UC Riverside

UC Riverside Electronic Theses and Dissertations

Title

The Derivatives and Properties of Sila-Diamondoids

Permalink

https://escholarship.org/uc/item/92q1181d

Author

Siu, Timothy C

Publication Date

2024

Peer reviewed|Thesis/dissertation

eScholarship.org Powered by the California Digital Library
University of California

UNIVERSITY OF CALIFORNIA
RIVERSIDE

The Derivatives and Properties of Sila-Diamondoids

A Dissertation submitted in partial satisfaction
of the requirements for the degree of

Doctor of Philosophy

in

Chemistry

by

Timothy C. Siu

September 2024

Dissertation Committee:
Dr. Timothy A. Su, Chairperson
Dr. Matthew Conley
Dr. Ana Bahamonde

Copyright by
Timothy C. Siu
2024

The Dissertation of Timothy C. Siu is approved:

_____

_____

_____

Committee Chairperson

University of California, Riverside

ACKNOWLEDGEMENTS

The journey I had undertaken in the last five years at UC Riverside could not have been completed without a vast support network that I have the pleasure of offering my thanks to below. First, I would like to give all glory to God without whom I could not have completed this journey. I would also like to thank Prof. Timothy A. Su for his guidance and support throughout the years. He was instrumental in teaching me how to pursue science with absolute rigor and taught me to effectively communicate complex concepts to a wide audience. As one of the first students of his laboratory, I think both of us are proud of how the lab has grown since we began in Summer 2019.

My passion for chemistry began at my undergraduate institution, Cal Poly Pomona, in the laboratory of Prof. Alex John. I was a below average student at best, but he still allowed me to conduct research in his laboratory. He allowed me to walk at Cal Poly Pomona so that I was ready to run at UC Riverside. Thank you for placing the stones I stepped on.

To my lab mates, especially Matthew Hight, Imex Aguirre Cardenas, Fernando Alfaro, Jacob Seo and Lan Pham, thank you all for making the laboratory a supportive environment. Even when things were heating up, we could find a reason to laugh it off. I hope the future of the laboratory will retain this quality.

To my undergraduate mentee, McKinley Durham, thank you for your extensive help in the synthetic work we've done together here. Without you, much of my thesis work would not have been possible. I still remember when Dr. Su and I first interviewed you during the COVID-19 pandemic. The enthusiasm and willingness to learn you

exhibited that day remained until the day you graduated. I wish you continued success as you begin your studies at UC Los Angeles.

To my grandmother: First, you had to raise your own family at an adolescent age in a war-torn Vietnam. Then you had to raise two children on your own in America before you helped raise my sister and I alongside my parents. Although I could not have always been present with you during my studies, I will always appreciate your sacrifices and support that shaped me into who I am today.

To my parents, Lynn and Kuang Siu, I know I was (and perhaps still am) the immature son who didn't take his future seriously. However, you both loved me unconditionally despite my flaws and I couldn't have asked for more as a son. My completion of this degree could not have been possible without your love and support.

To my sister, Jennifer Siu, I am extremely proud of how much you've grown in parallel with me. You truly exhibit qualities of a Jesus loving woman and inspire me to pursue my relationship with Him as well.

To the boys: It is rare that one finds quantity and quality within almost anything, but I am blessed to have both with you all. Although we may not see each other as often as the golden days, each of you remain in my thoughts and I know the vibes will continue as they had left off whenever we meet.

ABSTRACT OF THE DISSERTATION

The Derivatives and Properties of Sila-Diamondoids

by

Timothy C. Siu

Doctor of Philosophy, Graduate Program in Chemistry
University of California, Riverside, September 2024
Dr. Timothy A. Su, Chairperson

Bulk silicon's semiconducting properties has led to silicon being the defining material of the 21st century as seen in its widespread uses in modern technology. As electronics become increasingly smaller and more powerful, there has been much interest in exploring the behavior of silicon at the nanoscale. While silicon nanoparticles have promising applications as qubit hosts, bioimaging agents or lithium anodes, the heterogeneity of nanoparticle sizes, shapes and surfaces mask the elucidation of structure property relationships. By synthesizing silicon molecules from a "bottom-up" synthetic approach, atomic level precision is obtained and structure-property relationships in silicon nanoparticles are established. Inspired by the bulk silicon lattice, we sought to synthesize well-defined silicon clusters we have coined "sila-diamondoids".

Here, we report the optimization of the $AlCl_3$ catalyzed rearrangement towards sila-adamantane by adjusting conditions such as solvent, temperature, catalyst loading and concentration. This optimization has allowed us to synthesize sila-adamantane on

gram scales. We further demonstrated that sila-adamantane can be used as a building block material resulting in functionalized derivatives at the 1, 1,3 and 1,3,5,7 positions.

Next, we established a scope of SiAd functionalized with aurophillic linker groups (-CH_2SMe) to be studied in the context of single molecule electronic studies. We developed methods to functionalize SiAd($CH_2SMe)_2$ further and installed a scope of electronegative substituents at site specific locations about the cluster core. We intend to investigate the effects of electronegative substituents on the electronic environment of SiAds and how they relate to charge transport behavior.

In efforts to expand the use of SiAd as a material of interest, we dimerized two SiAd clusters between a linear oligosilane chain to form a type of oligosilane linked dumbbell structure. We then established a scope of oligosilane dumbbells with varying lengths or varying cluster sizes to probe their relative effects on optical properties.

Finally, we were able to synthesize a novel silicon analogue of carbon trishomocubane cubane cluster, which we have dubbed “sila-trishomocubane”. Investigation of the mechanism of formation of sila-trishomocubane allowed us to gain valuable insight into the driving forces of oligosilane isomerizations.

Table of Contents

Chapter 1: Introduction **1**

Chapter 2: Site Selective Functionalization of Sila-Adamantane and Its Ensuing Optical Effects 7

Introduction 7

Results and Discussion 11

Conclusion 24

Experimental 31

Chapter 3: Conductivity of the Molecular Analog of the Crystalline Unit Cell and Synthesis of Its Derivatives 112

Introduction 112

Results and Discussion 116

Conclusion 120

Experimental 124

Chapter 4: Oligosilane-Linked Sila-Adamantane Dumbbell Structures and Their Optical Properties 151

Introduction 151

Results and Discussion 152

Conclusion 161

Experimental 163

Chapter 5: Synthesis of a $Si_{10}C_1$ Trishomocubane 199

Introduction 199

Results and Discussion 201

Conclusion 203

Experimental 207

List of Figures

Figure 1.1 Proposed bottom-up approach builds up silicon components akin to building a house piece by piece whereas the top-down approach is akin to stripping down a large building into a house. 1

Figure 1.2 Methods of generating silyl anions from oligosilanes. a) Methyllithium preferentially cleaves internal (red) Si-Si bonds. b) Potassium *tert*-butoxide preferentially cleaves external (blue) Si-Si bonds.....2

Figure 1.3 Marschner's synthesis of sila-adamantane using potassium *tert*-butoxide silanide chemistry followed by Lewis acid catalyzed rearrangement. 3

Figure 1.4 Three sila-diamondoid structures sharing the same framework as bulk silicon are the subjects of my study. 4

Figure 2.1 a) Marschner's route to sila-adamantane 2. b) Developmental roadmap for functional adamantanes. Methods for functionalizing adamantane at its 1-, 2-, 3-, 5-, and 7-positions led to the creation of functional adamantane materials whose properties depend on their site of derivatization. c) This work discloses synthetic strategies for functionalizing sila-adamantane at five discrete locations within the cluster core, paving the way for functional silicon diamondoid materials. 9

Figure 2.2 a) Synthesis of tricyclic precursor 1 and sila-adamantane 2. i) Chlorotrimethylsilane, lithium, THF. ii) Potassium tert-butoxide, THF; 1,2-dichlorotetramethyldisilane. iii) Potassium tert-butoxide, 18-crown6, toluene; 1,2-dichlorotetramethyldisilane. iv) Potassium tert-butoxide, 18-crown-6, toluene; dichlorodimethylsilane. v) Potassium tert-butoxide, 18-crown-6, toluene; P6. vi) [CPh3][B(C6F5)4], toluene. b) Synthesis of P6. i) Lithium, THF. ii) Trifluoromethanesulfonic acid, pentane; triethylammonium chloride, ether. 11

Figure 2.3 a) ^{1}H NMR spectra of reaction aliquots for a representative isomerization of **1** with $AlCl_3$ track the presence of **1** (gray), **2** (red), **3** (blue), and **4** (orange) over the reaction timecourse. Asterisk (*) at 24 h timepoint denotes tetramethylsilane generated in situ. b) 2-cation **5** is 10.2 kcalmol ^{1} lower in free energy (ΔG^{298}) than exo-cation **6** based on gas-phase DFT calculations at the M06–2X/6–311G+(d,p) level of theory. Red-colored bonds indicate Si Si bonds that are coplanar with the silylium 3p orbital. Scheme illustrates proposed pathways for the generation of **2**, **3**, and **4**. c), d) Proposed pathways to explain product distribution in the isomerization of **1** with c) $AlCl_3$ or d) $AlCl_3$-$SiMe_3Cl$. Bottom plots show percent yield against reaction time, with yields determined from ^{1}H NMR spectra of reaction aliquots against cyclohexane or tetradecane internal standards. 12

Figure 2.4 a) One-pot multi-functionalization of sila-adamantane. i) Potassium tert-butoxide (2 equiv), 18-crown-6 (2 equiv), toluene; chloromethyl methyl sulfide, 99% yield.

ii) Potassium tert-butoxide (3 equiv), 18-crown-6 (3 equiv), toluene; chloromethyl methyl sulfide, 28% yield. iii) Potassium tert-butoxide (4 equiv), 18-crown-6 (4 equiv), toluene; chloromethyl methyl sulfide, 36% yield. b) Molecular structure of dianion **21** as determined by single-crystal X-ray diffraction (SCXRD). c) Sequential multi-functionalization of sila-adamantane. i) Potassium tert-butoxide (1 equiv), 18-crown-6 (1 equiv), toluene; p-toluenemethanesulfonate, 97% yield. ii) Potassium tert-butoxide (1 equiv), 18-crown-6 (1 equiv), toluene; chlorotriisopropylsilane, 44% yield. iii) Potassium tert-butoxide (1 equiv), 18-crown-6 (1 equiv), toluene; chloromethyl methyl sulfide, 71% yield. iv) Potassium tert-butoxide (1 equiv), 18-crown-6 (1 equiv), toluene; dibromoethane, 96% yield. SCXRD-determined structures have thermal ellipsoids plotted at 50% probability (**21**, **24**) or 30% probability (**20**). Solvent molecules and H atoms omitted for clarity. Si (blue), C (black), S (yellow), O (red), K (purple), Br 15

Figure 2.5 Experimental ultraviolet absorption spectra for 10 μM solutions of **11, 3, 4**, and **17** (solid black lines) in pentane. Blue star marks λ_3 peak position. Red star for **17** indicates the optically disallowed 285 nm peak corresponding to the 2e → $2a_1$ (HOMO → LUMO) transition. TD-DFT-calculated spectra (dotted gray line) at the PBE0/TZVP//BP86/TZVP level show normalized peaks plotted at 0.10 eV half-width at half height.....17

Figure 2.6 **(a)** Orbital correlation diagrams tracking the molecular orbitals relevant to ultraviolet absorption between the C_{3v}-symmetric **17** and **11** and C_s-symmetric **3**. The red levels track the fate of the $2a_1$ orbital (LUMO) for **11** upon 1- and 2-chloro substitution. The blue levels track the $1a_2$ → 3e transition that is a principal component of the λ_3 peak for **13**. **(b-d)** Orbital isosurfaces (isovalue = 0.035) for the $1a_2$ → 3e transition (**17, 11**) and 1a'' → 4a'' transition (**3**). Si (teal), C (gray), H (white), Cl (green), Ge (dark teal). In the bottom MO structures, the red labels "1" and "2" refer to the Si position discussed in the manuscript. As a consequence of spatially aligning the MO representations of **3** with **13** and **19**, the chlorine in **3** occupies the chemically equivalent 5-position. 21

Figure 2.7 **(a)** Molecular structures of chlorinated sila-adamantanes **17** and **3**. (**b**) Molecular structure of a T_d-symmetric silicon nanocrystal with a Si_{35} core. Atom coloring distinguishes non-chlorinated Si (black), chlorinated 3˚ Si (blue), chlorinated 2˚ Si (pink), Cl (green), and C (gray), with H atoms omitted for clarity. 22

Figure 2.8 (a) Marschner's reported route to **1** and **2**, with yields and scales reported from References [1–5]. (i) chlorotrimethylsilane, lithium, THF. (ii) methyllithium, toluene; 1,2-dichlorotetramethyldisilane. (iii) potassium *tert*-butoxide, 18-crown-6, toluene; 1,2-dibromotetramethyldisilane. (iv) potassium *tert*-butoxide, 18-crown-6, toluene; dichlorodimethylsilane. (v) potassium *tert*-butoxide, 18-crown-6, benzene; **P8**. (vi) aluminum chloride, cyclohexane; methyllithium. (b) Reported route to **P8**, with yields and scales reported from Supporting References [6–8]. (i) lithium, THF. (ii) aluminum chloride, hydrogen chloride, cyclohexane. (iii) phenylmagnesium bromide, THF. (iv) hydrogen bromide. 31

Figure 2.9 Overlay of ^{1}H NMR spectra comparing reaction mixture at 48-hour timepoint in isomerization reaction of **1** with $AlCl_3$ (1.7 equiv.) against isolated **3** and **4**. The reaction mixture NMR spectrum (top) is the same as the one shown in Fig. 2a of the main text, but with peaks shown at higher intensity. 32

Figure 2.10 LUMO isosurfaces (isovalue = 0.035) of (**a**) 2-cation **5** and (**b**) exo-cation **6**, with geometries optimized at the M06-2X/6-311+(d,p) level without symmetry constraints. Bonds highlighted in red indicate bonds that interact with silylium 3p orbital in the LUMO. 32

Figure 2.11 Experimental UV-vis absorbance spectrum of SiAd **2** measured in pentane plotted against computational spectra generated from gas-phase TD-DFT calculations at the following levels of theory: (A) PBE0/TZVP//BP86/TZVP, (B) PBE0/TZVP//M062X/6-311G(d,p), (C) PBE0/6-311+G(d,p)//M062X/6-311G(d,p), (D) M062X/6-311+G(d,p)//M062X/6-311G(d,p), (E) CAM-B3LYP/6-311+G(d,p)//M062X/6-311G(d,p). DFT-generated spectra have their extinction coefficients normalized. Calculated spectra are plotted at 0.10 eV half-width at half height. More details about the suitability of this functional and basis set can be found in the Computational Chemistry section of the Supporting Information. 33

Figure 2.12 Experimental and calculated absorption spectra of SiAd **2** and the calculated spectrum of **Si5** that represents an excised pentasilane fragment from **2** that is then passivated with hydride groups. The calculated spectrum of **Si5** tracks reasonably well with the experimental spectrum for the methylated analog $(SiMe_3)_3SiSiMe_2Si(SiMe_3)_3$ reported by Marschner and coworkers at ~245 nm.[9] 34

Figure 2.13 (a) Orbital energy diagram for the C_{2v}-symmetric **Si5** and T_d-symmetric **2**. (b) Orbital isosurfaces (isovalue=0.030) for molecular orbitals relevant for 235 nm transition for **Si5** and 221 and 240 nm transitions for **2**, showing oscillator strength and transition energies from TD-DFT calculations at the PBE0/TZVP level. More details can be found in the Computational Chemistry section of the Supporting Information. 35

Figure 2.14 (Left) Experimental UV-vis spectra for the functionalized sila-adamantanes, with extinction coefficient plotted against absorption wavelength from 10 µM solutions in pentane. (Right) Experimental spectrum (black dotted line) overlaid against line fit (red solid line) obtained from the 'Multipeak Fit' module of Igor Pro 8, in which Gaussian-shaped peaks were used to reconstruct the experimental spectrum. TD-DFT calculations (see Computational Chemistry section of Supporting Information) support the notion that the UV spectrum is comprised of multiple transitions and validate the multipeak model. The Gaussian peak most relevant to the experimental λ_3 peak is indicated with the blue solid line; its extinction coefficient is used for $\varepsilon_{3,\,\text{fitted}}$ in **Table 1** of the main text. ... 36-40

Figure 3.1 Sila-adamantane is isostructural with the unit cell of crystalline silicon; Methylthioether linked Sila-adamantane in a single molecule junction. 114

Figure 3.1 a) Illustration of “cutting out” pathways of SiAd while retaining the main backbone. b) 1D histogram of **1, 2**, and **3**. 116

Figure 3.3 General synthetic method towards functionalization of **1**. 118

Figure 3.4 General synthetic method towards functionalization of **SiAd** or **9** with chlorodimethylsilyl methyl sulfide 118

Figure 3.5 Method of installing linkers onto **12**. The inert 2-Cl acts as a directing group which results in a single isomer, **13**. 119

Figure 3.6 1D Histograms of **1**, **7**, and **12**.....120

Figure 4.1 Synthesis of symmetric dumbbell SiAds, **3 - 6**. 152

Figure 4.2 a) – d) Crystal structures of **3** through **6**. Bonds highlighted in purple display a gauche orientation. Solvent molecules and H atoms omitted for clarity. Si (blue), C (black). 153

Figure 4.3. Dihedral scans of **4** along the chain linkage (red) and along the cage-chain (dark red). Dihedral scan of a linear Si_4Me_8 provided for context (grey). 154

Figure 4.4 Experimental ultraviolet absorption spectra for 10 μM solutions of **1** and **3 – 6** in pentane. 155

Figure 4.5 Experimental ultraviolet absorption spectra for 10 μM solutions of **4**, **5**, and **6** (solid yellow, blue and green respectively) in pentane. TD-DFT-calculated spectra (dotted black line – gauche ; dotted gray line – anti) at the PBE0/TZVP//BP86/TZVP level. ...157

Figure 4.6 Synthesis of asymmetric dumbbell SiAd-Si_3Me_6-Si[2.2.1.] (**7**).....158

Figure 4.7 Synthesis of Si[2.2.1.]-$SiMe_2$-Si[2.2.1.] (**9**) 158

Figure 4.8 Experimental ultraviolet absorption spectra for 10 μM solutions of **3**, **7**, and **9** in pentane. 159

Figure 4.9 Molecular orbital diagrams of HOMO and LUMO of **9**, **7**, and **3**. Energy levels obtained from DFT-optimized structures at the M06-2X/6-31G**. MO surface plots of **9**, **7**, and **3** below. 160

Figure 4.10 Synthesis of functionalized dumbbell **10**. 161

Figure 5.1 a) Earliest examples of cubane, homocubane, bishomocubane and trishomocubane. b) Earliest examples of silacubane, oxahomocubane, oxabishomocubane.

c) This work discloses the first synthesis of sila-trishomocubane that contains Group 14 elements exclusively. 199

Figure 5.2 a) Synthesis of sila-trishomocubane, **3**, via isomerization of **2**. b) Crystal structure of **3**. H atoms and solvent molecules omitted for clarity. Si – blue, C – black. Core Si framework labelled 1 – 11 (4 is Carbon). 201

List of Tables

Table 2.1 Scope of monosubstituted sila-adamantanes with functional group-dependent NMR and ultraviolet absorption properties. 16

Table 2.2 Molecular orbital correlations between **17, 11,** and **3** calculated at the PBE0/TZVP//BP86/TZVP level of theory.....41 – 44

Table 2.3 Calculated vertical transitions for **11** and **17** of relevance to experimental absorption properties, ordered from highest to lowest energy for **11**. Gray shading provides a visual guide for transitions with $f < 0.05$. Blue shading provides a visual guide for **17** vertical transitions that are blue-shifted relative to their matching transition in **11**. Besides the weakly allowed HOMO to LUMO transition for **17**, only excited states with $f > 0.05$ and $\lambda > 200$ nm for either molecule **11** or **17** are shown in this comparison.....45

Table 3.1 Derivatives of **1** with yields. ***5** was prepared from **8**.....118

Table 4.1 Yields of dumbbell SiAds **3** - **6**. $n \leq 2$ could not be formed.....152

Table 4.2 Relevant dihedral angles for dumbbell SiAds. Si atoms labeled correspond to longest Si chain. Red - anti, blue – transoid, yellow – gauche 153

Table 4.3 Scope of dumbbell SiAds and their ultraviolet absorption properties. *Data obtained from ref. [5].....155

Table 4.4 Ultraviolet absorption properties of **3**, **7** and **9** 159

Table 5.1 Relevant Si-Si-Si bond angles for **3**. 201

Chapter 1: Introduction

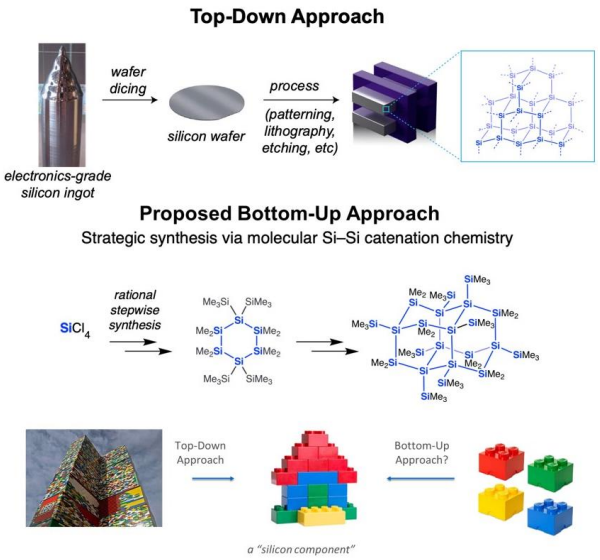


Figure 1.1 Proposed bottom-up approach builds up silicon components akin to building a house piece by piece whereas the top-down approach is akin to stripping down a large building into a house.

Bulk silicon's ability to act as a semiconductor played a critical role in the creation of the first computer in the 1940s, which used to take up an entire room.[1] Less than a hundred years later, we have cell phones that are essentially miniaturized computers that can fit into our pockets. As electronics are decreasing in size yet increasing in functionality, there is considerable interest in exploring the behavior of silicon at the nanoscale.

Currently, accessing nanoscale silicon materials require either a "top-down" or "bottom-up" approach. For example, the current state of the art of developing silicon computer chips is a top-down method that slices large ingots of silicon into wafers, followed by a laser etching process before the material is suitable for use in modern electronics.[2] However, there is a fundamental limit to the wavelength of a laser, which is within the nanometer size regime. As computer chips are reaching the sub-nanometer regime, it is necessary to consider alternative methods towards achieving electronics on a sub-nanometer scale.

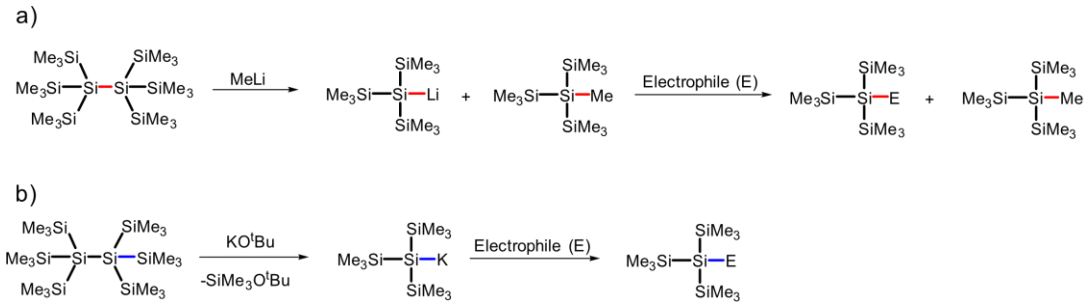


Figure 1.2 Methods of generating silyl anions from oligosilanes. a) Methyllithium preferentially cleaves internal (red) Si-Si bonds. b) Potassium *tert*-butoxide preferentially cleaves external (blue) Si-Si bonds.

The use of bottom-up synthetic methods may open doors for developing silicon materials at the Angstrom size regime, an order of magnitude smaller than nanometers. We utilize bottom-up approach involves using chemical methods to stitch together commercially available silicon starting materials into a sub-nanometer sized silicon molecule, akin to building a house brick by brick (Figure 1.1). A critical benefit of the bottom-up approach is that the materials being synthesized are atomically precise, where every single atom's identity and location is accounted for, allowing for the elucidation of meaningful structure property relationships that are unobstructed by potential structural abnormalities if the material were to be made by other means.

Accessing silicon clusters via bottom-up approaches may be difficult at times. While there exists a plethora of established methods to build complex organic compounds, the tool box for Si-Si bond formation reactions is significantly limited in comparison. Despite the limited scope of oligosilane functionalization methods, researchers have found that salt metathesis of silyl anions *in-situ* and electrophiles as an effective way to build up silicon clusters (Figure 1.2). Early silicon chemists such as

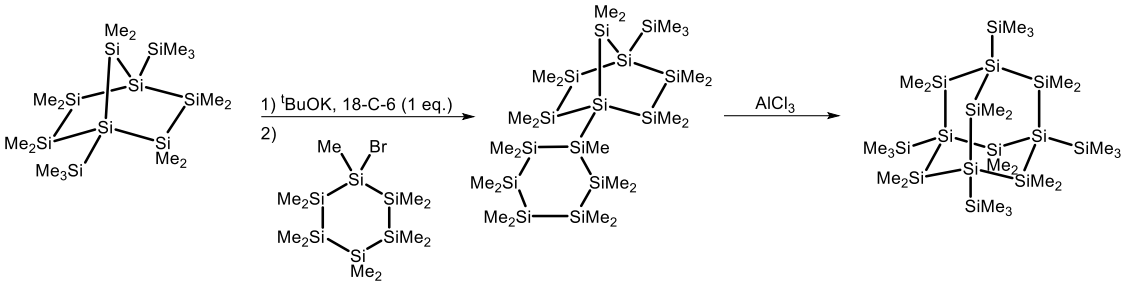


Figure 1.3 Marschner's synthesis of sila-adamantane using potassium *tert*-butoxide silanide chemistry followed by Lewis acid catalyzed rearrangement. Figure adapted from ref. [10].

Gilman and Hengge employed the use of lithium as a way to reductively cleave oligosilane compounds to yield silyl anions as silyl-lithiates.[3, 4] The silyl anions could then be quenched with an electrophile to yield a functionalized oligosilane. Gilman had also found that silyl-lithiates could be generated by subjecting an oligosilane to methyl lithium.[5] While these methods are quite effective for simpler oligosilanes such as tetrakis(trimethylsilyl)silane, the lithium or methyl lithium mediated cleavage often cleaves internal Si-Si bonds,[6] making these methods unattractive for use in more complex systems that contain multiple, symmetrically inequivalent internal Si-Si bonds.

Later, Marschner and co-workers had developed the chemistry of silyl anions further and found that the use of potassium *tert*-butoxide was an effective way to generate silyl-potassium complexes via cleavage of external Si-Si bonds.[7, 8] This has been seen as a viable alternative method of building up oligosilanes. Lithium and methyl lithium are pyrophoric reagents that can be difficult to control in their stoichiometry and may be unsafe to handle in large quantities. Potassium *tert*-butoxide is a much milder reagent in comparison, is much easier to control stoichiometrically, and is selective for external Si-Si

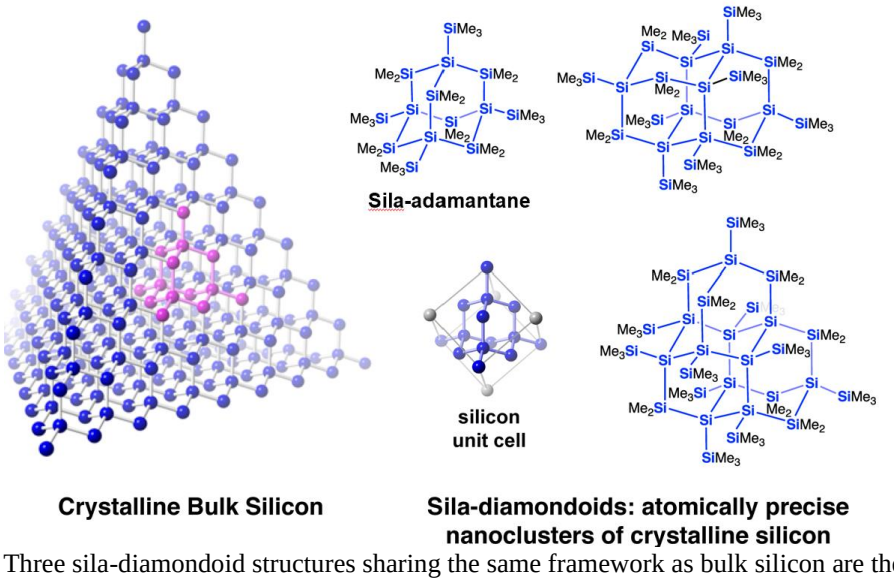


Figure 1.4 Three sila-diamondoid structures sharing the same framework as bulk silicon are the subjects of my study.

bonds. Marschner's group would continue to employ this method of functionalization to build up larger oligosilanes, including a precursor to sila-adamantane.

By subjecting a 1,4-disilylated bicyclo[2.2.1.]heptasilane to one equivalent of potassium *tert*-butoxide, they generated a silyl-anion which was subsequently quenched with undeamethylcyclohexasilanyl bromide to yield a tricyclic oligosilane. They then subjected the tricyclic starting material to a Lewis acid mediated rearrangement strategy adopted from the synthesis of adamantane[9] to produce sila-adamantane, the first silicon diamondoid (Figure 1.3).[10] Although the discovery of this molecule was indeed exciting, there has been very little experimental follow up studies for this class of silicon molecules, especially when compared to the plethora of known carbon diamondoids.

If sila-diamondoids are to be considered as an emerging class of materials, one must first consider the development of their more established carbon analogues, starting with adamantane. Adamantane was first found naturally in 1933 as a hydrocarbon extracted

from petroleum and bears the same framework as crystalline carbon.[11] It was then synthesized by Prelog in 1941, albeit in low yields, before an alternative, higher yielding synthetic pathway was developed by Schleyer in 1957.[9, 12] This higher yielding approach towards adamantane synthesis via Lewis acid isomerization of a commercially available *endo*-trimethylenenorbornane allowed for synthesis of adamantane in appreciable quantities for further study. As a result, a large scope of functionalized adamantanes were developed and these derivatives have found a wide range of biological applications.[13] As the scope of known diamondoids expanded from adamantane to higher order diamondoids up to tetramantane[14], the first sila-diamondoid was not prepared until 2005 by Marschner and co-workers. If sila-adamantane is to follow in the footsteps of its carbon analogue and grow into a more ubiquitous material, follow-up studies of the molecule is necessary.

Here, we decided targeted to target these "sila-diamondoids" because they share the same diamond framework as the crystalline bulk silicon used industrially for modern materials (Figure 1.4). Therefore, development of structure property relationships with these novel, smaller analogs of bulk silicon may reveal fundamentally interesting behaviors that can create avenues for new classes of sub-nanometer silicon materials. Although these sila-diamondoids may be of significant fundamental intrigue, their applications are masked by a lack of study due to the very limited scope of experimentally realized molecules. Herein we describe efforts to enlarge the scope of known sila-diamondoids and to study their ensuing physical properties which we hope will result in further exploration of this material.

References:

[1] Alice R. Burks, Arthur W., *The First Electronic Computer* (Ann Arbor: University of Michigan Press, 1989), 387

[2] Intel, "How Intel Manufactures Chips", Filmed 2020, Intel Corporation, 0:51

[3] Gilman, H.; Harrell, R.; Chang, K. Y.; Cottis, S. *Journal of Organometallic Chemistry* **1964**, *2* (5), 434–436.

[4] Hengge, E.; Wolfer, D. *Journal of Organometallic Chemistry* **1974**, *66* (3), 413–424.

[5] Gilman, H.; Smith, C. L. *Journal of Organometallic Chemistry* **1968**, *14* (1), 91–101.

[6] Apeloig, Y.; Yuzefovich, M.; Bendikov, M.; Bravo-Zhivotovskii, D.; Klinkhammer, K. *Organometallics* **1997**, *16* (6), 1265–1269.

[7] Marschner, C.. *European Journal of Inorganic Chemistry* **1998**, *1998* (2), 221–226.

[8] Marschner, C. *Organometallics* **2006**, *25* (9), 2110–2125.

[9] von R. Schleyer, P. *J. Am. Chem. Soc.* **1957**, *79* (12), 3292–3292.

[10] Fischer, J.; Baumgartner, J.; Marschner, C. *Science* **2005**, 310, 825

[11] Landa, S.; Macháček, V. *Collect. Czech. Chem. Commun.* **1933**, *5*, 1–5.

[12] Prelog, V.; Seiwerth, R. *Berichte der deutschen chemischen Gesellschaft (A and B Series)* **1941**, *74* (10), 1644–1648.

[13] Blanpied, T. A.; Clarke, R. J.; Johnson, J. W. *J. Neurosci.* **2005**, *25* (13), 3312–3322.

[14] Burns, W.; McKervey, M. A.; Mitchell, T. R. B.; Rooney, J. J. *J. Am. Chem. Soc.* **1978**, *100* (3), 906–911.

Chapter 2: Site-Selective Functionalization of Sila-Adamantane and Its Ensuing Optical Properties

Preface

This chapter presents a manuscript entitled "Site-Selective Functionalization of Sila-Adamantane and Its Ensuing Optical Properties" by Timothy C. Siu, Mario Imex Aguirre Cardenas, Jacob Seo, Kirllos Boctor, Miku G. Shimono, Isabelle T. Tran, Veronica Carta and Timothy A. Su, published in *Angewandte Chemie International Edition*. I synthesized all compounds and obtained all UV-vis data. Mr. Imex Aguirre Cardenas performed a mechanistic time point study and helped synthesize starting compounds. Mr. Jacob Seo, Mr. Kirllos Boctor, Ms. Miku G. Shimo and Ms. Isabelle Tran helped synthesize starting compounds. Crystallographic data was obtained by Dr. Veronica Carta. Theoretical calculations were performed by Dr. Timothy A. Su.

Introduction

Molecular silicon clusters are multicyclic compounds with skeletal cores composed of catenated silicon bonds. They can be classified into three categories based on the nature of their bonding:[1] saturated clusters,[2–4] unsaturated clusters (siliconoids),[5] and Zintl ion clusters.[6] These clusters are attractive molecular models for understanding the reactivity and properties of bulk silicon, the core material of consumer solar cells and integrated circuits. For example, the unsaturated vertices in siliconoid clusters have been described as models for studying the reactivity of dangling bonds at bulk silicon surfaces.[7,8] Saturated

cyclohexasilanes are emerging as materials of interest that are structurally precise analogs of the silicon semiconductor.[9]

Sila-adamantane (SiAd) is a saturated silicon cluster that bears particular intrigue in the context of nanoscale electronics, as its cluster core is isostructural with the diamond cubic unit cell of the silicon semiconductor (Figure 2.1).[10] It thus represents the ultimate limit of miniaturization for nanocrystalline silicon. Fischer, Baumgartner, and Marschner reported the first and only synthesis of SiAd through the sila-Wagner–Meerwein rearrangement of the strained tricyclic oligosilane **1** (Figure 2.1a),[10] reminiscent of Schleyer's isomerization synthesis of adamantane.[11] Despite its promise, the development of silicon diamondoids has remained in its infancy. While adamantanes with mixed tetrel-silicon cores such as Fritz's C_6Si_4 carborundane[12] and Wagner's recent Ge_xSi_y adamantanes[13] have been reported, no experimental studies on sila-adamantane have followed since its 2005 report, leaving much to be discovered about the mechanism of its synthesis, derivatization, and physical properties.

The absence of follow-up studies on sila-adamantane can be attributed in part to the difficulty of its synthesis. Whereas Schleyer's *endo*-trimethylenenorbornane precursor could be prepared quantitatively in a single-step from dicyclopentadiene, Marschner's route to **1** involves a convergent nine-step synthesis from commercial reagents (Figure 2.8).[10] While the large-scale synthesis of **1** and **2** is nontrivial, it is worth pursuing, as it would allow us to elucidate the fundamental reactivity and properties of silicon diamondoids. If we consider the developmental roadmap of carbon adamantane (Figure 2.1b), from its initial synthesis to eventual ubiquity, it becomes evident that that the next developmental stage for sila-adamantane is to establish strategies for its site-selective functionalization. In the same fashion that the regioselective functionalization of the organic adamantane[14–17] led to its subsequent use in therapeutics,[18] biological imaging probes,[19,20] ligands,[21,22] and materials,[23,24] the synthesis of functionalized sila-

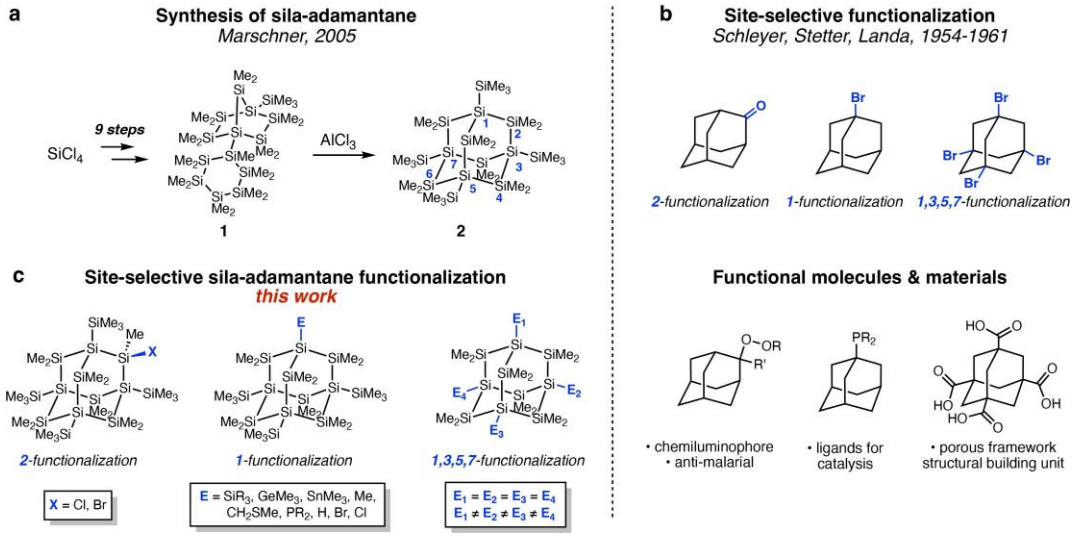


Figure 2.1 a) Marschner's route to sila-adamantane **2**. b) Developmental roadmap for functional adamantanes. Methods for functionalizing adamantane at its 1-, 2-, 3-, 5-, and 7-positions led to the creation of functional adamantane materials whose properties depend on their site of derivatization. c) This work discloses synthetic strategies for functionalizing sila-adamantane at five discrete locations within the cluster core, paving the way for functional silicon diamondoid materials.

adamantanes would dramatically advance the utility of silicon diamondoids. Indeed, approaches for the site-selective functionalization of related saturated,[25–32] unsaturated,[33–35] and Zintl ion[36–39] silicon clusters have led to the discovery of new properties and applications.

The present work discloses the gram-scale synthesis of sila-adamantane and its regioselective functionalization at five discrete silicon centers within its core (Figure 2.1c). These syntheses are guided by mechanistic insights that implicate an aluminate-stabilized silylium ion at the 2-position as the final intermediate in the isomerization synthesis of **2**. We can use these insights to mono-substitute sila-adamantane at its 2-position with halides, or tetra-substitute sila-adamantane at its 1-, 3-, 5-, and 7-positions with either the same or different functional groups. We show that these functionalization approaches may be used to control the optical properties of silicon diamondoids. These findings provide new insight into the atom-level origins of functionalization dependent luminescence in silicon nanocrystals.

Results and Discussion

We obtained **P4** (Figure 2.2) following precedented approaches by Marschner, Gilman, and Pannell on a large scale.[40–43] The clean mono-triflation of Si_6Me_{12} reported by Albers et al.[44] enabled efficient access to **P6** relative to the 4-step synthesis of its brominated analog in the previous route (Figure 2.8).[10] Coupling **P4** and **P6** together gave **1** on decagram-scale. Figure 2.3a shows NMR spectra of reaction aliquots from a representative isomerization of **1** to **2** via aluminum chloride in benzene. The unmarked peaks at the 24-hour timepoint correspond to unidentified intermediates that form over the course of isomerization. These intermediates largely disappear at the 48-hour timepoint, as they have coalesced into products with silicon adamantane cores, the most prominent of which belongs to the T_d-symmetric **2**. SiAd **2** forms in 53% NMR yield under these conditions, along with monochlorinated sila-adamantane byproducts that we have assigned as the C_s-symmetric 2-chlorinated **3**[45] (13% yield) and the C_{3v}-symmetric exocyclic-chlorinated **4** (6% yield) (Figure 1.3b, **3c**). These assignments were confirmed upon isolation of **3** from

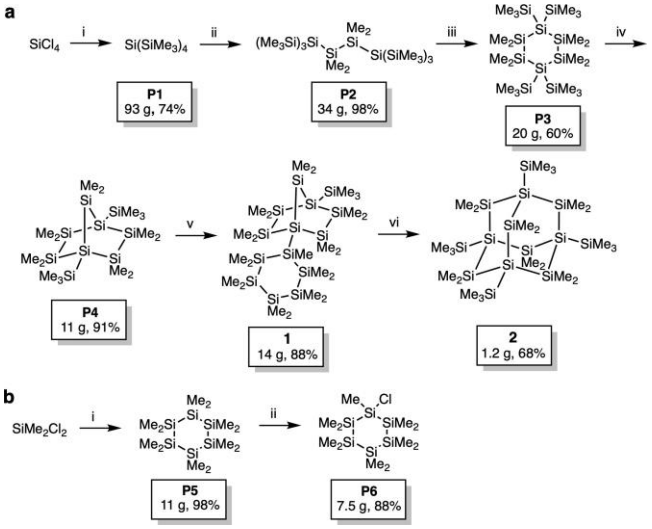


Figure 2.2 a) Synthesis of tricyclic precursor **1** and sila-adamantane **2**. i) Chlorotrimethylsilane, lithium, THF. ii) Potassium tert-butoxide, THF; 1,2-dichlorotetramethyldisilane. iii) Potassium tert-butoxide, 18-crown6, toluene; 1,2-dichlorotetramethyldisilane. iv) Potassium tert-butoxide, 18-crown-6, toluene; dichlorodimethylsilane. v) Potassium tert-butoxide, 18-crown-6, toluene; **P6**. vi) $[CPh_3][B(C_6F_5)_4]$, toluene. b) Synthesis of **P6**. i) Lithium, THF. ii) Trifluoromethanesulfonic acid, pentane; triethylammonium chloride, ether.

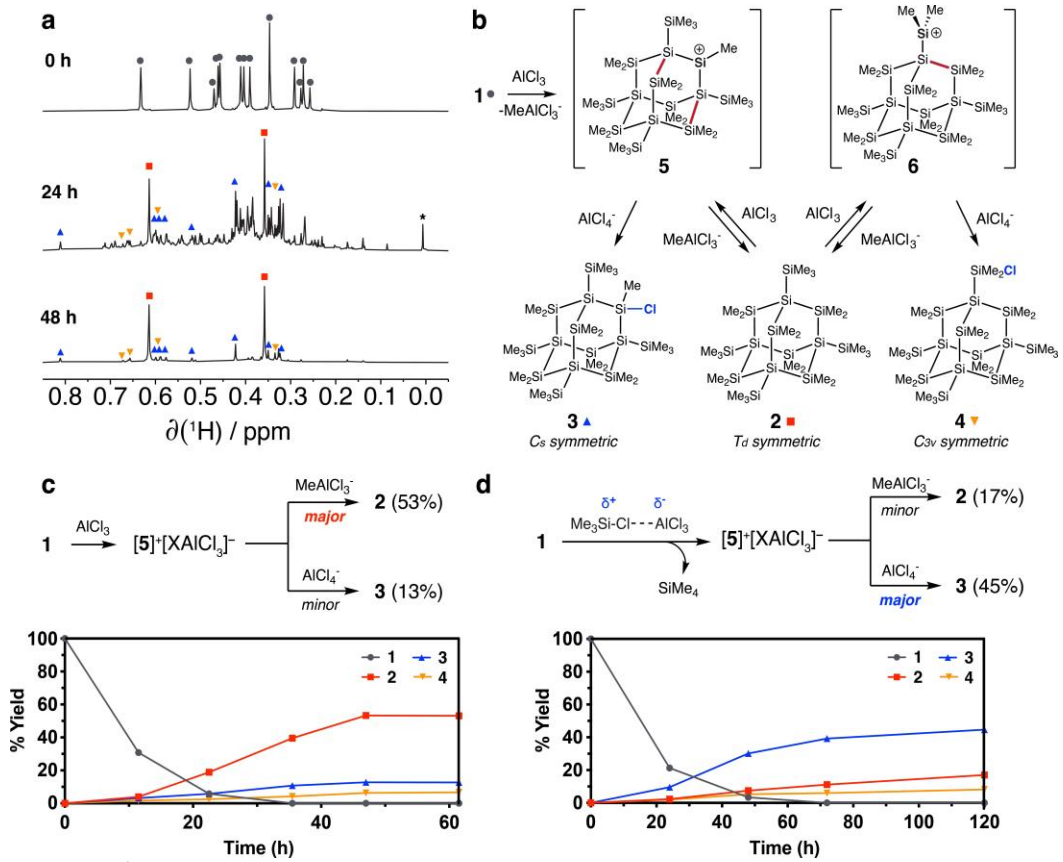


Figure 2.3 a) ^{1}H NMR spectra of reaction aliquots for a representative isomerization of **1** with $AlCl_3$ track the presence of **1** (gray), **2** (red), **3** (blue), and **4** (orange) over the reaction timecourse. Asterisk (*) at 24 h timepoint denotes tetramethylsilane generated in situ. b) 2-cation **5** is 10.2 kcalmol ^{1} lower in free energy (ΔG^{298}) than exo-cation **6** based on gas-phase DFT calculations at the M06–2X/6–311G+(d,p) level of theory. Red-colored bonds indicate Si Si bonds that are coplanar with the silylium 3p orbital. Scheme illustrates proposed pathways for the generation of **2**, **3**, and **4**. c), d) Proposed pathways to explain product distribution in the isomerization of **1** with c) $AlCl_3$ or d) $AlCl_3$-$SiMe_3Cl$. Bottom plots show percent yield against reaction time, with yields determined from ^{1}H NMR spectra of reaction aliquots against cyclohexane or tetradecane internal standards.

the reaction mixture and the independent synthesis of **4** from **2** (Figure 2.9). We note that a portion of **2** becomes chlorinated in the presence of aluminum chloride alone under our reaction conditions, leading to a distribution ratio of **2** (94%), **3** (2.6%), and **4** (3.4%) over the same 48-hour reaction period. While this pathway may partially account for the formation of **3** and **4** (Figure 2.3b), it does not explain the relative enrichment of **3** found in the $AlCl_3$-mediated rearrangement of **1** (Figure 2.3c).

We were particularly intrigued by the generation of **3**, both for its mechanistic implications and because the selective functionalization of secondary silicon centers over primary and quaternary silicon centers is rare. While mechanistic inquiry into sila-adamantane isomerization has not been directly explored, related work investigating sila-Wagner–Meerwein rearrangements by Kumada, West, Marschner, Albers, Müller, Pannell, and others in simpler oligosilanes provide a basic framework for how the reaction begins and ends.[44,46–55] Methyl transfer from **1** to the Lewis acid initiates a cascade of bond shift rearrangements to the lowest energy oligosilanyl cationic structure. Methyl transfer from [$MeAlCl_3$] to the final silylium intermediate terminates isomerization. Under this premise, terminal methylation must then occur at a silylium-like center located at either the exocyclic or 2-position. Gas-phase DFT calculations of the free cation indicate that the 2-cation **5** is 10.2 kcalmol ^{1} lower in free energy than the exo-cation **6** (Figure 2.9b), likely due to the stronger hyperconjugative stabilization from adjacent, coplanar Si Si bonds (Figure 2.10). The 2-cation is the proposed final intermediate in the isomerization synthesis of carbon adamantane for analogous reasons.[56] These factors, along with the enrichment of **3** relative to **4**, suggest that the 2-cation **5** is the favored final intermediate that forms in the isomerization of **1** to SiAd **2**.

The evolution of tetramethylsilane over the reaction course, as shown in the ^{1}H NMR spectrum of the 24-hour timepoint (Figure 2.3a), provides a key clue to how the chlorinated sila-adamantane **3** forms. Tetramethylsilane is a common byproduct that forms via redistribution reactions when oligosilanes are subjected to strong Lewis acids.[46,51,57] As tetramethylsilane is highly volatile, its evolution from the reaction mixture effectively

removes methyl donors from the reaction mixture that would otherwise methylate **5** via [$MeAlCl_3$] species to yield SiAd **2**. Presumably, in the absence of these methyl donors, the 2-cation is instead quenched by chloride donation from species such as [$AlCl_4$] counterions, leading to the formation of the chlorinated **3** (Figure 2.3b).

We employed the $SiMe_3Cl$-$AlCl_3$ system to probe this hypothesis (Figure 2.3d).[57] Methyl transfer from **1** to the activated $SiMe_3Cl$-$AlCl_3$ species leads to the generation of the volatile $SiMe_4$ and the removal of methyl donors from the reaction mixture that originally came from **1**. The net consequence is an enriched ratio of [$AlCl_4$] counteranions that may chlorinate **5** (Figure 2.3d). Indeed, inclusion of an equimolar amount of $SiMe_3Cl$ relative to **1** in the presence of $AlCl_3$ yields a 2.7-fold enrichment of **3** relative to **2** (Figure 2.3d), with **3** forming in 45% yield. Treatment of **1** with the $SiMe_3Br$-$AlBr_3$ system similarly gives 2Br-SiAd **7**, albeit in lower yields. Thus, the removal of methyl donors from the reaction medium allows us to install halides precisely at the 2-position of the SiAd core via nucleophilic tetrahaloaluminate counteranions.

Next, we sought to isolate **2** on gram-scale to establish its broader functionalization scope. It was challenging to accomplish this goal using aluminum chloride as the Lewis acid due to difficulties removing **3** from the reaction mixture. The silyl chloride in **3** is inert to aqueous workup, co-crystallizes with **2**, and elutes closely with **2** in hexanes via silica gel chromatography. Marschner and co-workers previously employed a methyllithium quench following isomerization. But while methyllithium readily displaces the accessible silyl chloride in **4**, it only partially does so for **3**. We hypothesized that the isomerization of **1** with Lewis acids containing non-nucleophilic counteranions would give fewer

byproducts and enable higher-yielding access to **2**. Indeed, the Lewis acid trityl tetrakis(pentafluorophenyl)borate $[CPh_3][B(C_6F_5)_4]$ enabled the facile isolation of **2** (68% yield) on gram-scale after silica plug purification (Figure 2.2a).[54,55]

With gram-scale quantities of **2** in hand, we sought to explore the scope of functionalization at its bridgehead positions (Figure 2.4, Table 2.1).[58,59] We mono-functionalized the silanide of **2** with electrophiles to access **4**, **8**–**17** (Table 2.1). Next, we sought to establish whether all four quaternary Si centers in SiAd **2** could be substituted. Treatment of **2** with two, three, or four equivalents of potassium *tert*-butoxide and 18-crown-6 followed by reaction with a chloromethyl methyl sulfide electrophile led

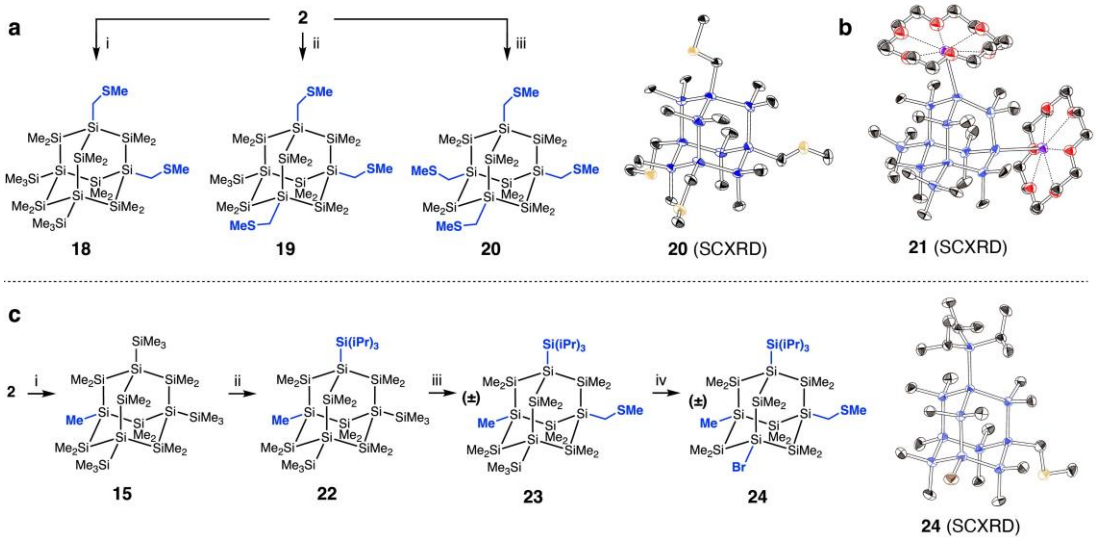
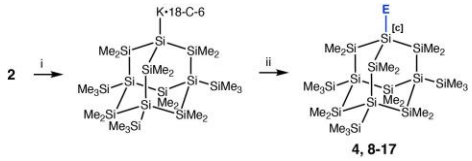


Figure 2.4 a) One-pot multi-functionalization of sila-adamantane. i) Potassium tert-butoxide (2 equiv), 18-crown-6 (2 equiv), toluene; chloromethyl methyl sulfide, 99% yield. ii) Potassium tert-butoxide (3 equiv), 18-crown-6 (3 equiv), toluene; chloromethyl methyl sulfide, 28% yield. iii) Potassium tert-butoxide (4 equiv), 18-crown-6 (4 equiv), toluene; chloromethyl methyl sulfide, 36% yield. b) Molecular structure of dianion **21** as determined by single-crystal X-ray diffraction (SCXRD). c) Sequential multi-functionalization of sila-adamantane. i) Potassium tert-butoxide (1 equiv), 18-crown-6 (1 equiv), toluene; p-toluenemethanesulfonate, 97% yield. ii) Potassium tert-butoxide (1 equiv), 18-crown-6 (1 equiv), toluene; chlorotriisopropylsilane, 44% yield. iii) Potassium tert-butoxide (1 equiv), 18-crown-6 (1 equiv), toluene; chloromethyl methyl sulfide, 71% yield. iv) Potassium tert-butoxide (1 equiv), 18-crown-6 (1 equiv), toluene; dibromoethane, 96% yield. SCXRD-determined structures have thermal ellipsoids plotted at 50% probability (**21**, **24**) or 30% probability (**20**). Solvent molecules and H atoms omitted for clarity. Si (blue), C (black), S (yellow), O (red), K (purple), Br (brown).

Table 2.1 Scope of monosubstituted sila-adamantanes with functional group-dependent NMR and ultraviolet absorption properties.



E	% yield[a]	EN [b]	@ ($_{29}$Si/ppm)[c]	λ_1 [nm], ε_1 [M $^{-1}$ cm $^{-1}$]	λ_3 [nm], ε_3 [M $^{-1}$ cm $^{-1}$]	$\varepsilon_{3,fit}$ [M $^{-1}$ cm $^{-1}$][f]
2	–	–	1.8	118.7	198, 11149	223, 14133
3	–	–	1.8	112.0	198, 9857	222, 11256
4	$SiMe_2Cl$	84%	1.8	115.8	198, 10190	223, 12696
8	$SiMe_2Ph$	33%	1.8	118.9	198, 10770	223, 9235
9	$SiPh_3$	54%	1.8	117.1	200, 16874	221, 7581
10	$SnMe_3$	98%	1.8	117.4	198, 10988	226, 11922
11	$GeMe_3$	60%	1.8	110.7	199, 10770	223, 11917
12	H	70%	2.1	99.7	198, 8518	218, 7903
13	$P(NEt_2)_2$	63%	2.1	87.7[d]	198, 11232	222, 8983
14	CH_2SMe	35%	2.5	70.6	199, 10053	216, 7909
15	Me	97%	2.5	68.9	199, 11388	215, 8380
16	Br	83%	2.8	12.7	198, 11374	215, sh[e]
17	Cl	21%	3.0	4.2	201, 11425	214, sh[e]

i) Potassium tert-butoxide, 18-crown-6, toluene. ii) electrophilic reagent. Key. [a] Isolated yields. Reactions executed on 0.05–0.2 mmol scales. [b] Pauling electronegativity of the substituent atom in **E** that is attached to 1-Si center. [c] ^{29}Si DEPT peak shift of 1-Si center relative to a tetramethylsilane internal standard. [d] $^1J_{SiP}$ =99 Hz. [e] Shoulder peak. [f] ε_3, fitted represents the extinction coefficient obtained from fitting experimental absorption data to Gaussian peak distributions extracted from Figure 2.14.

respectively to 1-,3-, 1-,3-,5-, and 1-,3-,5-,7-functionalized silaadamantanes **18**, **19**, and **20**[45] (Figure 2.4). We attempted to isolate the multianionic intermediate in this tetra-functionalization. Treatment of **2** with four equivalents of potassium *tert*-butoxide and 18-crown-6 predominately gave dianion **21**[45] (Figure 2.4b), suggesting that the tri-substituted **19** and tetra-substituted **20** undergo subsequent generation and quenching of anionic sites after the first two anionic sites are functionalized. In addition, we established that four unique functional groups at the 1-, 3-, 5-, and 7-positions can be installed on the sila-adamantyl core through successive mono-substitution reactions to yield the chiral sila-adamanane **24**[45] (Figure 2.4c) in 29% overall yield starting from **2**. To our knowledge, **4** represents the first example of four silanide centers being generated and functionalized in

a single-pot reaction for a neutral silicon cluster.[1,59] Tetrafunctionalized sila-adamantanes are anticipated to be useful material building blocks. Sila-adamantanes with four identical metal-linking groups may serve as a tetrahedral building blocks in framework materials;[24,60] sila-adamantanes with four unique substituents enable access to multifunctional materials with sila-diamondoid cores.[61,62]

Marschner and co-workers previously noted the wavelength of maximum absorption for **2** (223 nm) is blue-shifted compared to linear pentasilane chains (Figure 2.11–2.13). We sought to explore how mono-substitution on the sila-adamantane scaffold may further impact optical characteristics. The substituent groups in Table 2.1 systematically range from being highly σ-donating to σ-withdrawing. Their electronic impact is apparent in the downfield $\partial(^{29}Si)$ NMR shift of the SiAd 1-Si center that occurs as the substituent becomes increasingly electronegative (Table 2.1). Figure 2.5 and Figure 2.14 show the UV/Visible absorbance spectra for all molecules listed in Table 2.1. Figure 2.14 shows that the experimental spectra can be fit to a tetramodal peak distribution

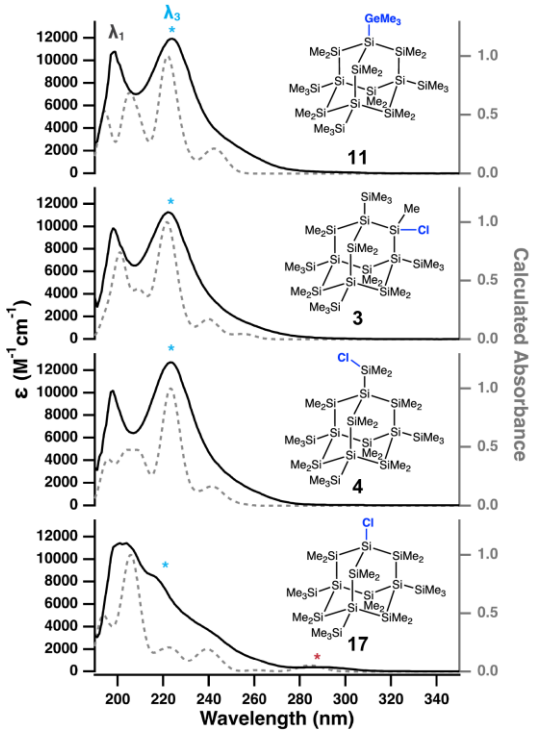


Figure 2.5 Experimental ultraviolet absorption spectra for 10 μM solutions of **11, 3, 4**, and **17** (solid black lines) in pentane. Blue star marks λ_3 peak position. Red star for **17** indicates the optically disallowed 285 nm peak corresponding to the 2e → $2a_1$ (HOMO → LUMO) transition. TD-DFT-calculated spectra (dotted gray line) at the PBE0/TZVP//BP86/TZVP level show normalized peaks plotted at 0.10 eV half-width at half height.

with maxima between 197– 201 nm, (λ_1), 203–208 nm (λ_2), 213–226 nm (λ_3), and 230–260 nm (λ_4). We focus particularly on λ_1 and λ_3 in Table 2.1, as these are the two readily identifiable peaks in the experimental absorbance spectra for all molecules. Whereas the extinction coefficient (ε_1) for λ_1 does not appreciably depend on substituent electronegativity, we find that the extinction coefficient (ε_3) for λ_3 inversely correlates with substituent electronegativity (Table 2.1). For example, functionalized sila-adamantanes with electropositive 1-substituents and $\partial(^{29}\text{Si})$ shifts between 119 to 110 ppm are largely indistinguishable from the UV absorbance spectrum of SiAd **2** (Figure 2.14)—this includes the 1-germylated **11**, 2-chlorinated **3**, and exocyclic chlorinated **4**, whose spectra are shown in Figure 2.5. As the substituent groups become increasingly electronegative, the extinction coefficient for λ_3 diminishes to the point where it becomes a shoulder peak in the spectra of the 1-halogenated sila-adamantanes **16** (Figure 2.14) and **17** (Figure 2.5). The fitted extinction coefficients ($\varepsilon_{3,\text{fit}}$) derived from the multipeak analysis in Figure 2.14 provides a numerical sense for how ε_3 is impacted by 1-halogenation.

These experimental observations led us to two questions: 1) why does ε_3 diminish as the 1-substituent becomes increasingly electron-withdrawing, and 2) why are the optical properties of sila-adamantane sensitive to chlorination at the 1-position, but not at the 2- or exocyclic positions?

Insights from time-dependent DFT (TD-DFT) calculations at the PBE0/TZVP//BP86/TZVP level of theory provide a framework for understanding the origins of these effects. To understand why ε_3 inversely correlates with substituent electronegativity, we compare **11**, which has an electron-donating 1-germyl substituent,

against **17**, which has an electron-withdrawing 1chloro substituent. Because **11** and **17** are both C_{3v}– symmetric, it is straightforward to correlate their MOs (Figure 2.6a, Table 2.2) and track how the associated vertical transitions in the λ_3 region change as the 1-substituent becomes increasingly σ-withdrawing (Table 2.2). Inspection of Table 2.2 reveals these λ_3 vertical transitions meet two principal fates in going from **11** to **17**: they either blue-shift to the λ_2 regions, or they become optically forbidden states with f<0.05.

The former is straightforward to rationalize, as chlorination dramatically lowers the energy of the filled $1a_1$ MO by 0.76 eV due to its $\sigma_{Si\,Cl}$ character (Table 2.2). The energetic stabilization of the $1a_1$ MO leads to blue-shifted vertical transitions that are apparent in the increased λ_2 intensity in the experimental and calculated absorbance spectra for **17** (Figure 2.5).

Analysis of MO character between **11** and **17** helps rationalize why many of the λ_3 transitions listed in Table 2.3 become dipole-forbidden upon 1-chlorination. For the sake of simplicity, we focus on just one of these transitions, $1a_2$! 3e (blue levels in Figure 2.6a), that has a vertical excitation energy of 5.62 eV (221 nm) for **11** and 5.55 eV (224 nm) for **17**. Figure 2.6b–c show the isosurfaces for the principal MOs that are involved. The occupied $1a_2$ MOs are indistinguishable in character for both **11** and **17** and are comprised from a cyclic ring of *gauche*-oriented $\sigma_{Si\text{-}Si}$ bonds distal from the Si(1) and Si(2) sites. However, the nature of the unoccupied 3e orbitals are quite different: the 3e MO for **11** features substantial σ*Si(1)-Si(2) and σ*Si(2)-CH3 character, while **17** does not. The $1a_2$! 3e transition dipole moment is visibly stronger for **11** than **17**, as the directional shift in

orbital density from the $1a_2$ to 3e orbitals is much larger for **11**, thus explaining the low oscillator strength observed for this transition in **17**.

Inspection of the $2a_1$ LUMO for **17** and **11** provides deeper insight into why the 3e orbitals for **17** lacks $\sigma^*_{Si(1)\text{-}Si(2)}$ and $\sigma^*_{Si(2)\text{-}CH3}$ character (Figure 1.6b–c). The $2a_1$ MO is 0.62 eV lower in energy for **17** than **11** due to its substantial $\sigma^*_{Si\,Cl}$ character (Figure 2.6a, Table 2.2). In addition, the $2a_1$ orbital of **17** shows substantial $\sigma^*_{Si(1)\text{-}Si(2)}$ character, as indicated by the thicker orbital character above Si(1), and substantial $\sigma^*_{Si(2)\text{-}CH3}$ character, as indicated by the puckering of orbital density in the cluster interior toward the Si(2) centers. Chloride substitution at the 1-position thus lowers the energies of the adjacent σ*Si(1)-Si(2) and σ*Si(2)-CH3 orbitals to such an extent that they become principal components of the $2a_1$ orbital instead of the 3e orbitals. This leads to the optical weakening of the $1a_2$! 3e transition and attenuation of the experimental λ_3 peak. This explanation can be generalized to the other transitions in Table 2.3 and broadly explains why ε_3 becomes diminished as increasingly σ-withdrawing groups are installed at the 1-position (Table 2.1), thus answering our first question.

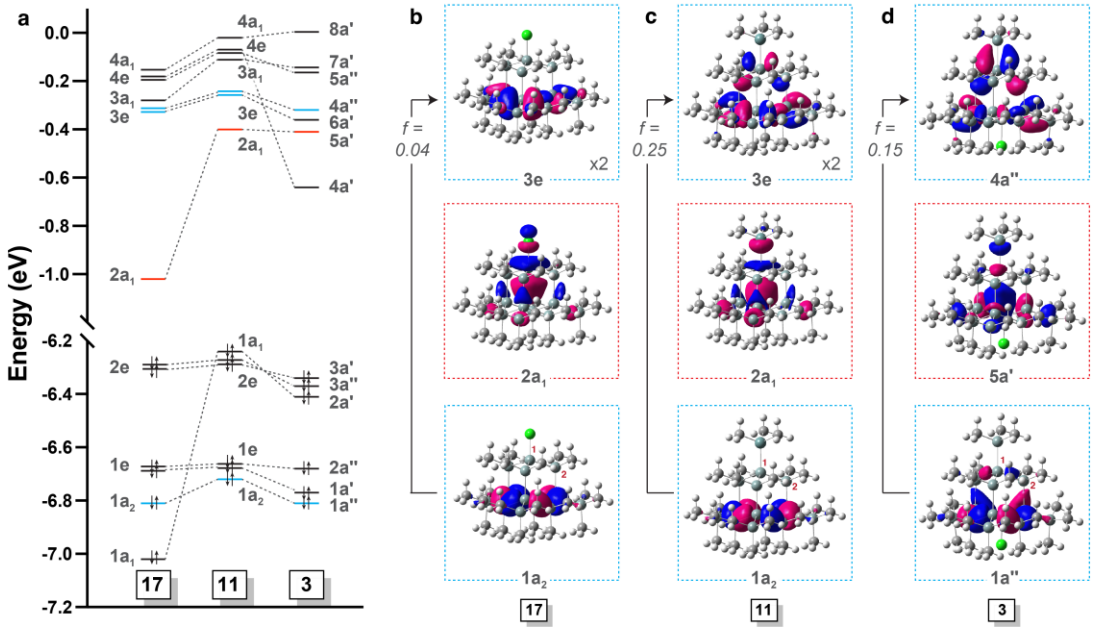


Figure 2.6 **(a)** Orbital correlation diagrams tracking the molecular orbitals relevant to ultraviolet absorption between the C_{3v}-symmetric **17** and **11** and C_s-symmetric **3**. The red levels track the fate of the $2a_1$ orbital (LUMO) for **11** upon 1- and 2-chloro substitution. The blue levels track the $1a_2$ → 3e transition that is a principal component of the λ_3 peak for **13**. **(b-d)** Orbital isosurfaces (isovalue = 0.035) for the $1a_2$ → 3e transition (**17, 11**) and 1a'' → 4a'' transition (**3**). Si (teal), C (gray), H (white), Cl (green), Ge (dark teal). In the bottom MO structures, the red labels "1" and "2" refer to the Si position discussed in the manuscript. As a consequence of spatially aligning the MO representations of **3** with **13** and **19**, the chlorine in **3** occupies the chemically equivalent 5-position.

TD-DFT analysis answers why 2-chlorination has a marginal impact on optical absorbance relative to 1-chlorination. The key $2a_1$ orbital for **11** and **17** described above correlates most strongly with the 5a' orbital of **3** (Figure 2.6a). Instead of lowering the 5a' orbital energy, however, chlorination in **3** lowers the 4a' orbital by 0.55 eV from the parent 4e orbital in **11**. This 4a' orbital does not play a major role in the vertical transitions in the λ_3 range for **3** the way that the 5a' MO does. Since the 5a' MO is energetically unaffected by chlorination in **3**, it does not perturb the character of the 4a'' MO. Indeed, Figure 5d shows that the orbitals relevant for the 1a'' ! 4a'' transition for **3** are similar in character to those of the $1a_2$! 3e transition for **11**. Because the 5a' MO is unaffected by 2-chlorination, the 4a'' MO of **3** maintains substantial $\sigma^*_{Si(1)\text{-}Si(2)}$ and $\sigma^*_{Si(2)\text{-}CH3}$ character, thus giving rise

to a significant transition moment dipole. This rationale explains why 2-chlorination is optically inert relative to 1chlorination. The same rationale may be applied for rationalizing why exocyclic chlorination in **4** does not affect λ_3 absorbance.

The optical absorbance spectra and TD-DFT-based rationalizations demonstrate how substituent electronics and the site of substitution dictate the optical properties of functionalized sila-adamantane clusters. These findings have broader implications in the context of the surface-sensitive nature of silicon nanocrystal (NC) optical absorbance (Figure 2.7).[63–65] Surface passivation with electronegative groups such as oxides and chlorides is commonly found on Si NC surfaces as either remnants of NC synthesis[66,67] or NC postfunctionalization processes.[68] These groups dramatically impact optical properties, particularly for small (<2 nm diameter) Si NCs. For example, surface oxide formation causes Si NCs to become indirect band gap materials with 1 eV red-shifted photoluminescence.[64,69] Several groups have computationally investigated Si_{35} diamondoids as models for Si NCs passivated with hydride, hydroxyl, or halide (F, Cl) groups (Figure 2.7b).[70–73] Zhou, Brus, and Friesner found that while hydride-passivated Si NCs experience optically allowed, direct-gap transitions at 5.21 eV (*f*= 0.22), passivation with hydroxyl or halide groups leads to

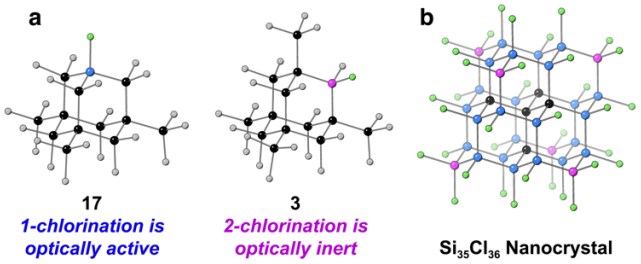


Figure 2.7 **(a)** Molecular structures of chlorinated sila-adamantanes **17** and **3**. (**b**) Molecular structure of a T_d-symmetric silicon nanocrystal with a Si_{35} core. Atom coloring distinguishes non-chlorinated Si (black), chlorinated 3˚ Si (blue), chlorinated 2˚ Si (pink), Cl (green), and C (gray), with H atoms omitted for clarity.

optically forbidden, indirect-gap transitions at 4.00 eV (*f*= 0.017) and 4.25 eV (*f*=0.019*)* respectively.[70,71]

These Si NC optical trends resonate with our experimental and computational findings on functionalized silaadamantane clusters (Figure 2.7a). Optically allowed λ_3 transitions for sila-adamantanes with electron-rich substituents become dipole-forbidden as the 1-substituent becomes increasingly electronegative. We also find the emergence of a dipole-forbidden, red-shifted peak (λ_5) in the 285–290 nm range for the 1-halogenated **16** and **17** (Figure 2.5, Figure 2.14). This λ_5 peak corresponds to the weakly allowed 2e ! $2a_1$ transition that redshifts from **11** (244 nm) to **17** (285) nm due to the energetic lowering of the $2a_1$ MO upon 1chlorination (Table 2.3). This bathochromic shift mirrors the one found in silicon nanocrystals as hydride surface groups are replaced with electronegative hydroxyl or halide groups.

It is even more interesting to consider that while the 1chlorination of sila-adamantane reproduces these experimental Si NC trends, 2-chlorination does not. Unlike **17**, **3** has strong dipole- allowed transitions in the λ_3 region. Its bathochromic λ_5 shift is far weaker than the one in **17**. We see no significant differences in the UV/Visible absorbance spectrum between **3** and **11**. If we are to consider silaadamantane as an atomically precise model system for Si NCs (Figure 2.7), the notion that 1-chlorination is optically active while 2-chlorination is relatively inert suggests that the dipole-forbidden transitions and red-shifted absorbance observed in Si NCs upon surface functionalization are also site-dependent effects. Though Si NCs are larger than silaadamantanes, they are also diamondoid structures that contain only two inequivalent surface sites: a tertiary site and a

secondary site that correspond respectively to the 1and 2-positions of sila-adamantane (Figure 2.7). One hypothesis that emerges from this comparison is that electronegative groups at tertiary surface sites have an outsized impact on Si NC photophysical properties relative to substituents at secondary surface sites. Such site-specific effects are difficult to study experimentally in silicon nanocrystals due to the structural imprecision in their methods of synthesis and surface functionalization. It is the atomically precise nature of sila-adamantane and the functionalization approaches described herein that allows us to probe the site specific origins of these related optical effects.

Conclusion

The present work expands the scope of what is known about sila-adamantane, from the mechanism of its isomerization synthesis to its regioselective derivatization and functionalization-dependent optical properties. Mechanistic insight supporting the 2-cation **5** as the final intermediate in the isomerization of **1** to **2** enabled us to develop synthetic approaches for installing halides at the 2-position via tetrahaloaluminate nucleophiles. Meanwhile, isomerizing **1** using a non-nucleophilic Lewis acid catalyst allowed gramscale access to **2**, enabling our functionalization studies of sila-adamantane at its 1-, 3-, 5-, and 7-positions with either the same or unique functional groups. Electronegative substituents at the 1-position of sila-adamantane lead to dipole-forbidden vertical transitions as an indirect consequence of lowering the energy of the adjacent $\sigma^*_{Si(1)\text{-}Si(2)}$ and $\sigma^*_{Si(2)\text{-}CH3}$ orbitals. These findings mirror the onset of redshifted, indirect band gaps when silicon nanocrystals are passivated with electronegative groups and offer atom-level rationales for Si NC behavior.

We anticipate that silicon diamondoids may be used to explore the atomistic origins of other properties of interest for nanocrystalline silicon, such as charge transport. Efforts are currently underway in our laboratory to use our siteselective functionalization strategies to probe single-molecule conductance in sila-adamantane-based molecular junctions. Based on the ordering of symmetric and antisymmetric frontier MOs in the present DFT study, we anticipate that electronic transport in sila-adamantane junctions will be sensitive to destructive σ-quantum interference effects. [29,30,74–76]

References

[1] Y. Heider, D. Scheschkewitz, *Chem. Rev.* **2021**, *121*, 9674–9718.

[2] A. Sekiguchi, T. Yatabe, S. Doi, H. Sakurai, *Phosphorus. Sulfur. Silicon Relat. Elem.* **1994**, *93*, 193–196.

[3] A. Sekiguchi, H. Sakurai, *Adv. Organomet. Chem.* **1995**, *37*, 1–38.

[4] E. Hengge, H. Stüger, in *The Chemistry of Organic Silicon Compounds, Vol. 2* (Eds.: Z. Rappoport, Y. Apeloig), Wiley, Chichester, UK, **1998**, pp. 2177–2216.

[5] Y. Heider, D. Scheschkewitz, *Dalt. Trans.* **2018**, *47*, 7104–7112.

[6] S. C. Sevov, J. M. Goicoechea, *Organometallics* **2006**, *25*, 5678–5692.

[7] D. Scheschkewitz, *Angew. Chem. Int. Ed.* **2005**, *44*, 2954–2956.

[8] J. M. Buriak, *Chem. Rev.* **2002**, *102*, 1271–1308.

[9] E. A. Marro, R. S. Klausen, *Chem. Mater.* **2019**, *31*, 2202–2211.

[10] J. Fischer, J. Baumgartner, C. Marschner, *Science* **2005**, *310*, 825.

[11] P. V. R. Schleyer, *J. Am. Chem. Soc.* **1957**, *79*, 3292–3292.

[12] G. Fritz, F. Diem, H. Köhler, D. Kummer, H. Scheer, *Angew. Chem. Int. Ed.* **1970**, *9*, 464–465.

[13] B. Köstler, M. Bolte, H. Lerner, M. Wagner, *Chem. Eur. J.* **2021**, *27*, 14401–14404.

[14] P. Von R. Schleyer, R. D. Nicholas, *J. Am. Chem. Soc.* **1961**, *83*, 182–187.

[15] S. Landa, S. Kriebel, E. Knobloch, *Chem. Listy* **1954**, *48*, 61–64.

[16] H. Stetter, M. Schwarz, A. Hirschhorn, *Chem. Ber.* **1959**, *92*, 1629–1635.

[17] H. Stetter, C. Wulff, *Chem. Ber.* **1960**, *93*, 1366–1371.

[18] L. Wanka, K. Iqbal, P. R. Schreiner, *Chem. Rev.* **2013**, *113*, 3516–3604.

[19] O. Green, T. Eilon, N. Hananya, S. Gutkin, C. R. Bauer, D. Shabat, *ACS Cent. Sci.* **2017**, *3*, 349–358.

[20] A. T. Aron, M. O. Loehr, J. Bogena, C. J. Chang, *J. Am. Chem. Soc.* **2016**, *138*, 14338–14346.

[21] L. Chen, P. Ren, B. P. Carrow, *J. Am. Chem. Soc.* **2016**, *138*, 6392–6395.

[22] K. A. Agnew-Francis, C. M. Williams, *Adv. Synth. Catal.* **2016**, *358*, 675–700.

[23] P. J. Krommenhoek, J. Wang, N. Hentz, A. C. Johnston-Peck, K. A. Kozek, G. Kalyuzhny, J. B. Tracy, *ACS Nano* **2012**, *6*, 4903–4911.

[24] B. Chen, M. Eddaoudi, T. M. Reineke, J. W. Kampf, M. O'Keeffe, O. M. Yaghi, *J. Am. Chem. Soc.* **2000**, *122*, 11559–11560.

[25] J. Tillmann, J. H. Wender, U. Bahr, M. Bolte, H.-W. Lerner, M. C. Holthausen, M. Wagner, *Angew. Chem. Int. Ed.* **2015**, *54*, 5429–5433.

[26] M. Bamberg, M. Bursch, A. Hansen, M. Brandl, G. Sentis, L. Kunze, M. Bolte, H.-W. Lerner, S. Grimme, M. Wagner, *J. Am. Chem. Soc.* **2021**, *143*, 10865–10871.

[27] T. Iwamoto, D. Tsushima, E. Kwon, S. Ishida, H. Isobe, *Angew. Chem. Int. Ed.* **2012**, *51*, 2340–2344.

[28] Y. Yokouchi, T. Iwamoto, *Organometallics* **2020**, *39*, 3301–3305.

[29] M. H. Garner, H. Li, Y. Chen, T. A. Su, Z. Shangguan, D. W. Paley, T. Liu, F. Ng, H. Li, S. Xiao, C. Nuckolls, L. Venkataraman, G. C. Solomon, *Nature* **2018**, *558*, 416–419.

[30] T. C. Siu, J. Y. Wong, M. O. Hight, T. A. Su, *Phys. Chem. Chem. Phys.* **2021**, *23*, 9643–9659.

[31] M. Zirngast, J. Baumgartner, C. Marschner, *Organometallics* **2008**, *27*, 6472–6478.

[32] A. Wallner, R. Emanuelsson, J. Baumgartner, C. Marschner, H. Ottosson, *Organometallics* **2013**, *32*, 396–405.

[33] Y. Heider, N. E. Poitiers, P. Willmes, K. I. Leszczyńska, V. Huch, D. Scheschkewitz, *Chem. Sci.* **2019**, *10*, 4523–4530.

[34] Y. Heider, P. Willmes, V. Huch, M. Zimmer, D. Scheschkewitz, *J. Am. Chem. Soc.* **2019**, *141*, 19498–19504.

[35] P. Willmes, K. Leszczyńska, Y. Heider, K. Abersfelder, M. Zimmer, V. Huch, D. Scheschkewitz, *Angew. Chem. Int. Ed.* **2016**, *55*, 2907–2910.

[36] L. J. Schiegerl, A. J. Karttunen, W. Klein, T. F. Fässler, *Chem. Sci.* **2019**, *28*, 9130–9139.

[37] S. Joseph, M. Hamberger, F. Mutzbauer, O. Härtl, M. Meier, N. Korber, *Angew. Chem. Int. Ed.* **2009**, *48*, 8770–8772.

[38] M. Waibel, F. Kraus, S. Scharfe, B. Wahl, T. F. Fässler, *Angew. Chem. Int. Ed.* **2010**, *49*, 6611–6615.

[39] F. S. Geitner, T. F. Fässler, *Chem. Commun.* **2017**, *53*, 12974–12977.

[40] H. Gilman, C. L. Smith, *J. Organomet. Chem.* **1967**, *8*, 245–253.

[41] S. M. Whittaker, M.-C. Brun, F. Cervantes-Lee, K. H. Pannell, *J. Organomet. Chem.* **1995**, *499*, 247–252.

[42] C. Kayser, G. Kickelbick, C. Marschner, *Angew. Chem. Int. Ed.* **2002**, *41*, 989–992.

[43] R. Fischer, T. Konopa, S. Ully, J. Baumgartner, C. Marschner, *J. Organomet. Chem.* **2003**, *685*, 79–92.

[44] L. Albers, J. Baumgartner, C. Marschner, T. Müller, *Chem. Eur. J.* **2016**, *22*, 7970–7977.

[45] Deposition Numbers 2143761, 2143763, 2143760, and 2143762 contain the supplementary crystallographic data for this paper. These data are provided free of charge by the joint Cambridge Crystallographic Data Centre and Fachinformationszentrum Karlsruhe Access Structures service.

[46] M. Ishikawa, J. Iyoda, H. Ikeda, K. Kotake, T. Hashimoto, M. Kumada, *J. Am. Chem. Soc.* **1981**, *103*, 4845–4850.

[47] S. Sharma, N. Caballero, H. Li, K. H. Pannell, *Organometallics* **1999**, *18*, 2855–2860.

[48] M. Ishikawa, M. Watanabe, J. Iyoda, H. Ikeda, M. Kumada, *Organometallics* **1982**, *1*, 317–322.

[49] T. A. Blinka, R. West, *Organometallics* **1986**, *5*, 128–133.

[50] H. Wagner, A. Wallner, J. Fischer, M. Flock, J. Baumgartner, C. Marschner, *Organometallics* **2007**, *26*, 6704–6717.

[51] H. Wagner, J. Baumgartner, C. Marschner, P. Poelt, *Organometallics* **2011**, *30*, 3939–3954.

[52] H. Wagner, J. Baumgartner, T. Müller, C. Marschner, *J. Am. Chem. Soc.* **2009**, *131*, 5022–5023.

[53] L. Albers, S. Rathjen, J. Baumgartner, C. Marschner, T. Müller, *J. Am. Chem. Soc.* **2016**, *138*, 6886–6892.

[54] L. Albers, M. A. Meshgi, J. Baumgartner, C. Marschner, T. Müller, *Organometallics* **2015**, *34*, 3756–3763.

[55] H. F. T. Klare, L. Albers, L. Süsse, S. Keess, T. Müller, M. Oestreich, *Chem. Rev.* **2021**, *121*, 5889–5985.

[56] E. M. Engler, M. Farcasiu, A. Sevin, J. M. Cense, P. V. R. Schleyer, *J. Am. Chem. Soc.* **1973**, *95*, 5769–5771.

[57] M. Ishikawa, M. Kumada, H. Sakurai, *J. Organomet. Chem.* **1970**, *23*, 63–69.
[58] C. Marschner, *Eur. J. Inorg. Chem.* **1998**, *1998*, 221–226.

[59] C. Marschner, in *Organosilicon Compounds* (Ed: V. Ya. Lee), Elsevier, **2017**, pp. 295–360.

[60] J. Bedard, N. J. Roberts, M. Shayan, K. L. Bamford, U. Werner-Zwanziger, K. M. Marczenko, S. S. Chitnis, *Angew. Chem. Int. Ed.* **2022**, *4*, DOI 10.1002/anie.202204851.

[61] V. Humblet, P. Misra, K. R. Bhushan, K. Nasr, Y. Sen Ko, T. Tsukamoto, N. Pannier, J. V. Frangioni, W. Maison, *J. Med. Chem.* **2009**, *52*, 544–550.

[62] G. R. Newkome, A. Nayak, R. K. Behera, C. N. Moorefield, G. R. Baker, *J. Org. Chem.* **1992**, *57*, 358–362.

[63] W. L. Wilson, P. F. Szajowski, L. E. Brus, *Science* **1993**, *262*, 1242–1244.

[64] M. V. Wolkin, J. Jorne, P. M. Fauchet, G. Allan, C. Delerue, *Phys. Rev. Lett.* **1999**, *82*, 197–200.

[65] Q. Li, Y. He, J. Chang, L. Wang, H. Chen, Y. W. Tan, H. Wang, Z. Shao, *J. Am. Chem. Soc.* **2013**, *135*, 14924–14927.

[66] R. K. Baldwin, K. A. Pettigrew, E. Ratai, M. P. Augustine, S. M. Kauzlarich, *Chem. Commun.* **2002**, *17*, 1822–1823.

[67] L. M. Wheeler, N. R. Neale, T. Chen, U. R. Kortshagen, *Nat. Commun.* **2013**, *4*, 2197.

[68] M. Dasog, J. Kehrle, B. Rieger, J. G. C. Veinot, *Angew. Chem. Int. Ed.* **2016**, *55*, 2322–2339.

[69] I. Vasiliev, J. R. Chelikowsky, R. M. Martin, *Phys. Rev. B* **2002**, *65*, 121302.

[70] Z. Zhou, L. Brus, R. Friesner, *Nano Lett.* **2003**, *3*, 163–167.

[71] Z. Zhou, R. A. Friesner, L. Brus, *J. Am. Chem. Soc.* **2003**, *125*, 15599–15607.

[72] A. Martínez, J. C. Alonso, L. E. Sansores, R. Salcedo, *J. Phys. Chem. C* **2010**, *114*, 12427–12431.

[73] E. Ramos, B. M. Monroy, J. C. Alonso, L. E. Sansores, R. Salcedo, A. Martínez, *J. Phys. Chem. C* **2012**, *116*, 3988–3994.

[74] M. H. Garner, H. Li, M. Neupane, Q. Zou, T. Liu, T. A. Su, Z. Shangguan, D. W. Paley, F. Ng, S. Xiao, C. Nuckolls, L. Venkataraman, G. C. Solomon, *J. Am. Chem. Soc.* **2019**, *141*, 15471–15476.

[75] S. Gunasekaran, J. E. Greenwald, L. Venkataraman, *Nano Lett.* **2020**, *20*, 2843–2848.

[76] F. Evers, R. Korytár, S. Tewari, J. M. Van Ruitenbeek, *Rev. Mod. Phys.* **2020**, *92*, 35001.

Experimental

Supporting Figures and Tables from Main Text

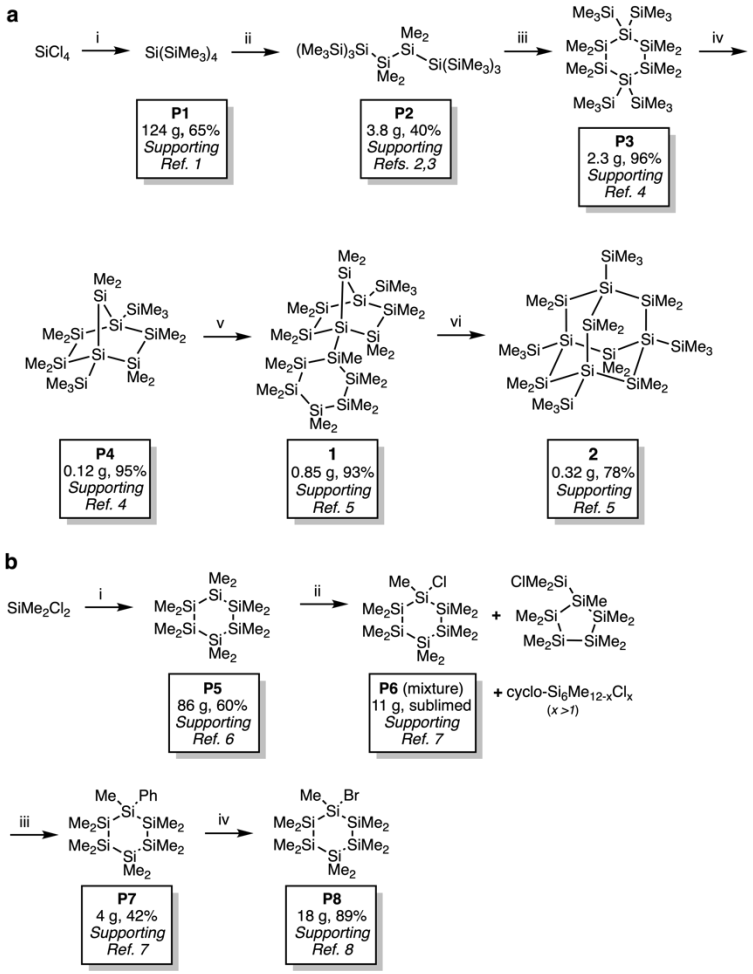


Figure 2.8 (a) Marschner's reported route to **1** and **2**, with yields and scales reported from References [1–5]. (i) chlorotrimethylsilane, lithium, THF. (ii) methyllithium, toluene; 1,2-dichlorotetramethyldisilane. (iii) potassium *tert*-butoxide, 18-crown-6, toluene; 1,2-dibromotetramethyldisilane. (iv) potassium *tert*-butoxide, 18-crown-6, toluene; dichlorodimethylsilane. (v) potassium *tert*-butoxide, 18-crown-6, benzene; **P8**. (vi) aluminum chloride, cyclohexane; methyllithium. (b) Reported route to **P8**, with yields and scales reported from Supporting References [6–8]. (i) lithium, THF. (ii) aluminum chloride, hydrogen chloride, cyclohexane. (iii) phenylmagnesium bromide, THF. (iv) hydrogen bromide.

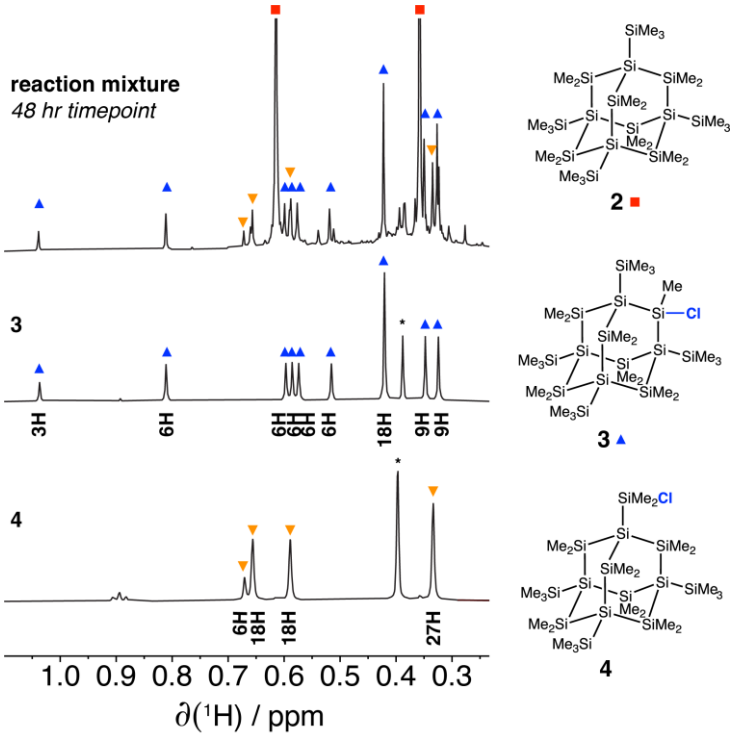


Figure 2.9 Overlay of ^{1}H NMR spectra comparing reaction mixture at 48-hour timepoint in isomerization reaction of **1** with $AlCl_3$ (1.7 equiv.) against isolated **3** and **4**. The reaction mixture NMR spectrum (top) is the same as the one shown in Fig. 2a of the main text, but with peaks shown at higher intensity.

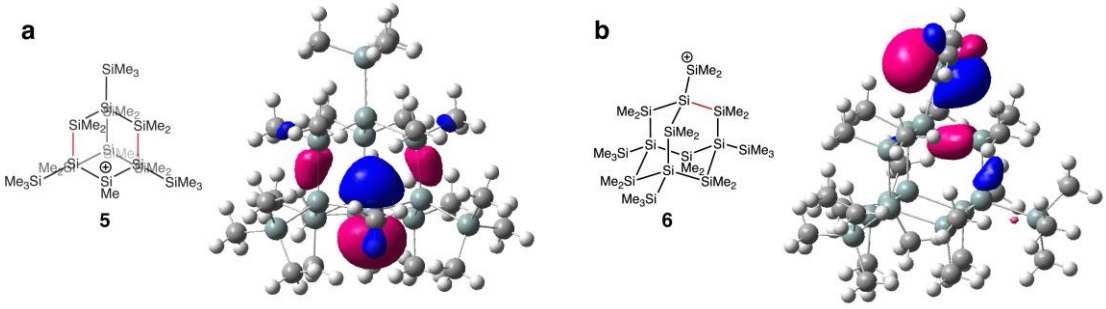


Figure 2.10 LUMO isosurfaces (isovalue = 0.035) of (**a**) 2-cation **5** and (**b**) exo-cation **6**, with geometries optimized at the M06-2X/6-311+(d,p) level without symmetry constraints. Bonds highlighted in red indicate bonds that interact with silylium 3p orbital in the LUMO.

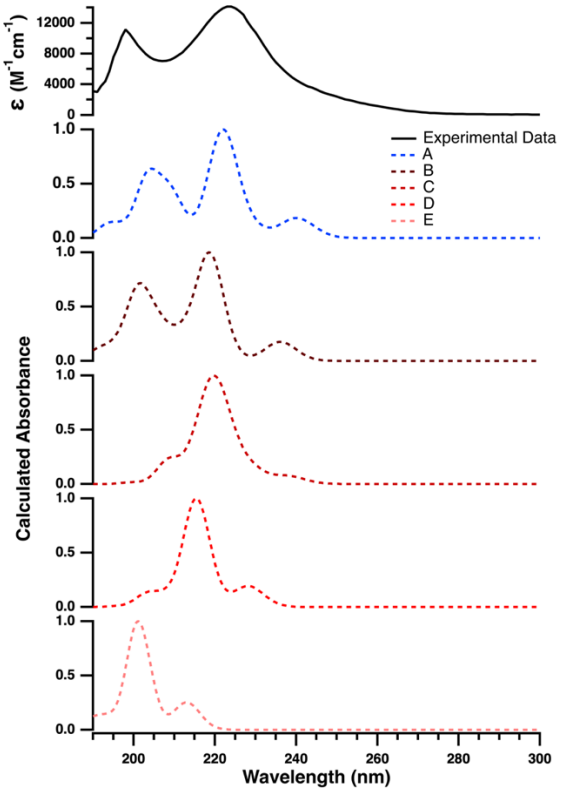


Figure 2.11 Experimental UV-vis absorbance spectrum of SiAd **2** measured in pentane plotted against computational spectra generated from gas-phase TD-DFT calculations at the following levels of theory: (A) PBE0/TZVP//BP86/TZVP, (B) PBE0/TZVP//M062X/6-311G(d,p), (C) PBE0/6-311+G(d,p)//M062X/6-311G(d,p), (D) M062X/6-311+G(d,p)//M062X/6-311G(d,p), (E) CAM-B3LYP/6-311+G(d,p)//M062X/6-311G(d,p). DFT-generated spectra have their extinction coefficients normalized. Calculated spectra are plotted at 0.10 eV half-width at half height. More details about the suitability of this functional and basis set can be found in the Computational Chemistry section of the Supporting Information.

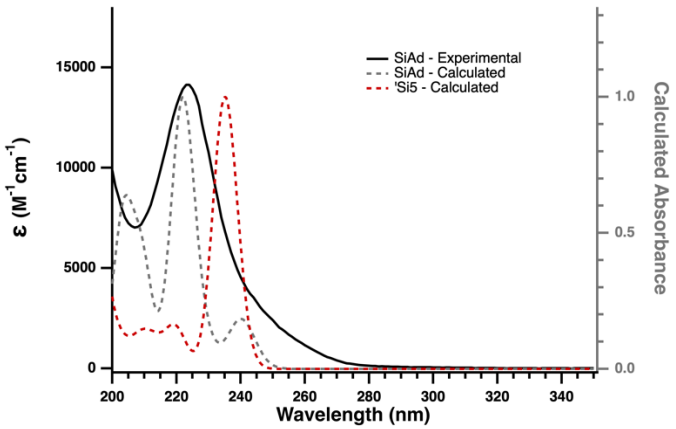


Figure 2.12 Experimental and calculated absorption spectra of SiAd **2** and the calculated spectrum of **Si5** that represents an excised pentasilane fragment from **2** that is then passivated with hydride groups. The calculated spectrum of **Si5** tracks reasonably well with the experimental spectrum for the methylated analog $(SiMe_3)_3SiSiMe_2Si(SiMe_3)_3$ reported by Marschner and coworkers at ~245 nm.[9]

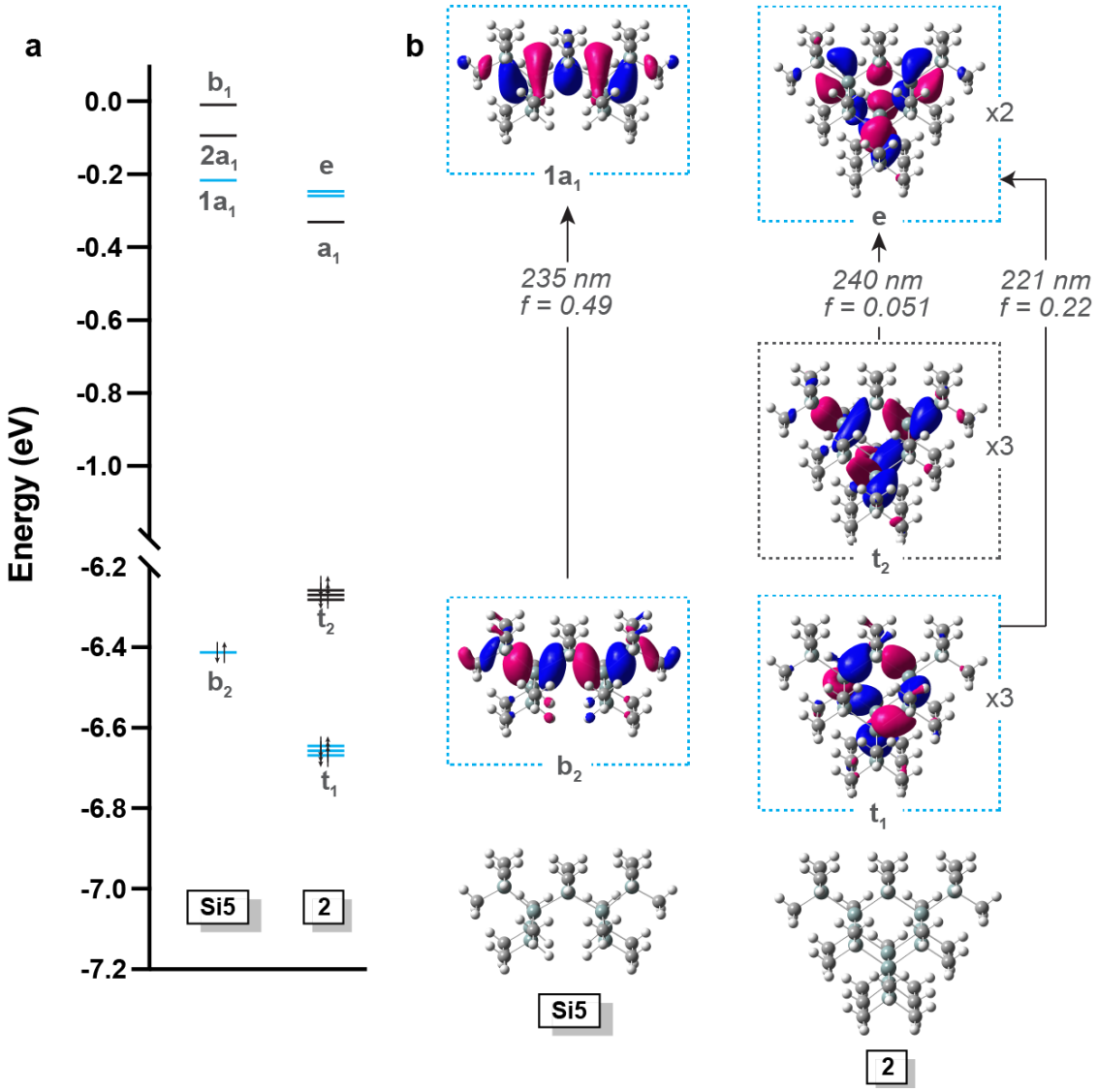
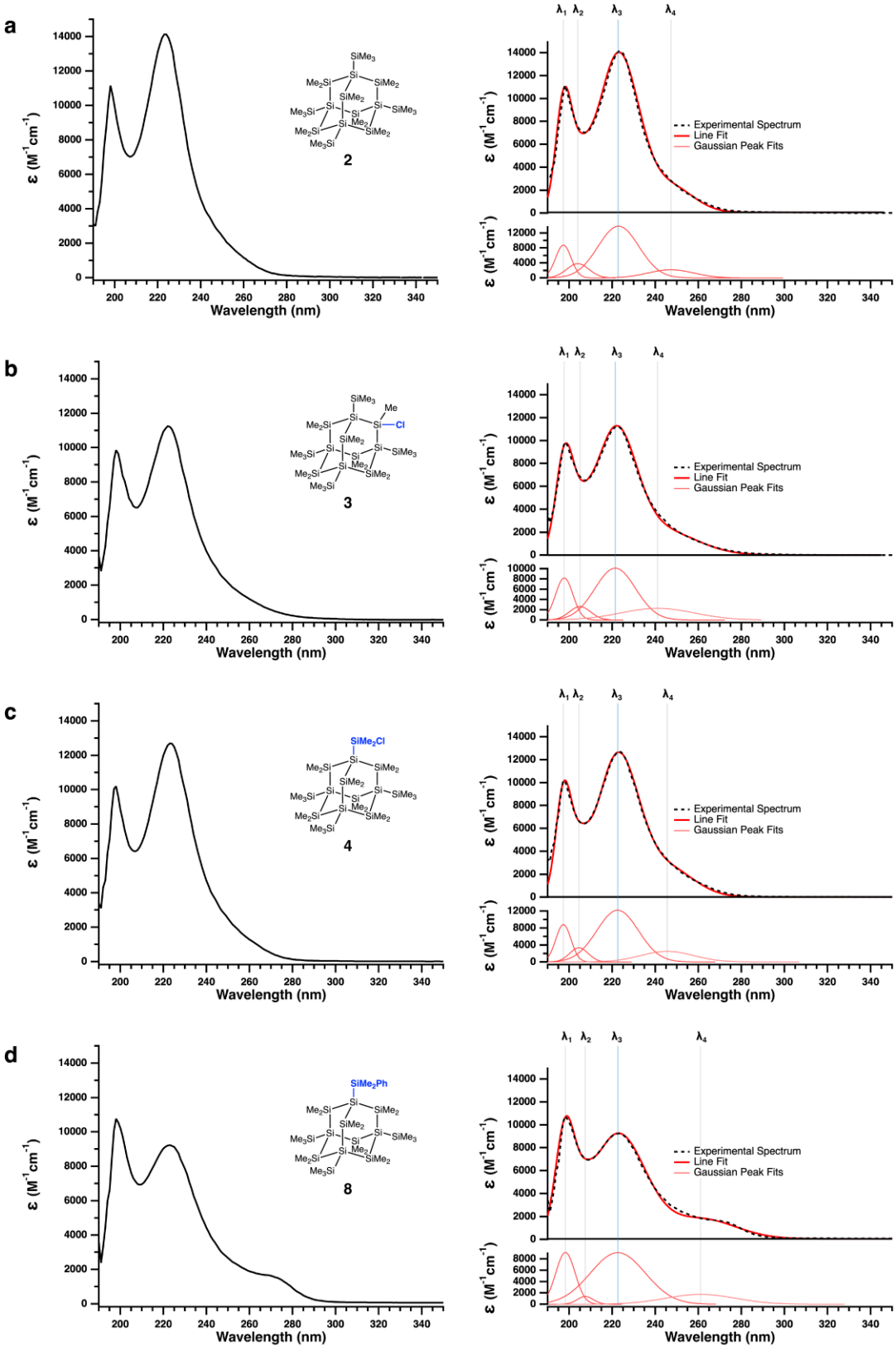
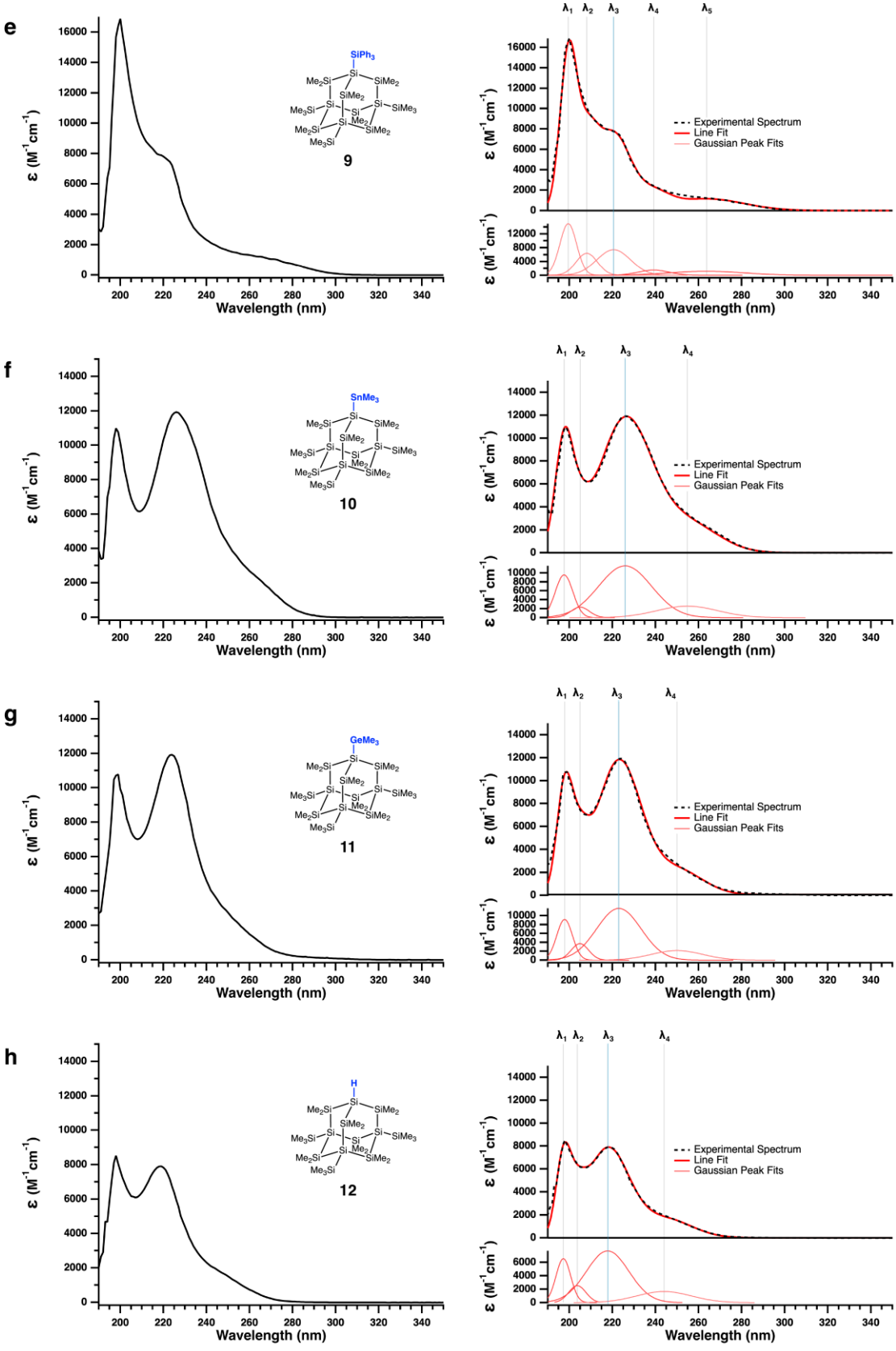
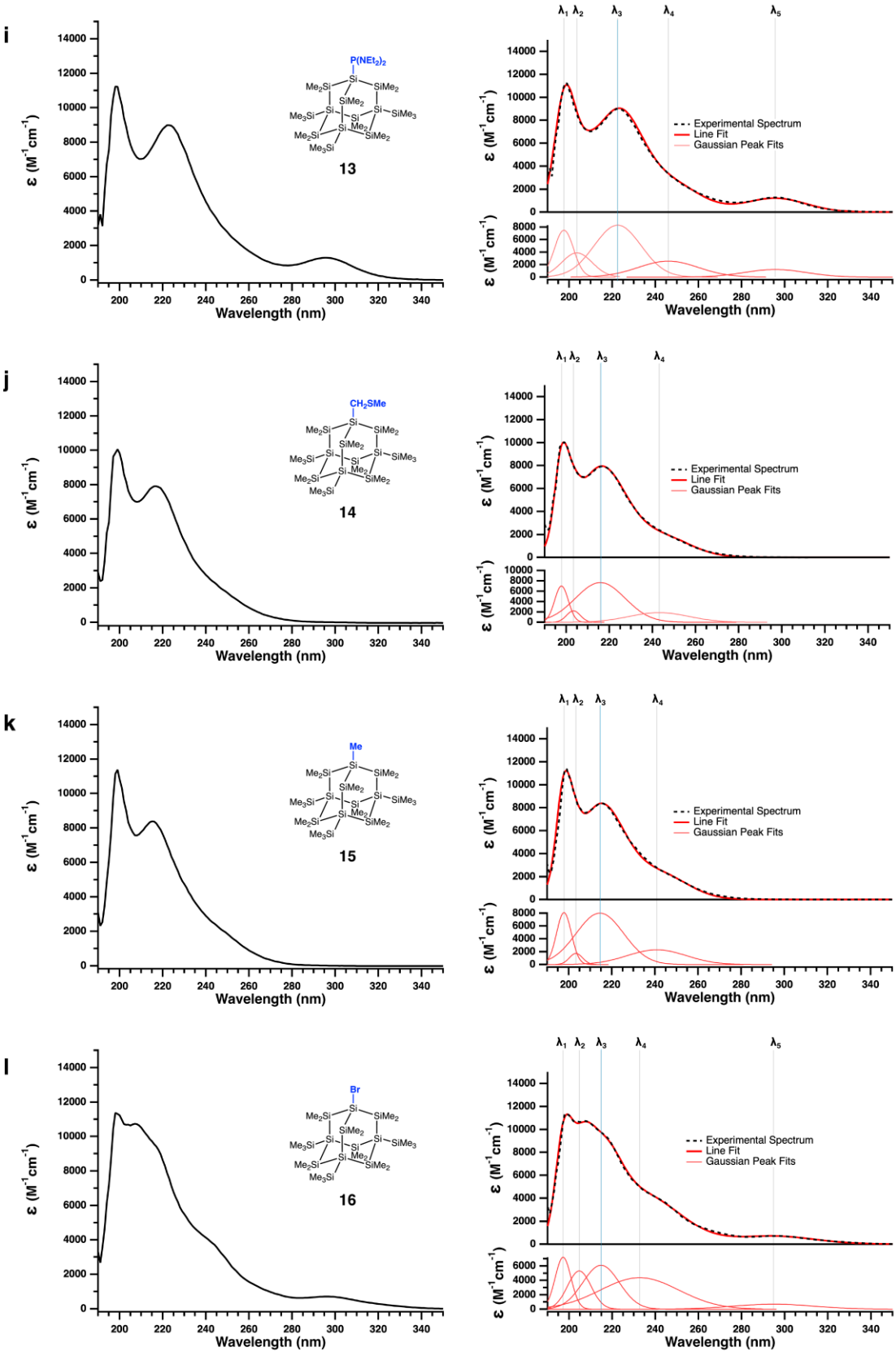


Figure 2.13 (a) Orbital energy diagram for the C_{2v}-symmetric **Si5** and T_d-symmetric **2**. (b) Orbital isosurfaces (isovalue=0.030) for molecular orbitals relevant for 235 nm transition for **Si5** and 221 and 240 nm transitions for **2**, showing oscillator strength and transition energies from TD-DFT calculations at the PBE0/TZVP level. More details can be found in the Computational Chemistry section of the Supporting Information.


a
b
c
d
ε (M⁻¹cm⁻¹)
Wavelength (nm)
λ1 λ2 λ3 λ4
Experimental Spectrum
Line Fit
Gaussian Peak Fits
2
3
4
8
SiMe3
SiMe2
Me3Si
Me2Si
Si
Me
Cl
SiMe2Cl
SiMe2Ph


e
f
g
h
ε (M⁻¹cm⁻¹)
Wavelength (nm)
λ1 λ2 λ3 λ4 λ5
λ1 λ2 λ3 λ4
Experimental Spectrum
Line Fit
Gaussian Peak Fits
SiPh3
SnMe3
GeMe3
H
Me2Si
SiMe2
Me3Si
9
10
11
12


i
P(NEt2)2
13
j
CH2SMe
14
k
Me
15
l
Br
16
ε (M-1cm-1)
Wavelength (nm)
λ1 λ2 λ3 λ4 λ5
Experimental Spectrum
Line Fit
Gaussian Peak Fits

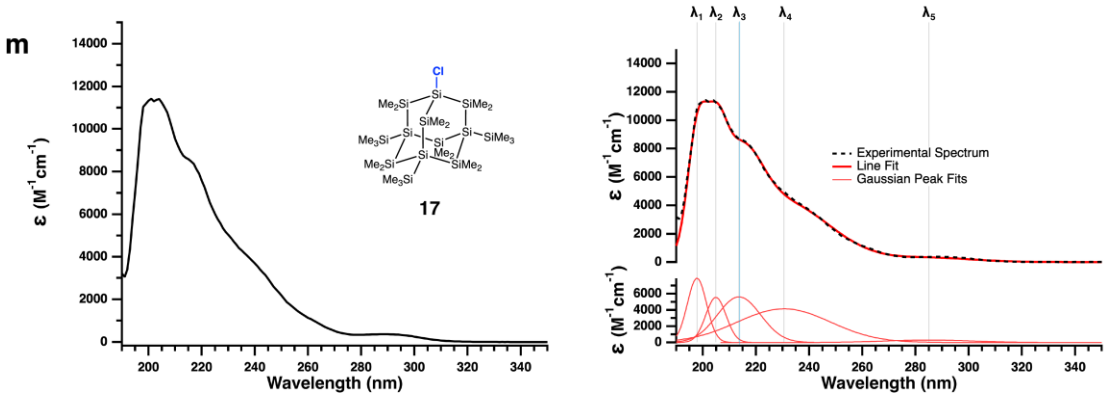
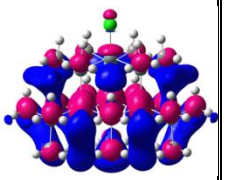
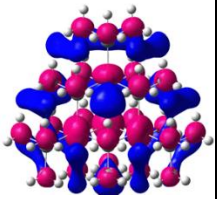
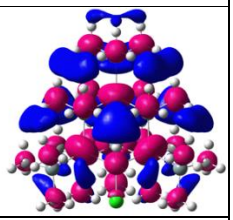
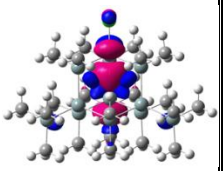
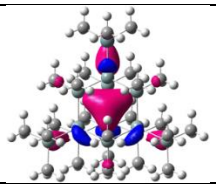
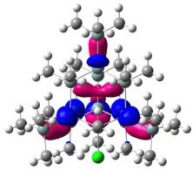
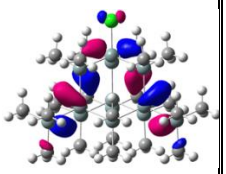
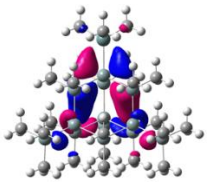
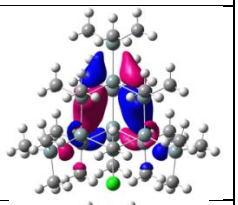
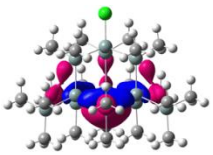
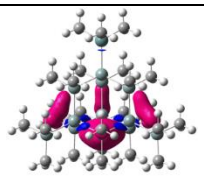
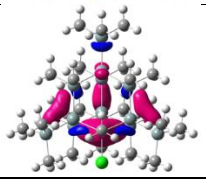
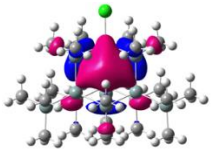
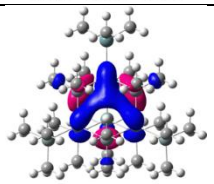
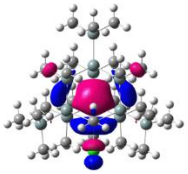
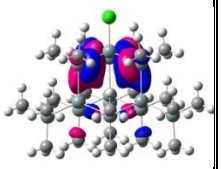
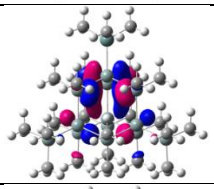
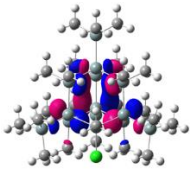
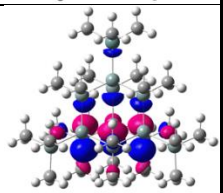
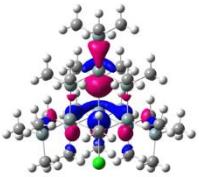
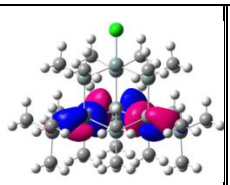
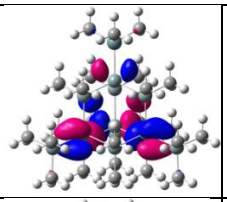
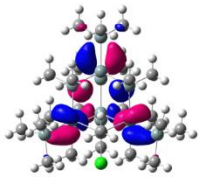
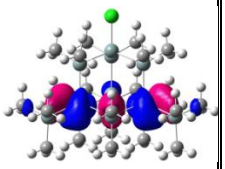
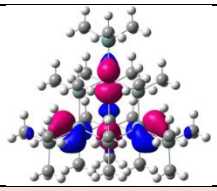
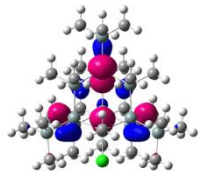
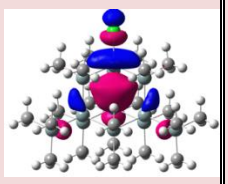
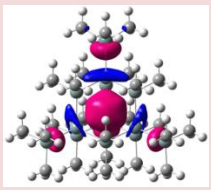
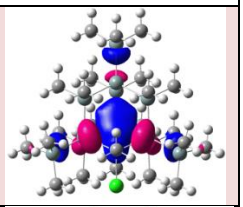
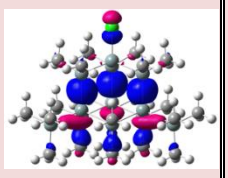
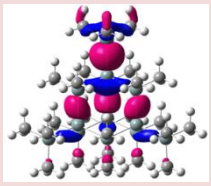
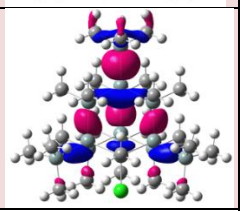
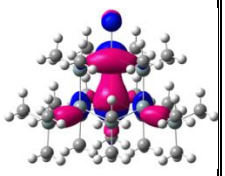
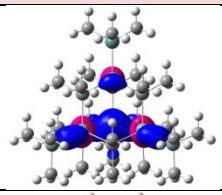
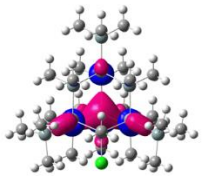
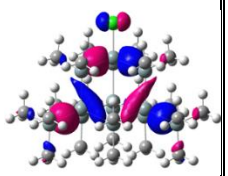
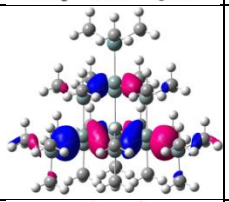
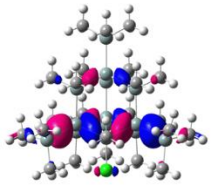
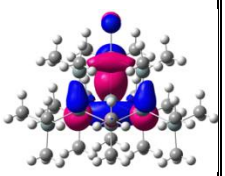
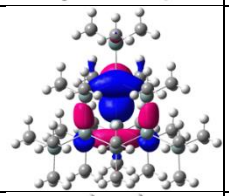
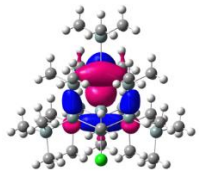
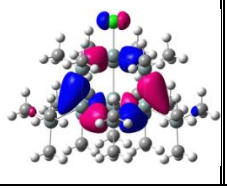
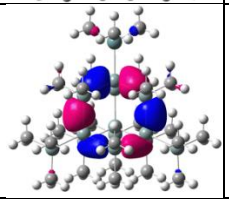
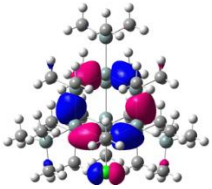
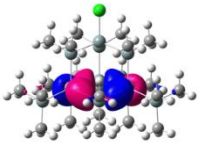
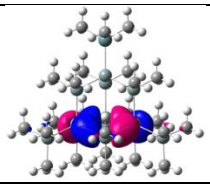
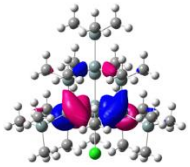

m
ε (M-1cm-1)
Wavelength (nm)
Cl
Me2Si
SiMe2
Me3Si
SiMe3
17
λ1 λ2 λ3 λ4 λ5
Experimental Spectrum
Line Fit
Gaussian Peak Fits

Figure 2.14 (Left) Experimental UV-vis spectra for the functionalized sila-adamantanes, with extinction coefficient plotted against absorption wavelength from 10 μM solutions in pentane. (Right) Experimental spectrum (black dotted line) overlaid against line fit (red solid line) obtained from the 'Multipeak Fit' module of Igor Pro 8, in which Gaussian-shaped peaks were used to reconstruct the experimental spectrum. TD-DFT calculations (see Computational Chemistry section of Supporting Information) support the notion that the UV spectrum is comprised of multiple transitions and validate the multipeak model. The Gaussian peak most relevant to the experimental λ_3 peak is indicated with the blue solid line; its extinction coefficient is used for $\varepsilon_{3,\,\text{fitted}}$ in **Table 1** of the main text.

Table 2.2 Molecular orbital correlations between **17, 11,** and **3** calculated at the PBE0/TZVP//BP86/TZVP level of theory.

*Molecular orbitals for **17***			*Molecular orbitals for **11***			*Molecular orbitals for **3***		
MO[a]	**Sym.[b]**	**Isosurface[c]**	**MO[a]**	**Sym.[b]**	**Isosurface[c]**	**MO[a]**	**Sym.[b]**	**Isosurface[c]**
204 (L+9)	$5a_1$		225 (L+9)	$5a_1$		220 (L+9)	10a’	
203 (L+8)	5e		224 (L+8)	5e		217 (L+8)	9a’	
202 (L+7)	5e		223 (L+7)	5e		218 (L+7)	6a’’	
201 (L+6)	$4a_1$		222 (L+6)	$4a_1$		219 (L+8)	8a’	
199 (L+4)	4e		221 (L+5)	4e		211 (L)	4a’	
200 (L+5)	4e		220 (L+4)	4e		215 (L+4)	5a’’	
198 (L+3)	$3a_1$		219 (L+3)	$3a_1$		216 (L+5)	7a’	

197 (L+2)	3e		218 (L+2)	3e		214 (L+3)	4a''	
196 (L+1)	3e		217 (L+1)	3e		213 (L+2)	6a'	
195 (L)	$2a_1$		216 (L)	$2a_1$		212 (L+1)	5a'	
189 (H-5)	$1a_1$		215 (H)	$1a_1$		208 (H-2)	3a'	
193 (H-1)	2e		214 (H-1)	2e		210 (H)	2a'	
194 (H)	2e		213 (H-2)	2e		209 (H-1)	3a''	
191 (H-3)	1e		212 (H-3)	1e		206 (H-4)	1a'	
192 (H-2)	1e		211 (H-4)	1e		207 (H-3)	2a''	

190 (H-4)	$1a_2$		210 (H-5)	$1a_2$		205 (H-5)	1a''	

Key. [a]Orbital numbers correspond to Gaussian16 output described in Computational Chemistry section of Supporting Information. “H” and “L” refer to HOMO and LUMO, respectively. [b]Mulliken label ordering starts from the HOMO-5 orbitals. [c]All orbitals plotted at isovalue=0.035 except the L+9 orbitals, which are plotted at isovalue=0.015.

Table 2.3 Calculated vertical transitions for **11** and **17** of relevance to experimental absorption properties, ordered from highest to lowest energy for **11**. Gray shading provides a visual guide for transitions with f < 0.05. Blue shading provides a visual guide for **17** vertical transitions that are blue-shifted relative to their matching transition in **11**. Besides the weakly allowed HOMO to LUMO transition for **17**, only excited states with f > 0.05 and λ > 200 nm for either molecule **11** or **17** are shown in this comparison.

Vertical Transitions for 11 (1-$GeMe_3$ substituted)						Vertical Transitions for 17 (1-Cl substituted)					
ES[a]	Transition[b]	Cont. (%)[c]	λ (nm)[d]	Energy (eV)[d]	*f*[e]	ES	Transition	Cont. (%)	λ (nm)	Energy (eV)	*f*
58, 59	**2e** (H-2, H-1) → **5a$_1$** (L+9)	89%	204.0	6.08	0.19	51, 52	**2e** (H-1, H) → **5a$_1$** (L+9)	73%	204.1	6.08	0.29
57	**1a$_1$** (H) → **5a$_1$** (L+9)	90%	204.6	6.06	0.20	75	**1a$_1$** (H-5) → **5a$_1$** (L+9)	3%	194.4	6.38	0.03
56	**1e** (H-4, H-3) → **5e** (L+7, L+8)	80%	209.0	5.93	0.14	69	**1e** (H-3, H-2) → **5e** (L+7, L+8)	78%	196.7	6.30	0.0000
54, 55	**1a$_2$** (H-5) → **5e** (L+7, L+8)	58%	209.1	5.93	0.080	76, 77	**1a$_2$** (H-4) → **5e** (L+7, L+8)	37%	193.4	6.41	0.080
45, 46	**1e** (H-4, H-3) → **4a$_1$** (L+6)	34%	215.6	5.75	0.009	34, 35	**1e** (H-2, H-3) → **4a$_1$** (L+6)	40%	218.6	5.67	0.056
36, 37	**1e** (H-4, H-3) → **3e** (L+1, L+2)	34%	220.7	5.62	0.25	30, 31	**1e** (H-3, H-2) → **3e** (L+1, L+2)	17%	223.5	5.55	0.042
	1a$_2$ (H-5) → **3e** (L+1, L+2)	27%					**1a$_2$** (H-4) → **3e** (L+1, L+2)	54%			
35	**1e** (H-4, H-3) → **2e** (L+1, L+2)	68%	221.5	5.60	0.15	23, 24	**1e** (H-3, H-2) → **3e** (L+1, L+2)	76%	226.7	5.47	0.030
34	**2e** (H-2, H-1) → **5e** (L+7, L+8)	78%	223.0	5.56	0.11	46	**2e** (H-1, H) → **5e** (L+7, L+8)	70%	209.2	5.93	0.030
28	**1a$_1$** (H) → **3a$_1$** (L+3)	58%	225.5	5.50	0.15	50	**1a$_1$** (H-5) → **3a$_1$** (L+3)	34%	207.1	5.99	0.12
10, 11	**1a$_1$** (H) → **4e** (L+4, L+5)	65%	237.0	5.23	0.0004	48, 49	**1a$_1$** (H-5) → **4e** (L+4, L+5)	37%	207.7	5.97	0.20
4, 5	**2e** (H-2, H-1) → **2a$_1$** (L)	78%	244.4	5.07	0.030	1, 2	**2e** (H-1, H) → **2a$_1$** (L)	88%	284.5	4.36	0.026

Key.[a]Excited state from TD-DFT (PBE0/TZVP//BP86/TZVP) calculation with N=80 states. A full list of the 80 excited states is provided in the Computational Chemistry section of the Supporting Information. [b]Primary vertical transition for each excited state, with Mulliken label ordering starting from the HOMO-5 orbitals. "H" refers to HOMO, "L" refers to LUMO. [c]Percent contribution of primary transition for each excited state. [d]Calculated energy for each transition. [e]Oscillator strength for each excited state.

General Synthesis and Characterization Information

All reactions were performed in oven-dried or flame-dried glassware, unless otherwise stated. Reaction vessels were fitted with Teflon magnetic stir bars and rubber septa and reactions were conducted under nitrogen or argon on a Schlenk manifold or in a nitrogen-filled glovebox. Reaction solvents were purged with argon and dried over activated alumina columns through a JC Meyer solvent purification system, then stored over 4 Å molecular sieves. Automated flash chromatography was performed using a Yamazen Smart Flash AKROS system with Yamazen Premium silica columns.

Materials. All chemicals were purchased from commercial sources and used without further purification unless otherwise stated. Trityl tetrakis(pentafluorophenyl)borate was purchased from Aaronchem or Strem, aluminum chloride (99.999%) was purchased from Sigma Aldrich.

Instrumentation. ^{1}H NMR, ^{13}C NMR and ^{29}Si NMR were recorded on Bruker NEO 400 (400 MHz) or Bruker AV 600 (600 MHz) spectrometers. Chemical shifts for ^{1}H NMR are reported in parts per million downfield from tetramethylsilane and are referenced to residual protium in NMR solvents ($CHCl_3$, δ 7.26; C_6H_6, δ 7.16). Chemical shifts for ^{13}C NMR are reported in parts per million downfield from tetramethylsilane and are referenced to the center peaks of residual solvents ($CHCl_3$, δ 77.16; C_6H_6, δ128.06). Chemical shifts for silicon are reported in parts per million downfield from tetramethylsilane and are referenced to a tetramethylsilane internal standard. To compensate for the low isotopic abundance of ^{29}Si, the DEPT pulse sequence was employed for the amplification of the signal. Chemical shifts for phosphorous and tin are reported downfield from 85% H_3PO_4

and tetramethylstannane external standards, respectively. Data are represented as follows: chemical shift, multiplicity (s = singlet, d = doublet, t = triplet, m = multiplet, br = broad), coupling constants in Hertz, and integration. High-resolution mass spectrometry (HRMS) was recorded on either an Agilent 7200 GCMS-QTOF in methane chemical ionization mode, or a Waters XEVO G2XS QToF mass spectrometer equipped with a UPC2 SFC inlet, electrospray ionization (ESI) probe, atmospheric pressure chemical ionization (APCI) probe, and atmospheric solids analysis probe (ASAP+). UV-visible absorption spectra taken with an Agilent Cary 60 UV-vis Spectrophotometer in 1 cm cuvettes at concentrations of 10 μM in pentane.

Reaction monitoring via ^{1}H NMR spectroscopy for Figure 1.3c, 1.3d

*Experiment shown in **Figure 1.3c** - Isomerization with $AlCl_3$ (1.7 equiv.)*

An oven-dried 15 mL pressure tube was equipped with a stir bar and charged with **1** (0.11 g, 0.14 mmol, 1.0 equiv.), $AlCl_3$ (0.031 g, 0.24 mmol, 1.7 equiv.), and tetradecane (0.072 mL, 0.28 mmol, 2.0 equiv.) as internal standard. The mixture was further diluted with 0.46 mL benzene and stirred at room temperature. Reaction aliquots were taken at the indicated timepoints in **Figure 2c** in the main text by dipping an oven-dried glass pipette tip into the heterogeneous reaction mixture stirring in the glovebox, rinsing the pipette tip with anhydrous benzene-*d6,* then filtering the solution with a 0.22 μm syringe filter into an NMR tube.

Percent yields at each timepoint were determined using the 'Line Fitting' function in MestReNova Version 14.1. The following peaks were used to determine concentration relative to tetradecane (∂ 0.92, t, 6H): **1** (∂ 0.63 ppm, 6H), **2** (∂ 0.61, 36H; 0.35, 36H), **3** (∂ 1.03, 3H; ∂ 0.59, 6H; ∂ 0.32, 9H), **4** (∂ 0.65, 18H; ∂ 0.33, 27H). Concentration values were determined each individual peak, averaged to account for differences in relaxation time, then plotted using Graphpad Prism 9.1.

*Experiment shown in **Fig. 1.3d** - Isomerization with $AlCl_3$ (1.7 equiv., $SiMe_3Cl$ (1.0 equiv.)*

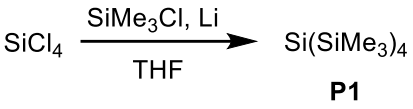
An oven-dried 15 mL pressure tube was equipped with a stir bar and charged with **1** (0.20 g, 0.27 mmol, 1.0 equiv.), $AlCl_3$ (0.061 g, 0.46 mmol, 1.7 equiv.), trimethylsilyl chloride (1.0 M solution in benzene, 0.27 mL, 0.27 mmol, 1.0 equiv.), and cyclohexane (0.086 mL, 0.60 mmol, 2.3 equiv.) as internal standard. The mixture was further diluted with 0.67 mL benzene and stirred at room temperature. Reaction aliquots were taken at the indicated timepoints in **Figure 2d** in the main text by dipping an oven-dried glass pipette tip into the heterogeneous reaction mixture stirring in the glovebox, rinsing the pipette tip with anhydrous benzene-*d6,* then filtering the solution with a 0.22 μm syringe filter into an NMR tube.

Percent yields at each timepoint were determined using the 'Line Fitting' function in MestReNova Version 14.1. The following peaks were used to determine concentration relative to cyclohexane (∂ 1.41, 12H): **1** (∂ 0.63 ppm, 6H), **2** (∂ 0.61, 36H; 0.35, 36H), **3** (∂ 1.03, 3H; ∂ 0.59, 6H; ∂ 0.32, 9H), **4** (∂ 0.65, 18H; ∂ 0.33, 27H). Concentration values were

determined from each individual peak, averaged to account for differences in relaxation time, then plotted using Graphpad Prism 9.1.

Synthetic Procedures and Characterization of Compounds

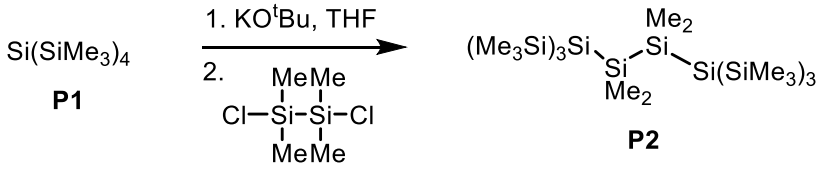
Preparation of **P1**



The synthesis for this compound was adapted from known procedures.[1] An oven-dried 1000 mL three-necked flask equipped with a 250 mL addition funnel, reflux condenser, septa, and stir bar was connected to a Schlenk manifold. The dropping funnel was charged with a mixture of chlorotrimethylsilane (177.94 g, 1.64 mol, 4.2 equiv.) and tetrachlorosilane (66.20 g, 0.39 mol, 1.0 equiv.). The flask was charged with a mixture of lithium granules (27.06 g, 3.90 mol, 10 equiv.) and THF (560 mL). The reaction flask was cooled with an ice-water bath and the reaction was stirred vigorously as the chlorotrimethylsilane-tetrachlorosilane mixture were added dropwise over 6 hours. During this period, the suspension adopted a golden-brown color. After addition was complete, the mixture was allowed to stir overnight at room temperature before being refluxed for 2 hours. The mixture was filtered through Celite and quenched with a 1 M hydrochloric acid solution (400 mL). The organic layer was separated from the aqueous layer, which was subsequently extracted with diethyl ether (3 x 500 mL). The combined organic layers were dried over magnesium sulfate and concentrated *in vacuo* to yield the crude product as a

yellow solid. The crude product was further purified by recrystallization in ethanol, yielding product **P1** as a white crystalline solid (93.18 g, 74% yield). ^{1}H NMR (400 MHz, $CDCl_3$) δ (ppm): 0.20 (s, 36 H). ^{13}C NMR (151 MHz, $CDCl_3$) δ 2.84. ^{29}Si NMR (119 MHz, $CDCl_3$) δ -9.86, -135.60.

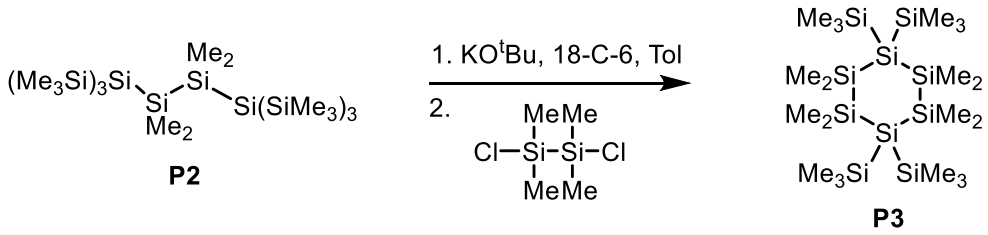
Preparation of **P2**



The synthesis for this compound was adapted from known procedures.[1] The synthesis for this compound was adapted from known procedures.[4] An oven-dried 2000 mL round-bottom flask was equipped with a stir bar and septum, then connected to a Schlenk manifold. **P1** (37.10 g, 0.12 mol, 1.0 equiv.) and potassium *tert*-butoxide (13.02 g, 0.12 mol, 1.0 equiv.) were added to the flask, followed by THF (1000 mL). The resulting orange mixture was left to stir overnight. The following day, the flask was concentrated to dryness *in vacuo* before toluene was added (1000 mL). The flask was then cooled to -78°C and left stirring for five minutes before 1,2-dichlorotetramethyldisilane (10.62 mL, 0.057 mol, 0.5 equiv.) was syringed into solution. The resulting white solution was warmed to room temperature while stirring overnight. The reaction was quenched with a 1 M hydrochloric acid solution (400 mL) and the organic and aqueous layers were separated. The aqueous layer was extracted with hexanes (3 x 600 mL) and the combined organic layers were brine-washed, dried over magnesium sulfate, then concentrated *in vacuo*. The crude product was

purified through silica gel chromatography with hexanes to yield **P3** as a white solid (34.16 g, 98% yield). ^{1}H NMR (400 MHz, $CDCl_3$) δ 0.38 (s, 12H), 0.24 (s, 54H). ^{13}C NMR (151 MHz, $CDCl_3$) δ 3.69, 0.17. ^{29}Si NMR (119 MHz, $CDCl_3$) δ -9.58, -29.95, -128.23.

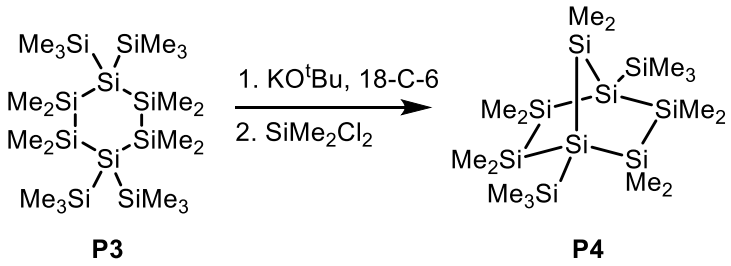
Preparation of **P3**



The synthesis for this compound was adapted from known procedures.[4] An oven-dried 2000 mL round-bottom flask was equipped with a stir bar and septum, then connected to a Schlenk manifold. **P2** (33.95 g, 0.55 mol, 1.0 equiv.), potassium *tert*-butoxide (12.46 g, 0.111 mol, 2.0 equiv.) and 18-crown-6 (29.32 g, 0.111 mol, 2.0 equiv.) were added to the flask, followed by toluene (1000 mL). The resulting orange mixture was left to stir overnight. The flask was first cooled to -78°C and left stirring for five minutes before 1,2-dichlorotetramethyldisilane (10.34 mL, 0.55 mol, 1.0 equiv.) was syringed into solution. The resulting white solution was warmed to room temperature while stirring overnight. The reaction was quenched with a 1 M hydrochloric acid solution (400 mL) and the organic and aqueous layers were separated. The aqueous layer was extracted with hexanes (3 x 600 mL) and the combined organic layers were brine-washed, dried over magnesium sulfate, then concentrated *in vacuo*. The crude product was purified through silica gel chromatography with hexanes to yield **P3** as a white solid (20.23 g, 60% yield). ^{1}H NMR

(400 MHz, $CDCl_3$) δ (ppm): 0.29 (s, 24H), 0.24 (s, 36H). ^{13}C NMR (151 MHz, $CDCl_3$) δ 3.87, -0.99. ^{29}Si NMR (119 MHz, $CDCl_3$) δ -8.25, -39.07, -131.98.

P4

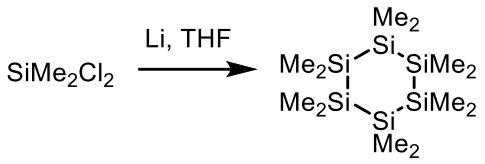


P3 **P4**

The synthesis for this compound was adapted from known procedures.[4] An oven-dried 500 mL Schlenk flask was equipped with a septum and stir bar. **P3** (13.65 g, 0.024 mol, 1.0 equiv.) potassium *tert*-butoxide (5.27 g, 0.048 mol, 2.0 equiv.) and 18-crown-6 (12.41 g, 0.048 mol, 2.0 equiv.) were added to the flask, followed by toluene (350 mL). The resulting orange solution was stirred overnight. A separate 1000 mL Schlenk flask with a stir bar and septum was charged with dichlorodimethylsilane (0.920 g, 0.024 mol, 1.0 equiv.) and toluene (350 mL). The orange dianion solution was cannulated into the flask containing dichlorodimethylsilane dropwise. The cannulation was terminated once a pale orange color persisted in the receiving flask. The reaction was left to stir for two hours before the reaction was quenched with a 1 M hydrochloric acid solution (250 mL) and the organic and aqueous layers were separated. The aqueous layer was extracted with hexanes (3 x 350 mL) and the combined organic layers were brine-washed, dried over magnesium sulfate, then concentrated *in vacuo* to yield the crude product as a waxy solid. This material was purified through silica gel chromatography with hexanes to yield **P4** as a white solid

(10.60 g, 91% yield). ^{1}H NMR (400 MHz, C_6D_6) δ 0.51 (s, 6H), 0.39 (s, 12H), 0.38 (s, 12H), 0.32 (s, 18H). ^{13}C NMR (151 MHz, C_6D_6) δ 3.45, 0.87, -0.52, -1.55. ^{29}Si NMR (119 MHz, C_6D_6) δ -5.45, -16.94, -31.39, -121.72.

Preparation of **P5**

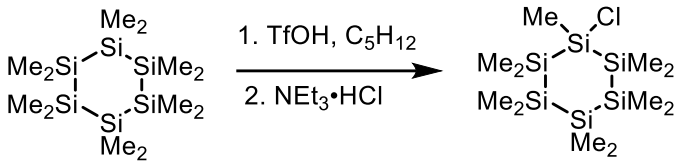


P5

The synthesis for this compound was adapted from known procedures.[6] An oven-dried 1000 mL two-necked flask was equipped with a stir bar, septa, and an oven-dried dropping funnel. The dropping funnel was charged with dichlorodimethylsilane (32.14 g, 0.249 mol, 1.0 equiv.) and THF (220 mL). The reaction flask was charged with granules (10.37 g, 1.49 mol, 6.0 equiv.) and THF (300 mL). The reaction was cooled in an ice-water bath and stirred for five minutes before the dichlorodimethylsilane solution was added to the flask dropwise over 8 hours. During the dropwise addition, the color of suspension becomes cloudy white. After addition was completed, the mixture was allowed to stir overnight before the mixture was filtered through Celite and subsequently quenched with water (200 mL). The organic and aqueous layers were separated, and the aqueous layer was extracted with hexanes (3 x 300 mL). The combined organic layers were dried over magnesium sulfate and concentrated *in vacuo,* re-dissolved in hexanes, then filtered over a Celite plug to yield the product as a white solid (10.89 g, 98% yield). ^{1}H NMR (600 MHz, $CDCl_3$) δ

0.13 (s, 36H). ^{13}C NMR (151 MHz, $CDCl_3$) δ -5.95. ^{29}Si NMR (119 MHz, $CDCl_3$) δ -42.17.

Preparation of **P6**

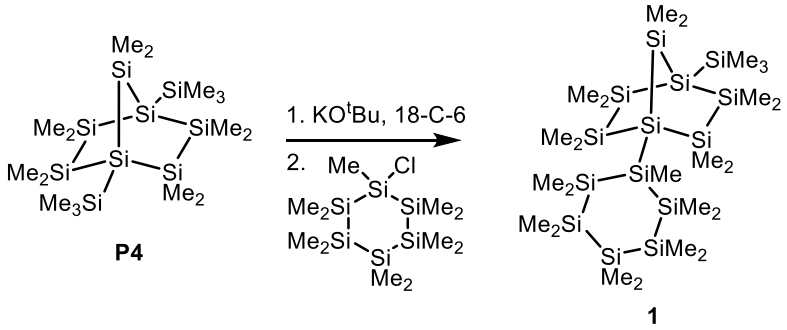


P5 **P6**

The synthesis for this compound was adapted from known procedures.[14] An oven-dried 100 mL Schlenk flask equipped with a stir bar and septum was charged with **P5** (8.00 g, 23.93 mmol, 1.0 equiv.) and anhydrous pentane (20 mL). Trifluoromethanesulfonic acid (4.05 mL, 45.85 mmol, 2.0 equiv.) was syringed into the reaction flask to give a biphasic yellow-brown reaction mixture. The pentane layer was aliquoted and monitored by ^{1}H NMR for the disappearance of starting material after 2 hours. Additional trifluoromethanesulfonic acid (1.75 mL, 19.82 mmol, 0.83 equiv.) was added and stirred for 2 hours. The mixture was then concentrated *in vacuo*. Anhydrous diethyl ether (30 mL) was added, followed by triethylammonium chloride (9.04 g, 65.67 mmol, 2.83 equiv.) under a positive nitrogen flow. The resulting biphasic mixture was stirred for 2 hours before being subjected to a -78°C bath to freeze the ionic liquid layer. The ether layer was decanted into a separate Erlenmeyer flask. Dry pentane (50 mL) was added to extract the ionic liquid layer, which was re-frozen before decanting the pentane layer into the Erlenmeyer flask. This process was repeated twice more. The organic layers were combined into a separate

250 mL Erlenmeyer flask and passed through dried celite into a 250 mL round bottom flask. The organic layers were concentrated *in vacuo* to yield the compound as a white fluffy solid (7.50 g, 88% yield). ^{1}H NMR (400 MHz, C_6D_6) δ 0.61 (s, 3H), 0.36 (s, 6H), 0.25 (s, 6H), 0.23 (s, 6H), 0.22 (s, 6H), 0.19 (s, 3H), 0.16 (s, 3H). ^{13}C NMR (151 MHz, C_6D_6) δ 3.44, 0.06, -5.75, -5.80, -6.12, -6.16, -6.73. ^{29}Si NMR (119 MHz, C_6D_6) δ 16.78, -39.18, -41.82, -42.05.

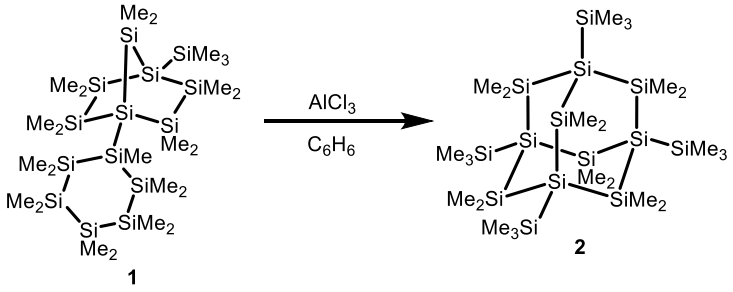
Preparation of **1**



The synthesis for this compound was adapted from known procedures.[5] An oven-dried 1000 mL Schlenk flask was equipped with a stir bar and septum before adding **P4** (10.60 g, 21.49 mmol, 1.0 equiv.), potassium *tert*-butoxide (2.41 g, 21.49 mmol, 1.0 equiv.) and 18-crown-6 (5.68 g, 21.49 mmol, 1.0 equiv.). Toluene (300 mL) was added to the reaction mixture, and the resulting solution was stirred overnight. **P6** (7.94 g, 21.49 mmol, 1.0 equiv.) and toluene (300 mL) were added to a separate 1000 mL Schlenk flask equipped with a stir bar and septum. The silanide solution was cannulated dropwise into the flask containing **P6**. The cannulation was terminated once a pale-yellow color persisted. The reaction mixture was stirred for two hours before the reaction was quenched with a 1 M

hydrochloric acid solution (200 mL). The organic and aqueous layers were separated, and the aqueous layer was extracted with hexanes (3 x 300 mL). The combined organic layers were brine-washed, dried over magnesium sulfate, then concentrated in vacuo to yield the crude material as a white wax. The product was purified via silica gel chromatography in hexanes to yield **1** as a white solid (14.20 g, 88% yield). ^{1}H NMR (400 MHz, C_6D_6) δ 0.63 (s, 6H), 0.52 (s, 6H), 0.47 (s, 3H), 0.46 (s, 6H), 0.45 (s, 6H), 0.41 (s, 6H), 0.40 (s, 6H), 0.39 (s 6H), 0.34 (s 9H), 0.29 (s, 6H), 0.27 (3H), 0.27 (s, 6H), 0.25 (s, 3H). ^{13}C NMR (151 MHz, C_6D_6) δ 3.45, 1.74, 1.07, -0.43, -0.68, -1.41, -2.46, -3.98, -4.26, -4.30, -4.91, -6.25, -6.74. ^{29}Si NMR (119 MHz, C_6D_6) δ -9.36, -25.15, -26.14, -26.98, -31.31, -34.28, -37.02, -59.70, -112.79, -128.94.

Preparation of ***2*** *(SiAd) via aluminum chloride*

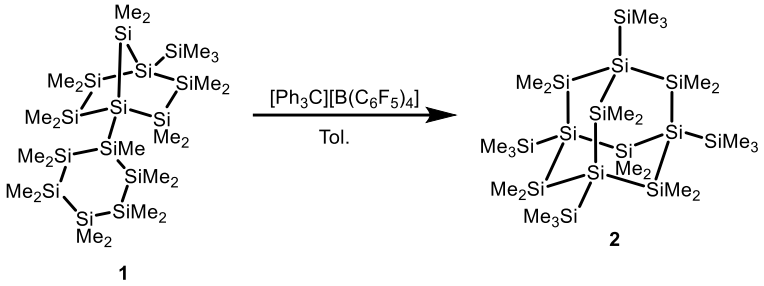


In a procedure adapted from Marschner and coworkers,[5] an oven-dried, 15 mL pressure tube equipped with a stir bar was brought into the glovebox and charged with **1** (1.0 g, 1.33 mmol, 1.0 equiv.), $AlCl_3$ (0.30 g, 2.25 mmol, 1.7 equiv.) and benzene (5 mL). The resulting cloudy mixture was stirred for 48 hours before the reaction was determined to be complete by ^{1}H NMR monitoring. The reaction mixture was removed from the glovebox and

quenched with a 1 M hydrochloric acid solution (7 mL). The aqueous layer was extracted with hexanes (3x50 mL). The organic layers were combined, washed with brine, dried over magnesium sulfate, then concentrated *in vacuo* to yield a white crude solid. This material was purified via flash column chromatography in hexanes to yield pure SiAd **2** (0.39 g, 39% yield) as a white solid. ^{1}H NMR (400 MHz, C_6D_6) δ 0.61 (s, 36H), 0.35 (s, 36H). ^{13}C NMR (101 MHz, C_6D_6) δ 5.03, 4.14. ^{29}Si-DEPT NMR (79 MHz, C_6D_6) δ -4.68, -25.88, -118.71.

Note: At room temperature, a reaction concentration of ≥0.26 M is key to observing reproducible isomerization outcomes under these conditions. We did not observe isomerization on these timescales and under these conditions at room temperature with 0.13 M solutions. The purity of $AlCl_3$ also impacts the isomerization: while anhydrous $AlCl_3$ purchased from Sigma-Aldrich (99.999% purity) enabled isomerization at room temperature on a two-day timescale, anhydrous $AlCl_3$ purchased from Strem (99.99% purity) typically required an extra day to isomerize. At room temperature, 0.85 equivalents of $AlCl_3$ did not lead to appreciable isomerization over a five-day period, though this quantity was sufficient for isomerization at higher temperatures (50 ˚C). Less time is required to achieve complete isomerization of **1** at higher temperatures: for example, the reaction is completed in 30 minutes at 80˚C in benzene with 1.7 equivalents of $AlCl_3$. However, we generally obtained lower isolated yields at higher temperatures.

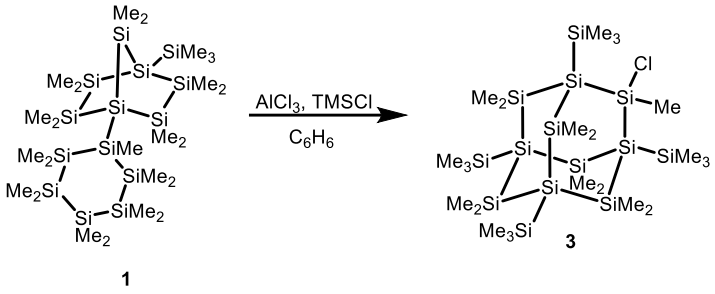
Preparation of ***2*** *(SiAd) via trityl tetrakis(pentafluorophenyl)borate*



1 **2**

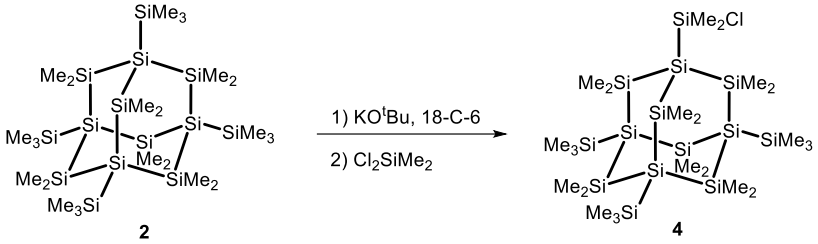
An oven-dried 50 mL pressure tube equipped with a stir bar was brought into the glovebox and charged with **1** (1.76 g, 2.33 mmol, 1.0 equiv.), trityl tetrakis(pentafluorophenyl)borate (0.22 g, 0.23 mmol, 0.10 equiv.) and toluene (8.5 mL). The red reaction mixture was stirred vigorously at room temperature for 48 hours before the reaction was deemed complete via ^{1}H NMR monitoring. The biphasic mixture was removed from the glovebox and subjected to a -78°C dry ice/acetone bath to freeze the denser polar phase. The nonpolar phase was pipetted out, then subjected to an aqueous work up with a 1 M hydrochloric acid solution (10 mL). The organic layer was separated, and the aqueous layer was extracted with hexanes (3x50 mL). The organic layers were combined, washed with brine, dried over magnesium sulfate, then concentrated *in vacuo* to yield a white waxy crude solid. The material was dissolved in hexanes and purified via flash column chromatography in hexanes to yield SiAd **2** (1.20 g, 68% yield) as a white solid. The material may also be purified by recrystallization in hexanes. ^{1}H NMR (400 MHz, C_6D_6) δ 0.61 (s, 36H), 0.35 (s, 36H). ^{13}C NMR (101 MHz, C_6D_6) δ 5.03, 4.14. ^{29}Si-DEPT NMR (79 MHz, C_6D_6) δ -4.68, -25.88, -118.71.

Preparation of ***3*** *(2Cl-SiAd)*



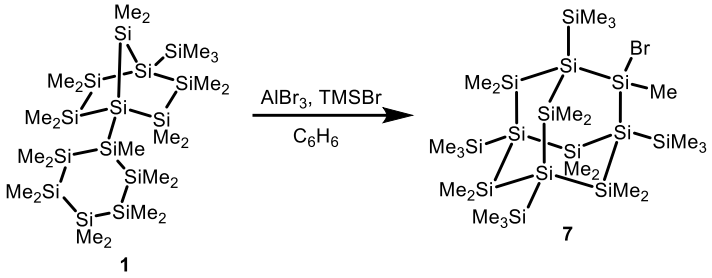
A 4 mL vial equipped with a stir bar was brought into a glovebox and charged with **1** (0.075 g, 0.10 mmol, 1.0 equiv.), $AlCl_3$ (0.023 g, 0.17 mmol, 1.7 equiv.), trimethylsilyl chloride (1.0 M solution in benzene, 0.10 mL, 0.10 mmol, 1.0 equiv.), and benzene (0.15 mL). The cloudy mixture was stirred for 48 hours before the reaction was determined to be complete by ^{1}H NMR monitoring. The vial was removed from the glovebox and quenched with a 1 M hydrochloric acid solution (2 mL). The aqueous layer was extracted with hexanes (3x10 mL) and the combined organic layers were brine-washed, dried over magnesium sulfate, then concentrated *in vacuo* to yield a white-yellow solid. The crude product was purified via flash column chromatography in hexanes to yield **3** as a white solid (0.016 g, 21% yield). ^{1}H NMR (600 MHz, C_6D_6) δ 1.03 (s, 3H), 0.81 (s, 6H), 0.59 (s, 6H), 0.58 (s, 6H), 0.57 (s, 6H), 0.51 (s, 6H), 0.42 (s, 18H), 0.35 (s, 9H), 0.32 (s, 9H). ^{13}C NMR (151 MHz, $CDCl_3$) δ 10.06, 4.90, 4.84, 4.56, 3.79, 3.69, 3.62, 3.27, 1.18. ^{29}Si-DEPT NMR (79 MHz, $CDCl_3$) δ 31.64, -4.06, -4.52, -4.54, -25.37, -26.02, -27.63, -111.99, -118.96, -118.97. HRMS (TOF MS CI+) for $[C_{23}H_{69}ClSi_{14}]$: calculated = 772.1858, found = 772.1871 $[M]^{+}$. Crystals suitable for single-crystal X-ray diffraction studies were grown by methanol vapor diffusion into a concentrated toluene solution.

Preparation of ***4*** *(1SiMe₂Cl-SiAd)*



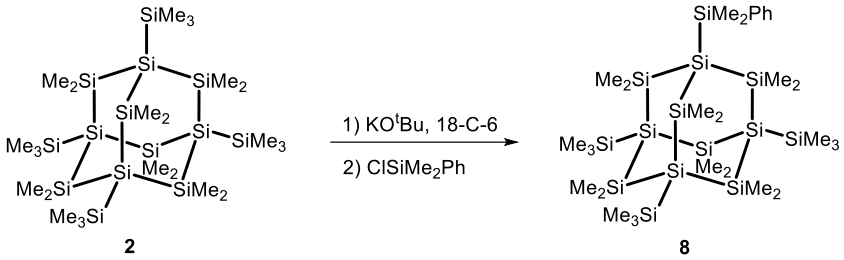
An oven-dried 10 mL Schlenk flask equipped with a stir bar was brought into a glovebox and charged with **2** (0.075 g, 0.10 mmol, 1.0 equiv.), potassium tert-butoxide (0.011 g, 0.10 mmol 1.0 equiv.), 18-crown-6 (0.026 g, 0.10 mmol 1.0 equiv.) and toluene (2 mL). The resulting orange mixture was left to stir for 16 hours. Then, the flask was taken out of the glovebox and connected to a Schlenk manifold upon which dichlorodimethylsilane (6.0 µL, 0.050 mmol, 1.0 equiv.) was added and the reaction mixture turned colorless. The mixture was allowed to stir for 3 hours before the reaction was quenched with a 1 M hydrochloric acid solution (5 mL). The aqueous layer was extracted with hexanes (3x10 mL) and the combined organic layers were brine-washed, dried over magnesium sulfate, then concentrated *in vacuo* to yield a white solid. The product was further purified by recrystallization in hexanes to yield **4** as a white solid (0.065 g, 84% yield). ^{1}H NMR (600 MHz, C_6D_6) δ 0.67 (s, 6H), 0.65 (s, 18H), 0.59 (s, 18H), 0.33 (s, 27H). ^{13}C NMR (151 MHz, $CDCl_3$) δ 9.87, 4.87, 3.83, 3.79, 3.52. ^{29}Si-DEPT NMR (119 MHz, $CDCl_3$) δ 34.15, -4.69, -26.29, -26.82, -115.80, -118.47. HRMS (TOF MS ASAP+) for $[C_{22}H_{66}ClSi_{14}]^+$: calculated = 757.1623, found = 757.1635 $[M\text{-}CH_3]^+$.

Preparation of ***7*** *(2Br-SiAd)*



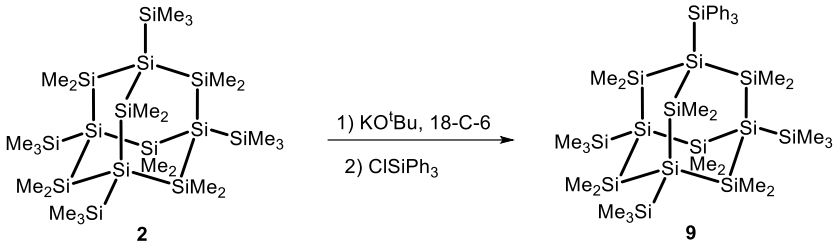
An oven-dried 4 mL vial equipped with a stir bar was brought into a glovebox and charged with **1** (0.11 g, 0.14 mmol, 1.0 equiv.), $AlBr_3$ (0.064 g, 0.24 mmol, 1.7 equiv.), trimethylsilyl bromide (18.5 µL, 0.14 mmol, 1.0 equiv.), benzene (0.45 mL, 5.0 mmol) and tetradecane as an internal standard (73 µL, 0.28 mmol, 2.0 equiv.). The opaque orange-red solution was stirred for 17 days. The vial was then taken out of the glovebox, quenched with acetone (1 mL) and subjected to an aqueous workup with a 1 M hydrochloric acid solution (2 mL). The aqueous layer was extracted with hexanes (3x5 mL) and the combined organic layers were brine-washed, dried over magnesium sulfate, then concentrated *in vacuo* to give a colorless crude solid. Purification with flash silica gel chromatography with hexanes yielded **7** as a colorless solid (6 mg, 6% yield). ^{1}H NMR (400 MHz, C_6D_6) δ 1.22 (s, 3H), 0.84 (s, 6H), 0.59 (s, 6H), 0.58 (s, 6H), 0.57 (s, 6H), 0.52 (s, 6H), 0.43 (s, 18H), 0.34 (s, 9H), 0.32 (s, 9H). ^{29}Si-DEPT NMR (79 MHz, C_6D_6) δ 21.12, -3.88, -4.84, -4.92, -25.67, -26.57, -27.24, -112.07, -118.96, -119.34. HRMS (TOF MS ASAP+) for $[C_{23}H_{69}BrSi_{14}]$: calculated = 818.1337, found = 818.1334 $[M]^+$

Preparation of ***8*** *(1SiMe$_2$Ph-SiAd)*



An oven-dried 10 mL Schlenk flask equipped with a stir bar was brought into a glovebox and charged with **2** (0.075 g, 0.10 mmol, 1.0 equiv.), potassium tert-butoxide (0.011 g, 0.10 mmol, 1.0 equiv.) and 18-crown-6 (0.026 g, 0.10 mmol, 1.0 equiv.). The solids were then dissolved in toluene (2 mL) and the resulting orange mixture was left to stir for 16 hours. The flask was taken out of the glovebox and connected to a Schlenk manifold upon which chlorodimethylphenylsilane (0.017 μL, 0.10 mmol, 1.0 equiv.) was added and the reaction mixture turned colorless. The mixture was allowed to stir for 3 hours before the reaction was quenched with a 1 M hydrochloric acid solution (5 mL). The aqueous layer was extracted with hexanes (3x10 mL) and the combined organic layers were brine-washed, dried over magnesium sulfate, then concentrated *in vacuo* to yield a white solid. The crude product was purified via flash column chromatography in hexanes to yield **8** as a white solid (0.025 g, 33% yield). ^{1}H NMR (400 MHz, C_6D_6) δ 7.58 – 7.55 (m, 2H), 7.25 – 7.21 (m, 3H), 0.61 (s, 6H), 0.59 (s, 9H), 0.58 (s, 9H), 0.51 (s, 18H), 0.33 (s, 27H). ^{13}C NMR (151 MHz, $CDCl_3$) δ 142.06, 134.20, 128.62, 127.98, 4.91, 3.84, 3.79, 3.53, 2.89. ^{29}Si-DEPT NMR (119 MHz, $CDCl_3$) δ -4.92, -10.25, -25.83, -26.43, -118.36, -118.89. HRMS (TOF MS ASAP+) for [$C_{39}H_{78}Si_{14}$]: calculated = 814.2560, found = 814.2551 $[M]^+$

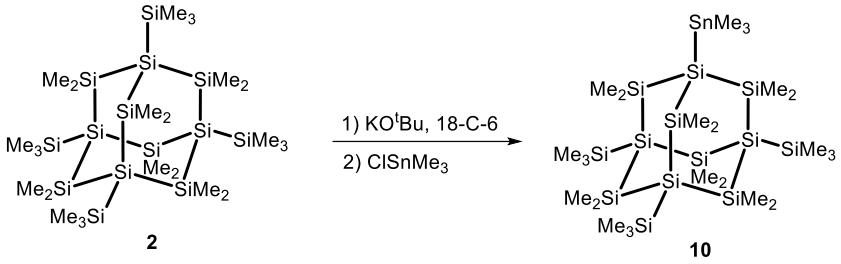
Preparation of ***9*** *(1SiPh$_3$-SiAd)*



An oven-dried 10 mL Schlenk flask equipped with a stir bar was brought into a glovebox and charged with **2** (0.10 g, 0.13 mmol, 1.0 equiv.), potassium tert-butoxide (0.015 g, 0.13 mmol, 1.0 equiv.) and 18-crown-6 (0.035 g, 0.13 mmol 1.0 equiv.). The solids were then dissolved in toluene (2.0 mL) and capped with a septum. The resulting orange mixture was left to stir for 16 hours. The flask was taken out of the glovebox, connected to a Schlenk manifold, and subjected to positive pressure nitrogen. The septum was then removed, upon which chlorotriphenylsilane (0.039 g, 0.10 mmol, 1.0 equiv.) was added under a positive nitrogen flow, after which the reaction mixture turned colorless. The flask was recapped with a septum, and the mixture was allowed to stir for 3 more hours before the reaction was quenched with a 1 M hydrochloric acid solution (5 mL). The aqueous layer was extracted with hexanes (3 x 10 mL) and the combined organic layers were brine-washed, dried over magnesium sulfate, then concentrated *in vacuo* to yield a white solid. The crude product was further purified by washing with cold hexanes to yield **9** as a white solid (0.067 g, 54% yield). ^{1}H NMR (400 MHz, C_6D_6) δ 7.86 – 7.84 (m, 6H), 7.70 – 7.68 (m, 3H), 7.26 – 7.22 (m, 6H), 0.58 (s, 9H), 0.57 (s, 9H), 0.45 (s, 18H), 0.30 (s, 27H). ^{13}C NMR (151 MHz, $CDCl_3$) δ 137.12, 136.68, 129.12, 127.93, 5.04, 4.42, 3.83, 3.79. ^{29}Si NMR (79 MHz,

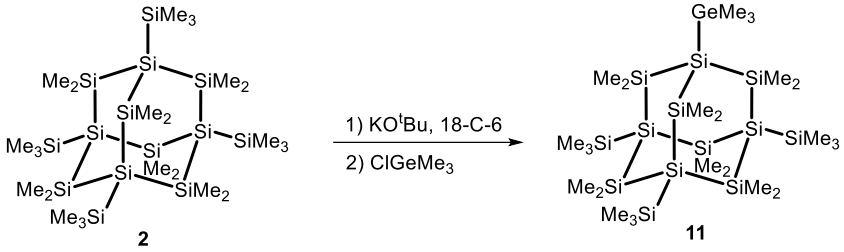
C_6D_6) δ -4.68, -11.04, -24.58, -26.61, -116.05, -117.12. HRMS (TOF MS ASAP+) for [$C_{39}H_{78}Si_{14}$]: calculated = 939.2883, found = 939.2834 $[M]^+$

Preparation of ***10*** *(1SnMe₃-SiAd)*



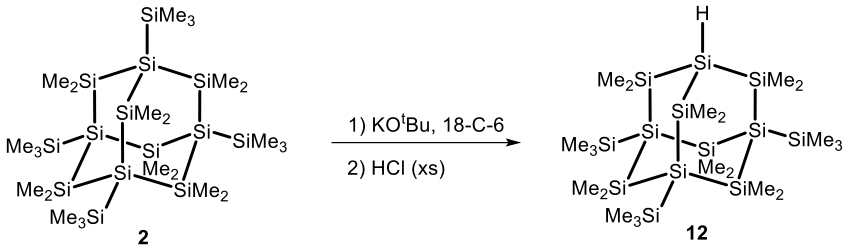
An oven-dried 10 mL Schlenk flask equipped with a stir bar was brought into a glovebox and charged with **2** (0.075 g, 0.10 mmol 1.0 equiv.), potassium tert-butoxide (0.011 g, 0.10 mmol, 1.0 equiv.), 18-crown-6 (0.026 g, 0.10 mmol, 1.0 equiv.) and toluene (2 mL). The resulting orange mixture was left to stir for 16 hours. Then, chlorotrimethyltin (0.0199 g, 0.100 mmol, 1.0 equiv.) was added under positive nitrogen flow, after which the reaction mixture turned colorless. The mixture was allowed to stir for 3 more hours before the flask was taken out of the glovebox and the reaction was quenched with a 1 M hydrochloric acid solution (5 mL). The aqueous layer was extracted with hexanes (3x10 mL) and the combined organic layers were brine-washed, dried over magnesium sulfate, then concentrated *in vacuo* to yield **10** as a white solid. (0.082 g, 98% yield). ^{1}H NMR (400 MHz, C_6D_6) δ 0.60 (s, 9H), 0.59 (s, 9H), 0.57 (s, 18H), 0.42 (s, 9H), 0.34 (s, 27H). ^{13}C NMR (151 MHz, C_6D_6) δ 4.90, 4.27, 4.16, 4.08, -5.88. ^{29}Si-DEPT NMR (119 MHz, C_6D_6) δ -4.62, -24.54, -25.67, -117.39, -118.26. ^{119}Sn NMR (149 MHz, C_6D_6) δ -64.36. HRMS (TOF MS ASAP+) for [$C_{24}H_{72}Si_{13}Sn$]: calculated = 844.1652, found = 844.1653 $[M]^+$

Preparation of ***11*** *(1GeMe₃-SiAd)*



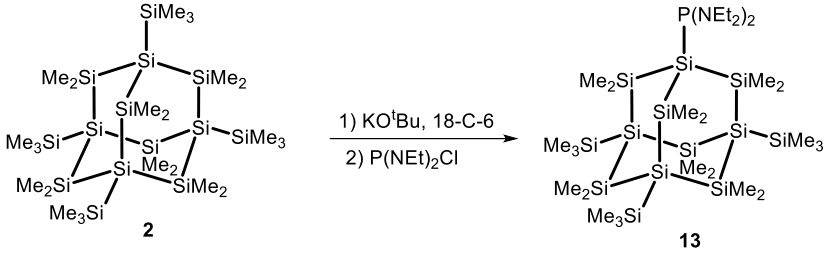
An oven-dried 10 mL Schlenk flask equipped with a stir bar was brought into a glovebox and charged with **2** (0.050 g, 0.066 mmol, 1.0 equiv.), potassium tert-butoxide (0.0074 g, 0.066 mmol, 1.0 equiv.) and 18-crown-6 (0.018 g, 0.066 mmol, 1.0 equiv.) and toluene (2 mL). The resulting orange mixture was left to stir for 16 hours. The flask was then taken out of the glovebox and connected to a Schlenk manifold upon which chlorotrimethylgermanium (8.2 μL, 0.066 mmol, 1.0 equiv.) was added. The mixture was allowed to stir for 3 more hours before the reaction was quenched with a 1 M hydrochloric acid solution (5 mL). The aqueous layer was extracted with hexanes (3x10 mL) and the combined organic layers were brine-washed, dried over magnesium sulfate, then concentrated *in vacuo* to yield **11** as a white solid. (0.050 g, 60% yield). ^{1}H NMR (600 MHz, C_6D_6) δ 0.61 (s, 9H), 0.60 (s, 18H), 0.57 (s, 9H) 0.50 (s, 9H), 0.35 (s, 27H). ^{13}C NMR (151 MHz, C_6D_6) δ 4.97, 4.58, 4.13, 4.07, 4.01. ^{29}Si-DEPT NMR (119 MHz, C_6D_6) δ -4.67, -25.52, -25.88, -110.71, -118.18. HRMS (TOF MS ASAP+) for [$C_{24}H_{72}GeSi_{13}$]: calculated = 798.1850, found = 798.1837 $[M]^+$

Preparation of ***12*** *(1H-SiAd)*



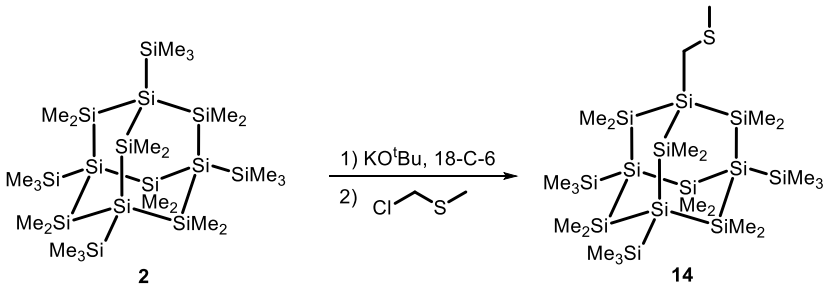
An oven-dried 10 mL Schlenk flask equipped with a stir bar was brought into a glovebox and charged with **2** (0.075 g, 0.10 mmol, 1.0 equiv.), potassium tert-butoxide (0.011 g, 0.10 mmol, 1.0 equiv.), 18-crown-6 (0.026 g, 0.10 mmol, 1.0 equiv.) and toluene (2 mL). The resulting orange mixture was left to stir for 16 hours. Then, the flask was taken out of the glovebox and connected to a Schlenk manifold upon which excess amounts of a 1 M hydrochloric acid solution (5 mL) was added and the reaction mixture turned colorless. The mixture was allowed to stir for 3 more hours before the aqueous layer was extracted with hexanes (3x10 mL) and the combined organic layers were brine-washed, dried over magnesium sulfate, then concentrated *in vacuo* to yield **12** as a white solid. (0.048 g, 70% yield). ^{1}H NMR (600 MHz, C_6D_6) δ 3.50 (s, 1H), 0.68 (s, 9H), 0.55 (s, 9H), 0.54 (s, 18H), 0.31 (s, 27H). ^{13}C NMR (101 MHz, C_6D_6) δ 4.78, 4.13, 3.96, 3.32. ^{29}Si-DEPT NMR (79 MHz, C_6D_6) δ -4.52, -25.36, -29.20, -99.67, -118.21. HRMS (TOF MS CI+) for $[C_{21}H_{64}Si_{13}]$: calculated = 680.2009, found = 680.2028 $[M]^+$

Preparation of ***13*** *(1P(NEt₂)₂-SiAd)*



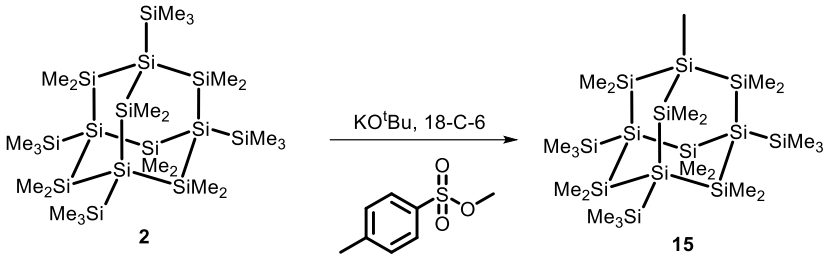
An oven-dried 10 mL Schlenk flask equipped with a stir bar was brought into a glovebox and charged with **2** (0.045 g, 0.060 mmol, 1.0 equiv.), potassium tert-butoxide (0.0067 g, 0.060 mmol, 1.0 equiv.), 18-crown-6 (0.016 g, 0.060 mmol, 1.0 equiv.) and toluene (2 mL). The resulting orange mixture was left to stir for 16 hours. Then, bis(diethylamino)chlorophosphine (12.55 µL, 0.0597 mmol, 1.0 equiv.) was added the reaction mixture and the mixture turned colorless. The mixture was allowed to stir for about 3 hours before being concentrated to dryness. The resulting solids were washed with dry pentane and the mixture was syringe filtered with a 0.22 µm syringe filter. Upon evaporation of the pentane filtrate, the crude product was obtained as a white waxy solid. The crude material was triturated with diethyl ether to obtain **13** as a white solid (0.032 g, 63% yield). ^{1}H NMR (400 MHz, C_6D_6) δ 3.27 – 3.10 (m, 8H), 1.11 (t, J = 7.1 Hz, 12H) 0.72 (s, 18H), 0.65 (s, 9H), 0.63 (s, 9H), 0.38 (s, 27H). ^{13}C NMR (151 MHz, C_6D_6) δ 15.14, 5.09, 4.09, 4.01, 3.58, 0.22. ^{29}Si NMR (119 MHz, C_6D_6) δ -4.70, -26.26 (d, $^{2}J_{SiP}$ = 17 Hz), -26.26, -87.69 (d, $^{1}J_{SiP}$ = 99 Hz) -115.51 (d, $^{3}J_{SiP}$ = 5.8 Hz). ^{31}P NMR (243 MHz, C_6D_6) δ 111.59. HRMS could not be obtained due to the ambient sensitivity of the product.

Preparation of ***14*** *(1CH₂SMe-SiAd)*



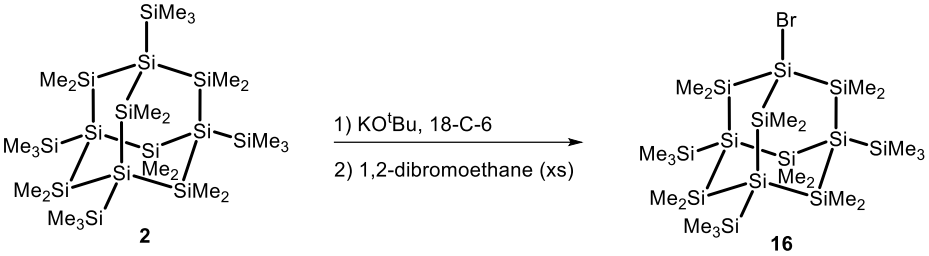
An oven-dried 10 mL Schlenk flask equipped with a stir bar was brought into a glovebox and charged with **2** (0.075 g, 0.10 mmol, 1.0 equiv.), potassium tert-butoxide (0.011 g, 0.10 mmol, 1.0 equiv.), 18-crown-6 (0.026 g, 0.10 mmol, 1.0 equiv.) and toluene (2 mL). The resulting orange mixture was left to stir for 16 hours. The flask was taken out of the glovebox and connected to a Schlenk manifold upon which chloromethyl methyl sulfide (8.5 µL, 0.10 mmol, 1.0 equiv.) was added and the reaction mixture turned colorless. The mixture was allowed to stir for 3 hours before the reaction was quenched with a 1 M hydrochloric acid solution (5 mL). The aqueous layer was extracted with hexanes (3x10 mL) and the combined organic layers were brine-washed, dried over magnesium sulfate, then concentrated *in vacuo* to yield a white solid. The crude product was further purified by flash chromatography using a gradient from 100% hexanes to 35% dichloromethane in hexanes to yield **14** as a white solid (0.024 g, 35% yield). ^{1}H NMR (400 MHz, $CDCl_3$) δ 2.26 (s, 2H), 2.19 (s, 3H), 0.48 (s, 18H), 0.47 (s, 9H), 0.46 (s, 9H), 0.27 (s, 27H). ^{13}C NMR (151 MHz, C_6D_6) δ 21.95, 15.80, 4.85, 4.11, 3.89, 2.27. ^{29}Si-DEPT NMR (119 MHz, $CDCl_3$) δ -4.75, -25.99, -29.18, -70.63, -116.73. HRMS (TOF MS ASAP+) for $[C_{22}H_{65}SSi_{13}]$: calculated = 725.1807, found = 725.1813 $[M\text{-}CH_3]^+$

Preparation of ***15*** *(1Me-SiAd)*



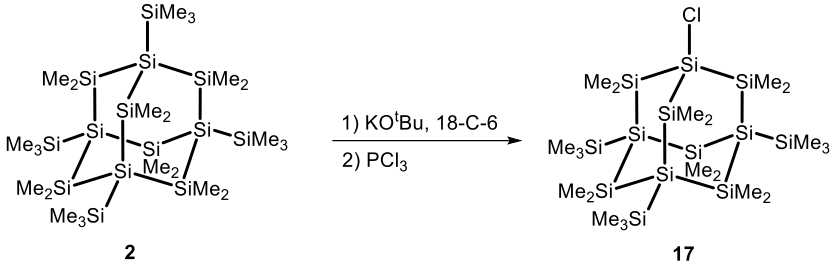
An oven-dried 10 mL Schlenk flask equipped with a stir bar was brought into a glovebox and charged with **2** (0.091 g, 0.12 mmol, 1.0 equiv.), potassium tert-butoxide (0.014 g, 0.12 mmol, 1.0 equiv.) and 18-crown-6 (0.032 g, 0.12 mmol, 1.0 equiv.). The solids were then dissolved in toluene (2 mL) and the resulting orange mixture was left to stir for 16 hours. Then, the flask was taken out of the glovebox, connected to a Schlenk manifold, and subjected to positive pressure nitrogen. The septum was then removed, upon which methyl-p-toluenesulfonate (0.023 g, 0.12 mmol, 1.0 equiv.) was added under positive nitrogen flow, after which the reaction mixture turned colorless. The mixture was allowed to stir for 3 more hours before the reaction was quenched with a 1 M hydrochloric acid solution (5 mL). The aqueous layer was extracted with hexanes (3x10 mL) and the combined organic layers were brine-washed, dried over magnesium sulfate, then concentrated *in vacuo* to yield **15** as a white solid. (0.082 g, 97% yield). ^{1}H NMR (600 MHz, C_6D_6) δ 0.60 (s, 9H), 0.59 (s, 9H), 0.50 (s, 18H), 0.34 (s, 27H), 0.28 (s, 3H). ^{13}C NMR (151 MHz, C_6D_6) δ 4.82, 4.15, 3.97, 1.15, -13.99. ^{29}Si-DEPT NMR (119 MHz, C_6D_6) δ 4.66, -20.75, -24.97, -68.88, -112.34. HRMS (TOF MS ASAP+) for [$C_{22}H_{66}Si_{13}$]: calculated = 694.2165, found = 694.2162 [M]+

Preparation of ***16*** *(1Br-SiAd)*



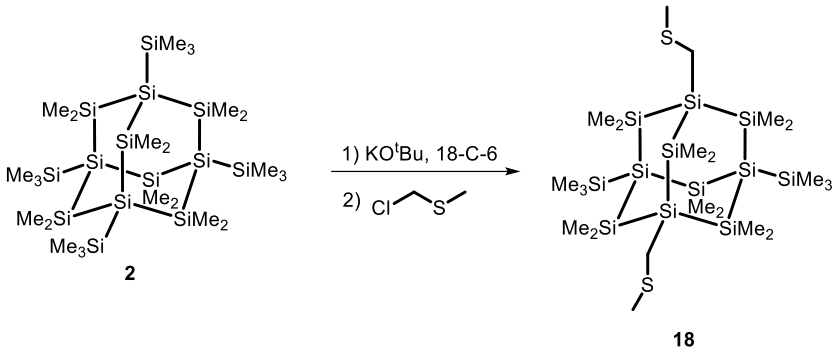
An oven-dried 10 mL Schlenk flask equipped with a stir bar was brought into a glovebox and charged with **2** (0.075 g, 0.10 mmol, 1.0 equiv.), potassium tert-butoxide (0.011 g, 0.10 mmol, 1.0 equiv.), 18-crown-6 (0.026 g, 0.10 mmol, 1.0 equiv.) and toluene (2 mL). The resulting yellow solution was left to stir for 16 hours before excess 1,2 dibromoethane (0.17 mL, 2.0 mmol, 20 equiv.) was syringed in upon which, the solution turned colorless. The mixture was allowed to stir for 3 more hours before being concentrated to dryness. The resulting salts were washed with dry pentane and the mixture was syringe filtered with a 0.22 μm syringe filter. Upon evaporation of the pentane solution, **16** was obtained as a white waxy solid (0.063 g, 83% yield). ^{1}H NMR (400 MHz, C_6D_6) δ 0.61 (s, 18H), 0.54 (s, 9H), 0.54 (s, 9H), 0.28 (s, 27H). ^{13}C NMR (151 MHz, C_6D_6) δ 4.51, 4.04, 3.62, 0.62. ^{29}Si-DEPT NMR (79 MHz, C_6D_6) δ -4.39, -12.70, -25.51, -28.58, -113.02. HRMS (TOF MS ASAP+) for [$C_{21}H_{63}Si_{13}Br$]: calculated = 760.1097, found = 760.1100 $[M]^+$

Preparation of ***17*** *(1Cl-SiAd)*



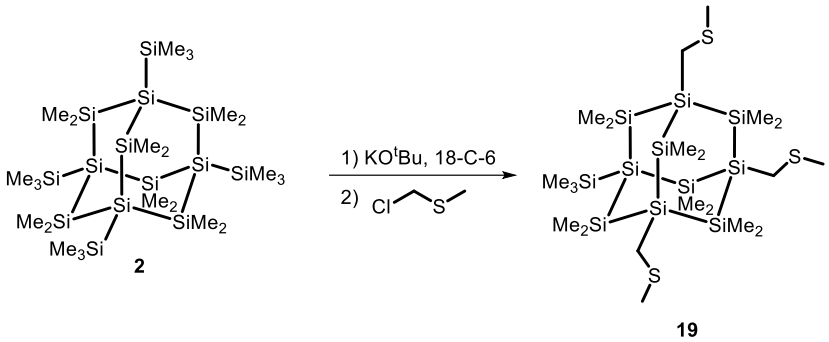
An oven-dried 10 mL Schlenk flask equipped with a stir bar was brought into a glovebox and charged with **2** (0.050 g, 0.066 mmol, 1.0 equiv.), potassium tert-butoxide (0.0075 g, 0.066 mmol, 1.0 equiv.), 18-crown-6 (0.018 g, 0.066 mmol, 1.0 equiv.) and toluene (2 mL). The resulting yellow solution was left to stir for 16 hours before the solution was subjected to a -78°C bath. Once cooled, PCl_3 (14.50 µL, 0.17 mmol, 2.50 equiv.) was syringed into the flask upon which, the solution turned colorless. The mixture was allowed to stir for 3 more hours before being concentrated to dryness. The resulting salts were washed with dry pentane and the mixture was syringe filtered with a 0.22 µm syringe filter. Upon evaporation of the pentane solution, the crude product was obtained as a white, waxy solid. The crude product was further purified by silica gel chromatography with hexanes to yield pure **17** as a white solid (0.010 g, 21% yield). ^{1}H NMR (400 MHz, C_6D_6) δ 0.62 (s, 18H), 0.55 (s, 9H), 0.55 (s, 9H), 0.29 (s, 27H). ^{13}C NMR (151 MHz, C_6D_6) δ 4.51, 3.99, 3.53, 0.25. ^{29}Si NMR (119 MHz, C_6D_6) δ -4.21, -4.33, -25.58, -27.36, -112.81. HRMS (TOF MS ASAP+) for $[C_{21}H_{63}Si_{13}Cl]$: calculated = 714.1619, found = 714.1616 $[M]^+$

Preparation of ***18*** *(1-,3-($CH_2SMe)_2$-SiAd)*



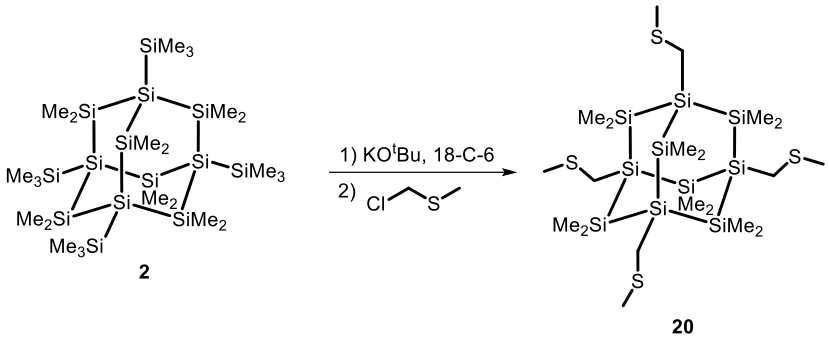
An oven-dried 10 mL Schlenk flask equipped with a stir bar was brought into a glovebox and charged with **2** (0.10 g, 0.13 mmol, 1.0 equiv.), potassium tert-butoxide (0.030 g, 0.27 mmol, 2.0 equiv.) and 18-crown-6 (0.070 g, 0.27 mmol, 2.0 equiv.). The resulting orange mixture was left to stir for 16 hours. Then, the flask was taken out of the glovebox and connected to a Schlenk manifold upon which chloro methyl methyl sulfide (22.3 µL, 0.27 mmol, 2.0 equiv.) was added and the reaction mixture turned colorless. The mixture was allowed to stir for 3 hours before the reaction was quenched with a 1 M hydrochloric acid solution (5 mL). The aqueous layer was extracted with hexanes (3x10 mL) and the combined organic layers were brine-washed, dried over magnesium sulfate, then concentrated *in vacuo* to yield a white solid. The crude product was further purified by flash chromatography using a gradient from 100% hexanes to 35% dichloromethane in hexanes to yield **18** as a white solid (0.096 g, 99% yield). ^{1}H NMR (400 MHz, $CDCl_3$) δ 2.26 (s, 4H), 2.19 (s, 6H), 0.50 (s, 6H), 0.48 (s, 12H), 0.47 (s, 12H), 0.46 (s, 6H), 0.27 (s, 18H). ^{13}C NMR (151 MHz, $CDCl_3$) δ 22.23, 15.75, 4.62, 3.58, 1.94, 1.65, 0.30. ^{29}Si NMR (119 MHz, $CDCl_3$) δ -4.39, -25.84, -28.92, -30.84, -67.96, -118.09. HRMS (TOF MS ASAP+) for [$C_{22}H_{65}S_2Si_{12}$]: calculated = 729.1759, found = 729.1728 $[M+H]^+$

Preparation of ***19*** *(1-,3-,5-($CH_2SMe)_3$-SiAd)*



An oven-dried 10 mL Schlenk flask equipped with a stir bar was brought into a glovebox and charged with **2** (0.075 g, 0.10 mmol, 1.0 equiv.), potassium tert-butoxide (0.034 g, 0.30 mmol, 3.0 equiv.), 18-crown-6 (0.079 g, 0.30 mmol, 3.0 equiv.) and toluene (2 mL). The resulting orange mixture was left to stir for 16 hours. Then, the flask was taken out of the glovebox, and connected to a Schlenk manifold upon which chloro methyl methyl sulfide (25.1 µL, 0.300 mmol, 3.0 equiv.) was added and the reaction mixture turned colorless. The mixture was allowed to stir for 3 hours before the reaction was quenched with a 1 M hydrochloric acid solution (5 mL). The aqueous layer was extracted with hexanes (3x10 mL) and the combined organic layers were brine-washed, dried over magnesium sulfate, then concentrated *in vacuo* to yield a white solid. The crude product was further purified by flash chromatography using a gradient from 100% hexanes to 35% dichloromethane in hexanes to yield **19** as a white solid (0.020 g, 28% yield). ^{1}H NMR (400 MHz, $CDCl_3$) δ 2.25 (s, 6H), 2.19 (s, 9H), 0.50 (s, 9H), 0.48 (s, 9H), 0.46 (s, 18H), 0.27 (s, 9H). ^{13}C NMR (101 MHz, $CDCl_3$) δ 22.20, 15.59, 4.55, 1.66, 0.37, 0.07. ^{29}Si-DEPT NMR (119 MHz, $CDCl_3$) δ -3.89, -28.83, -31.08, -67.90, -123.10. HRMS (TOF MS ASAP+) for $[C_{21}H_{61}S_3Si_{11}]$: calculated = 717.1397, found = 717.1365 $[M+H]^+$

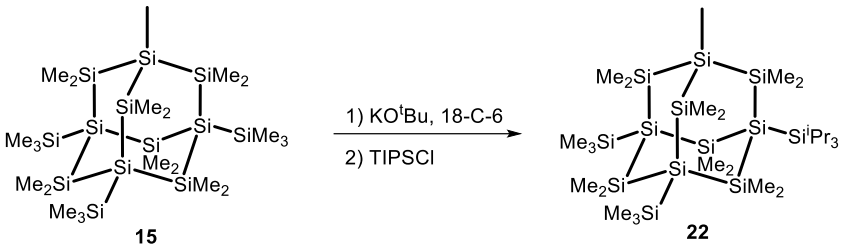
20 *(1-, 3- ,5-, 7-$(CH_2SMe)_4$-SiAd)*



An oven-dried 10 mL Schlenk flask equipped with a stir bar was brought into a glovebox and charged with **2** (0.050 g, 0.066 mmol 1.0 equiv.), potassium tert-butoxide (0.030 g, 0.27 mmol, 4.0 equiv.), 18-crown-6 (0.070 g, 0.27 mmol, 4.0 equiv.) and toluene (3 mL). The resulting dark orange mixture was left to stir for 16 hours. Then, the flask was taken out of the glovebox and connected to a Schlenk manifold upon which chloromethyl methyl sulfide (22.2 µL, 0.27 mmol, 4.0 equiv.) was added and the reaction mixture turned colorless. The mixture was stirred for 3 hours before the reaction was quenched with a 1 M hydrochloric acid solution (5 mL). The aqueous layer was extracted with hexanes (3 x 10 mL) and the combined organic layers were brine-washed, dried over magnesium sulfate, then concentrated *in vacuo* to yield a colorless oil. The crude product was further purified by flash chromatography using a gradient from 100% hexanes to 40% dichloromethane in hexanes to yield **20** as a white waxy solid (0.017 g, 36% yield). ^{1}H NMR (400 MHz, $CDCl_3$) δ 2.26 (s, 8H), 2.19 (s, 12H), 0.48 (s, 36H). ^{13}C NMR (101 MHz, $CDCl_3$) δ 22.19, 15.13, 0.08. ^{29}Si-DEPT NMR (119 MHz, $CDCl_3$) δ -30.99, -69.88. HRMS (TOF MS ASAP+) for $[C_{20}H_{57}S_4Si_{10}]$: calculated = 705.1036, found = 705.1039 $[M+H]^+$. Crystals

suitable for single-crystal X-ray diffraction studies were grown by methanol vapor diffusion into a concentrated toluene solution.

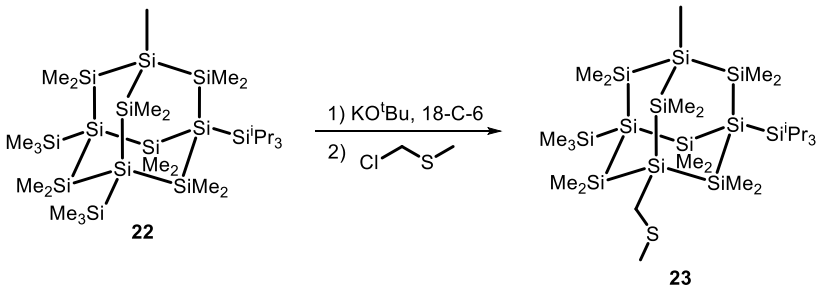
Preparation of ***22*** *(1Me-3Si^{i}Pr$_3$-SiAd)*



An oven-dried 10 mL Schlenk flask equipped with a stir bar was brought into a glovebox and charged with **15** (0.17 g, 0.25 mmol, 1.0 equiv.), potassium tert-butoxide (0.028 g, 0.25 mmol, 1.0 equiv.), 18-crown-6 (0.065 g, 0.25 mmol, 1.0 equiv.) and toluene (2 mL). The resulting orange mixture was left to stir for 16 hours. Then, the flask was taken out of the glovebox, and connected to a Schlenk manifold upon which chlorotriisopropylsilane (22.0 µL, 0.25 mmol, 1.0 equiv.) was added the reaction mixture that turned colorless over a 3-hour time period. The reaction was then quenched with a 1 M hydrochloric acid solution (5 mL). The aqueous layer was extracted with hexanes (3x10 mL) and the combined organic layers were brine-washed, dried over magnesium sulfate, then concentrated *in vacuo* to yield a white solid. The crude product was further purified by recrystallization in ethanol to yield **22** as a white solid (0.090 g, 44% yield). ^{1}H NMR (400 MHz, C_6D_6) δ 1.36 – 1.32 (m, 3H, overlapping with grease), 1.28 – 1.26 (d, J = 8, 18H), 0.63 (s, 6H), 0.62 (s, 6H), 0.61 (s, 3H), 0.60 (s, 3H), 0.54 (s, 6H), 0.51 (s, 12H), 0.37 (s, 18H), 0.34 (s, 3H). ^{13}C NMR (151 MHz, C_6D_6) δ 20.50, 15.35, 5.50, 5.30, 5.04, 4.08, 3.91, 2.16, 1.18, 1.05, -

13.68. ^{29}Si-DEPT NMR (119 MHz, C_6D_6) δ 16.47, -4.72, -24.02, -26.33, -29.10, -30.34, -72.58, -113.83, -114.79. HRMS (TOF MS ASAP+) for [$C_{27}H_{75}Si_{13}$]: calculated = 763.2869, found = 763.2884 $[M\text{-}CH_3]^+$

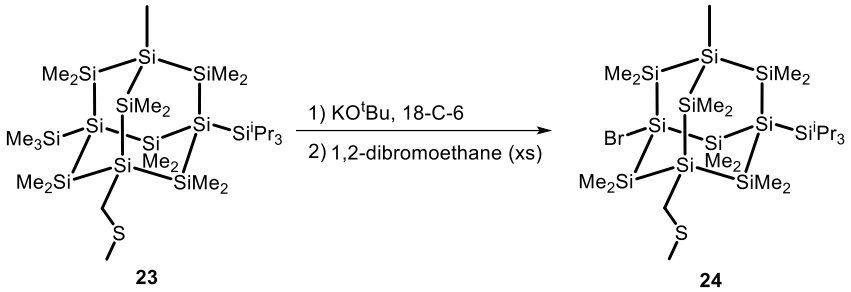
Preparation of ***23*** *(1Me-3Si^{i}Pr$_3$-5SMe-SiAd)*



An oven-dried 10 mL Schlenk flask equipped with a stir bar was brought into a glovebox and charged with **22** (0.090 g, 0.12 mmol, 1.0 equiv.), potassium tert-butoxide (0.013 g, 0.12 mmol, 1.0 equiv.) and 18-crown-6 (0.030 g, 0.12 mmol, 1.0 equiv.). The resulting orange mixture was left to stir for 16 hours. Then, the flask was taken out of the glovebox, and connected to a Schlenk manifold upon which chloro methyl methyl sulfide (9.6 µL, 0.12 mmol, 1.0 equiv.) was added and the reaction mixture turned colorless. The mixture was allowed to stir for 3 hours before the reaction was quenched with a 1 M hydrochloric acid solution (5 mL). The aqueous layer was extracted with hexanes (3x10 mL) and the combined organic layers were brine-washed, dried over magnesium sulfate, then concentrated *in vacuo* to yield **23** as a waxy, white solid. (0.063 g, 71% yield). ^{1}H NMR (600 MHz, C_6D_6) δ 2.34 (s, 2H), 1.93 (s, 3H), 1.37 – 1.35 (m, 3H, overlapping with grease), 1.26 – 1.25 (d, J = 6 Hz, 18H), 0.73 (s, 3H), 0.68 (s, 3H), 0.65 (s, 3H), 0.65 (s, 3H), 0.65 (s, 3H), 0.60 (s, 3H), 0.59 (s, 3H), 0.59 (s, 3H), 0.53 (s, 3H), 0.52 (s, 3H), 0.50 (s, 3H),

0.49 (s, 3H), 0.35 (s, 9H), 0.29 (s, 3H). ^{13}C NMR (151 MHz, C_6D_6) δ 21.93, 20.46, 16.31, 15.34, 14.40, 5.33, 4.95, 3.20, 2.88, 2.73, 2.18, 1.98, 1.72, 1.19, 0.90, 0.18, -0.55, -13.37. ^{29}Si-DEPT NMR (79 MHz, C_6D_6) δ 16.68, -4.19, -23.65, -27.47, -28.58, -28.80, -29.91, -31.13, -66.70, -70.01, -115.49, -116.45. HRMS (TOF MS ASAP+) for [$C_{27}H_{75}Si_{12}S$]: calculated = 767.2820 found = 767.2878 $[M+H]^+$

Preparation of ***24*** *(1-Me, 3-Si^{i}Pr$_3$, 5-CH$_2$SMe, 7-Br-SiAd)*



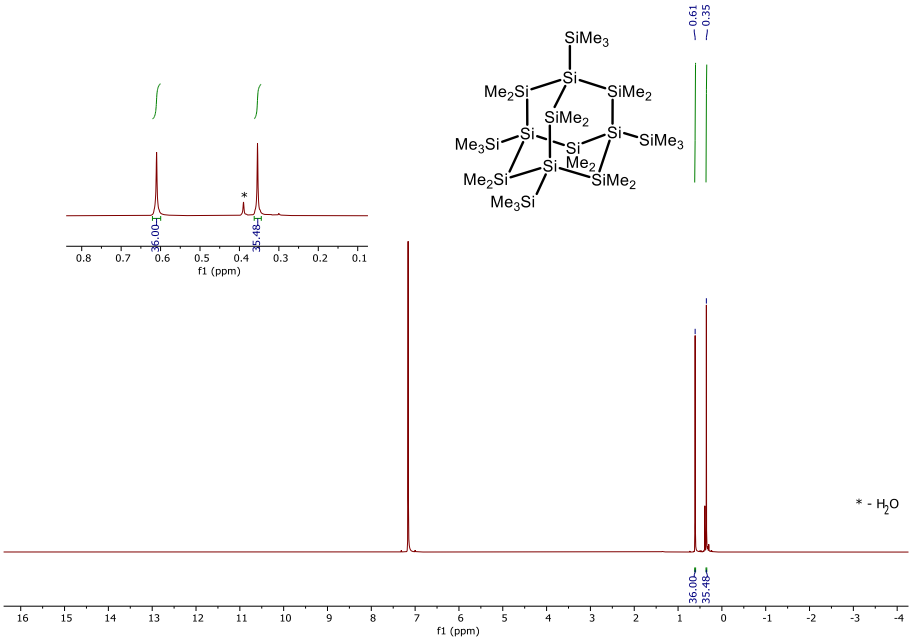
An oven-dried 10 mL Schlenk flask equipped with a stir bar was brought into a glovebox and charged with **23** (0.062 g, 0.081 mmol, 1.0 equiv.), potassium tert-butoxide (0.0091 g, 0.081 mmol, 1.0 equiv.), 18-crown-6 (0.021 g, 0.081 mmol, 1.0 equiv.) and toluene (2 mL). The resulting orange mixture was left to stir for 16 hours. Then, the flask was taken out of the glovebox and connected to a Schlenk manifold upon which excess 1,2-dibromoethane (0.14 mL, 1.61 mmol, 20 equiv.) was added the reaction mixture and the mixture turned colorless. The mixture was allowed to stir for 3 hours before being concentrated to dryness. The resulting salts were washed with dry pentane and the mixture was syringe filtered with a 0.22 μm syringe filter. Upon evaporation of the pentane filtrate, **24** was obtained as a white semisolid (0.060 g, 96% yield). ^{1}H NMR (400 MHz, C_6D_6) δ 2.28 (s, 2H), 1.91 (s, 3H), 1.37 – 1.36 (m, 3H, overlapping with grease), 1.20 (d, J = 5.8 Hz, 18H), 0.76 (s, 3H),

0.67 (s, 3H), 0.66 (s, 3H), 0.65 (s, 3H), 0.61 (s, 3H), 0.60 (s 3H), 0.59 (s, 3H), 0.53 (s, 3H), 0.50 (s, 3H), 0.49 (s, 3H), 0.46 (s, 3H), 0.46 (s, 3H), 0.26 (s, 3H). ^{13}C NMR (151 MHz, C_6D_6) δ 21.78, 20.29, 16.10, 15.39, 14.42, 2.92, 2.69, 1.93, 1.74, 1.45, 0.14, -0.10, -1.13, -1.17, -1.59, -1.94, -13.06. ^{29}Si-DEPT NMR (119 MHz, C_6D_6) δ 17.89, -9.69, -26.92, -27.07, -28.04, -29.19, -29.44, -31.52, -65.91, -70.32, -122.22. HRMS (TOF MS ASAP+) for [$C_{24}H_{66}Si_{11}BrS$]: calculated = 773.1531, found = 773.1540 $[M+H]^+$. Crystals suitable for single-crystal X-ray diffraction studies were grown by methanol vapor diffusion into a concentrated toluene solution.

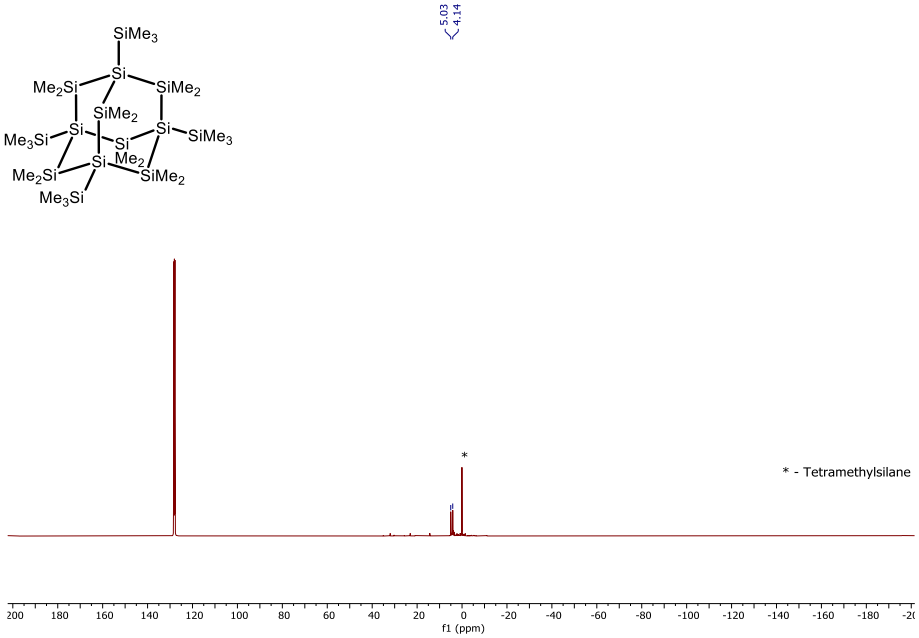
NMR Spectra

NMR Spectra of **2**

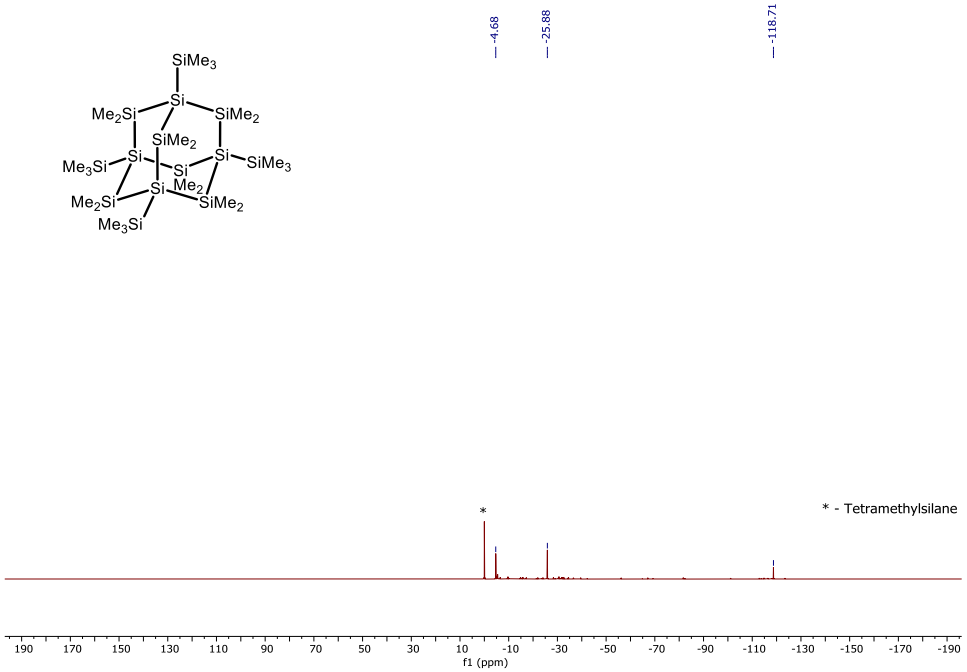
^{1}H NMR Spectrum (400 MHz, C_6D_6):



^{13}C NMR Spectrum (101 MHz, C_6D_6):

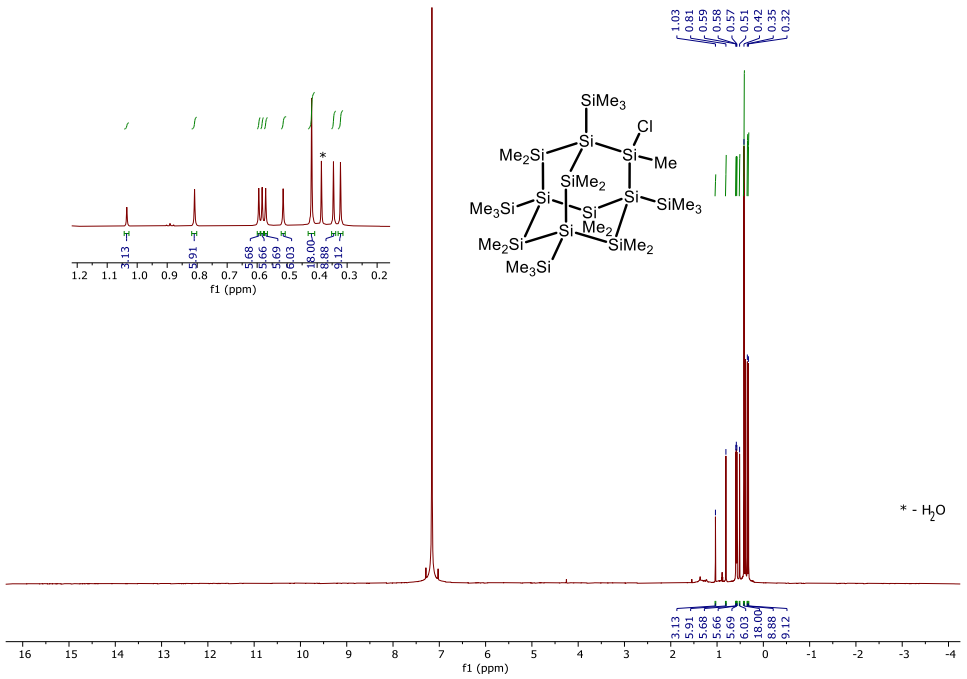


^{29}Si-DEPT NMR Spectrum (79 MHz, C_6D_6):

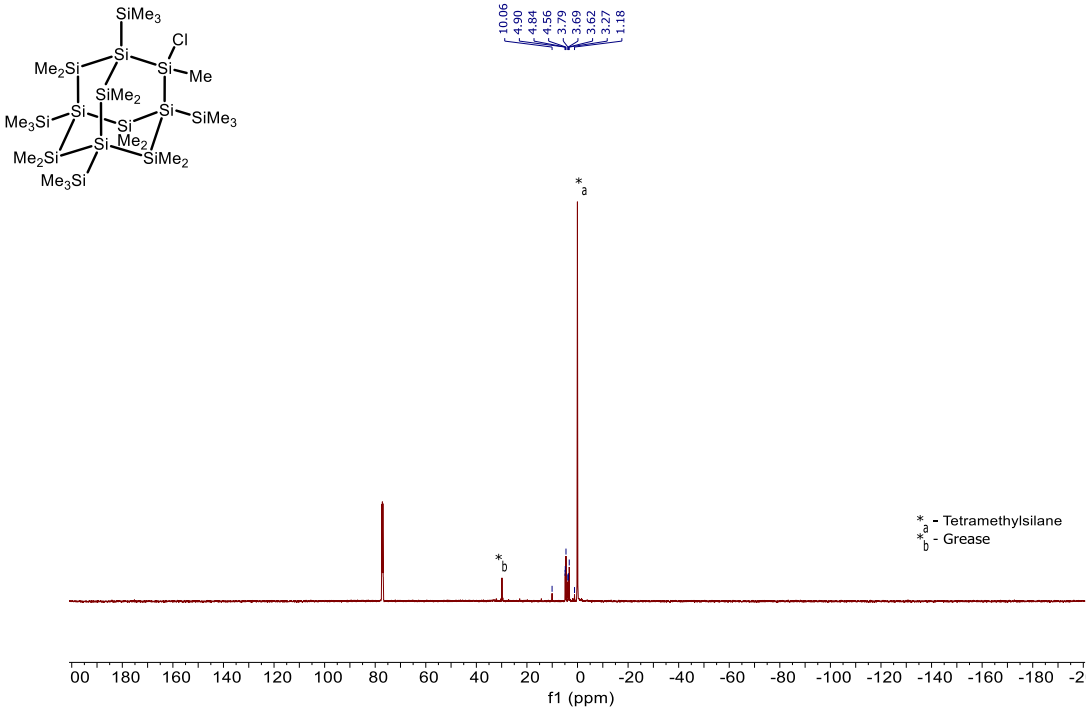


NMR Spectra of **3** (*2Cl-SiAd*)

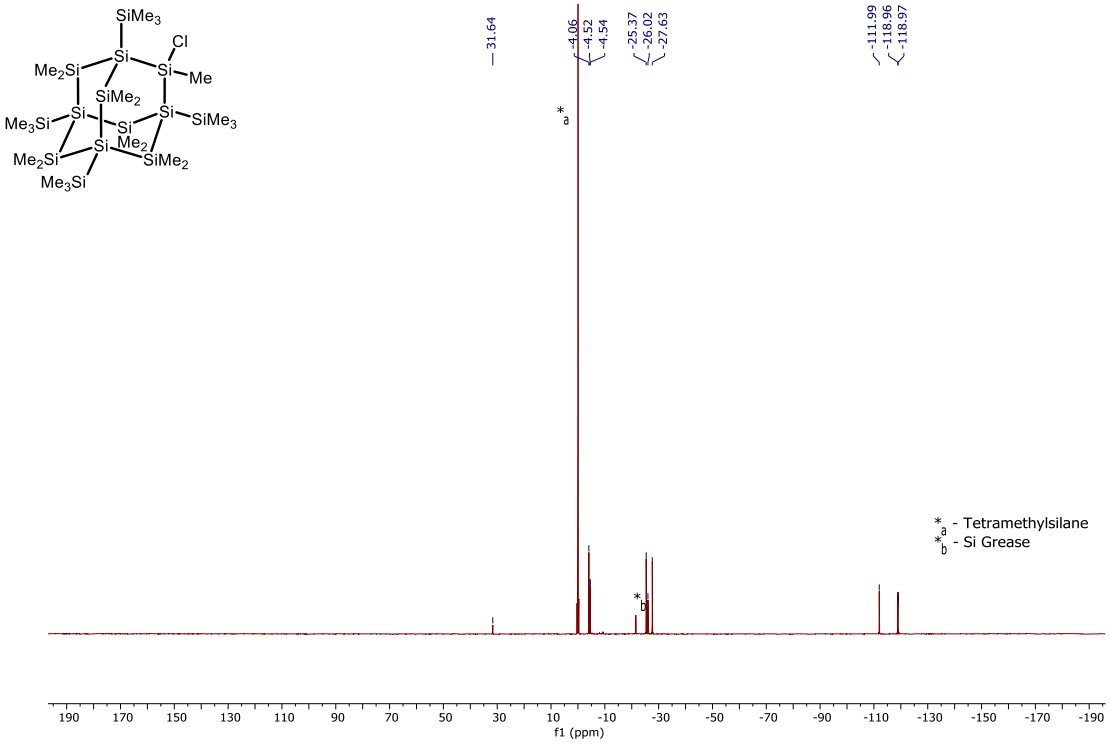
^{1}H NMR Spectrum (600 MHz, C_6D_6):



^{13}C NMR Spectrum (151 MHz, $CDCl_3$):

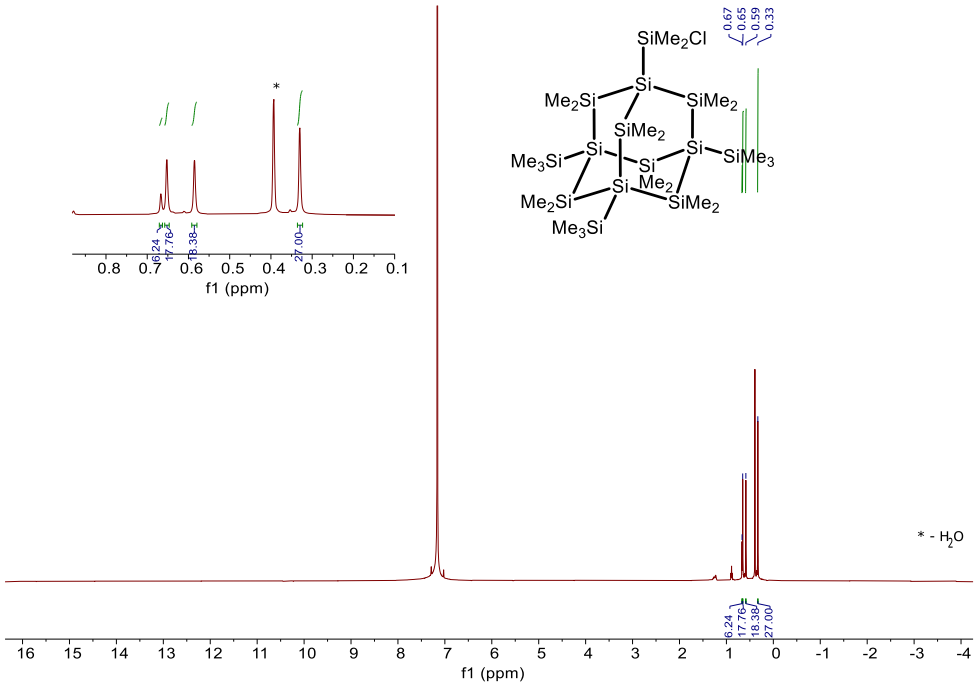


^{29}Si-DEPT NMR Spectrum (79 MHz, $CDCl_3$):

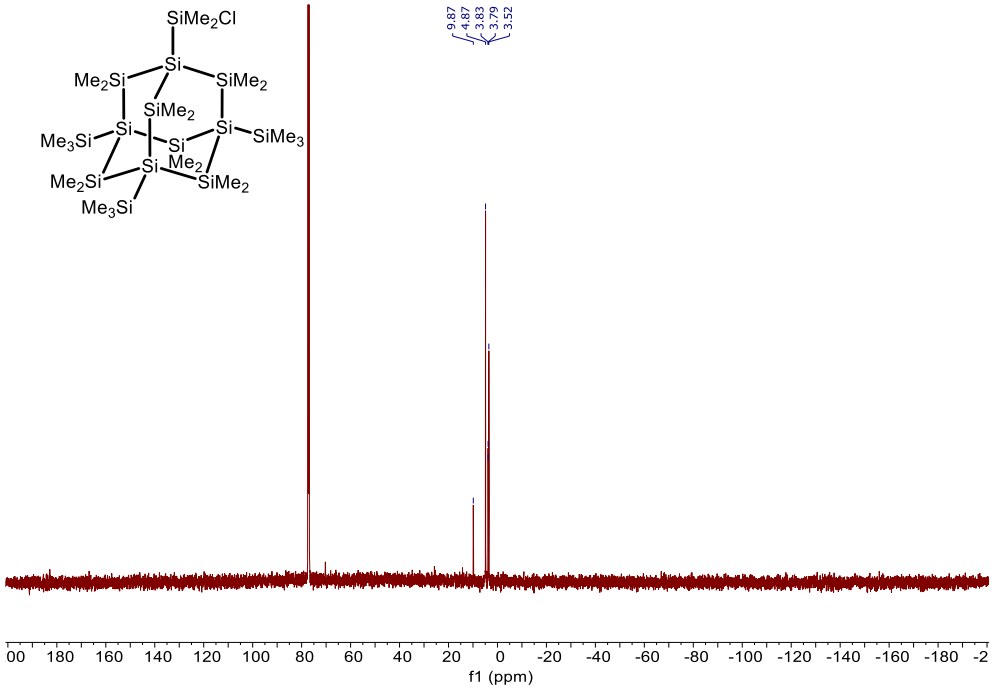


NMR Spectra of **4** (*1SiMe$_2$Cl-SiAd*)

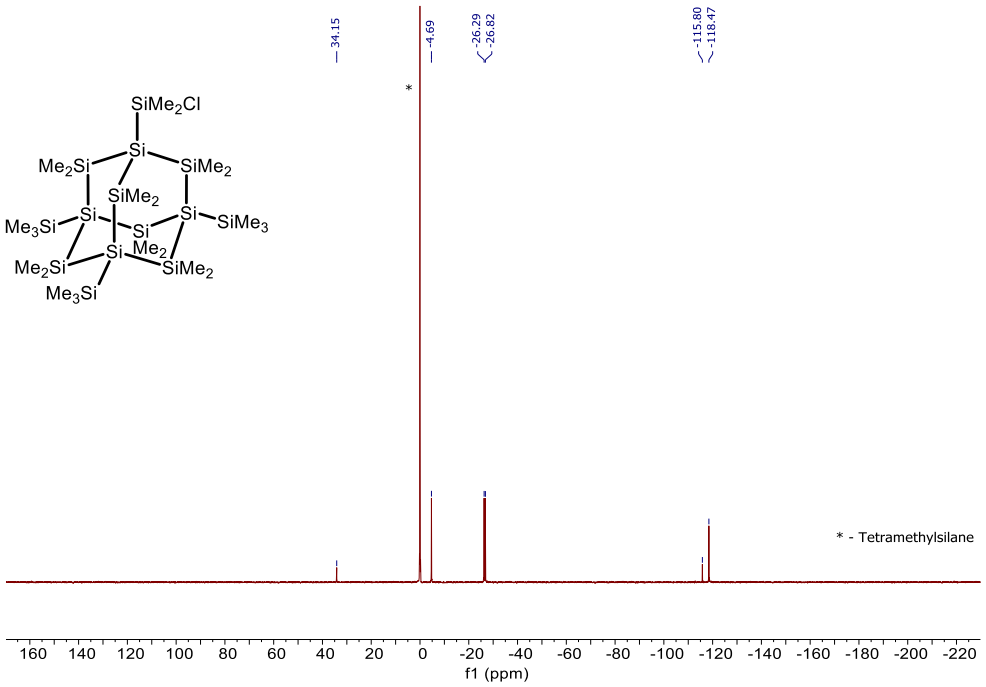
^{1}H NMR Spectrum (600 MHz, C_6D_6)



^{13}C NMR Spectrum (151 MHz, $CDCl_3$):

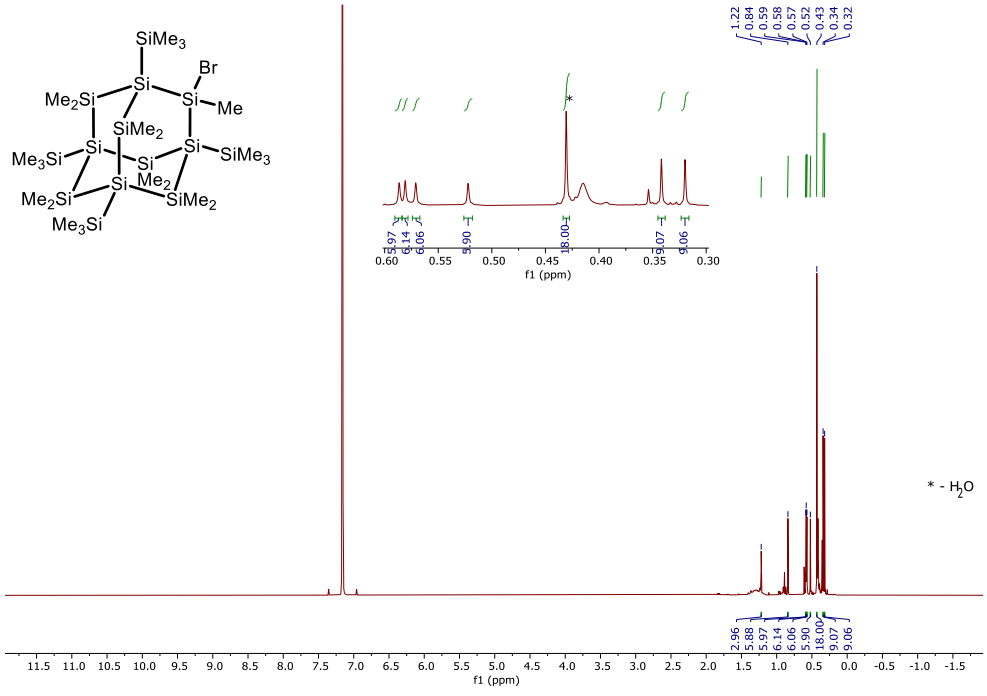


^{29}Si-DEPT NMR Spectrum (119 MHz, $CDCl_3$)

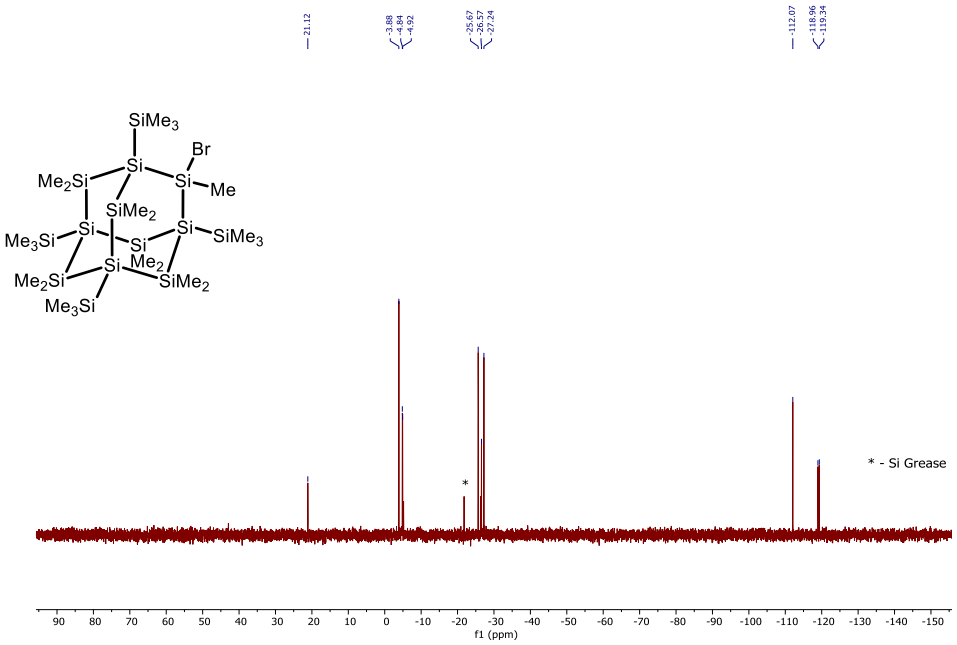


NMR Spectra of **7** (*2Br-SiAd*)

^{1}H NMR Spectrum (400 MHz, C_6D_6)

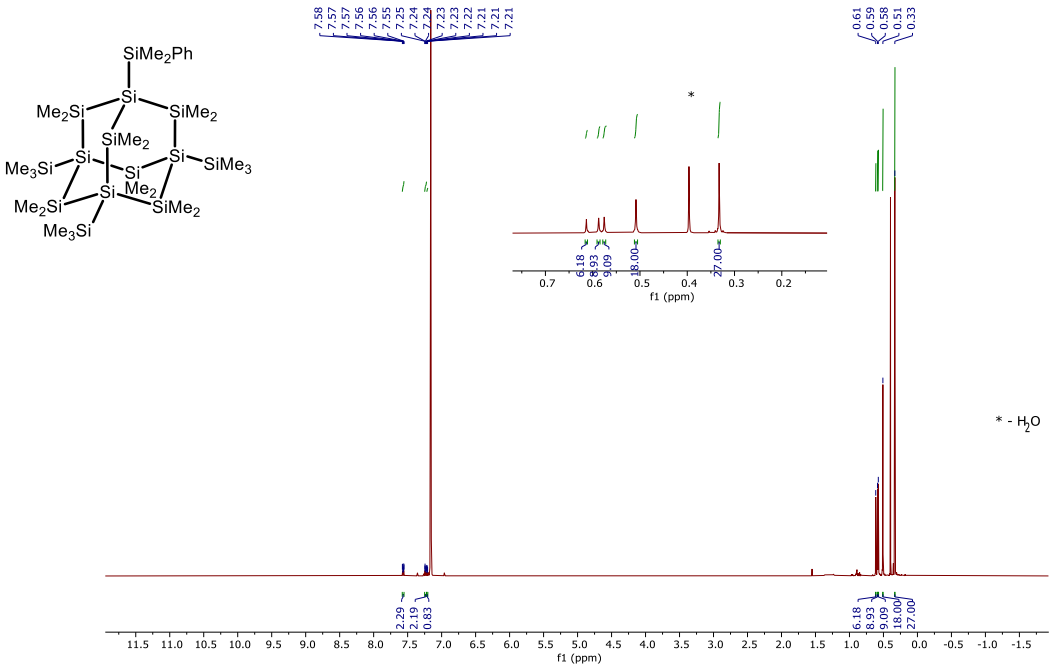


^{29}Si-DEPT NMR Spectrum (79 MHz, C_6D_6):

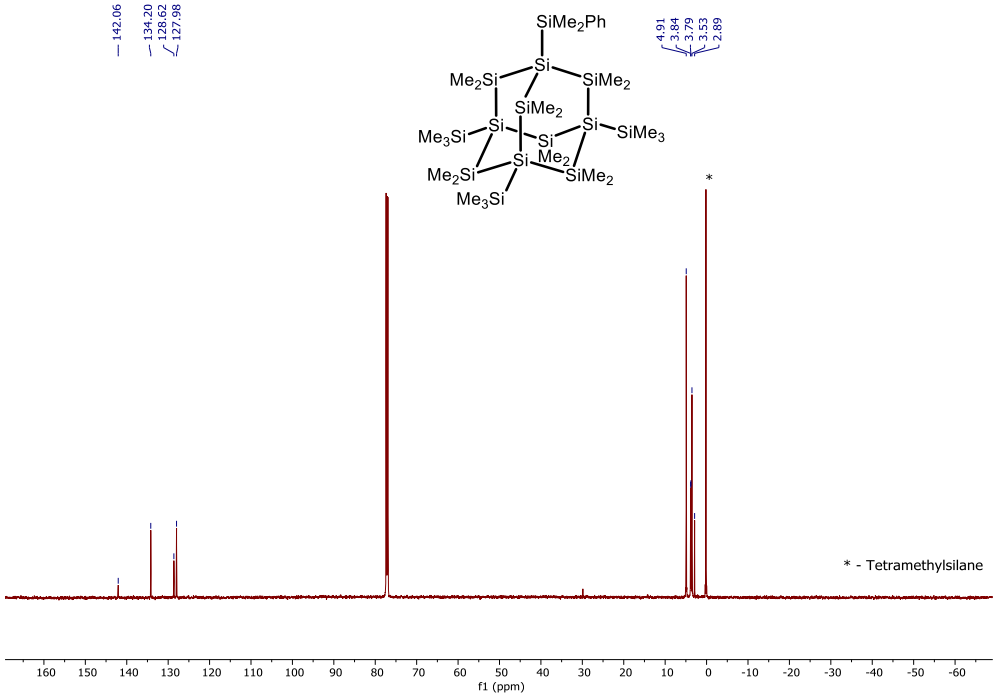


NMR Spectra of **8** (*1SiMe$_2$Ph-SiAd*)

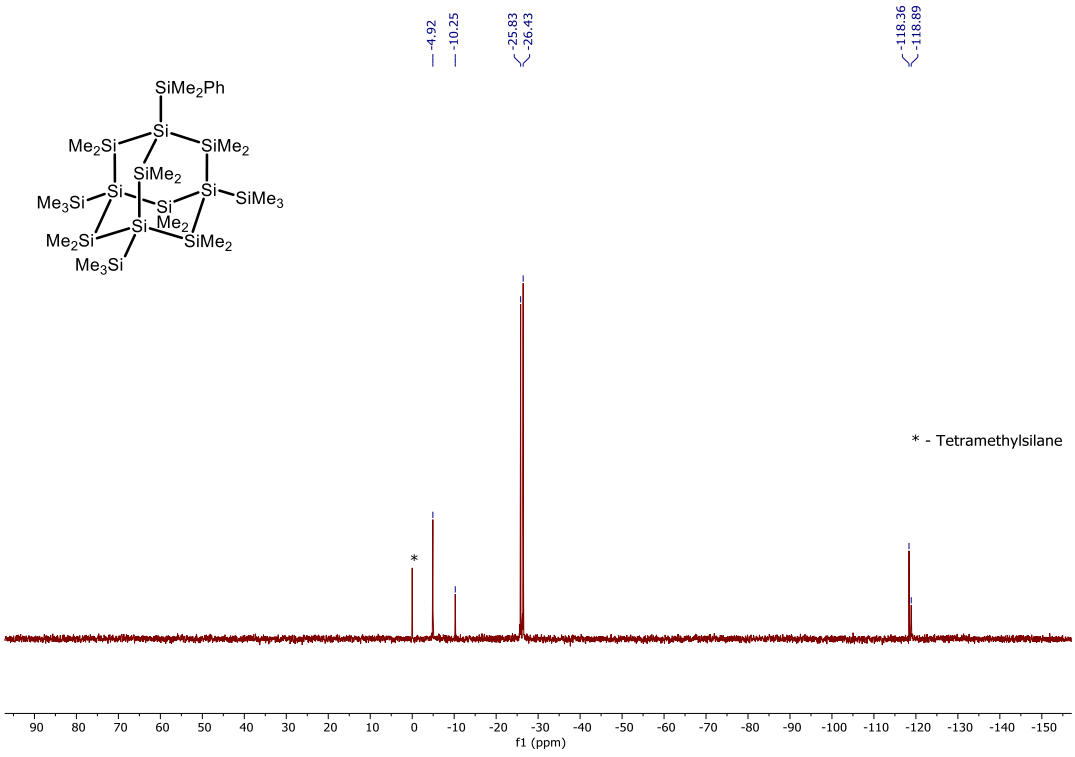
^{1}H NMR Spectrum (400 MHz, C_6D_6):



^{13}C NMR Spectrum (151 MHz, $CDCl_3$):

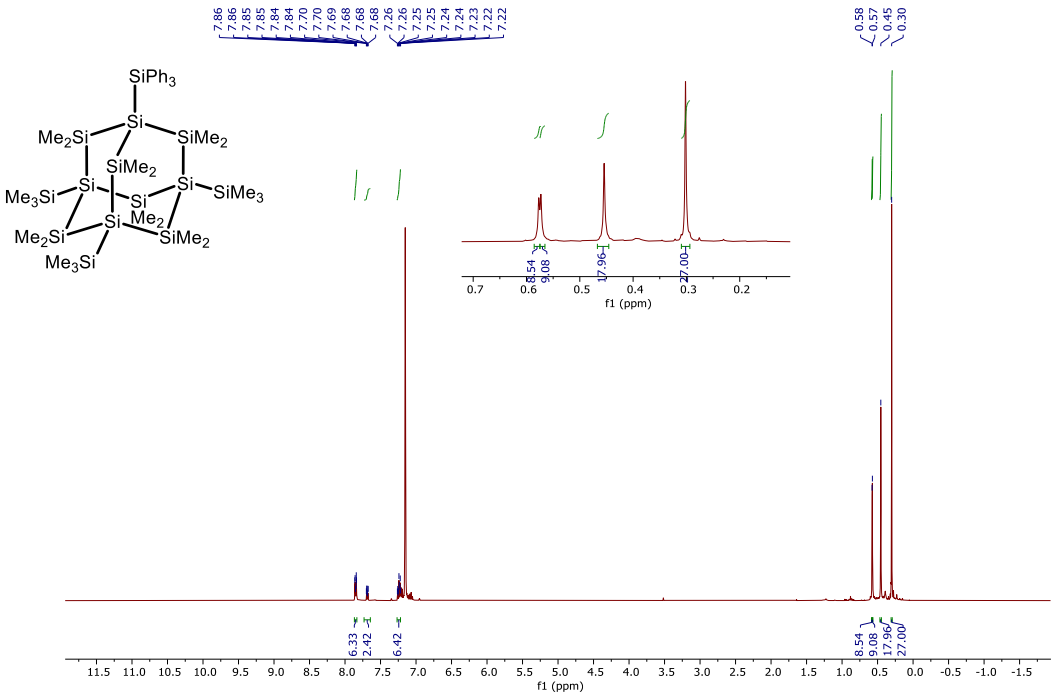


^{29}Si-DEPT NMR Spectrum (119 MHz, $CDCl_3$):

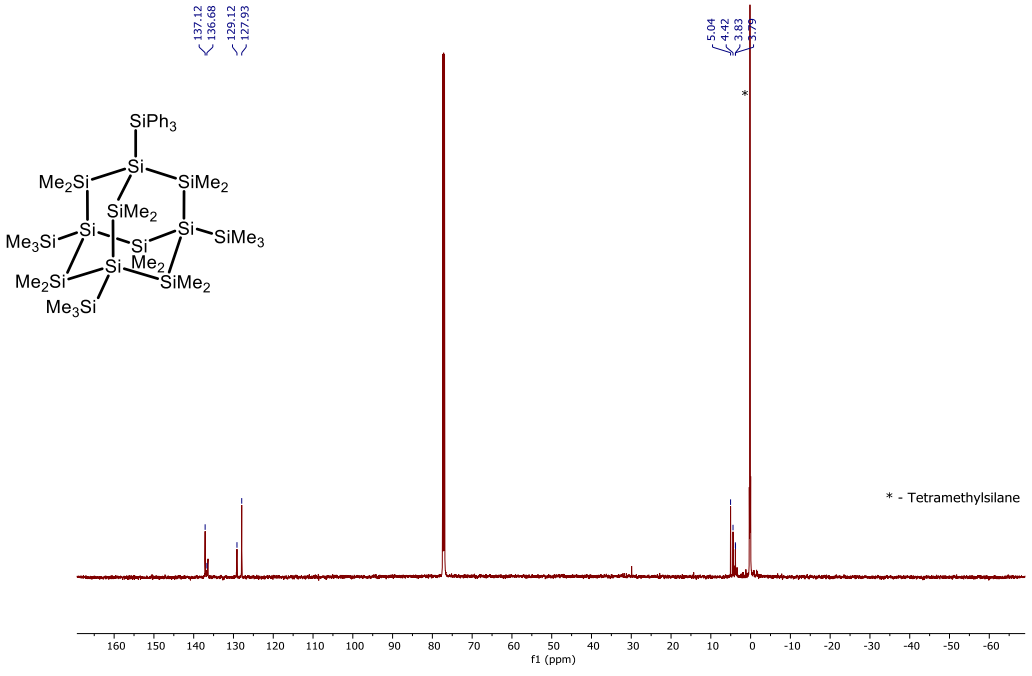


NMR Spectra of **9** (*1SiPh₃-SiAd*)

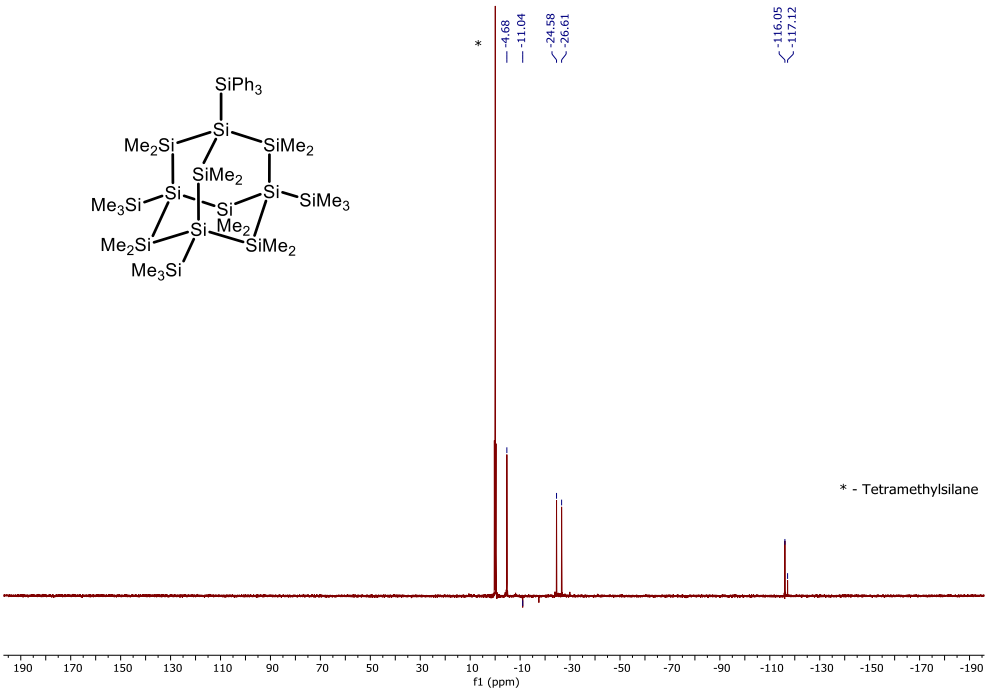
^{1}H NMR Spectrum (400 MHz, C_6D_6):



^{13}C NMR Spectrum (151 MHz, C_6D_6):

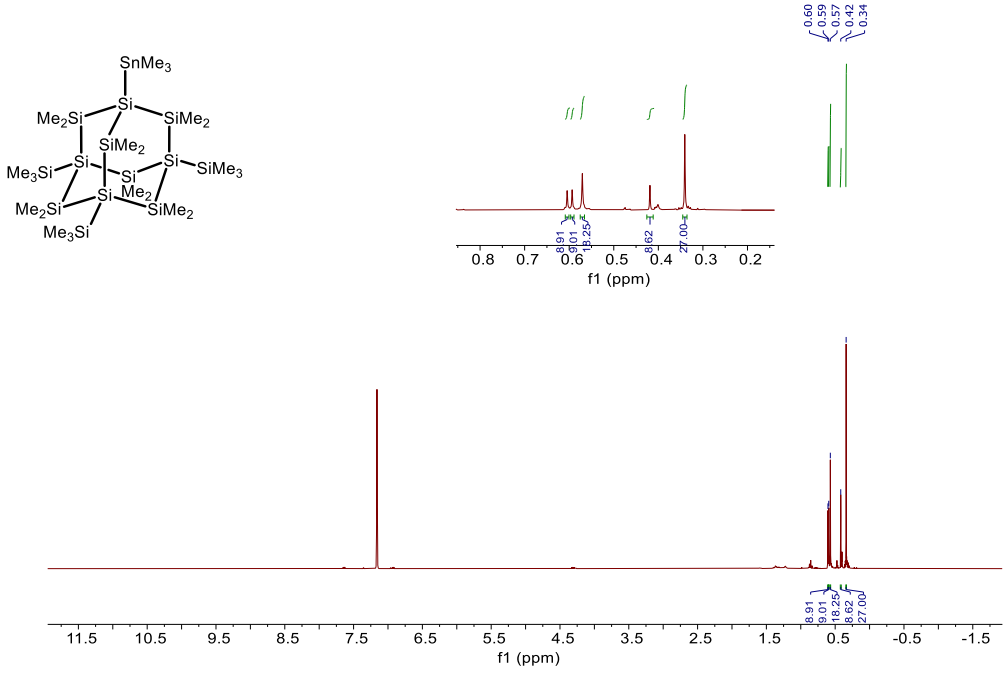


^{29}Si-DEPT NMR Spectrum (79 MHz, C_6D_6):

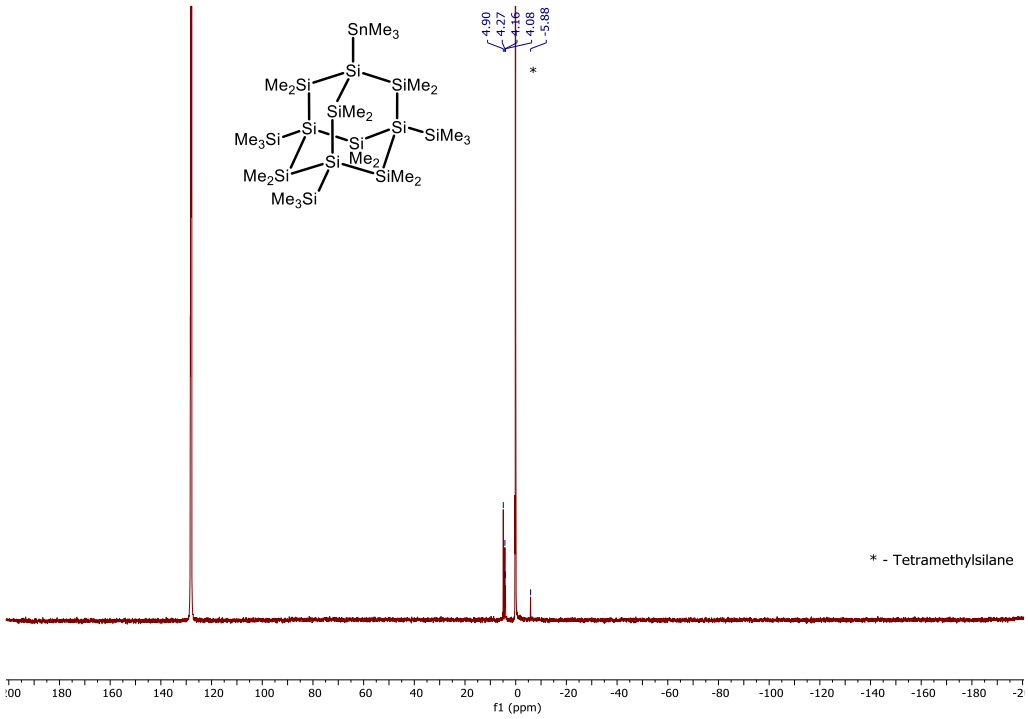


NMR Spectra of **10** (*1SnMe$_3$-SiAd*)

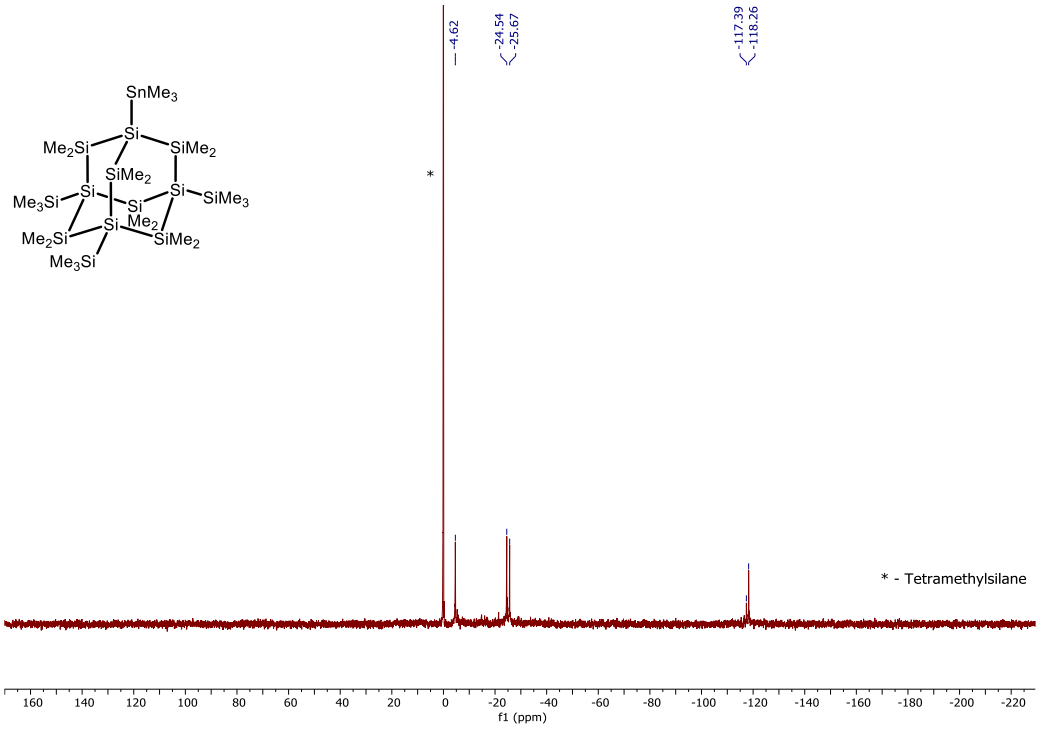
^{1}H NMR Spectrum (400 MHz, C_6D_6):



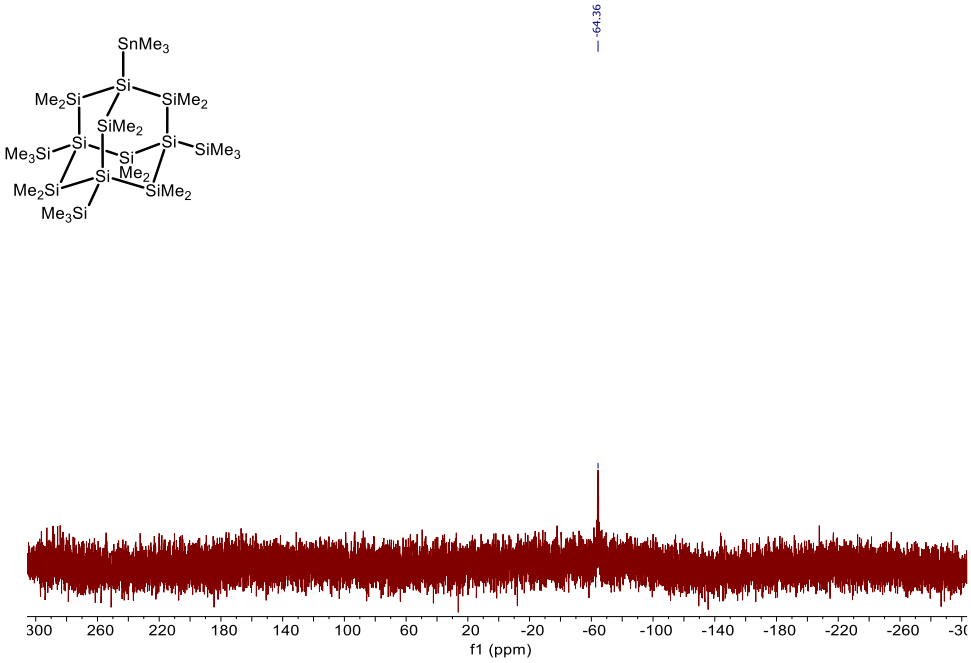
^{13}C NMR Spectrum (151 MHz, C_6D_6):



^{29}Si-DEPT NMR Spectrum (119 MHz, C_6D_6):

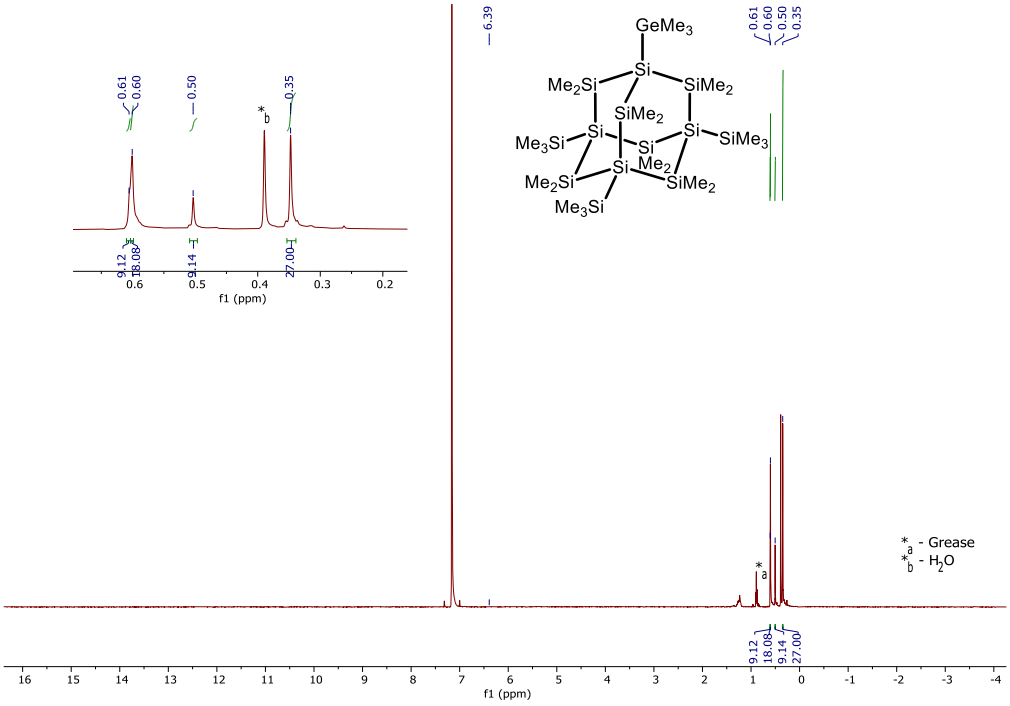


^{119}Sn NMR Spectrum (149 MHz, C_6D_6):

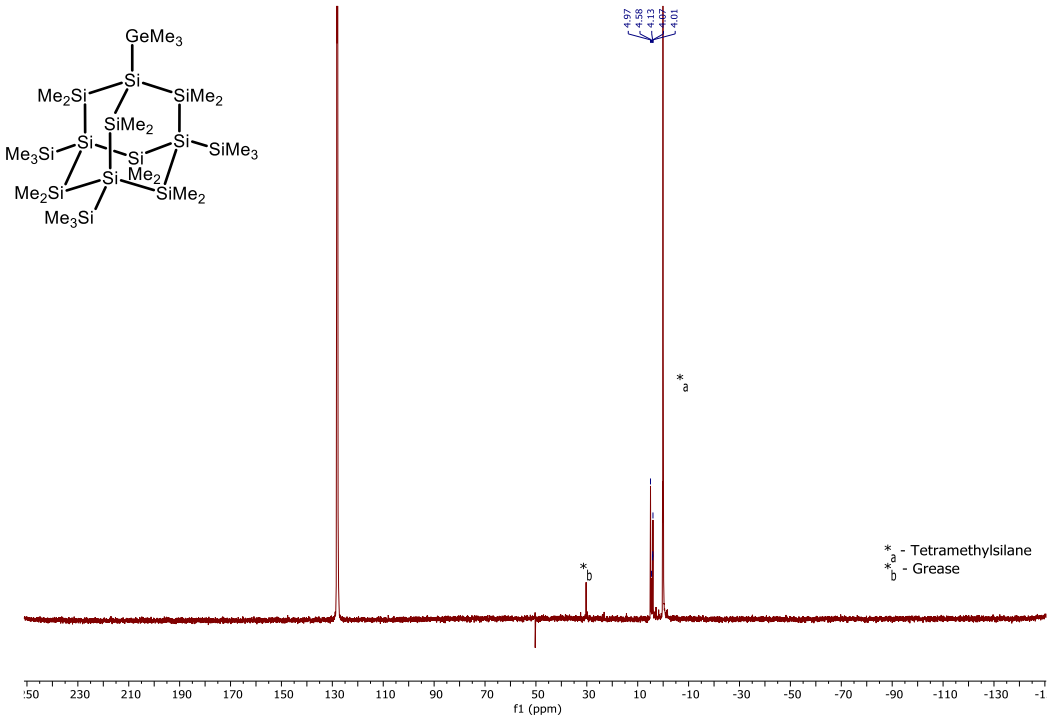


NMR Spectra of **11** (*1GeMe₃-SiAd*)

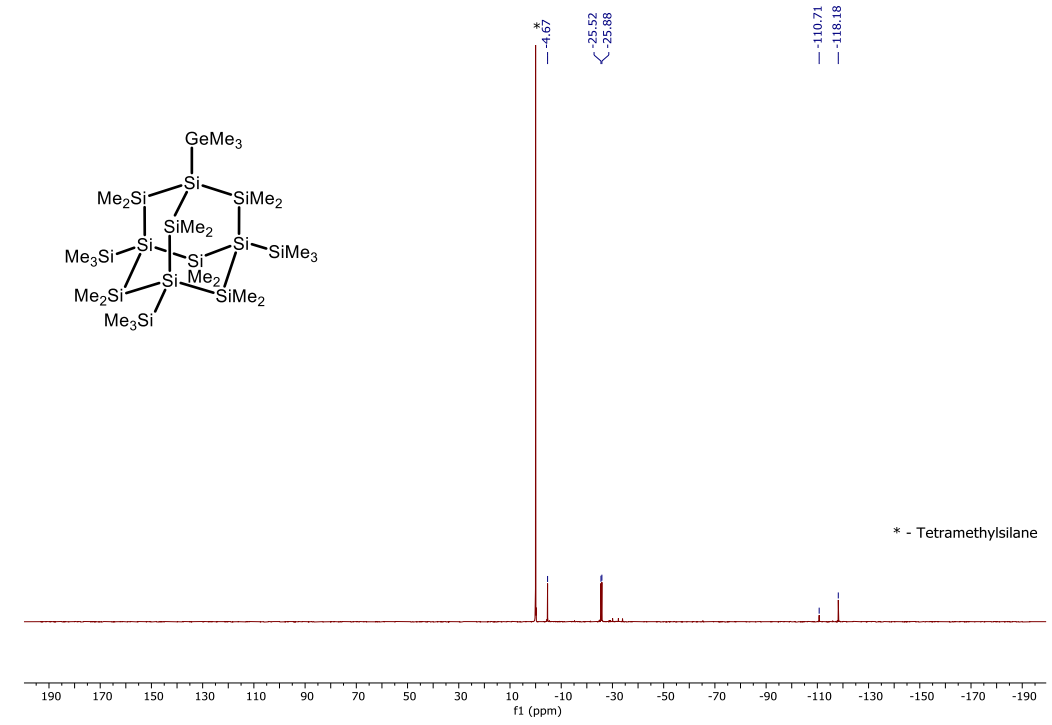
^{1}H NMR Spectrum (600 MHz, C_6D_6):



^{13}C NMR Spectrum (151 MHz, C_6D_6):

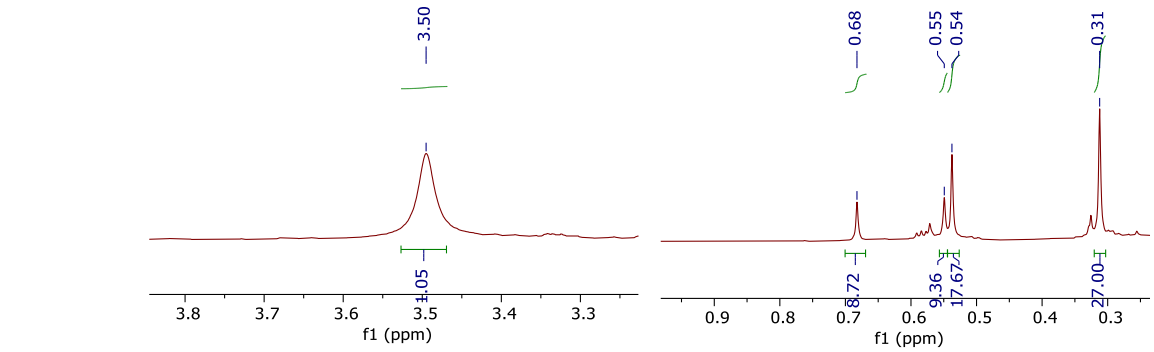


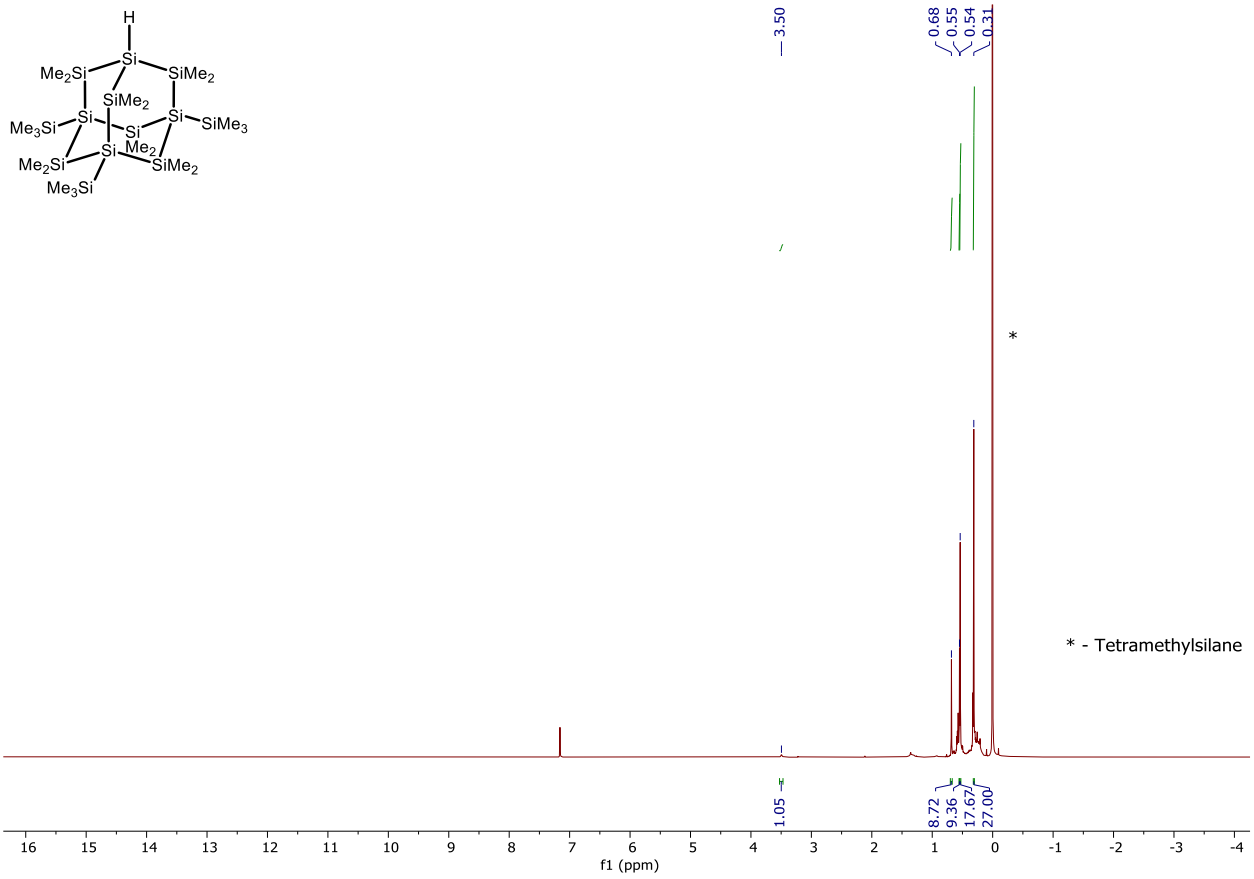
^{29}Si-DEPT NMR Spectrum (119 MHz, C_6D_6):



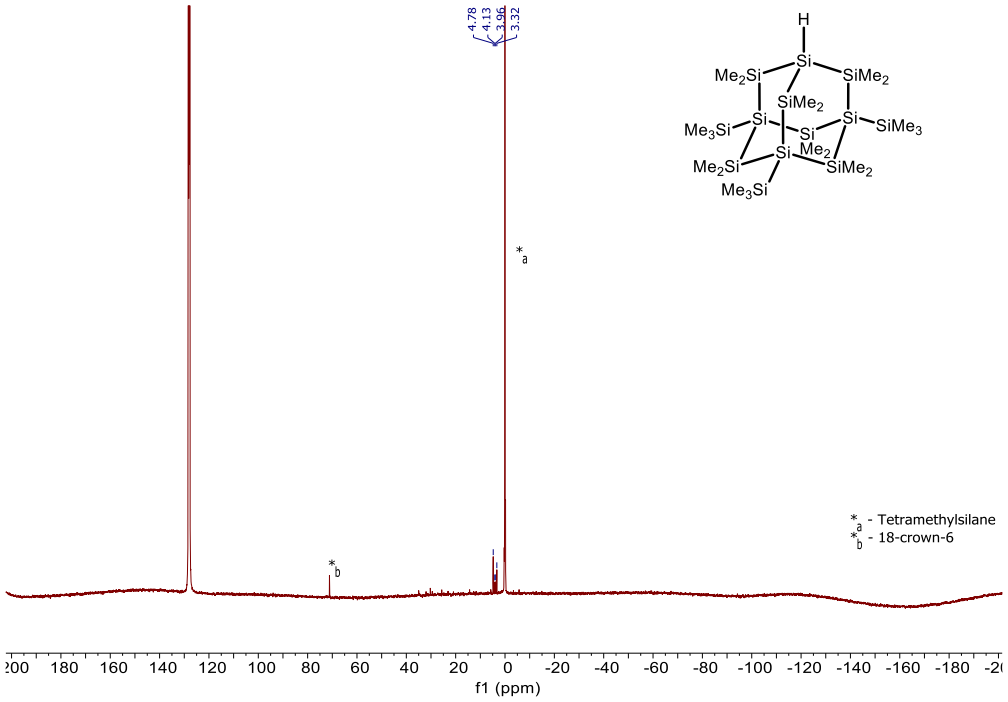
NMR Spectra of **12** (*1H-SiAd*)

^{1}H NMR Spectrum (600 MHz, C_6D_6):

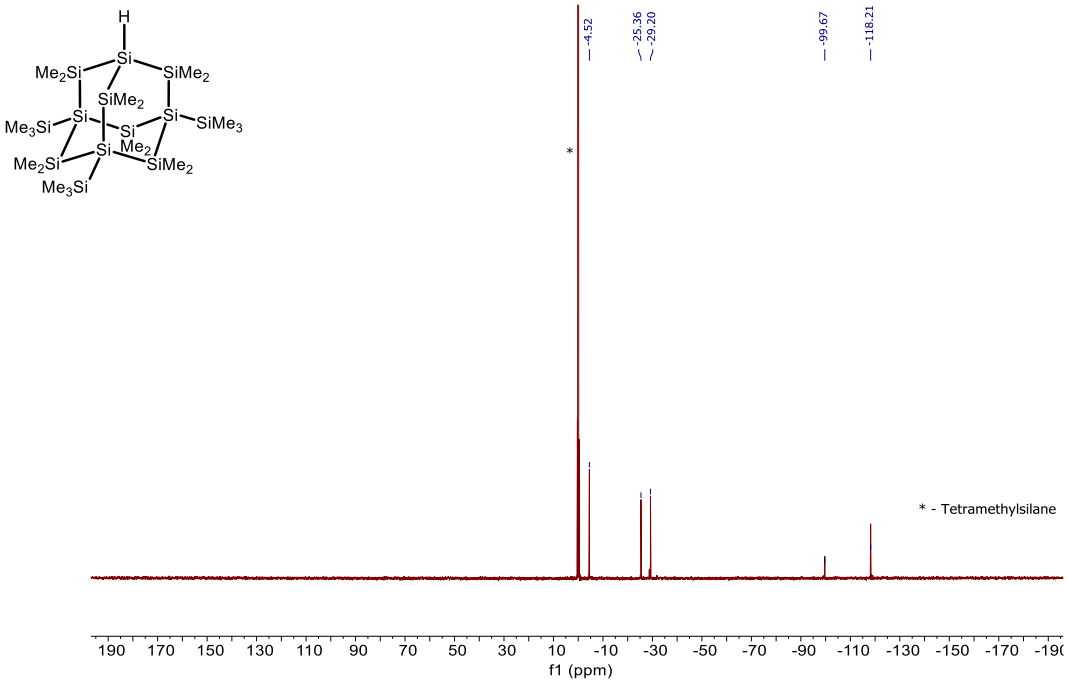




^{13}C NMR Spectrum (101 MHz, C_6D_6):

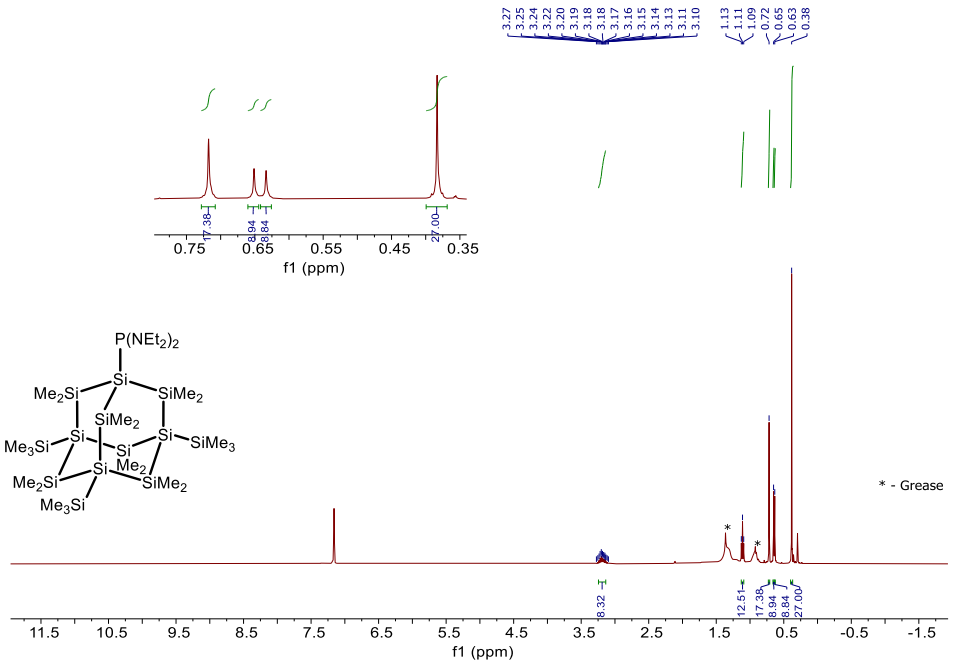


^{29}Si-DEPT NMR Spectrum (79 MHz, C_6D_6):

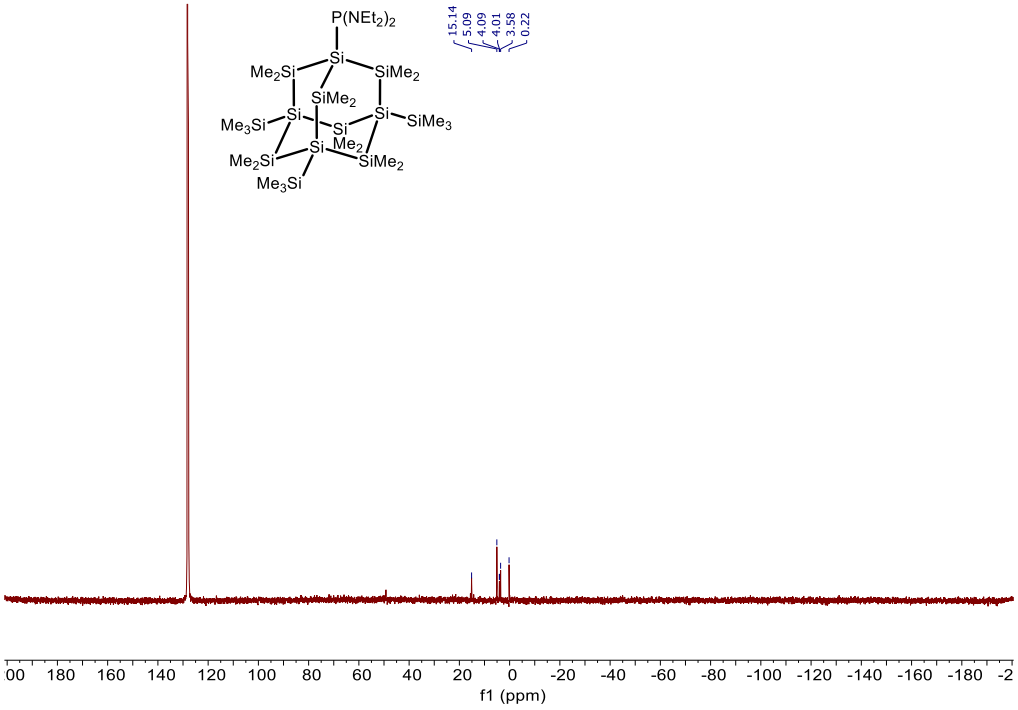


NMR Spectra of **13** (*1P(NEt$_2$)$_2$-SiAd*)

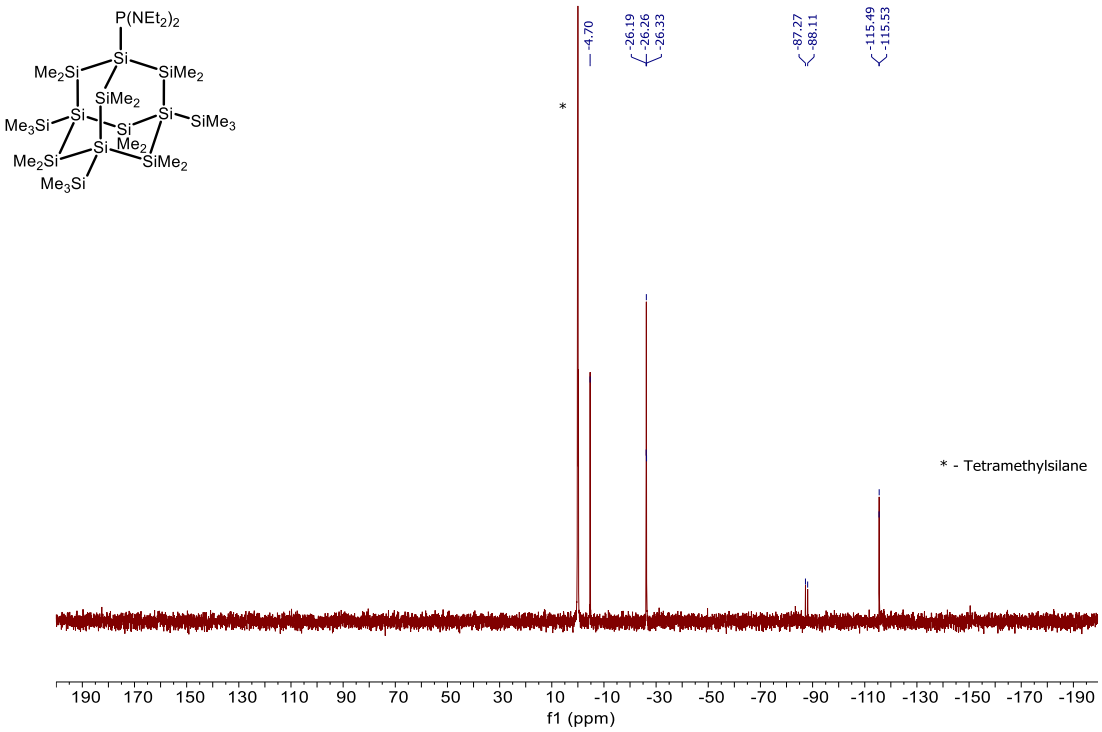
^{1}H NMR Spectrum (400 MHz, C_6D_6):



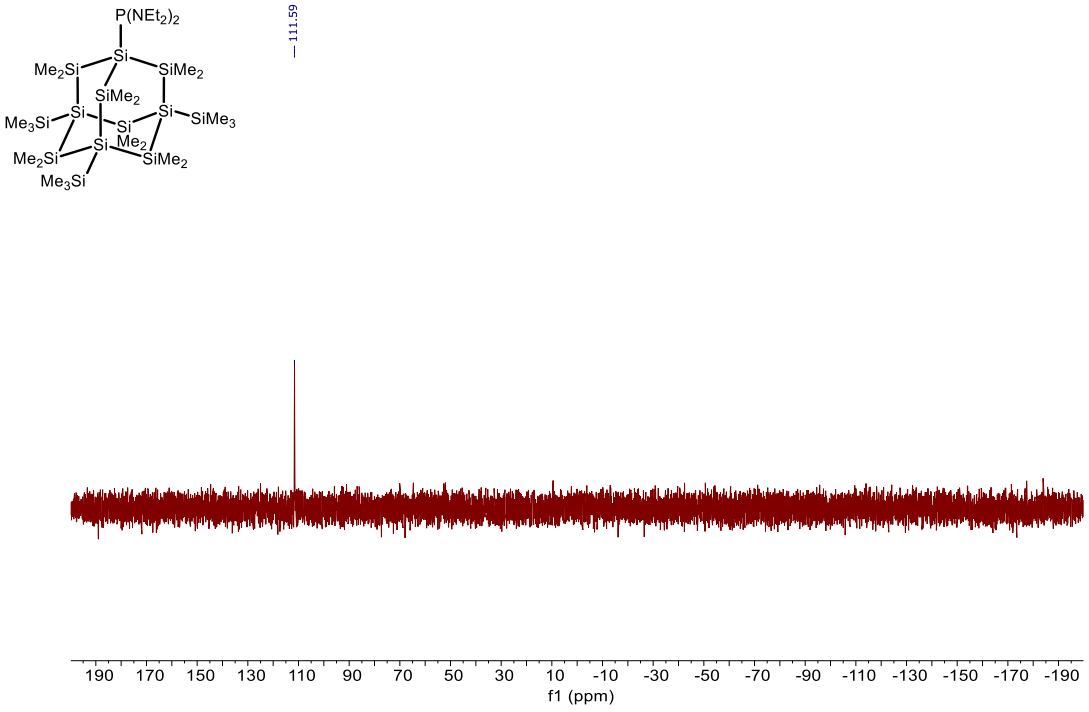
^{13}C NMR Spectrum (151 MHz, C_6D_6):



^{29}Si-DEPT NMR Spectrum (119 MHz, C_6D_6):

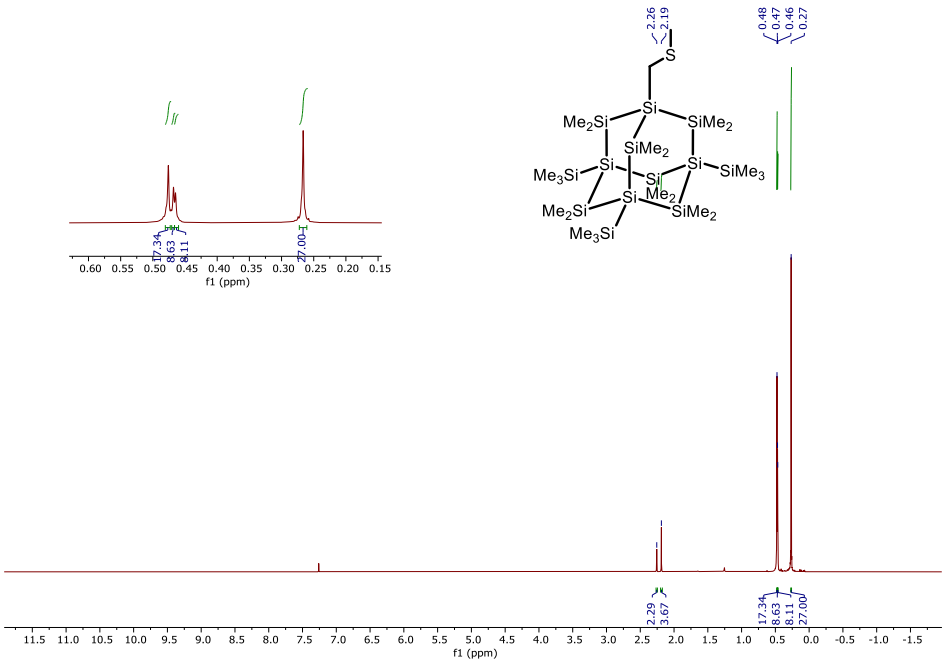


^{31}P NMR Spectrum (243 MHz, C_6D_6):

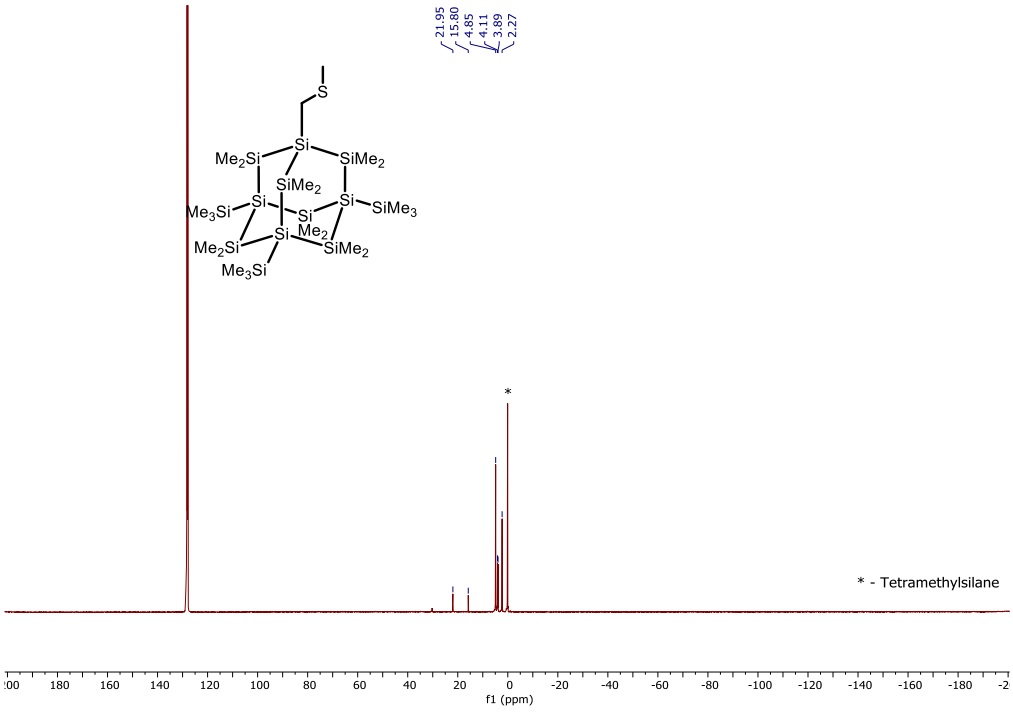


NMR Spectra of **14** (*1CH₂SMe-SiAd*)

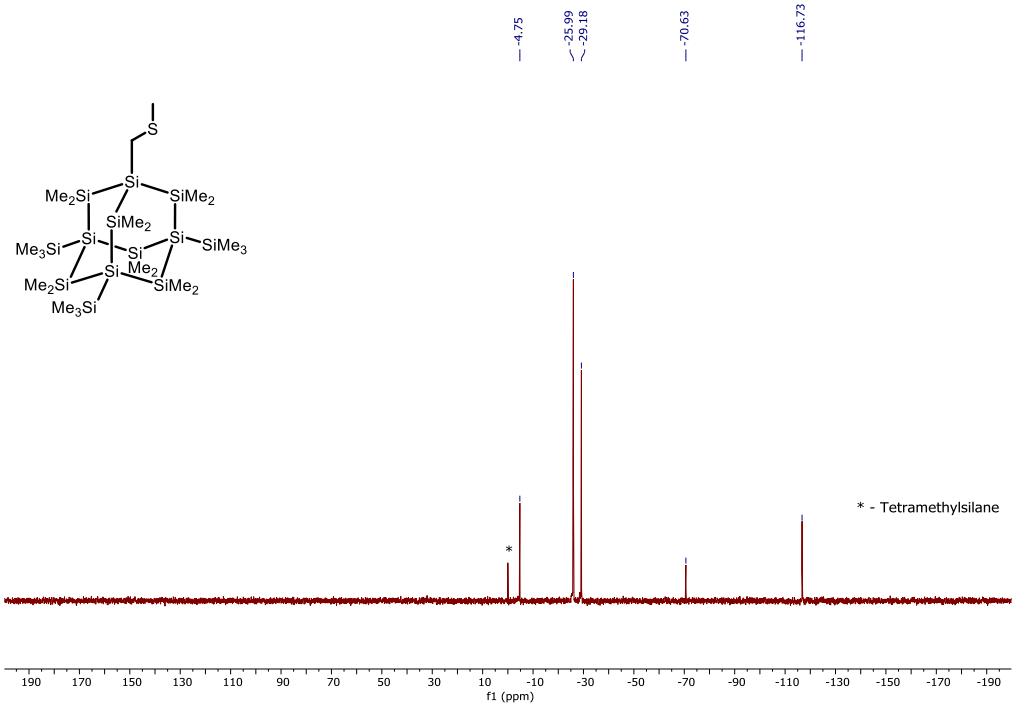
^{1}H NMR Spectrum (400 MHz, $CDCl_3$):



^{13}C NMR Spectrum (151 MHz, $CDCl_3$):

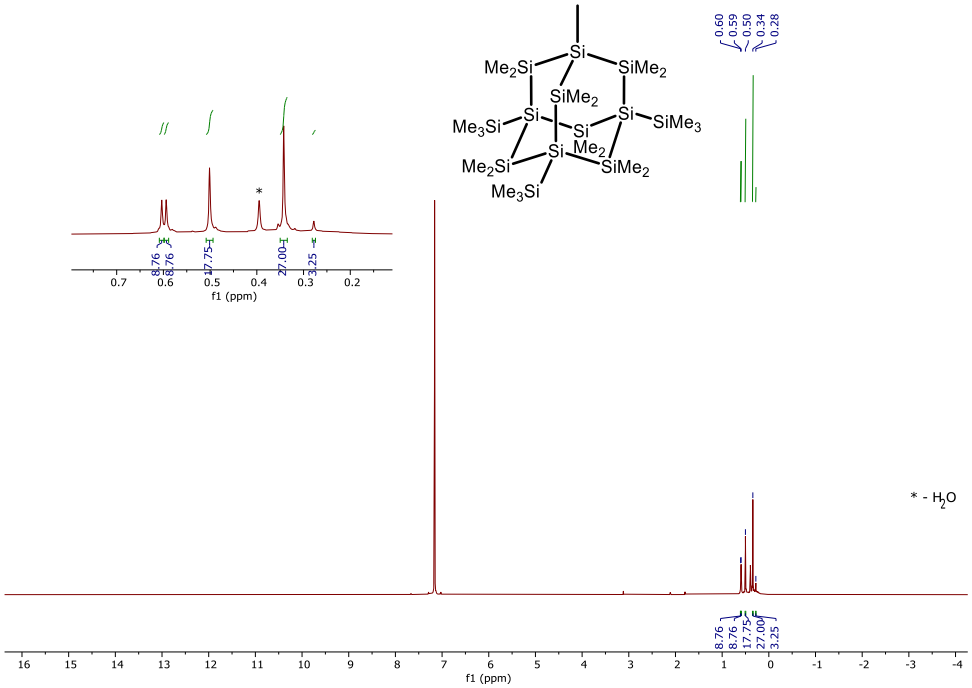


^{29}Si-DEPT NMR Spectrum (119 MHz, $CDCl_3$):

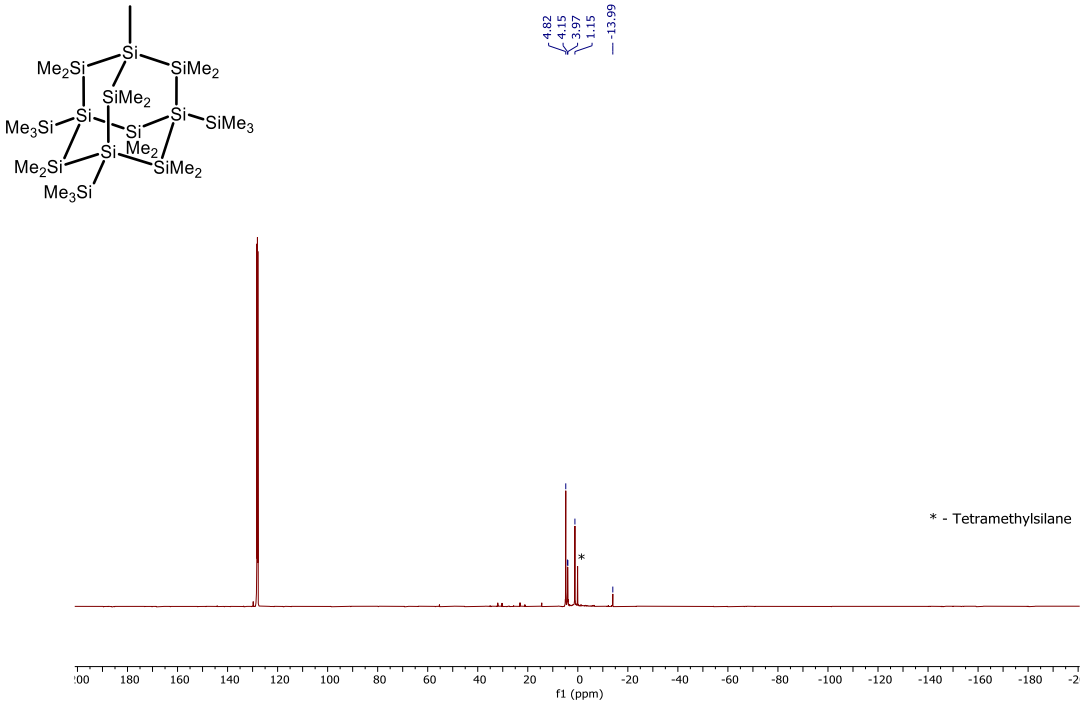


NMR Spectra of **15** (*1Me-SiAd*)

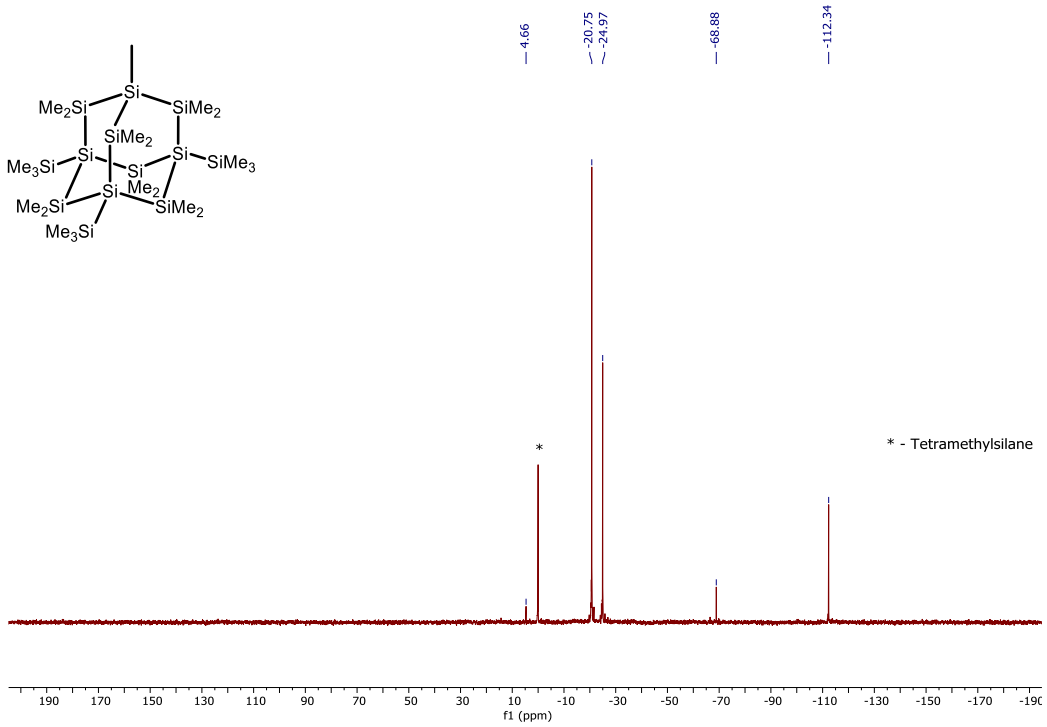
^{1}H NMR Spectrum (600 MHz, C_6D_6):



^{13}C NMR Spectrum (151 MHz, C_6D_6):

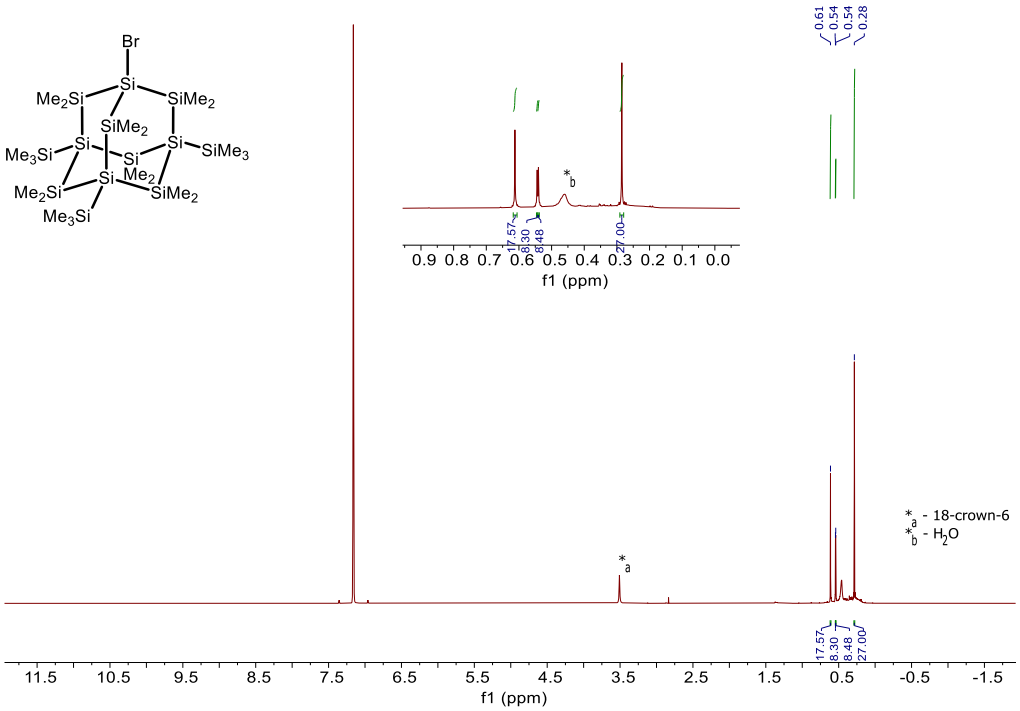


^{29}Si-DEPT NMR Spectrum (119 MHz, C_6D_6):

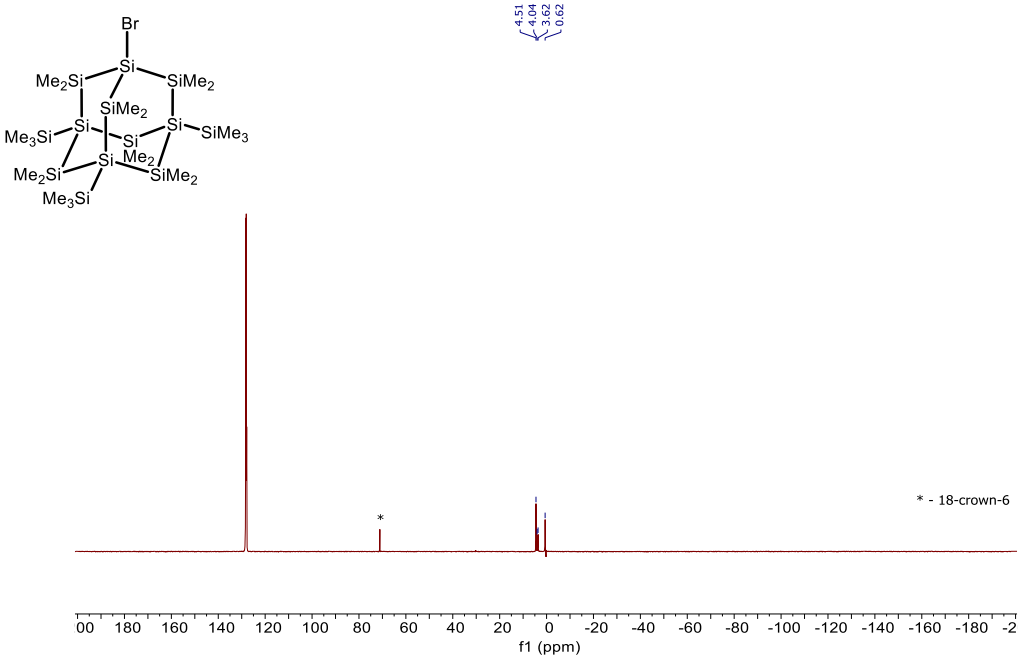


NMR Spectra of **16** (*1Br-SiAd*)

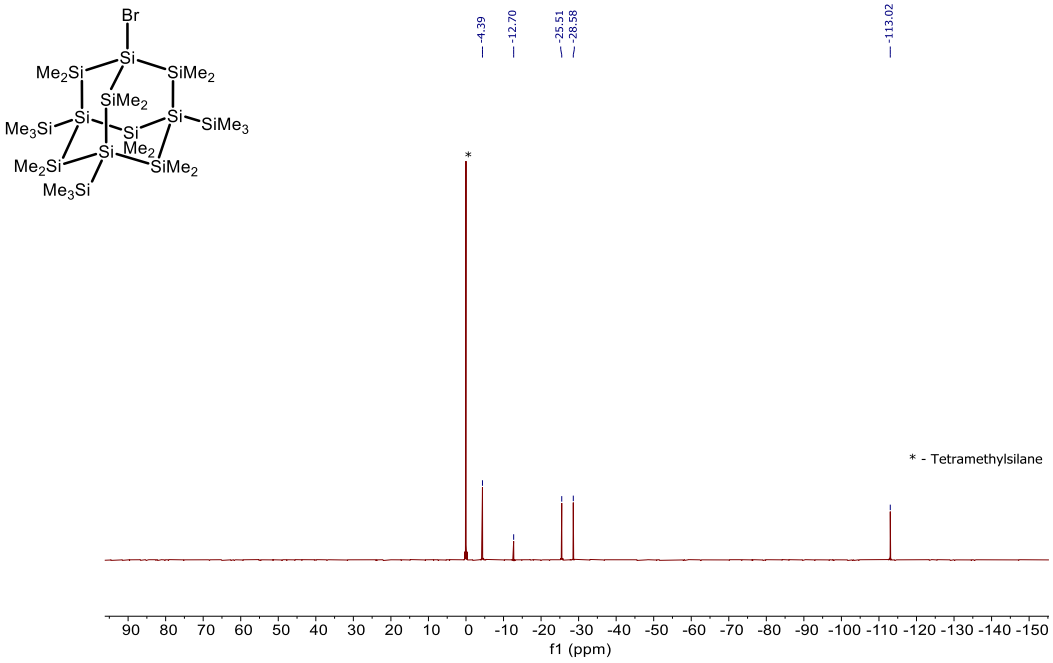
^{1}H NMR Spectrum (400 MHz, C_6D_6):



^{13}C NMR Spectrum (151 MHz, C_6D_6):

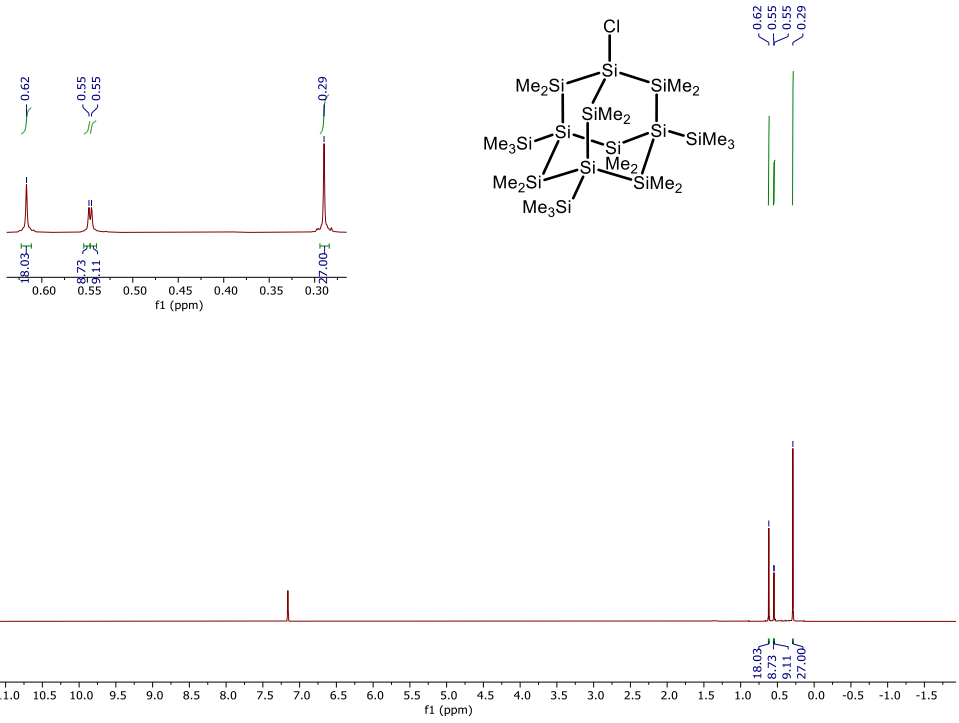


^{29}Si-DEPT NMR Spectrum (79 MHz, C_6D_6):

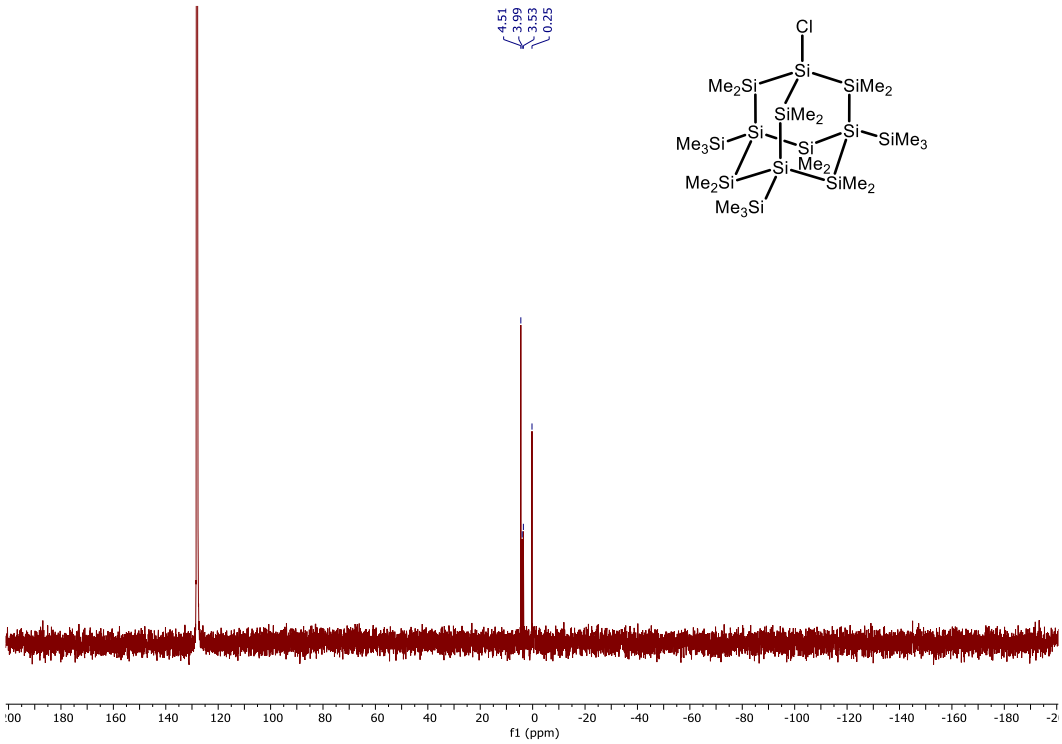


NMR Spectra of **17** (*1Cl-SiAd*)

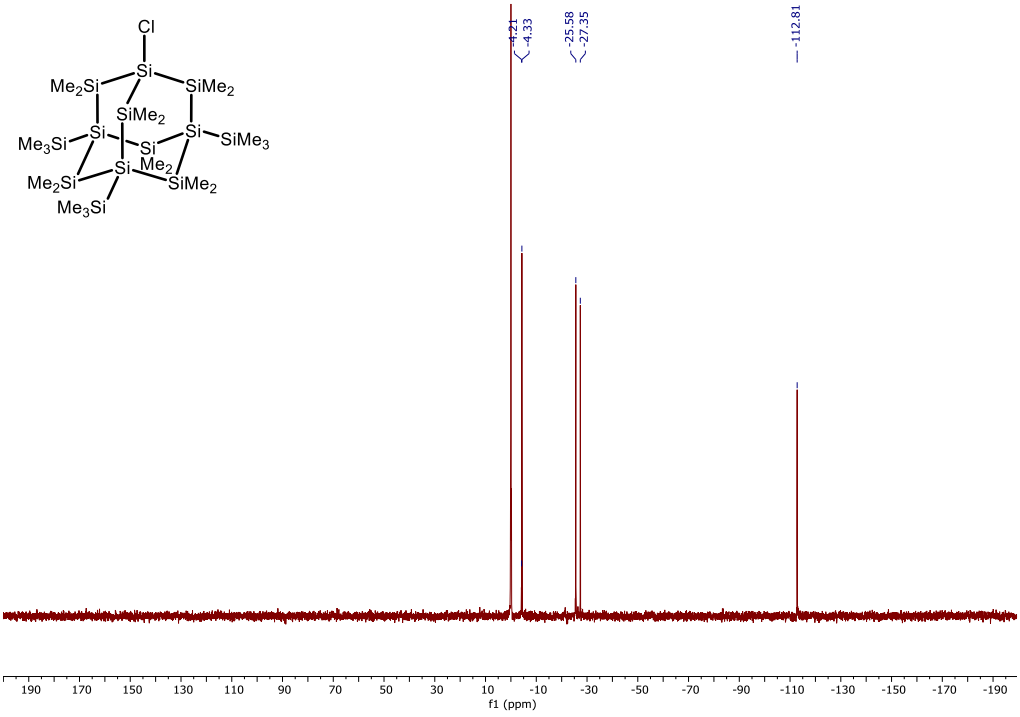
^{1}H NMR Spectrum (400 MHz, C_6D_6)



^{13}C NMR Spectrum (151 MHz, C_6D_6)

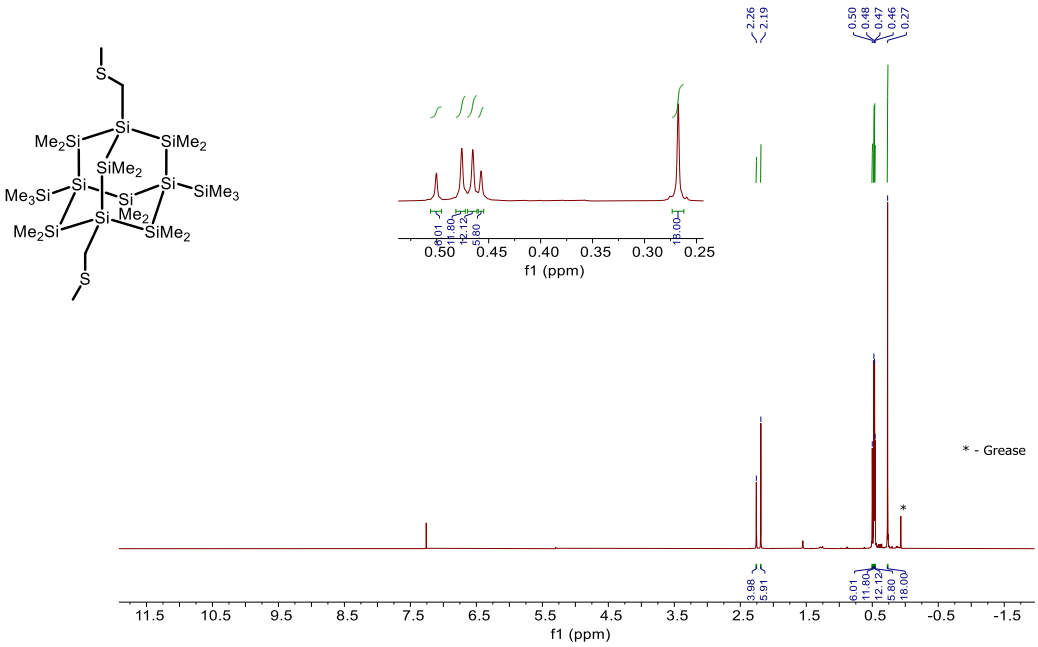


^{29}Si-DEPT NMR Spectrum (119 MHz, C_6D_6)

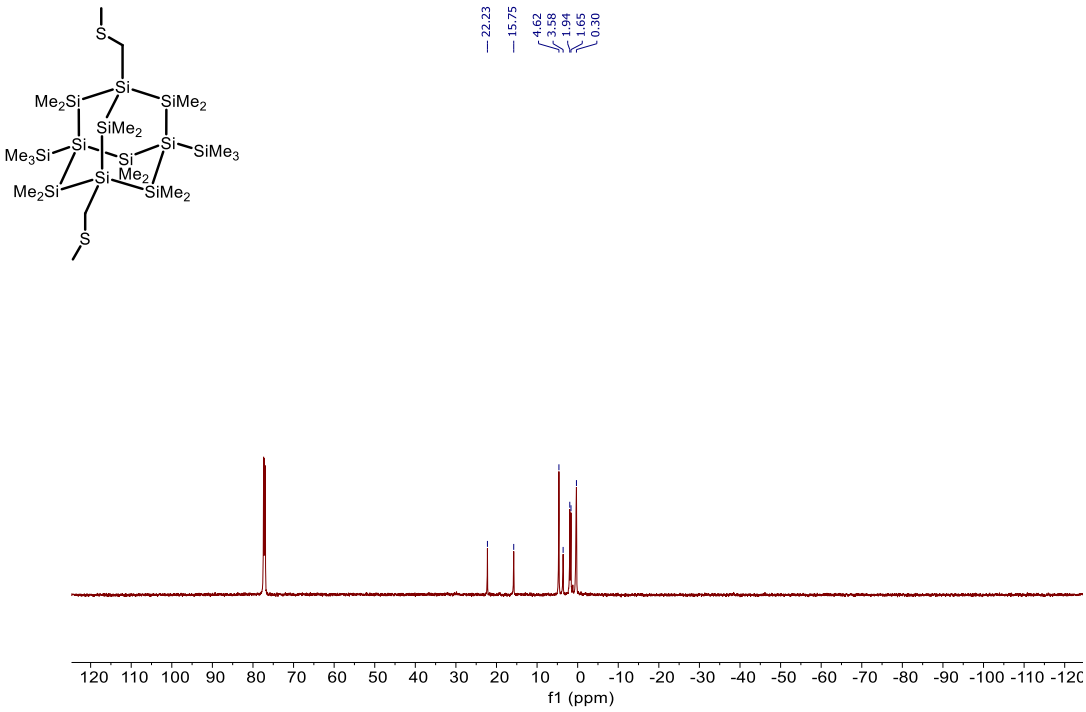


NMR Spectra of **18** (*1-,3-(CH$_2$SMe)$_2$-SiAd*)

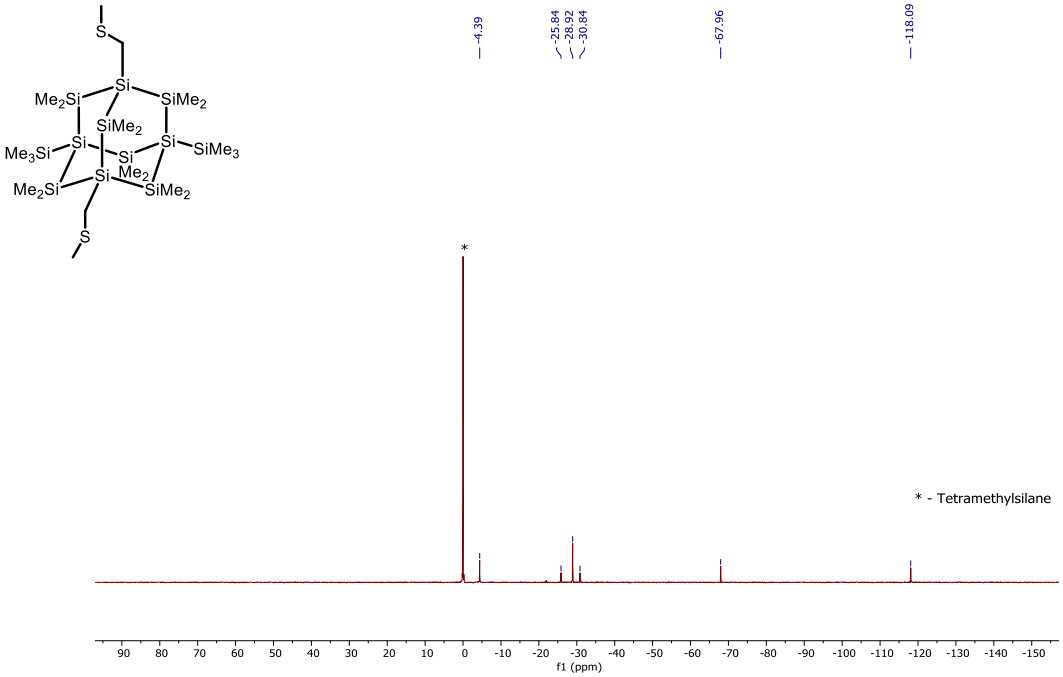
^{1}H NMR Spectrum (400 MHz, $CDCl_3$):



^{13}C NMR Spectrum (151 MHz, $CDCl_3$):

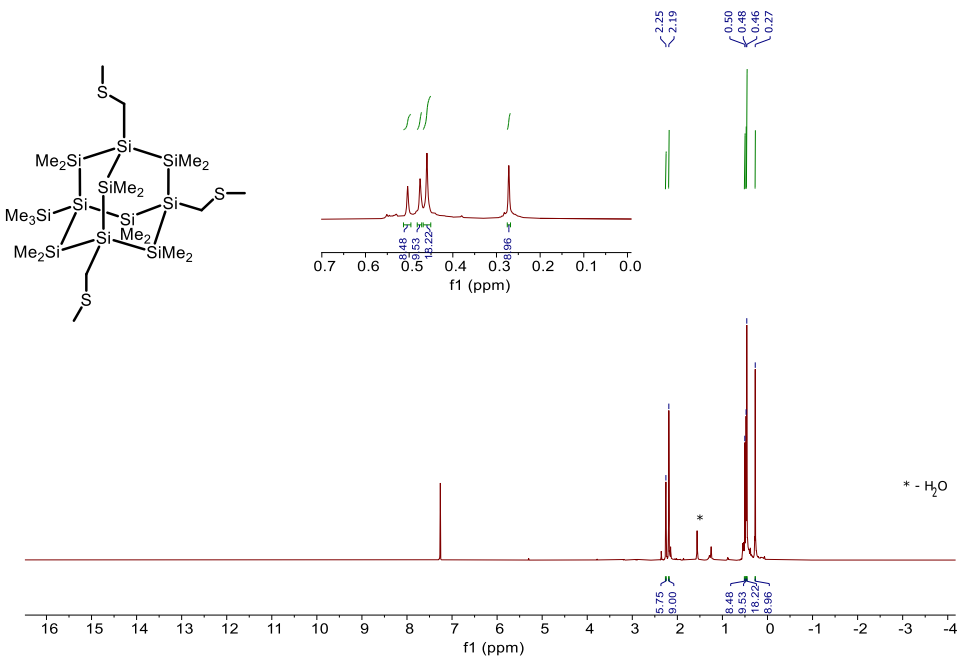


^{29}Si-DEPT NMR Spectrum (119 MHz, $CDCl_3$):

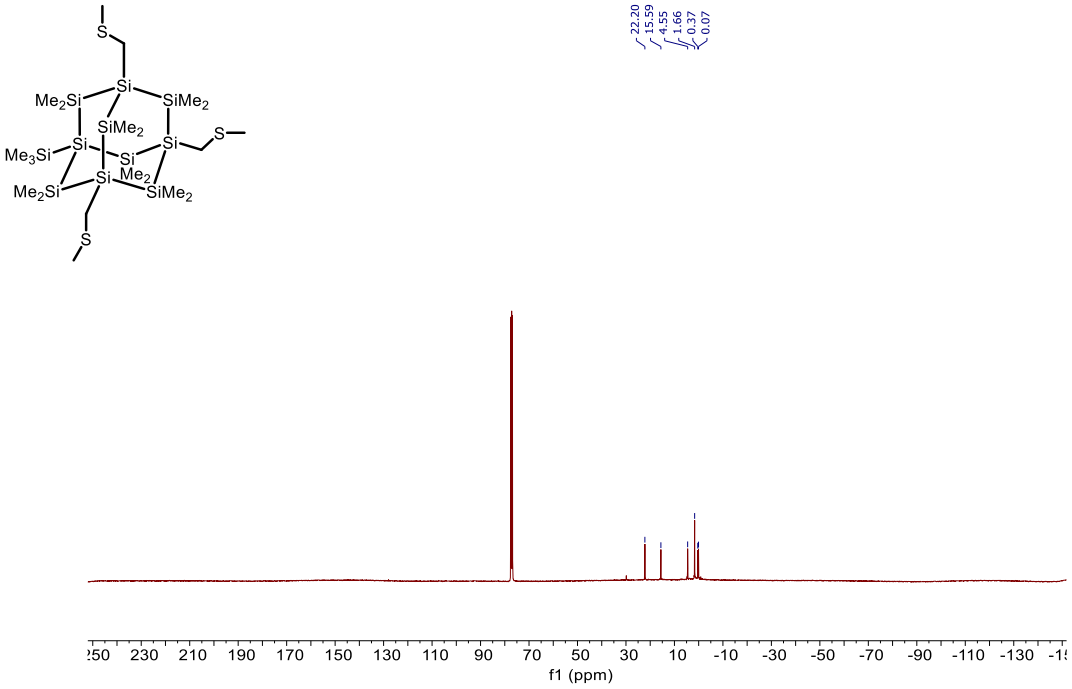


NMR Spectra of **19** (*1-,3-,5-(CH$_2$SMe)$_3$-SiAd*)

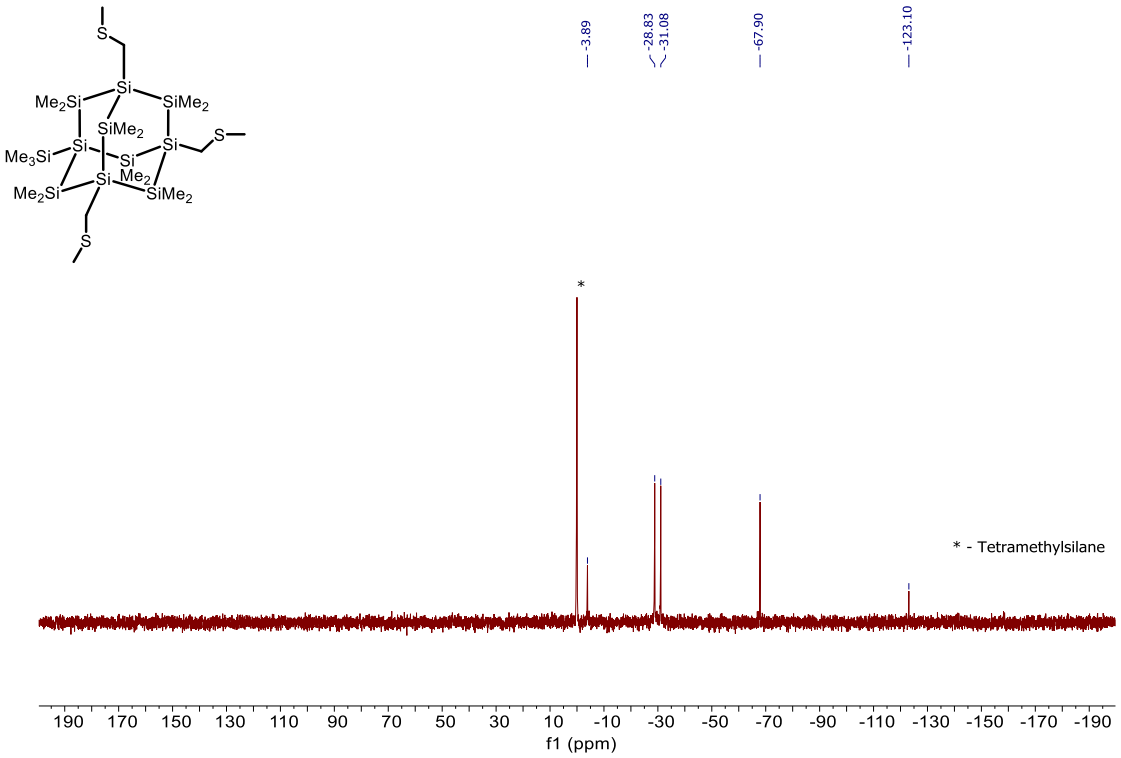
^{1}H NMR Spectrum (400 MHz, $CDCl_3$):



^{13}C NMR Spectrum (101 MHz, $CDCl_3$):

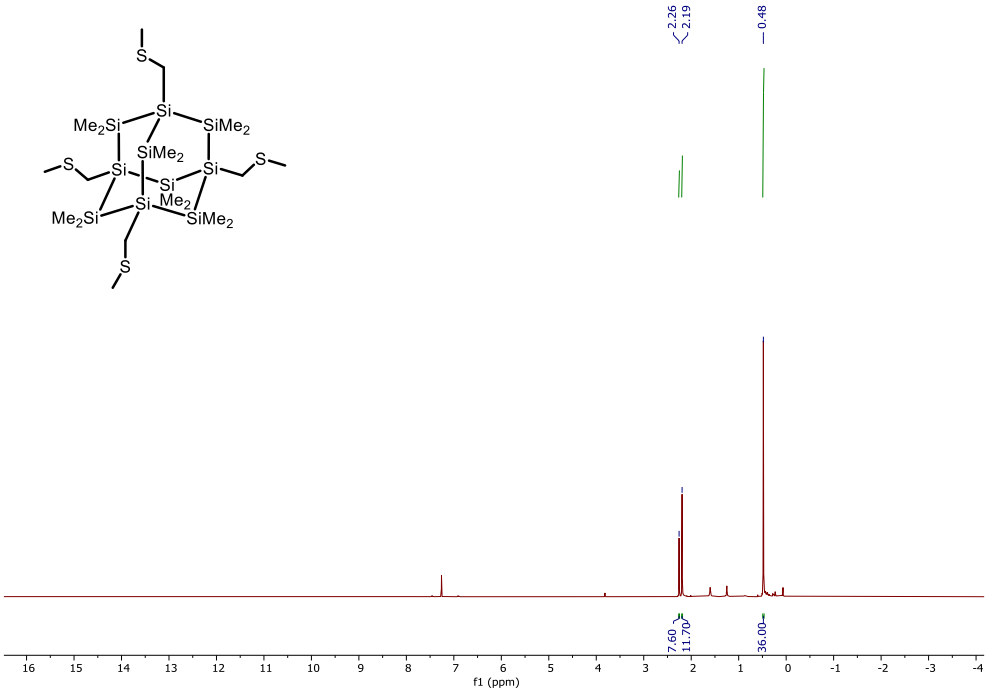


^{29}Si-DEPT NMR Spectrum (119 MHz, $CDCl_3$):

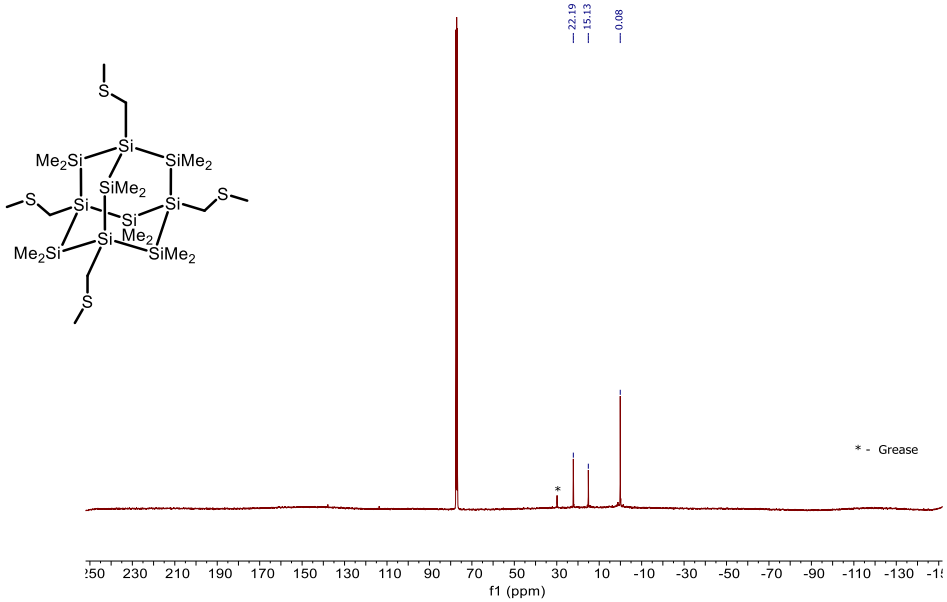


NMR Spectra of **20** (*1-, 3- ,5-, 7-$(CH_2SMe)_4$-SiAd)*

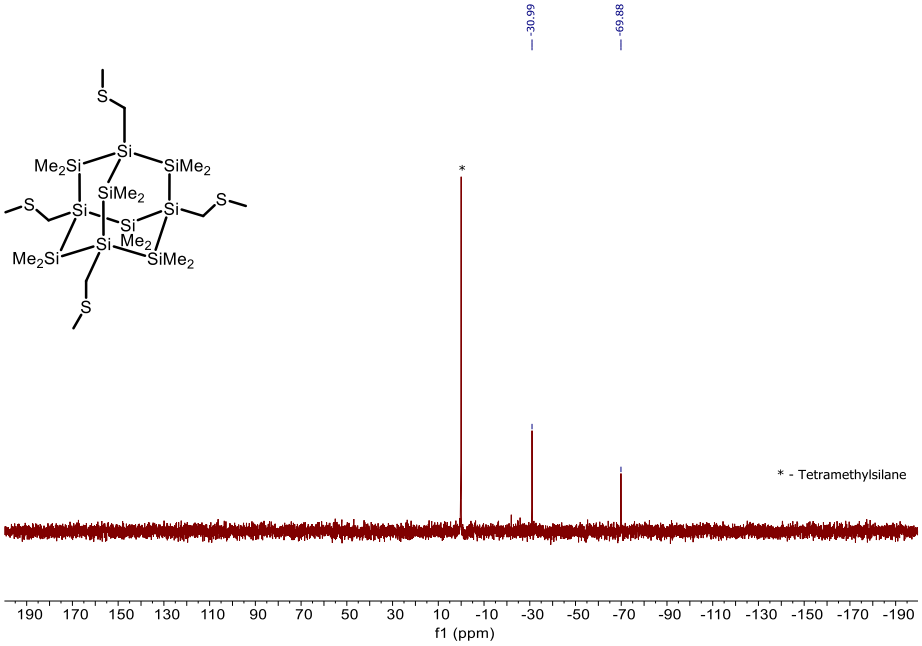
^{1}H NMR Spectrum (400 MHz, $CDCl_3$):



^{13}C NMR Spectrum (101 MHz, $CDCl_3$):

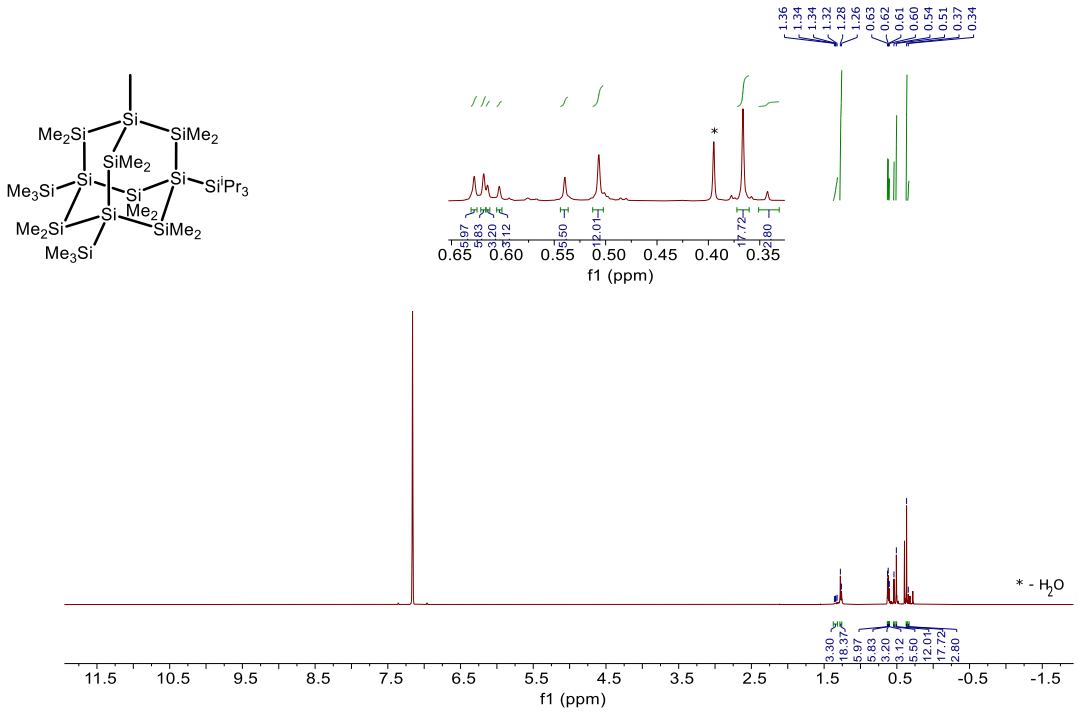


^{29}Si-DEPT NMR Spectrum (119 MHz, $CDCl_3$):

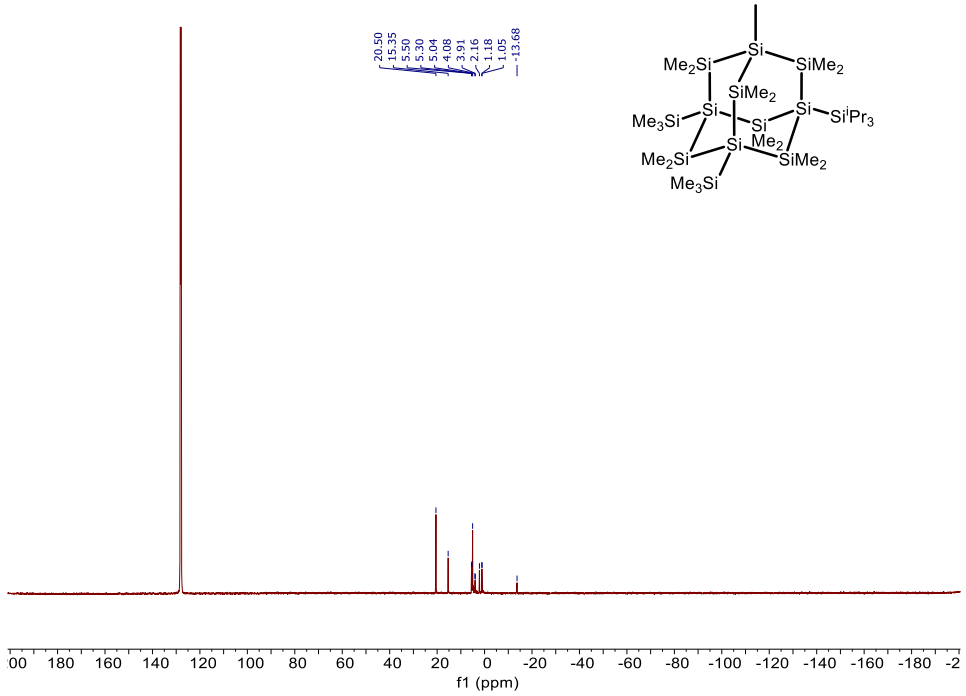


NMR Spectra of **22** (*1Me-3Si^{i}Pr$_3$-SiAd*)

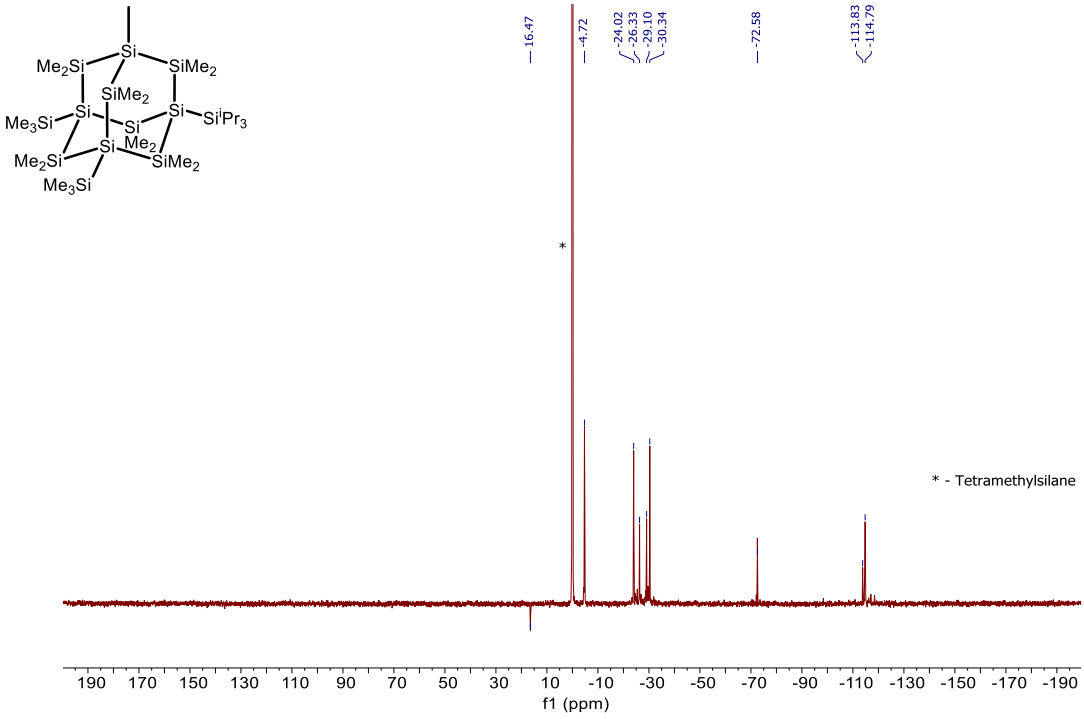
^{1}H NMR Spectrum (400 MHz, C_6D_6):



^{13}C NMR Spectrum (151 MHz, C_6D_6):

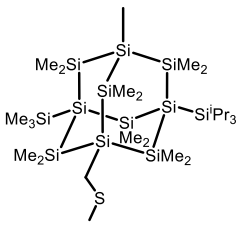


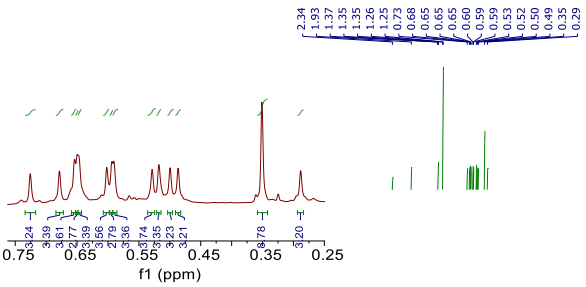
^{29}Si-DEPT NMR Spectrum (119 MHz, C_6D_6):

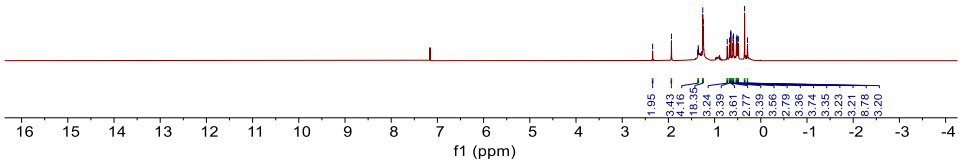


NMR Spectra of **23** (*1Me-3Si^{i}Pr$_3$-5SMe-SiAd*)

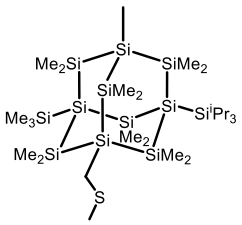
^{1}H NMR Spectrum (600 MHz, C_6D_6):

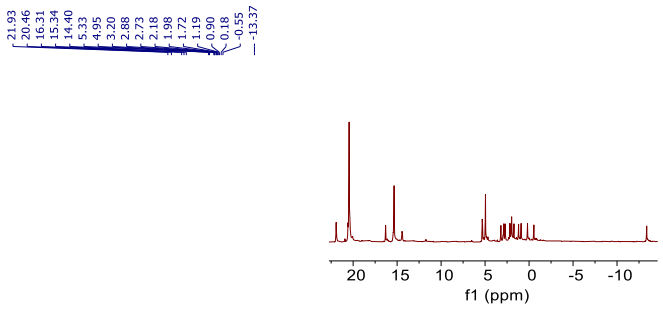


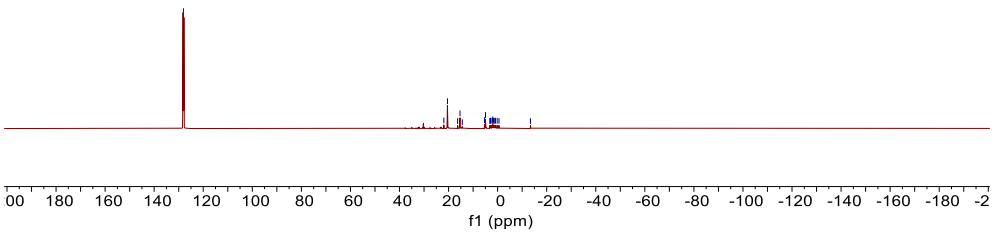




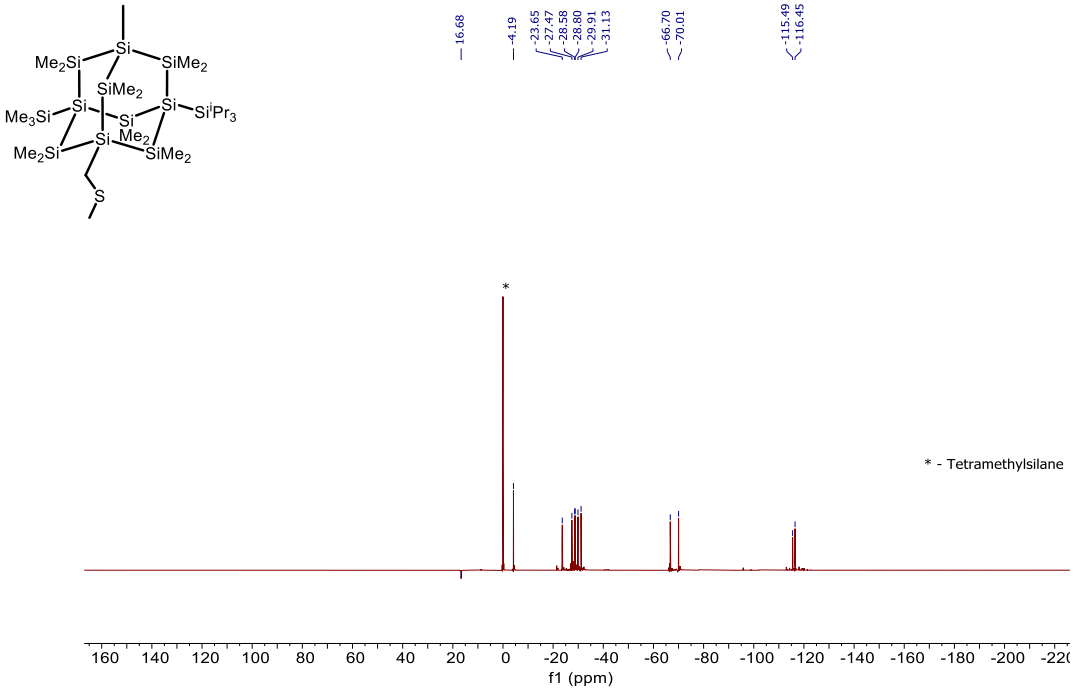
^{13}C NMR Spectrum (151 MHz, C_6D_6):





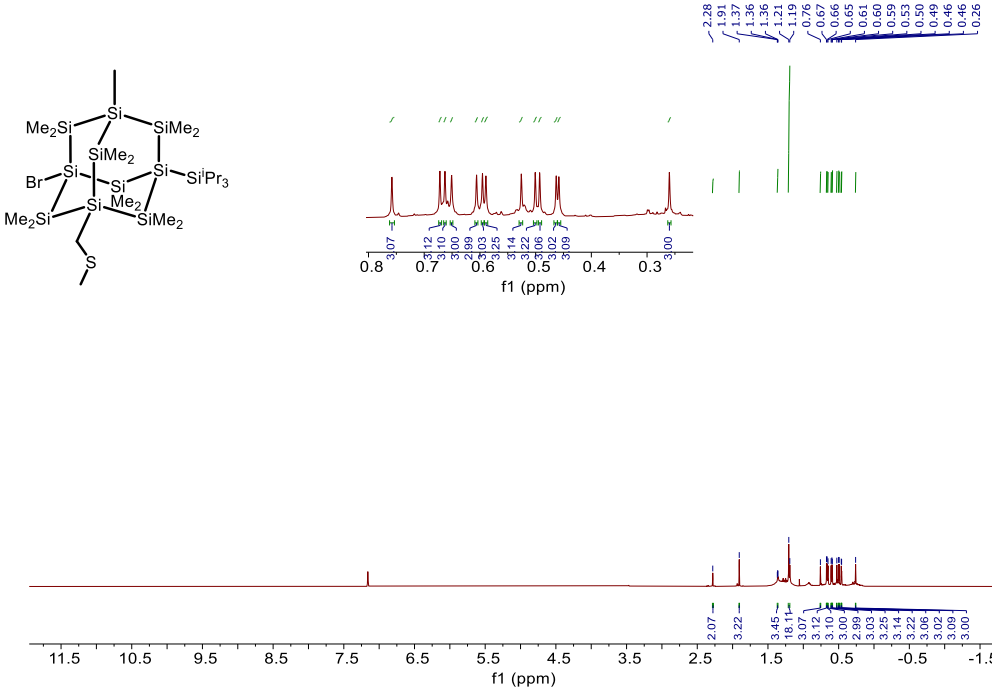


^{29}Si NMR Spectrum (79 MHz, C_6D_6):

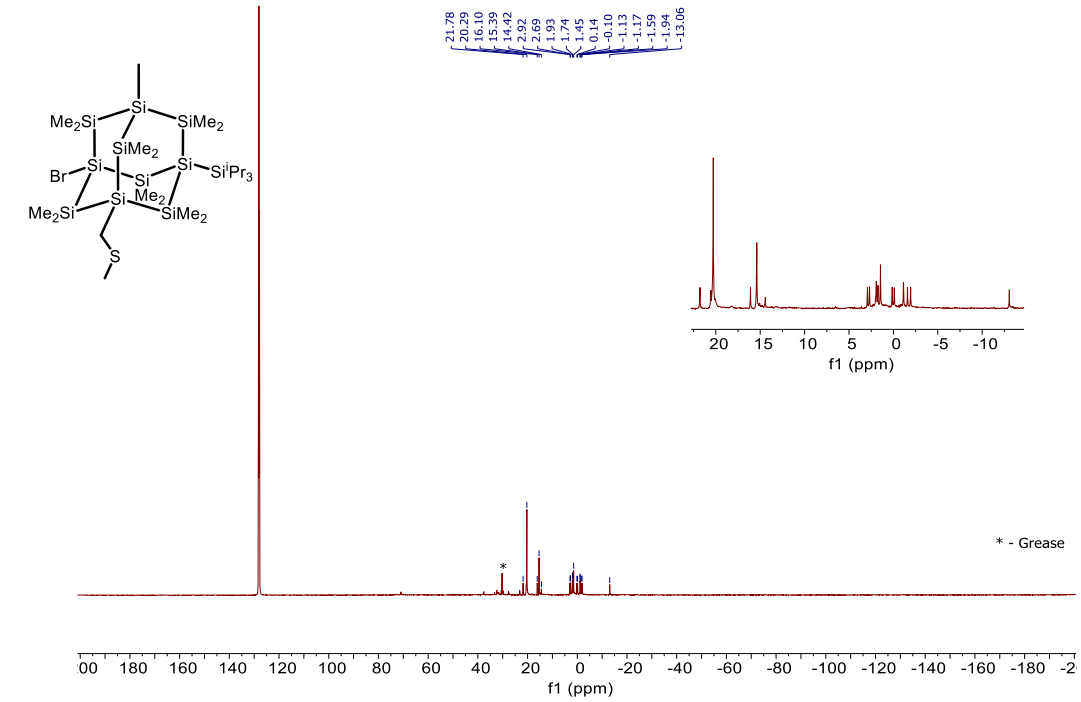


NMR Spectra of **24** (*1-Me, 3-Si^{i}Pr$_3$, 5-CH$_2$SMe, 7-Br-SiAd*)

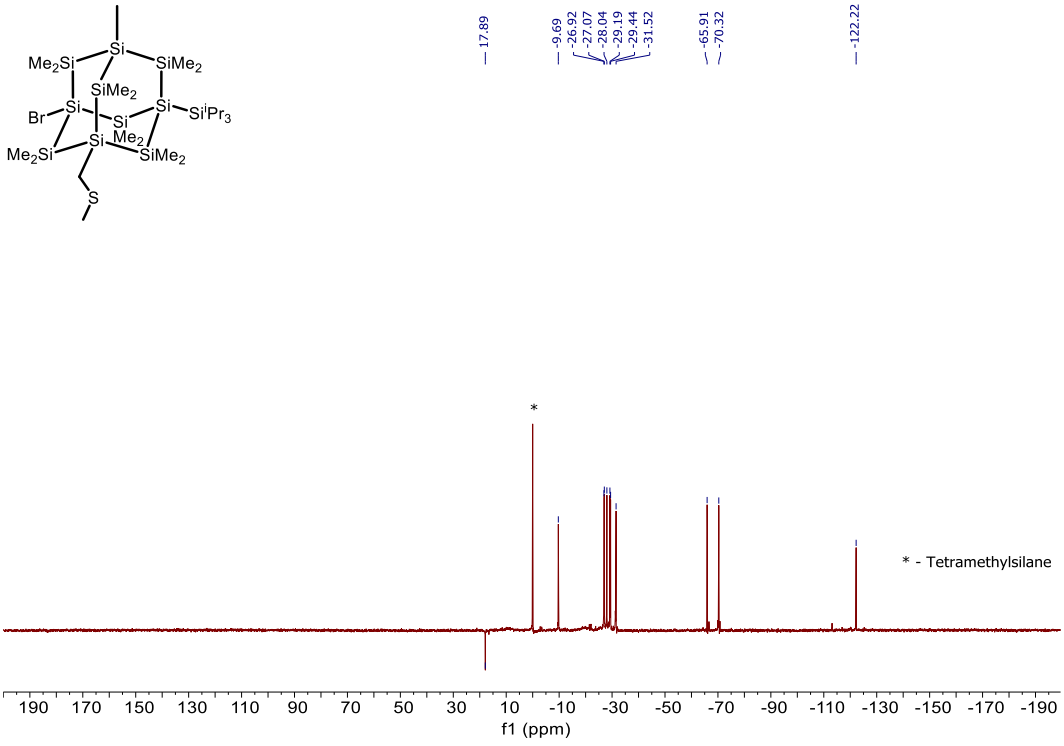
^{1}H NMR Spectrum (400 MHz, C_6D_6):



^{13}C NMR Spectrum (151 MHz, C_6D_6):



^{29}Si-DEPT NMR Spectrum (119 MHz, C_6D_6):



Computational Chemistry

Further computational details and crystallographic information can be found in the supporting information in Siu, T. C.; Imex Aguirre Cardenas, M.; Seo, J.; Boctor, K.; Shimono, M. G.; Tran, I. T.; Carta, V.; Su, T. A. *Angewandte Chemie International Edition* **2022**, *61* (31), e202206877.

References

[1] H. Gilman, C. L. Smith, *J. Organomet. Chem.* **1967**, *8*, 245–253.

[2] S. M. Whittaker, M.-C. Brun, F. Cervantes-Lee, K. H. Pannell, *J. Organomet. Chem.* **1995**, *499*, 247–252.

[3] C. Kayser, G. Kickelbick, C. Marschner, *Angew. Chem. Int. Ed.* **2002**, *41*, 989–992.

[4] R. Fischer, T. Konopa, S. Ully, J. Baumgartner, C. Marschner, *J. Organomet. Chem.* **2003**, *685*, 79–92.

[5] J. Fischer, J. Baumgartner, C. Marschner, *Science* **2005**, *310*, 825.

[6] H. Gilman, R. A. Tomasi, *J. Org. Chem.* **1963**, *28*, 1651–1653.

Chapter 3: Conductivity of the Molecular Analog of the Crystalline Unit Cell and Synthesis of Its Derivatives

Preface

This chapter presents a manuscript in progress. I synthesized all compounds except molecules **2** and **3**. Mr. Matthew O. Hight performed most STM-BJ measurements. Ms. Ashley E. Pimentel performed some STM-BJ measurements. Mr. McKinley Durham and Ms. Anika Manapul assisted in synthesis. All calculations were performed by Ms. Ashley E. Pimentel and Prof. Timothy A. Su. Mr. Joshua Y. Wong and Ms. Jennifer Nguyen synthesized molecules **2** and **3**. Crystallographic data was obtained by Dr. Veronica Carta. Theoretical calculations were performed by Dr. Timothy A. Su.

Introduction:

Crystalline silicon is at the heart of modern technology and the ability to refine and harness it as a semiconductor material has led to the dawn of an information era whereby data contained in and processed by silicon is of increasing value and importance. At the core of this information era is the development of dense arrays of transistors comprised of crystalline bulk silicon for which silicon's earth abundance coupled with its favorable semiconductor properties have made it the premier transistor material. Rapid advancement in information processing bandwidth and speed of commercial microprocessors has been enabled by continued efforts to produce denser silicon transistor arrays containing higher numbers of silicon transistors. The continued miniaturization of silicon microelectronics

has scaled well with the overall capability and efficiency of silicon microelectronics, consistently doubling every two years and is known colloquially as Moore's law.

As crystalline silicon components have become smaller, unwanted quantum charge transport has become an exponentially more difficult engineering problem. Currently, quantum leakage current plagues modern silicon microelectronics and is a cause of poor power efficiency, increased heat generation, and poor signal integrity.[1] Despite this, clever engineering approaches to mitigating and insulating against quantum leakage have enabled the continuum of Moore's law well into the 20th century and has led to the development of silicon component features that are small enough to earn an angstrom unit of measurement.[2] In the angstrom era of silicon microelectronics, we are rapidly approaching the fundamental limit of the miniaturization of bulk crystalline silicon: single molecules. Despite the race for smaller and smaller silicon microarchitecture, quantum charge transport in crystalline silicon remains poorly understood due to the ballistic conducting nature at the single molecule scale, highlighting the importance of understanding quantum charge transport in crystalline silicon at the single molecule scale.

Single-molecule conductance studies are a ripe platform for interrogating how atom-level effects such as strain, doping, and defects at an atomically precise level impact molecular silicon's electronic properties. Molecular silicon exhibits a wide variety of interesting properties due in large part to silicon's strong sigma conjugation. This sigma-conjugation, particularly in silanes, depends strongly on the dihedrals of the molecular backbone[3,4,5] and has been demonstrated to dictate silicon's conductance properties. Manipulating sigma conjugation via fixation of silicon dihedral angles in cluster molecules

has enabled the observation of silicon wires with a wide range of conductance values and have been demonstrated to exhibit DQI, a phenomenon originally observed in pi-systems[6] entirely within their sigma conjugated systems.[7]

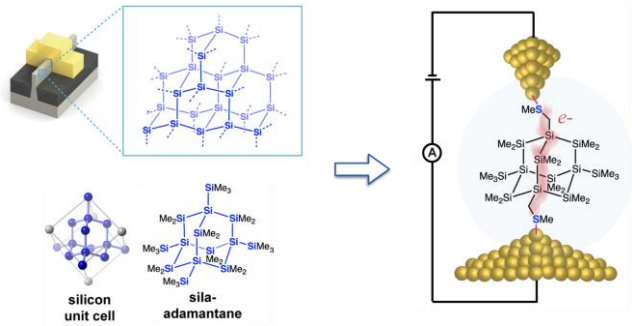


Figure 3.1 Sila-adamantane is isostructural with the unit cell of crystalline silicon; Methylthioether linked Sila-adamantane in a single molecule junction.

Until now, most of the emphasis has been placed on the transport properties of linear polysilanes, cyclic clusters, and bicyclic clusters.[8,9] Cluster molecules have been particularly useful in uncovering the properties of conductive molecular silicon as they constrain the molecular backbone in a fixed conformation and have given rise to a number of interesting fundamental insights. It has been previously demonstrated that bicyclic silane systems are essentially structurally constrained linear silanes in that they do not act as fully conjugated cyclic systems where all through bond paths contribute significantly to charge transport.[10] This works because the bicyclic cluster arms significantly influence the conformation of the aurophilic linker groups and serve to restrict the stereochemistry in a manner which aligns with the backbone but do not themselves drastically influence conductance. In turn, this alignment of the electrode linker groups serves to influence conductance through the linear portion of the molecular backbone.

Sila-adamantane is a tricyclic silicon cluster with tetrahedral geometry throughout, reminiscent of the diamond-like structure of bulk crystalline silicon (Figure 3.1). The

enhanced symmetry imparted by the additional bridging silicon atom removes the steric influence of the cluster arms responsible for alignment of the electrode linker groups with the linear molecular backbone. Recent chemistry to control the functionalization has allowed us to control the functionalization of **SiAd** in a site-selective manner and install electrode-linking endgroups enabling the study of their charge transport properties at the single molecule scale through the STM-BJ technique.[11]

To briefly describe the STM-BJ technique adapted from a prior review article, [12] a measurement of a single molecule starts with dropping a dilute solution (μM to mM) of the target molecule onto the surface of a gold substrate electrode. Then, contact is made between a gold STM tip and the flat gold substrate. The STM tip is pulled apart until an atomically thin metal-metal point contact is formed; this metal-metal point contact has a conductance value of G_0 (77.5 μS), which serves as our unit of conductance. As the tip retracts further, a target molecule functionalized with electrode linker groups can form a junction between the tip and the gold substrate. The tip then retracts even further which breaks the junction between the molecule and the gold tip electrode. The conductance data generated from this process is repeated 10,000 times per molecule by repeatedly forming and breaking contact with the electrodes. The data is then compiled to form 1D and 2D histograms that represent an average conductance value of the electrode-molecule-electrode junction.

Results and Discussion

To consider silicon diamondoids as new materials of interest and possible model systems, we thought it crucial to first evaluate the basics of how this molecule conducts electricity. Molecules in this study were designed to probe how the enhanced dimensionality and symmetry of SiAd impacts quantum transport in molecular silicon wires (figure 3.2). Along this end, a bicyclic Si-[3.3.1] containing identical cluster arms, but lacking the additional bridgehead silicon atom of SiAd was synthesized according to previously reported methods.[12] To briefly describe the synthesis of linker-functionalized molecules, we react dianions of **SiAd** and **Si-[3.3.1],** generated with two equivalents of potassium tert-butoxide, with chloromethyl methyl sulfide to obtain the cluster molecules with electrode linking functionality as **1** and **3** respectively.[13] **2** represents a non-cyclic analog of both **Si-[3.3.1]** and **SiAd** and was synthesized according to previously reported methods.[14]

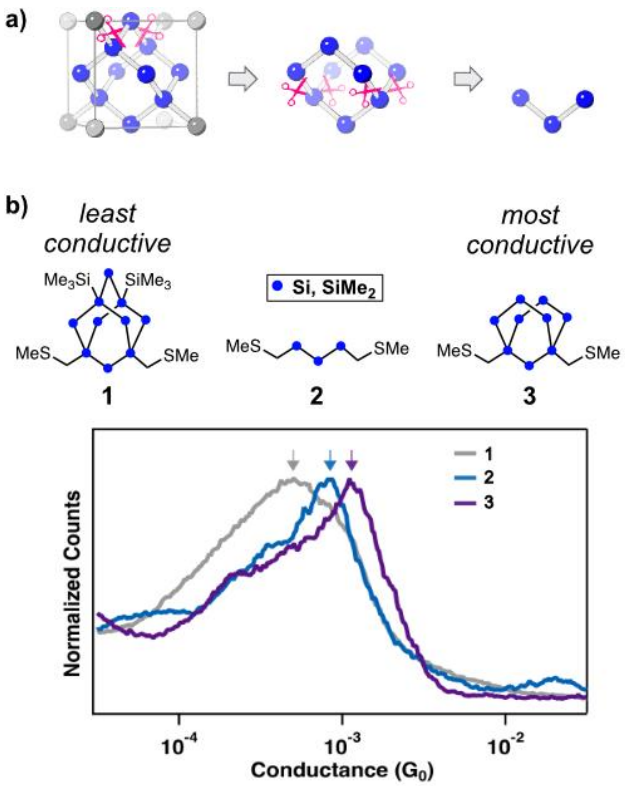


Figure 3.2 a) Illustration of "cutting out" pathways of SiAd while retaining the main backbone. b) 1D histogram of **1, 2**, and **3**.

With modified dimensionalities of SiAd successfully synthesized in the forms of **1**,**2**, and **3**, we were able to obtain conductance measurements for each. The 1D histogram in

Figure 3.2b. show that **1** is less conductive than **2** and three times less conductive than **3**. The significant variation in conductivity is surprising since **1**, **2**, and **3** share identical linker to linker molecular backbones. We are conducting ongoing investigations into the rationale behind this variation in conductivity.

In addition to probing the dimensionality of SiAd, we wanted to consider the effects of functional groups at the 5 and 7 positions of SiAd and how that would impact charge transport properties. To do so, we generated SiAd functionalized with electron withdrawing groups at E_1 or E_2 positions (Figure 3.3, Table 3.1). Given the stability of the CH_2SMe groups to potassium *tert*-butoxide attack, we began with generation of the anion or dianion of **1** and quenched with varying electrophiles to yield **2 – 6**. Attempts at dichlorination or debromination of **1** were unsuccessful via dianion generation and subsequent quenching with excess of PCl_3 or of 1,2-dibromoethane, thus only the mono-chlorinated (**5**) and mono-brominated (**4**) derivatives were synthesized.

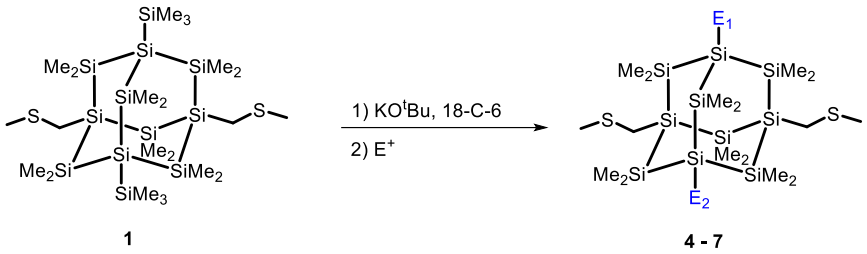


Figure 3.3 General synthetic method towards functionalization of **1**.

Table 3.1 Derivatives of **1** with yields. ***5** was prepared from **8**.

Compound	E_1	E_2	Yield
4	-Me	-$SiMe_3$	32%
5*	-Me	-Me	99%
6	-Br	-$SiMe_3$	83%
7	-Cl	-$SiMe_3$	98%

We also considered SiAd clusters with Si_1 linker groups that were one dimethylsilylene unit longer to remove stereochemical effects imparted by the cluster core on the linker groups (Figure 3.4). The synthesis of SiAd clusters with Si_1 linkers (**9**) requires the quenching of a SiAd dianion with chlorodimethylsilyl methyl sulfide, a compound

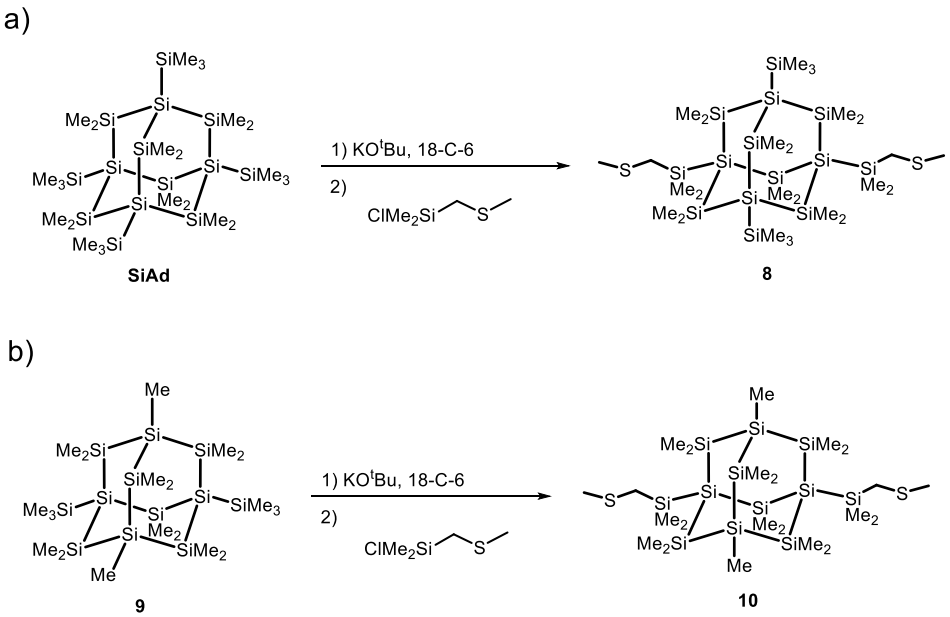
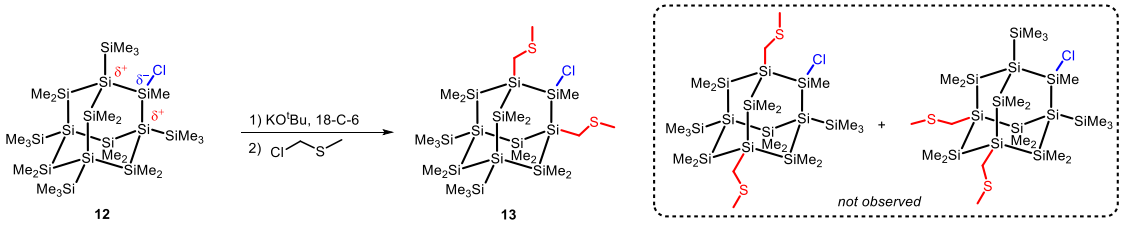


Figure 3.4 General synthetic method towards functionalization of **SiAd** or **9** with chlorodimethylsilyl methyl sulfide.



12 13

Figure 3.5 Method of installing linkers onto **12**. The inert 2-Cl acts as a directing group which results in a single isomer, **13**.

synthesized by previously reported methods.[14] Due to the sensitivity of the Si_1 linker to potassium *tert*-butoxide cleavage, preinstallation of functional groups were necessary before the Si_1 linkers were installed (Figure 3.4b). The sensitivity of the Si_1 linkers also limited the scope of derivatives to only include functional groups that are tolerant to potassium *tert*-butoxide.

We are probing the relationship between conductivity and clusters functionalized at the 2-position vs the 5-position and no chlorination. To synthesize these clusters, we generate a dianion of **12**, made from a previously reported method, and quench with chloro methyl methyl sulfide. It is interesting to note that the chlorine group at the 2-position is quite stable and inert to nucleophilic attack, due to the Si – Cl σ* orbital being protected within the cluster core. Even treatment of **12** with methyl magnesium bromide or methyl lithium would yield incomplete methylation. The difficulty in displacing the chloride can be used towards our advantage when considering the chloride as a directing group for further functionalization. For example, when reacting the 2-ClSiAd with two equivalents of potassium *tert*-butoxide, there are four possible exocyclic trimethylsilyl sites available to be cleaved. Upon quenching the dianion with chloro methyl methyl sulfide, we exclusively observe one of three possible isomers of the resulting 2-ClSiAd$(CH_2SMe)_2$ (Figure 3.5) This provides evidence that the chloro group at the 2-position acts as a relatively inert

directing group that allows for preferential cleavage of adjacent trimethylsilyl groups at the 1 and 3 positions.

With **12** successfully synthesized, we compared the conductivity between SiAd and its chlorinated derivatives at two different positions (Figure 3.6). Interestingly, chlorination at the 2-position (**12**) is less conductive than **1**, while chlorination at the 5-position (**5**) is the most conductive. We are currently investigating the nuances that give rise to this variation in conductivity across chlorination at different sites.

Conclusions

Here, we describe the methods of functionalization of sila-adamantanes that contain aurophillic linker groups. We demonstrate that the -CH_2SMe linker groups are not susceptible to potassium *tert*-butoxide attack and that **1** can be functionalized further. We note that the -$SiMe_2CH_2SMe$ groups are susceptible to potassium *tert*-butoxide attack, which requires functional groups to be preinstalled prior to the addition of the Si1 linker groups. We also demonstrate that the chloro group present in **12** is unreactive towards most nucleophiles and serves as a directing group allowing for selective fashioning of the -CH_2SMe linker groups. We are investigating the relationship between electronegative substitution on the cluster core

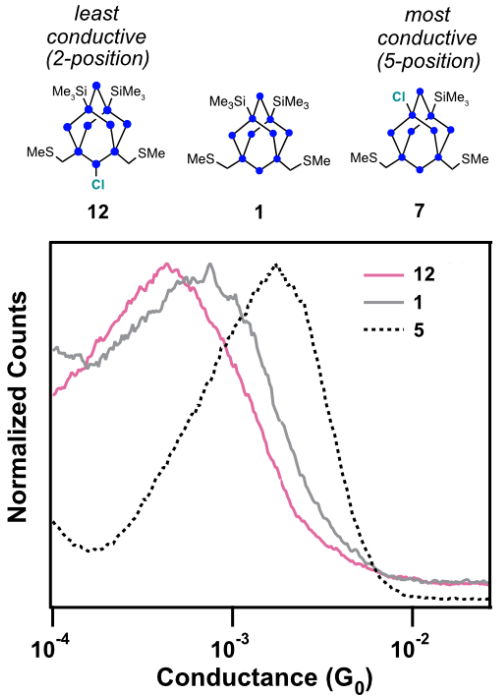


Figure 3.6 1D Histograms of **1**, **7**, and **12**.

and how it perturbs their molecular orbital environments and in turn, charge transport properties.

References:

[1] M. T. Bohr. *IEEE Trans. Nanotechnol.* **2002**, *1* (1), 56–62.

[2] M. T. Bohr. Logic Technology Scaling to Continue Moore's Law. In *2018 IEEE*

[3] *2nd Electron Devices Technology and Manufacturing Conference (EDTM)*; 2018; pp 1–3.

[4] Tsuji, H.; Michl, J.; Tamao, K. *Half Century Polysilane Chem.* **2003**, *685* (1), 9–14.

[5] Bande, A.; Michl, J. *Chem. – Eur. J.* **2009**, *15* (34), 8504–8517.

[6] Emanuelsson, R.; Löfås, H.; Wallner, A.; Nauroozi, D.; Baumgartner, J.; Marschner, C.; Ahuja, R.; Ott, S.; Grigoriev, A.; Ottosson, H. *Chem. – Eur. J.* **2014**, *20* (30), 9304–9311.

[7] Solomon, G. C.; Herrmann, C.; Hansen, T.; Mujica, V.; Ratner, M. A. *Nat. Chem.* **2010**, *2* (3), 223–228.

[8] Garner, M. H.; Li, H.; Chen, Y.; Su, T. A.; Shangguan, Z.; Paley, D. W.; Liu, T.; Ng, F.; Li, H.; Xiao, S.; Nuckolls, C.; Venkataraman, L.; Solomon, G. C. *Nature* **2018**, *558*

[9] Li, H.; Garner, M. H.; Shangguan, Z.; Zheng, Q.; Su, T. A.; Neupane, M.; Li, P.; Velian, A.; Steigerwald, M. L.; Xiao, S.; Nuckolls, C.; Solomon, G. C.; Venkataraman, L. *Chem. Sci.* **2016**, *7* (9), 5657–5662.

[10] McDermott, S.; George, C. B.; Fagas, G.; Greer, J. C.; Ratner, M. A. *J. Phys. Chem. C* **2009**, *113* (2), 744–750.

[11] Li, H.; Garner, M. H.; Shangguan, Z.; Chen, Y.; Zheng, Q.; Su, T. A.; Neupane, M.; Liu, T.; Steigerwald, M. L.; Ng, F.; Nuckolls, C.; Xiao, S.; Solomon, G. C.; Venkataraman, L *J. Am. Chem. Soc.* **2018**, *140* (44), 15080–15088.

[12] Siu, T. C.; Imex Aguirre Cardenas, M.; Seo, J.; Boctor, K.; Shimono, M. G.; Tran, I. T.; Carta, V.; Su, T. A. *Angew. Chem. Int. Ed.* **2022**, *61* (31), e202206877.

[13] Siu, T. C.; Wong, J. Y.; Hight, M. O.; Su, T. A. *Phys. Chem. Chem. Phys.* **2021**, *23*, 9643–9659.

[14] Zirngast, M.; Baumgartner, J.; Marschner, C. *Organometallics* **2008**, *27* (24), 6472–6478.

[15] Su, T. A.; Li, H.; Steigerwald, M. L.; Venkataraman, L.; Nuckolls, C. *Nat. Chem.* **2015**, *7* (3), 215–220.

Experimental

General Synthesis and Characterization Information

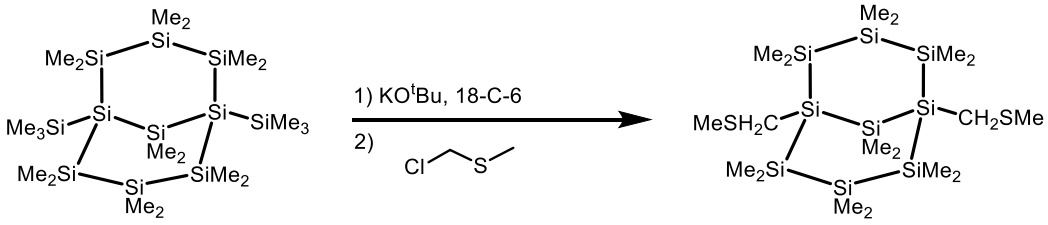
All reactions were performed in oven-dried or flame-dried glassware, unless otherwise stated. Reaction vessels were fitted with Teflon magnetic stir bars and rubber septa and reactions were conducted under nitrogen or argon on a Schlenk manifold or in a nitrogen-filled glovebox. Reaction solvents were purged with argon and dried over activated alumina columns through a JC Meyer solvent purification system, then stored over 4 Å molecular sieves. Automated flash chromatography was performed using a Yamazen Smart Flash AKROS system with Yamazen Premium silica columns.

Materials. All chemicals were purchased from commercial sources and used without further purification unless otherwise stated. **SiAd**, **11**[1], **Si[3.3.1.]**,[2], **2** and chlorodimethylsilyl methylsulfide[3] were prepared from literature procedures.

Instrumentation. ^{1}H NMR, ^{13}C NMR and ^{29}Si NMR were recorded on Bruker NEO 400 (400 MHz) or Bruker AV 600 (600 MHz) spectrometers. Chemical shifts for ^{1}H NMR are reported in parts per million downfield from tetramethylsilane and are referenced to residual protium in NMR solvents ($CHCl_3$, δ 7.26; C_6H_6, δ 7.16). Chemical shifts for ^{13}C NMR are reported in parts per million downfield from tetramethylsilane and are referenced to the center peaks of residual solvents ($CHCl_3$, δ 77.16; C_6H_6, δ128.06). Chemical shifts for silicon are reported in parts per million downfield from tetramethylsilane and are referenced to a tetramethylsilane internal standard. To compensate for the low isotopic abundance of ^{29}Si, the DEPT pulse sequence was employed for the amplification of the signal. Data are represented as follows: chemical shift, multiplicity (s = singlet, d = doublet,

t = triplet, m = multiplet, br = broad), coupling constants in Hertz, and integration. High-resolution mass spectrometry (HRMS) was recorded on either an Agilent 7200 GCMS-QTOF in methane chemical ionization mode, or a Waters XEVO G2XS QToF mass spectrometer equipped with a UPC2 SFC inlet, electrospray ionization (ESI) probe, atmospheric pressure chemical ionization (APCI) probe, and atmospheric solids analysis probe (ASAP+). High-resolution mass spectrometry (HRMS) was recorded on either an Agilent 7200 GCMS-QTOF in methane chemical ionization mode, or a Waters XEVO G2XS QToF mass spectrometer equipped with a UPC2 SFC inlet, electrospray ionization (ESI) probe, atmospheric pressure chemical ionization (APCI) probe, and atmospheric solids analysis probe (ASAP+). Low-resolution mass spectrometry (LRMS) was measured on a MALDI-TOF mass spectrometer instrument in the Analytical Chemistry Facility at UC Riverside.

Preparation of **2**

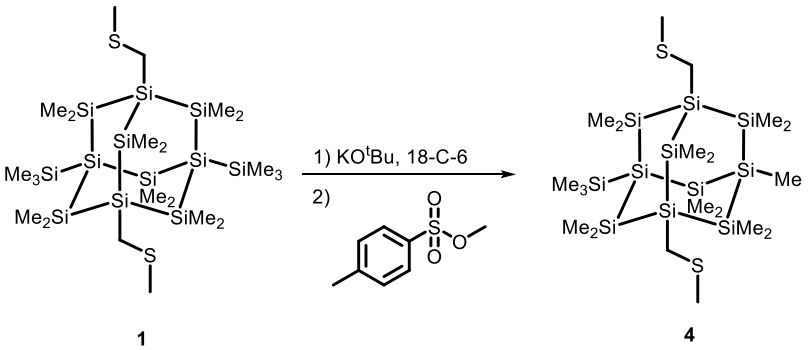


Si[3.3.1.] **2**

An oven-dried 20 mL vial was brought into the glovebox and charged with **Si[3.3.1]**, which was prepared from literature procedures[12] (0.100 g, 0.164 mmol, 1.0 equiv.), potassium *tert*-butoxide (0.037 g, 0.328 mmol, 2.0 equiv.), 18-C-6 (0.087 g, 0.328 mmol, 2.0 equiv.) and toluene (2 mL). The resulting orange mixture was left to stir overnight.

The following day, chloromethyl methyl sulfide (26.80 µL, 0.2 mmol, 2.0 equiv.) was added in dropwise upon which the reaction mixture turned colorless. The mixture was allowed to stir for 3 hours before the reaction was taken out of the glovebox and quenched with a 1 M hydrochloric acid solution (5 mL). The aqueous layer was extracted with hexanes (3x10 mL) and the combined organic layers were brine-washed, dried over magnesium sulfate, then concentrated *in vacuo* to yield a white semisolid. The crude product was further purified by flash column chromatography using a gradient from 100% hexanes to 30% dichloromethane in hexanes to yield **2** as a white semisolid (0.012 g, 12.2% yield). ^{1}H NMR (400 MHz, C_6D_6) δ 2.23 (s, 4H), 1.94 (s, 6H), 0.55 (s, 12H), 0.49 (s, 12H), 0.45 (s, 6H), 0.25 (s, 6H), 0.23 (s, 6H). ^{13}C NMR (151 MHz, C_6D_6) δ 128.17, 128.01, 127.85, 4.64, 2.99, 0.88, 0.00, -0.47, -3.52, -5.11. ^{29}Si NMR (119 MHz, C_6D_6) δ -35.09, -36.48, -43.54, -73.98. LRMS (MALDI-TOF MS) for [$C_{18}H_{52}S_2Si_9$]: calculated = 585.1512, found = 585.1530 $[M+H]^+$

Preparation of **4**

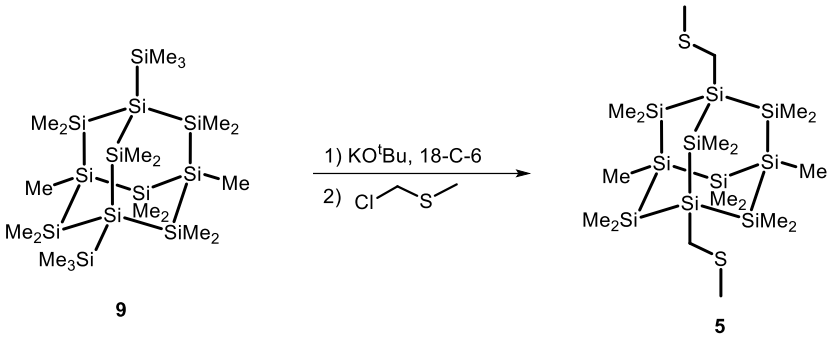


1 **4**

An oven-dried 10 mL Schlenk flask was brought into the glovebox and charged with **1** (0.024 g, 0.033 mmol, 1.0 equiv.), potassium *tert*-butoxide (0.0040 g, 0.033 mmol, 2.0

equiv.), 18-C-6 (0.0090 g, 0.033 mmol, 2.0 equiv.) and toluene (2 mL). The resulting orange mixture was left to stir overnight. Then, the flask was taken out of the glovebox, connected to a Schlenk manifold, and subjected to positive pressure nitrogen. The septum was then removed, upon which methyl-p-toluenesulfonate (0.0070 g, 0.033 mmol, 2.0 equiv.) was added under positive nitrogen flow, after which the reaction mixture turned colorless. The mixture was allowed to stir for 3 hours before the reaction was taken out of the glovebox and quenched with a 1 M hydrochloric acid solution (10 mL). The aqueous layer was extracted with hexanes (3x15 mL) and the combined organic layers were brine-washed, dried over magnesium sulfate, then concentrated *in vacuo* to yield a white solid. The crude product was further purified by flash column chromatography using a gradient from 100% hexanes to 40% dichloromethane in hexanes to yield **4** as a white solid (0.007 g, 32% yield). ^{1}H NMR (600 MHz, $CDCl_3$) δ 2.29 (s, 4H), 2.22 (s, 6H), 0.53 (s, 3H), 0.50 (s, 3H), 0.49 (s, 3H), 0.43 (s, 6H), 0.41 (s, 6H), 0.39 (s, 6H), 0.30 (s, 9H), 0.23 (s, 3H). ^{13}C NMR (101 MHz, $CDCl_3$) δ 22.08, 15.56, 4.40, 1.57, 1.07, 0.57, 0.33, -0.08, -0.70, -0.94, -13.99. ^{29}Si NMR (79 MHz, $CDCl_3$) δ -4.05, -28.60, -29.60, -30.91, -31.63, -67.87, -71.55, -123.06. HRMS (TOF MS ASAP+) for [$C_{20}H_{58}Si_{11}S_2Na$]: calculated = 692.1261 found = 693.0877 $[M+Na]^+$.

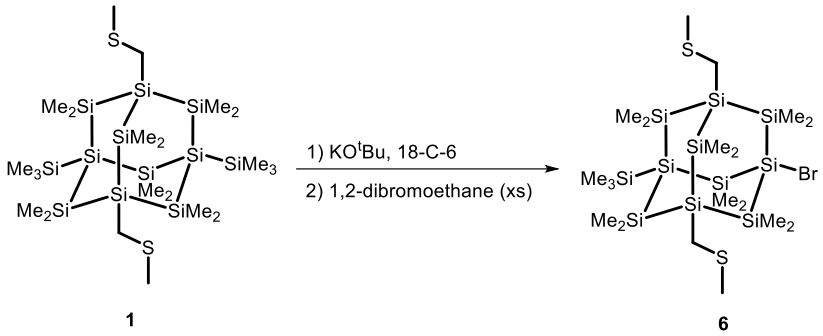
Preparation of **5**



9 **5**

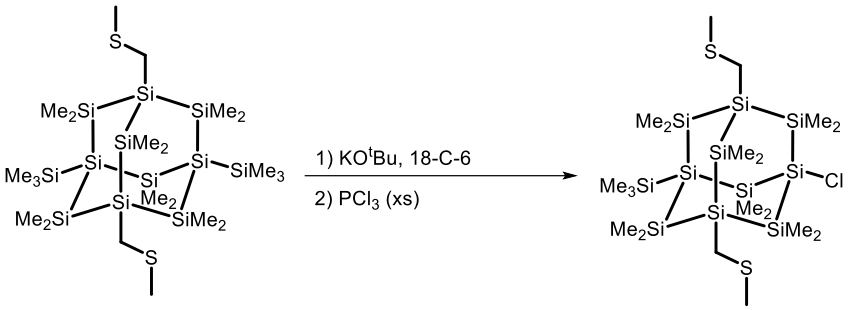
An oven-dried 20 mL vial was brought into the glovebox and charged with **9** (0.064 g, 0.1 mmol, 1.0 equiv.), potassium *tert*-butoxide (0.022 g, 0.2 mmol, 2.0 equiv.), 18-C-6 (0.053 g, 0.2 mmol, 2.0 equiv.) and toluene (5 mL). The resulting orange mixture was left to stir overnight. Then, the flask was taken out of the glovebox and connected to a Schlenk manifold upon which chloro methyl methyl sulfide (16.75 μL, 0.27 mmol, 2.0 equiv.) was added and the reaction mixture turned colorless. The mixture was allowed to stir for 3 hours before the reaction was taken out of the glovebox and quenched with a 1 M hydrochloric acid solution (10 mL). The aqueous layer was extracted with hexanes (3x15 mL) and the combined organic layers were brine-washed, dried over magnesium sulfate, then concentrated *in vacuo* to yield a white solid. The crude product was further purified by flash column chromatography using a gradient from 100% hexanes to 40% dichloromethane in hexanes to yield **5** as a white solid (0.060 g, 99% yield). ^{1}H NMR (400 MHz, $CDCl_3$) δ 2.26 (s, 4H), 2.19 (s, 6H), 0.47 (s, 6H), 0.38 (s, 12H), 0.38 (s, 12H), 0.28 (s, 6H), 0.21 (s, 6H). ^{13}C NMR (151 MHz, $CDCl_3$) δ 22.17, 15.29, 0.10, -0.84, -1.75, -14.28. ^{29}Si NMR (119 MHz, $CDCl_3$) δ -30.68, -31.42, -32.19, -69.65, -74.31. HRMS (TOF MS ASAP+) for [$C_{18}H_{52}Si_{10}S_2$]: calculated = 612.1203, found = 611.1270 $[M]^+$.

Preparation of **6**



An oven-dried 10 mL Schlenk flask was brought into the glovebox and charged with **1** (0.030 g, 0.041 mmol, 1.0 equiv.), potassium *tert*-butoxide (0.0050 g, 0.041 mmol, 1.0 equiv.), 18-C-6 (0.011 g, 0.041 mmol, 1.0 equiv.) and toluene (2 mL). The resulting yellow solution was left to stir for 16 hours before excess 1,2 dibromoethane (0.10 mL, 0.82 mmol, 20 equiv.) was syringed in upon which, the solution turned colorless. The mixture was allowed to stir for 3 more hours before being concentrated to dryness. The resulting salts were washed with dry pentane and the mixture was syringe filtered with a 0.22 μm syringe filter. Upon evaporation of the pentane solution, **6** was obtained as a white waxy solid (0.025 g, 83% yield). ^{1}H NMR (600 MHz, C_6D_6) δ 2.27 (s, 4H), 1.90 (s, 6H), 0.73 (s, 3H), 0.73 (s, 6H), 0.69 (s, 6H), 0.65 (s, 3H), 0.59 (s, 6H), 0.59 (s, 12H), 0.27 (s, 9H). ^{13}C NMR (151 MHz, C_6D_6) δ 21.76, 15.77, 4.40, 1.97, 1.67, 0.74, 0.33, 0.01, -0.64, -0.93. ^{29}Si NMR (119 MHz, C_6D_6) δ -2.56, -12.03, -21.37, -28.10, -29.21, -30.44, -66.32, -125.35. HRMS (TOF MS ASAP+) for [$C_{19}H_{56}Si_{11}S_2Br$]: calculated = 737.0450, found = 737.0478 $[M+H]^+$.

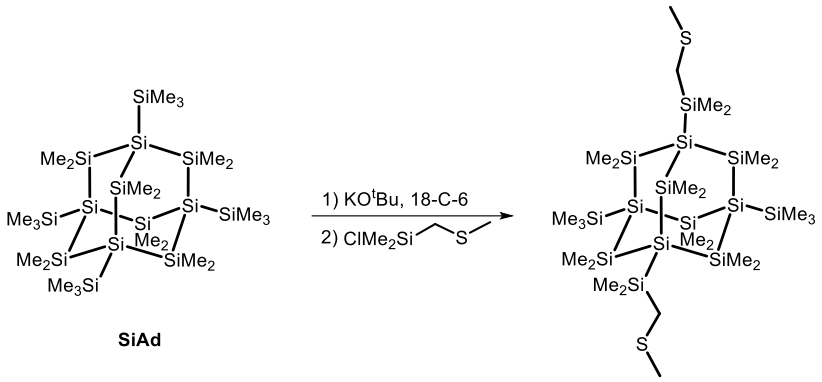
Preparation of **7**



1 **7**

An oven-dried 10 mL Schlenk flask was brought into the glovebox and charged with **1** (0.026 g, 0.036 mmol, 1.0 equiv.), potassium *tert*-butoxide (0.004 g, 0.0036 mmol, 1.0 equiv.), 18-C-6 (0.009 g, 0.036 mmol, 1.0 equiv.) and toluene (2 mL). The resulting yellow solution was left to stir for 16 hours before excess PCl_3 (0.06 mL, 0.71mmol, 20 equiv.) was syringed in upon which, the solution turned colorless. The mixture was allowed to stir for 3 more hours before being concentrated to dryness. The resulting salts were washed with dry pentane and the mixture was syringe filtered with a 0.22 μm syringe filter. Upon evaporation of the pentane solution, **7** was obtained as a white waxy solid (0.024 g, 98% yield). ^{1}H NMR (600 MHz, C_6D_6) δ 2.27 (s, 4H), 1.90 (s, 6H), 0.73 (s, 3H), 0.73 (s, 6H), 0.69 (s, 6H), 0.65 (s, 3H), 0.59 (s, 6H), 0.59 (s, 12H), 0.27 (s, 9H). ^{13}C NMR (151 MHz, C_6D_6) δ 21.76, 15.77, 4.40, 1.97, 1.67, 0.74, 0.33, 0.01, -0.64, -0.93. ^{29}Si NMR (119 MHz, C_6D_6) δ -2.56, -12.03, -21.37, -28.10, -29.21, -30.44, -66.32, -125.35. HRMS (TOF MS ASAP+) for [$C_{19}H_{56}Si_{11}S_2Cl$]: calculated = 693.0954, found = 693.0919 $[M+H]^+$.

Preparation of **8**

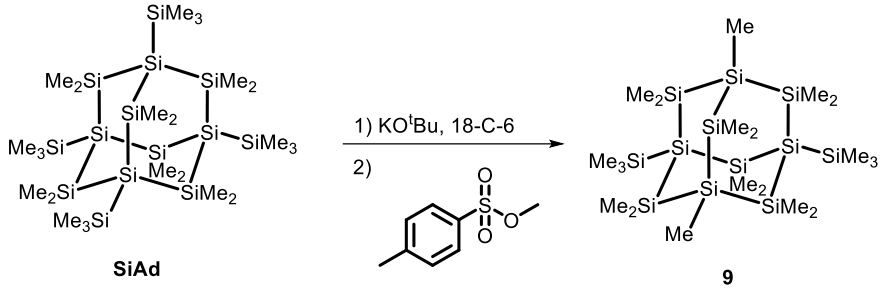


SiAd **8**

An oven-dried 20 mL vial was brought into the glovebox and charged with **SiAd** (0.075 g, 0.1 mmol, 1.0 equiv.), potassium *tert*-butoxide (0.022 g, 0.2 mmol, 2.0 equiv.), 18-C-6 (0.053 g, 0.2 mmol, 2.0 equiv.) and toluene (2 mL). The resulting orange mixture was left to stir overnight. The following day, chloro dimethyl silane methyl sulfide (26.80 µL, 0.2 mmol, 2.0 equiv.) was added in dropwise upon which the reaction mixture turned colorless. The mixture was allowed to stir for 3 hours before the reaction was taken out of the glovebox and quenched with a 1 M hydrochloric acid solution (5 mL). The aqueous layer was extracted with hexanes (3x10 mL) and the combined organic layers were brine-washed, dried over magnesium sulfate, then concentrated *in vacuo* to yield a colorless oil. The crude product was further purified by flash column chromatography using a gradient from 100% hexanes to 40% dichloromethane in hexanes to yield **8** as a white solid (0.054 g, 64% yield). ^{1}H NMR (600 MHz, $CDCl_3$) δ 2.17 (s, 6H), 1.99 (s, 4H), 0.50 (s, 6H), 0.48 (s, 24H), 0.46 (s, 6H), 0.36 (s, 12H), 0.27 (s, 18H). ^{13}C NMR (151 MHz, $CDCl_3$) δ 24.86, 20.79, 4.93, 4.18, 3.99, 3.83, 2.33. ^{29}Si NMR (119 MHz, $CDCl_3$) δ -3.80, -4.76, -26.18, -

26.29, -26.41, -118.48, -118.77. LRMS (MALDI-TOF MS) for [$C_{26}H_{76}S_2Si_{14}$ – $SiMe_3$]: calculated = 772.1763, found = 772.15 $[M - SiMe_3]^+$

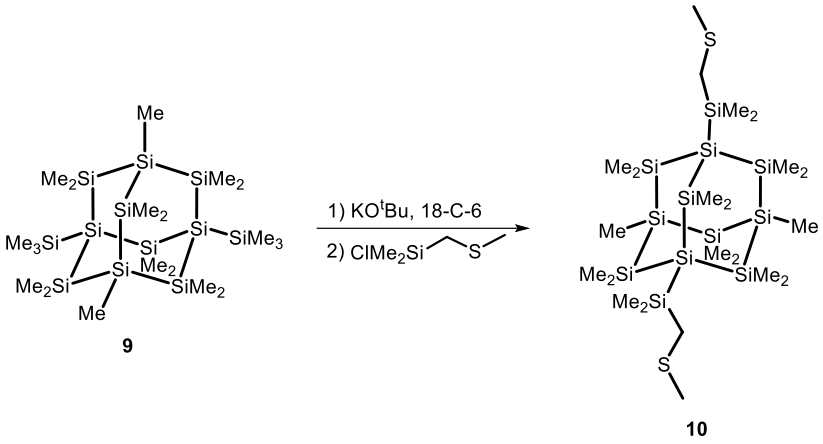
Preparation of **9**



An oven-dried 10 mL Schlenk flask was brought into the glovebox and charged with **SiAd**, prepared from literature procedures[11] (0.24 g, 0.31 mmol, 1.0 equiv.), potassium *tert*-butoxide (0.071 g, 0.62 mmol, 2.0 equiv.), 18-C-6 (0.17 g, 0.62 mmol, 2.0 equiv.) and toluene (5 mL). The resulting orange mixture was left to stir overnight. Then, the flask was taken out of the glovebox, connected to a Schlenk manifold, and subjected to positive pressure nitrogen. The septum was then removed, upon which methyl-p-toluenesulfonate (0.12 g, 0.62 mmol, 2.0 equiv.) was added under positive nitrogen flow, after which the reaction mixture turned colorless. The mixture was allowed to stir for 3 hours before the reaction was taken out of the glovebox and quenched with a 1 M hydrochloric acid solution (10 mL). The aqueous layer was extracted with hexanes (3x15 mL) and the combined organic layers were brine-washed, dried over magnesium sulfate, then concentrated *in vacuo* to yield a white solid. The crude product was purified via flash column chromatography in hexanes to yield pure **9** as a white solid (0.19 g, 94% yield). ^{1}H NMR (400 MHz, C_6D_6) δ 0.58 (s, 6H), 0.49 (s, 12H), 0.49 (s, 12H), 0.42 (s,

6H), 0.33 (s, 18H), 0.29 (s, 6H). ^{13}C NMR (101 MHz, C_6D_6) δ 4.64, 3.96, 1.15, 0.97, -1.40, -13.62. ^{29}Si NMR (79 MHz, C_6D_6) δ -4.44, -24.97, -29.12, -31.59, -71.11, -118.33. HRMS (TOF MS ASAP+) for [$C_{20}H_{60}Si_{12}Na$]: calculated = 658.1746, found = 662.1603 $[M+Na]^+$

Preparation of **10**

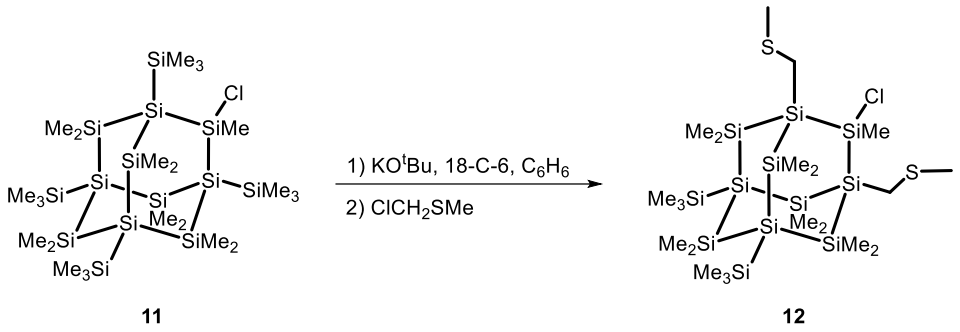


9 **10**

An oven-dried 20 mL vial was brought into the glovebox and charged with $SiAdMe_2$ (0.064 g, 0.1 mmol, 1.0 equiv.), potassium *tert*-butoxide (0.022 g, 0.2 mmol, 2.0 equiv.), 18-C-6 (0.053 g, 0.2 mmol, 2.0 equiv.) and toluene (2 mL). The resulting orange mixture was left to stir overnight. The following day, chloro dimethyl silane methyl sulfide (26.89 µL 0.2 mmol, 2.0 equiv.) was added in dropwise upon which the reaction mixture turned colorless. The mixture was allowed to stir for 3 hours before the reaction was taken out of the glovebox and quenched with a 1 M hydrochloric acid solution (5 mL). The aqueous layer was extracted with hexanes (3x10 mL) and the combined organic layers were brine-washed, dried over magnesium sulfate, then concentrated *in vacuo* to yield a colorless oil. The crude product was further purified by flash column chromatography using a gradient

from 100% hexanes to 40% dichloromethane in hexanes to yield **10** as a white solid (0.029 g, 40% yield). ^{1}H NMR (400 MHz, $CDCl_3$) δ 2.17 (s, 6H), 1.98 (s, 4H), 0.49 (s, 6H), 0.38 (S, 12H), 0.38 (s, 12H), 0.35 (s, 12H), 0.29 (s, 6H), 0.20 (s, 6H). ^{13}C NMR (151 MHz, $CDCl_3$) δ 24.56, 20.76, 3.94, 1.96, 1.00, 0.83, -1.58, -13.71. ^{29}Si NMR (119 MHz, $CDCl_3$) δ -3.61, -25.12, -29.51, -32.05, -71.27, -118.53.

Preparation of **12**



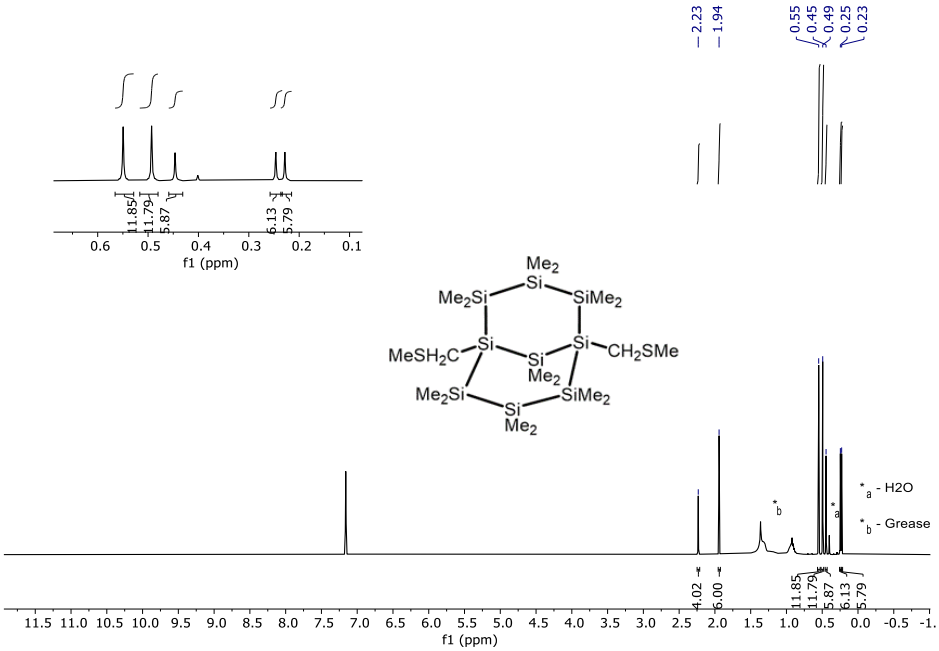
11 **12**

An oven-dried 20 mL vial was brought into the glovebox and charged with **11** (0.010 g, 0.13 mmol, 1.0 equiv.), potassium *tert*-butoxide (0.0020 g, 0.013 mmol, 2.0 equiv.), 18-C-6 (0.0040 g, 0.2 mmol, 2.0 equiv.) and benzene (5 mL). The resulting orange mixture was left to stir overnight. Then, the flask was taken out of the glovebox and connected to a Schlenk manifold upon which chloro methyl methyl sulfide (1.1 μL, 0.0131 mmol, 2.0 equiv.) was added and the reaction mixture turned colorless. The mixture was allowed to stir for 3 hours before the reaction was taken out of the glovebox and quenched with a 1 M hydrochloric acid solution (10 mL). The aqueous layer was extracted with hexanes (3x15 mL) and the combined organic layers were brine-washed, dried over magnesium sulfate, then concentrated *in vacuo* to yield a white solid. The crude product was further

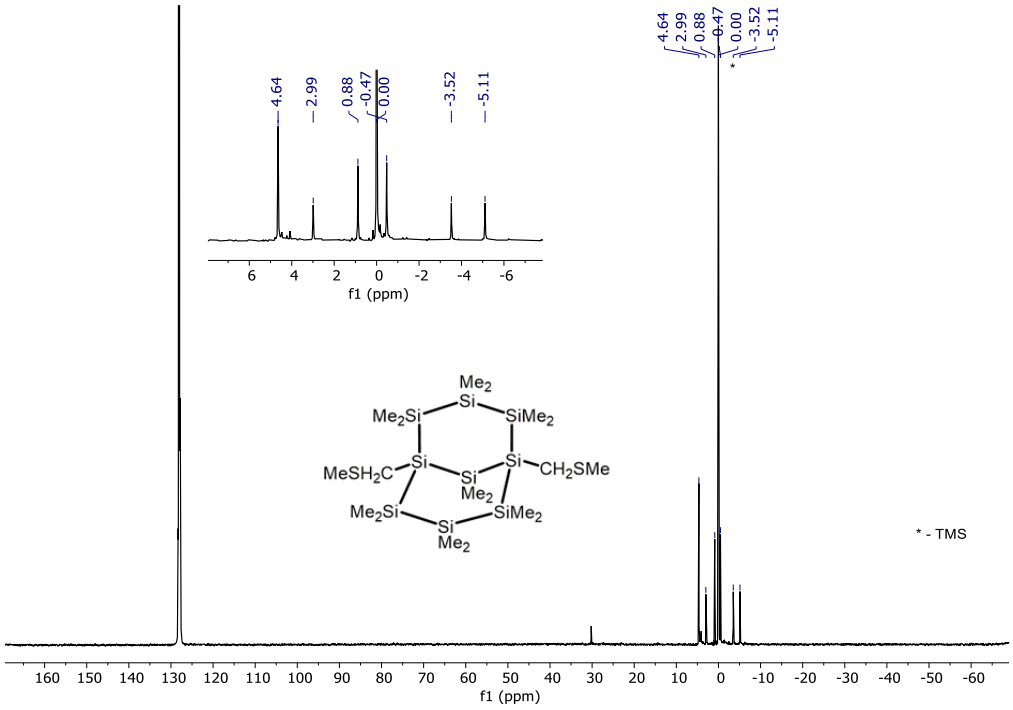
purified by flash column chromatography using a gradient from 100% hexanes to 40% dichloromethane in hexanes to yield **12** as a white solid (0.0040 g, 40% yield). ^{1}H NMR (600 MHz, $CDCl_3$) δ 2.36 (s, 2H), 2.36 (s, 2H), 2.21 (s, 6H), 0.55 (s, 6H), 0.54 (s, 6H), 0.51 (s, 6H), 0.48 (s, 6H), 0.47 (s, 6H), 0.28 (s, 9H), 0.28 (s, 9H). ^{13}C NMR (101 MHz, C_6D_6) δ 32.35, 21.68, 14.96, 14.39, 4.62, 3.79, 2.24, 1.90, 1.50, 1.25. ^{29}Si NMR (79 MHz, $CDCl_3$) δ -4.00, -4.14, -21.95, -25.80, -28.26, -30.30, -64.59, -117.02, -117.69. HRMS (TOF MS ASAP+) for $[C_{21}H_{62}Si_{12}S_2Cl]$: calculated = 751.1194, found = 751.1191 $[M+H]^+$.

NMR Spectra of **2**

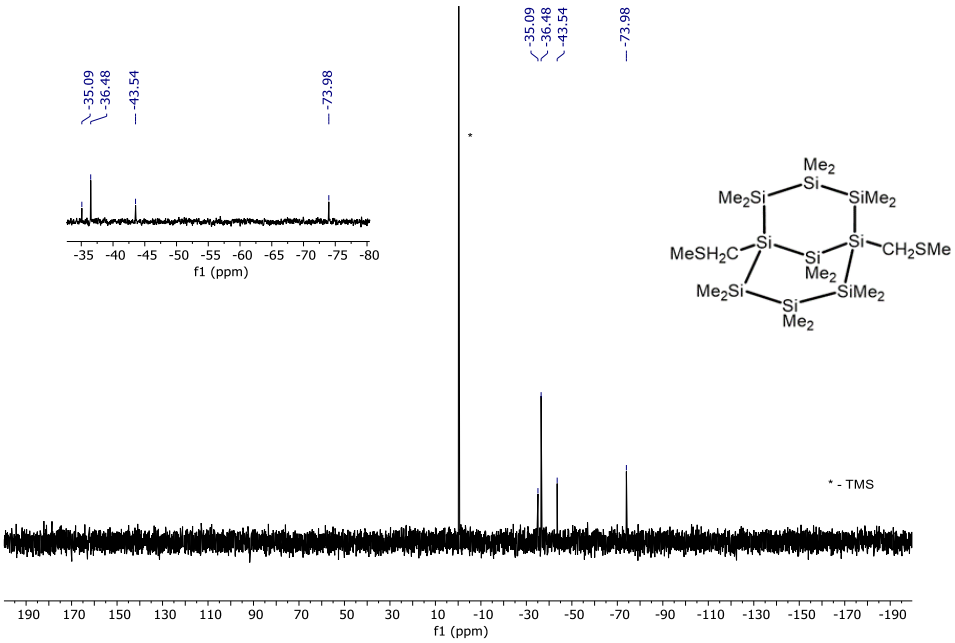
^{1}H NMR (400 MHz, C_6D_6)



^{13}C NMR (151 MHz, C_6D_6)

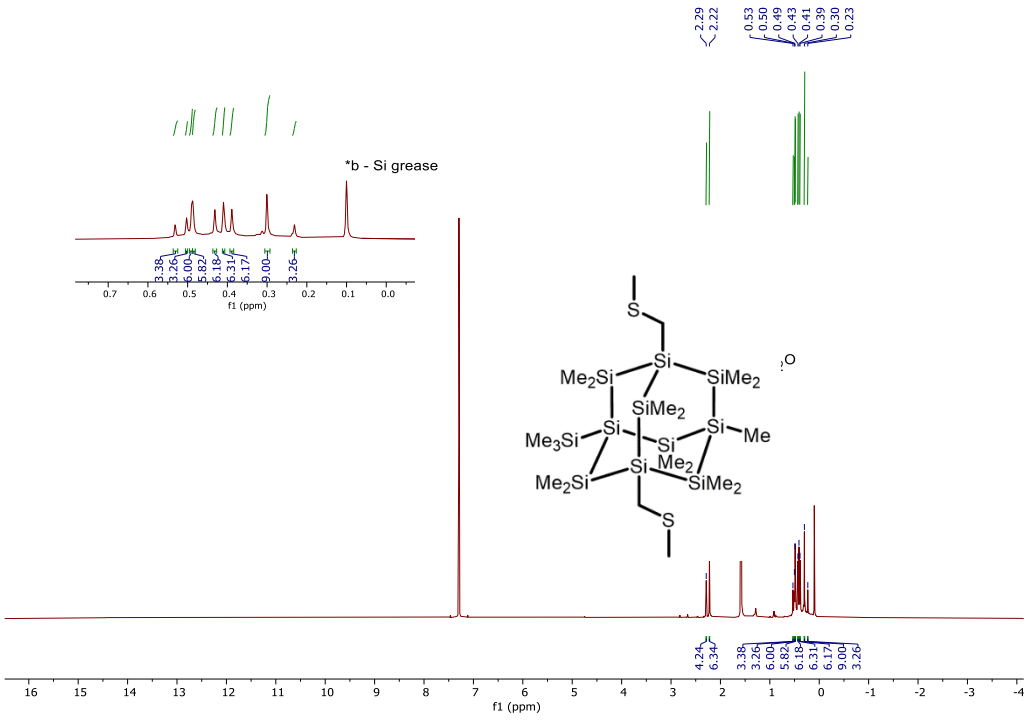


^{29}Si NMR (119 MHz, C_6D_6)

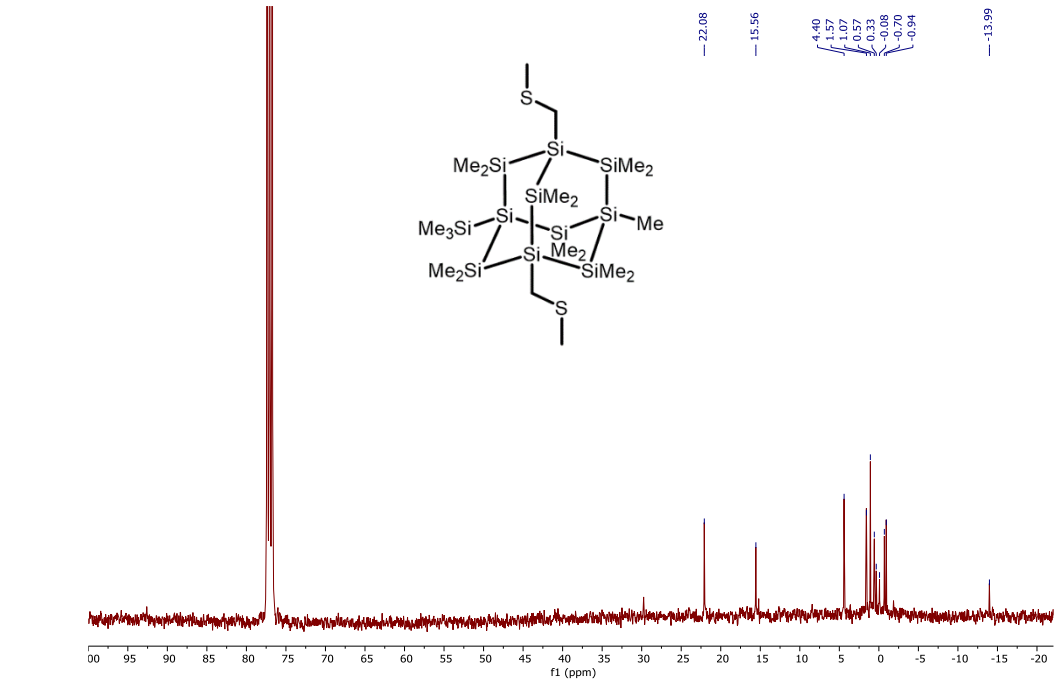


NMR Spectra of **4**

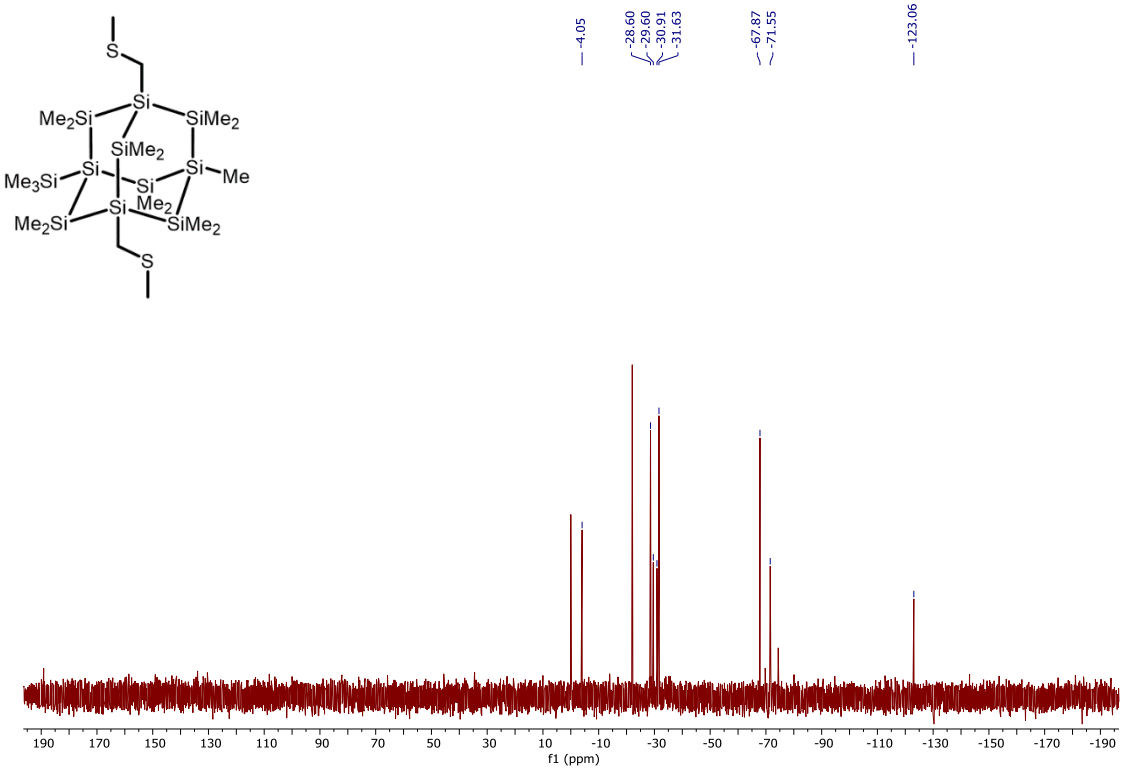
^{1}H NMR (600 MHz, $CDCl_3$)



^{13}C NMR (101 MHz, $CDCl_3$)

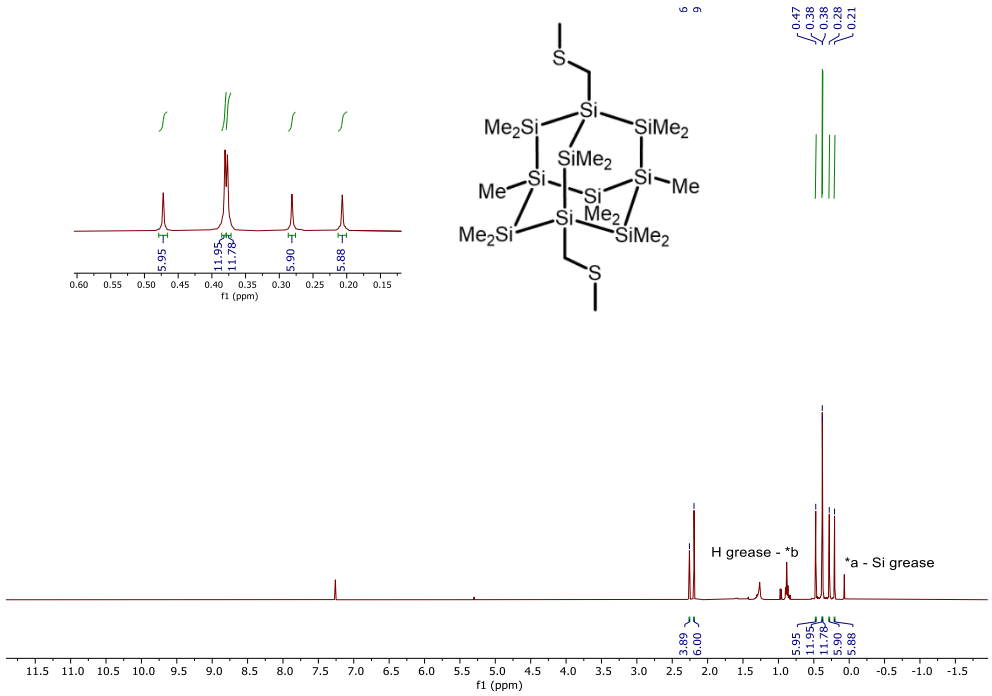


^{29}Si NMR (79 MHz, $CDCl_3$)

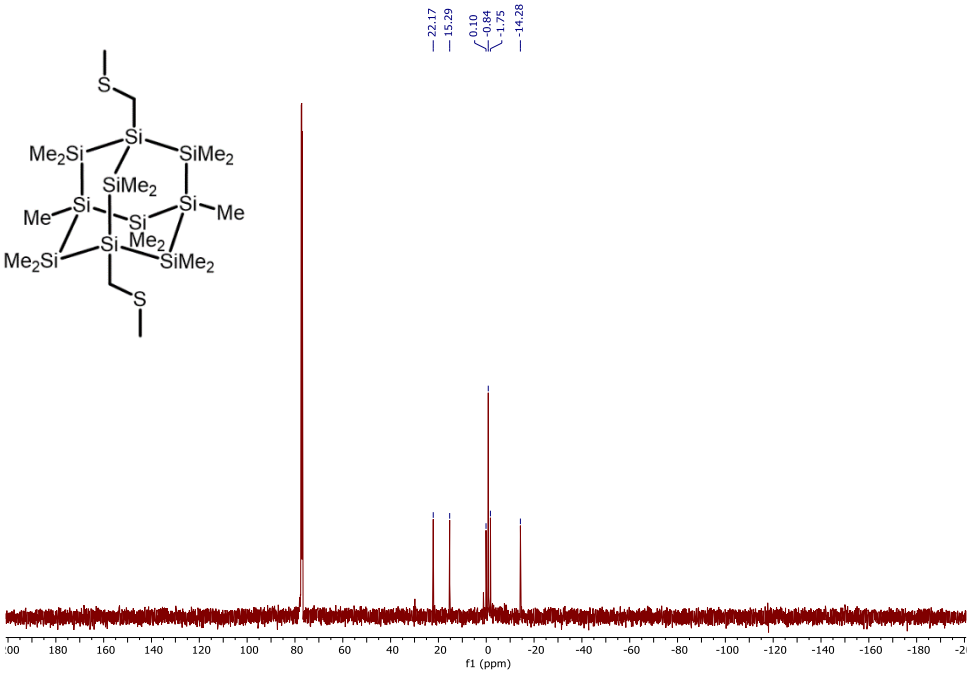


NMR Spectra of **5**

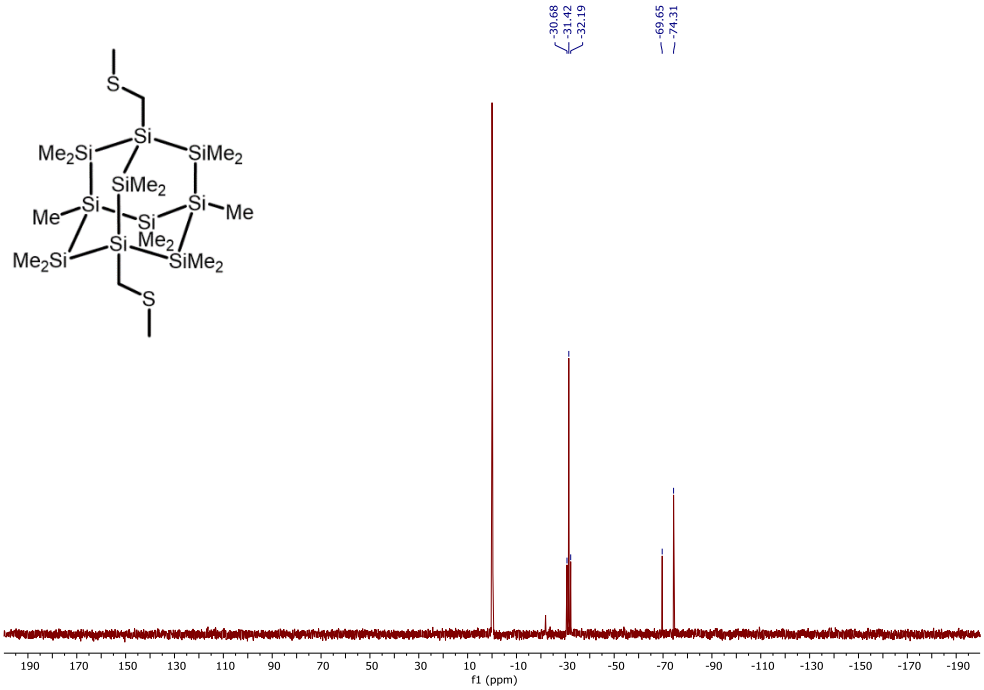
^{1}H NMR (400 MHz, $CDCl_3$)



^{13}C NMR (151 MHz, $CDCl_3$)

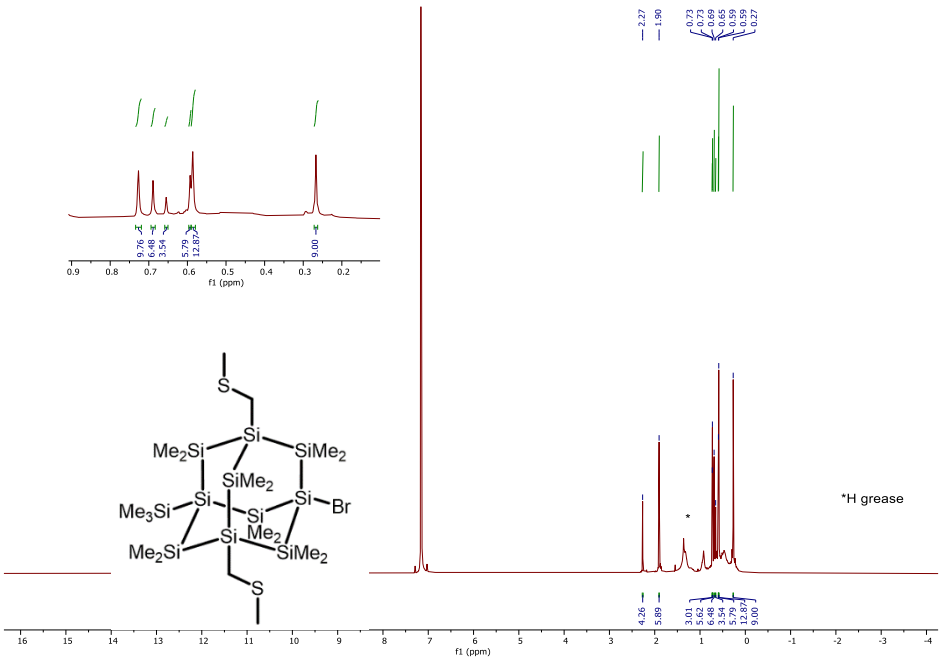


^{29}Si NMR (119 MHz, $CDCl_3$)

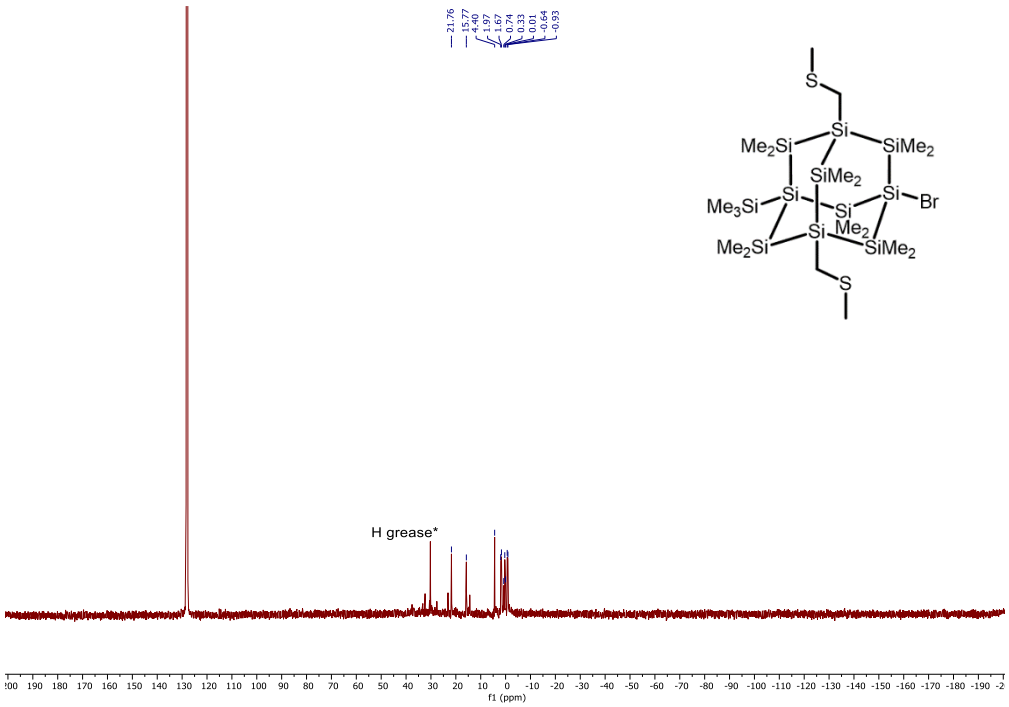


NMR Spectra of **6**

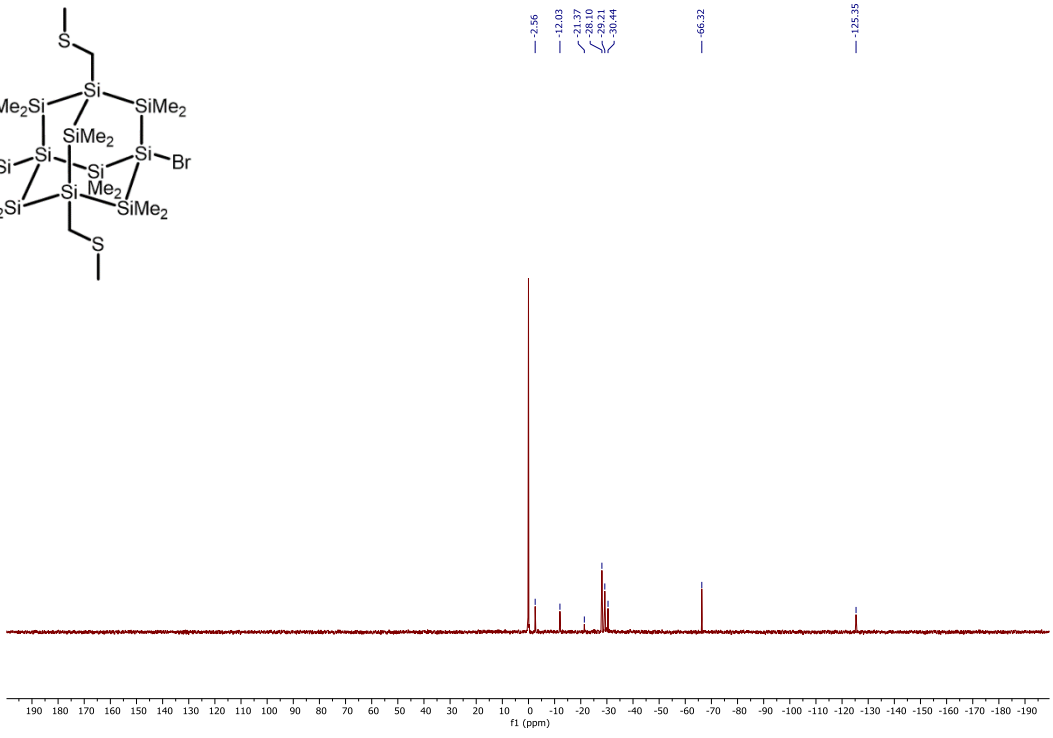
^{1}H NMR (600 MHz, C_6D_6)



^{13}C NMR (151 MHz, C_6D_6)

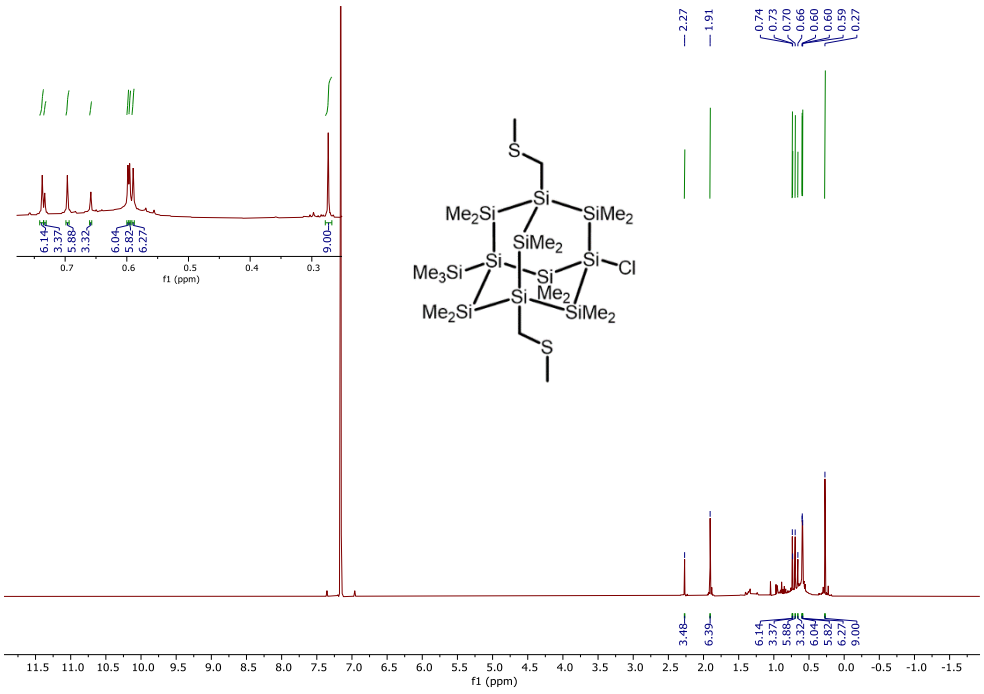


^{29}Si NMR (119 MHz, C_6D_6)

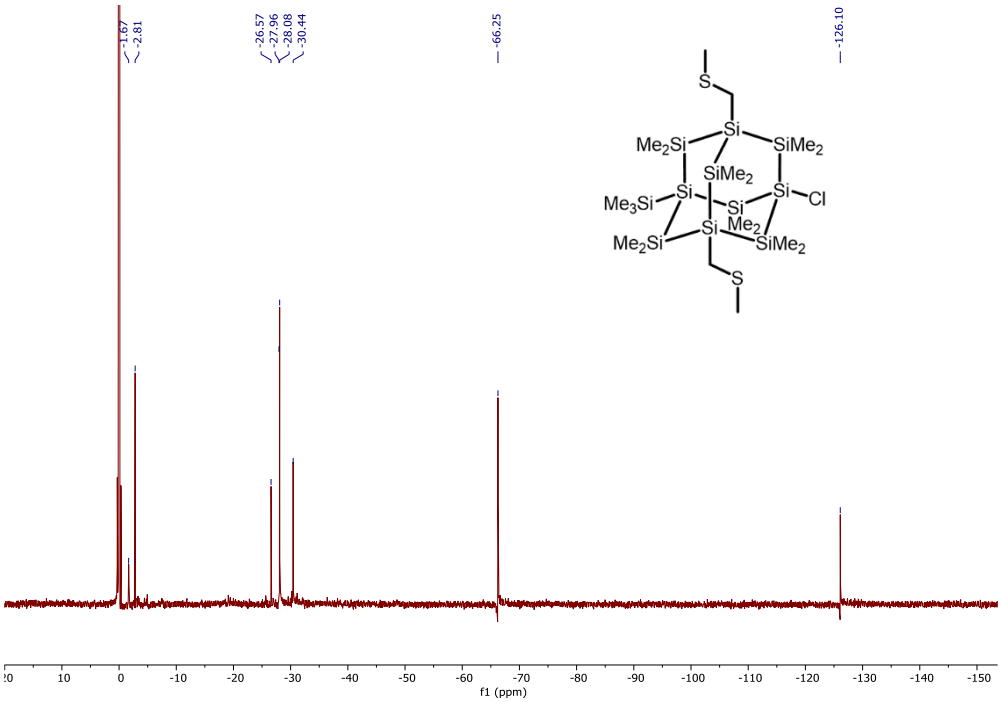


NMR Spectra of **7**

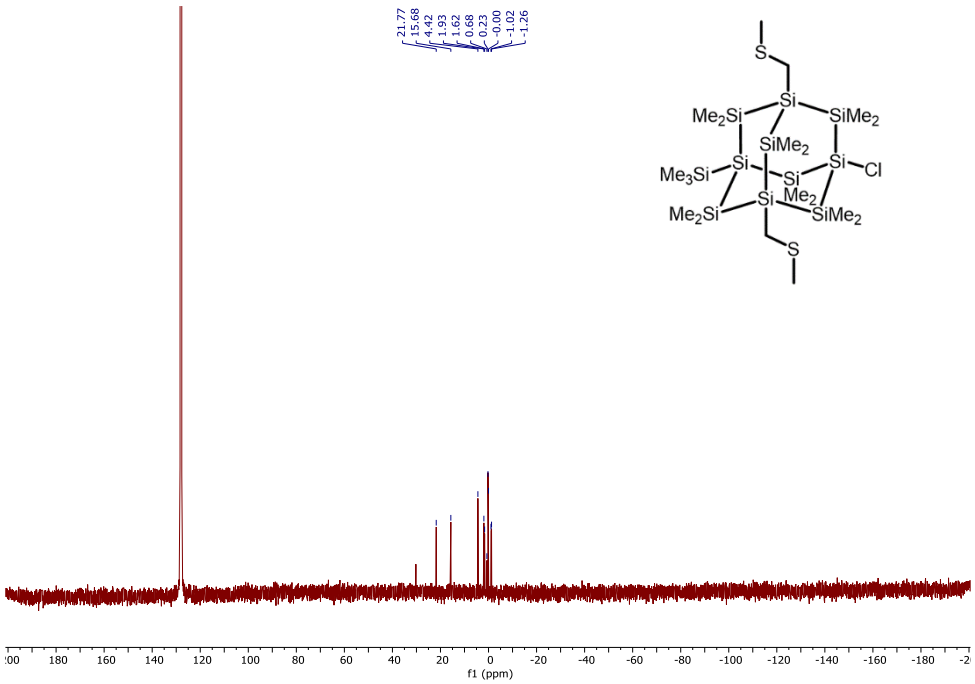
^{1}H NMR (600 MHz, C_6D_6)



^{13}C NMR (151 MHz, C_6D_6)

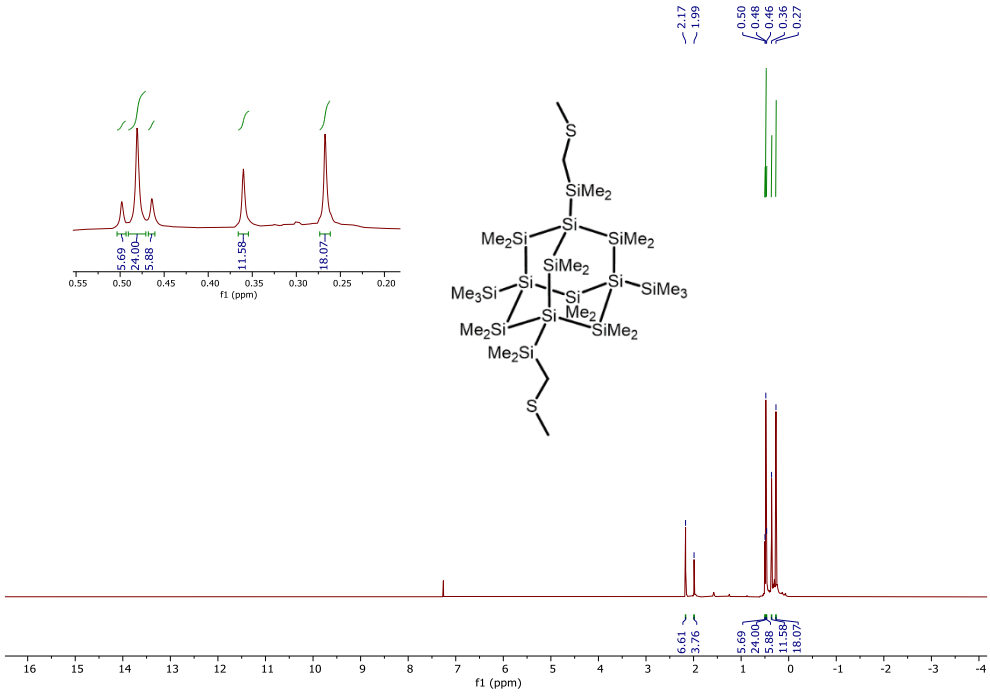


^{29}Si NMR (119 MHz, C_6D_6)

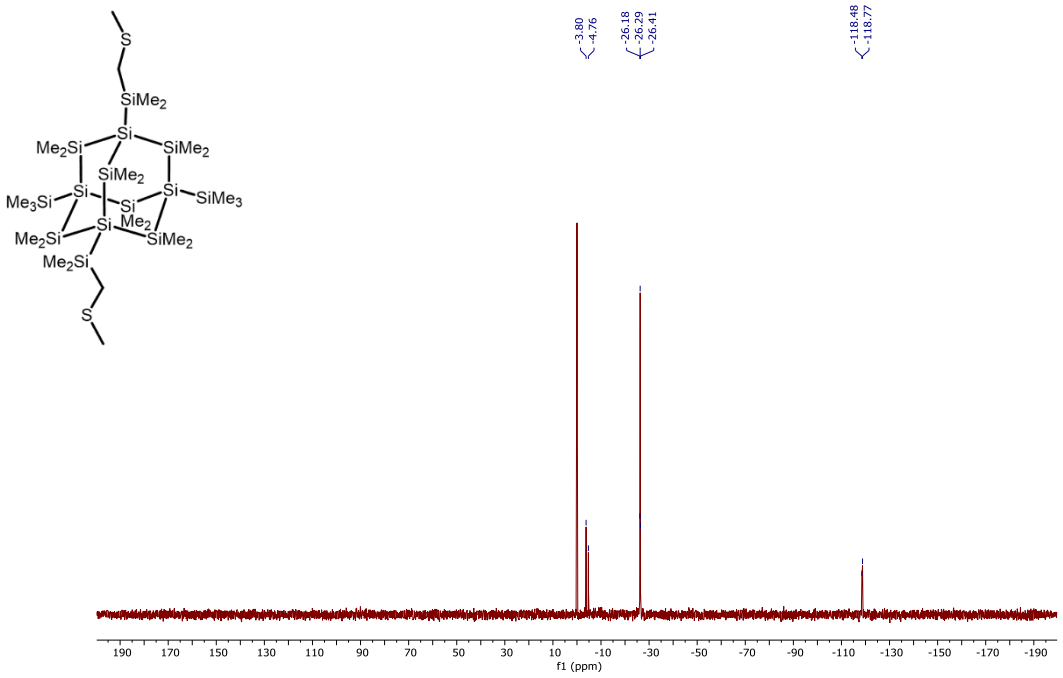


NMR Spectra of **8**

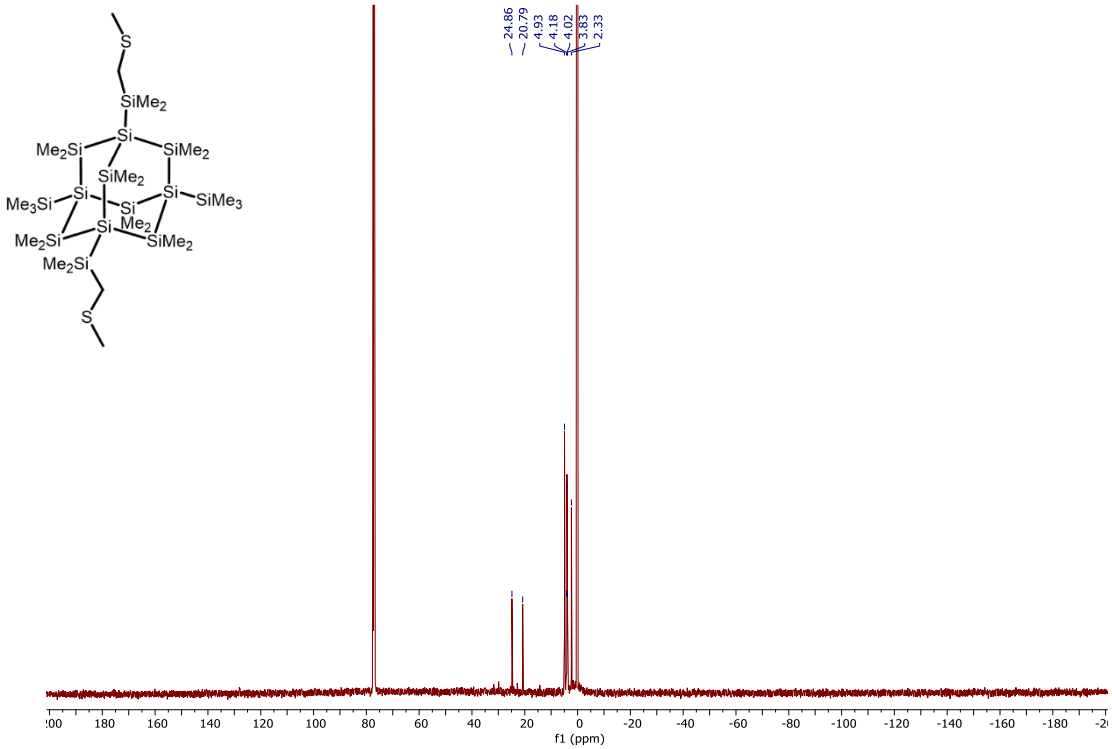
^{1}H NMR (600 MHz, $CDCl_3$)



^{13}C NMR (151 MHz, $CDCl_3$)

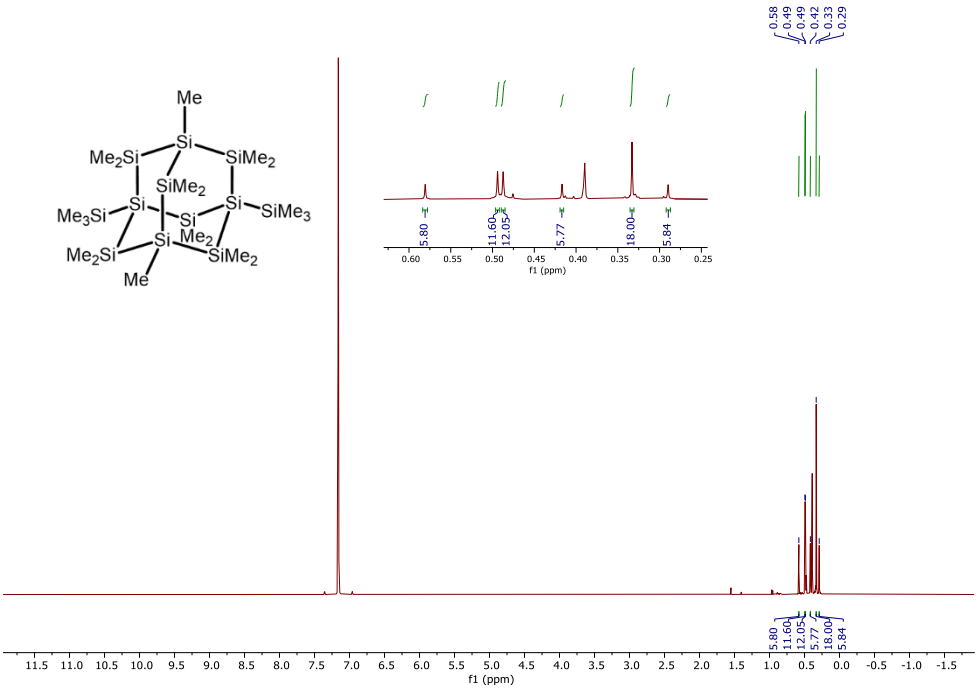


^{29}Si NMR (119 MHz, $CDCl_3$)

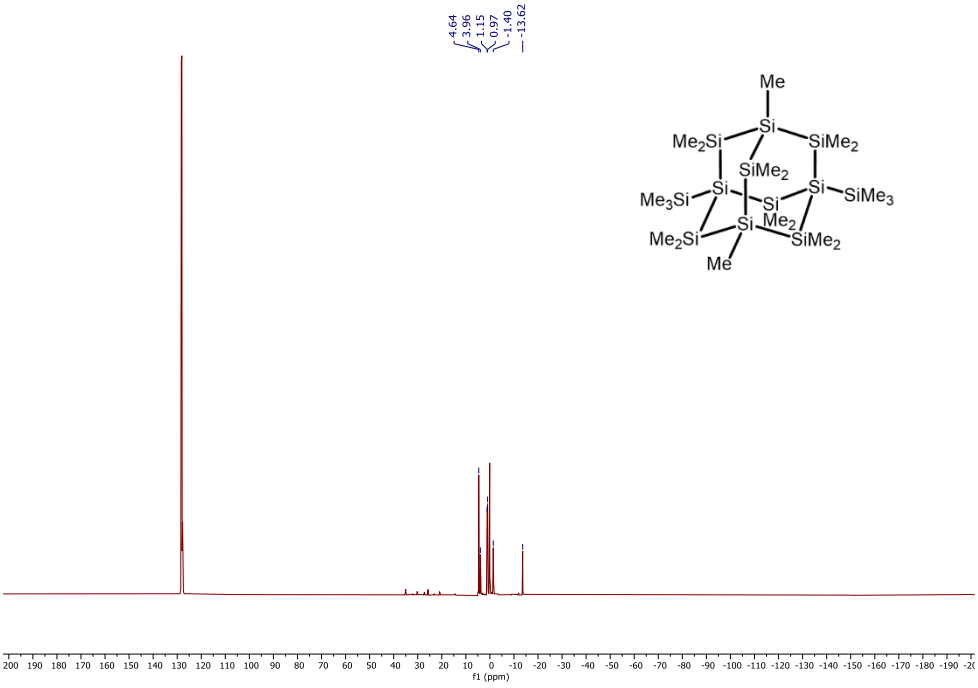


NMR Spectra of **9**

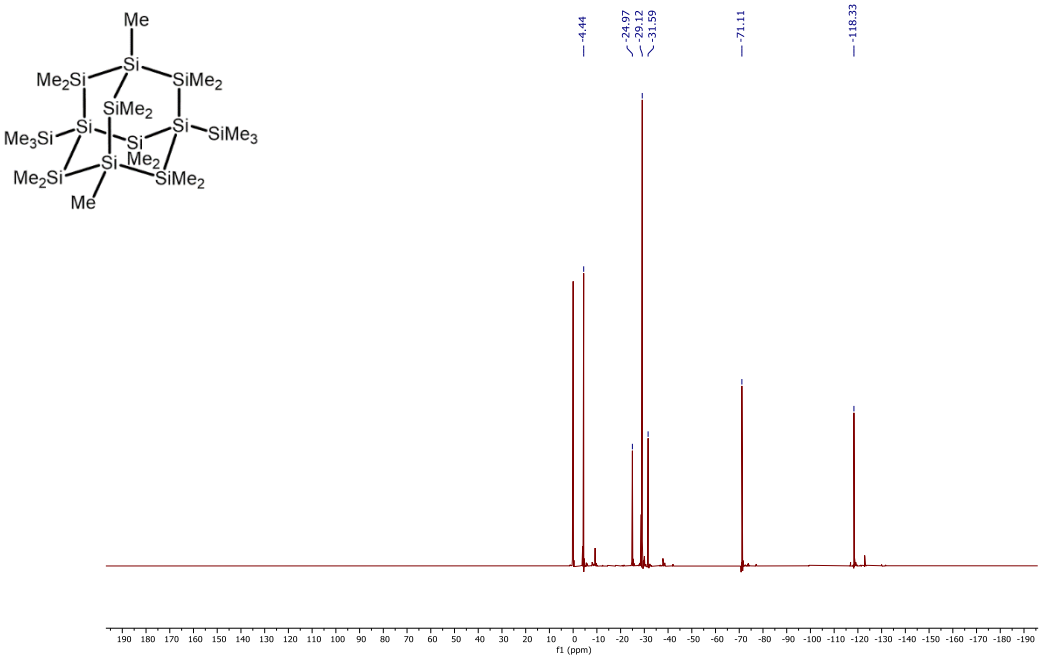
^{1}H NMR (400 MHz, C_6D_6)



^{13}C NMR (101 MHz, C_6D_6)

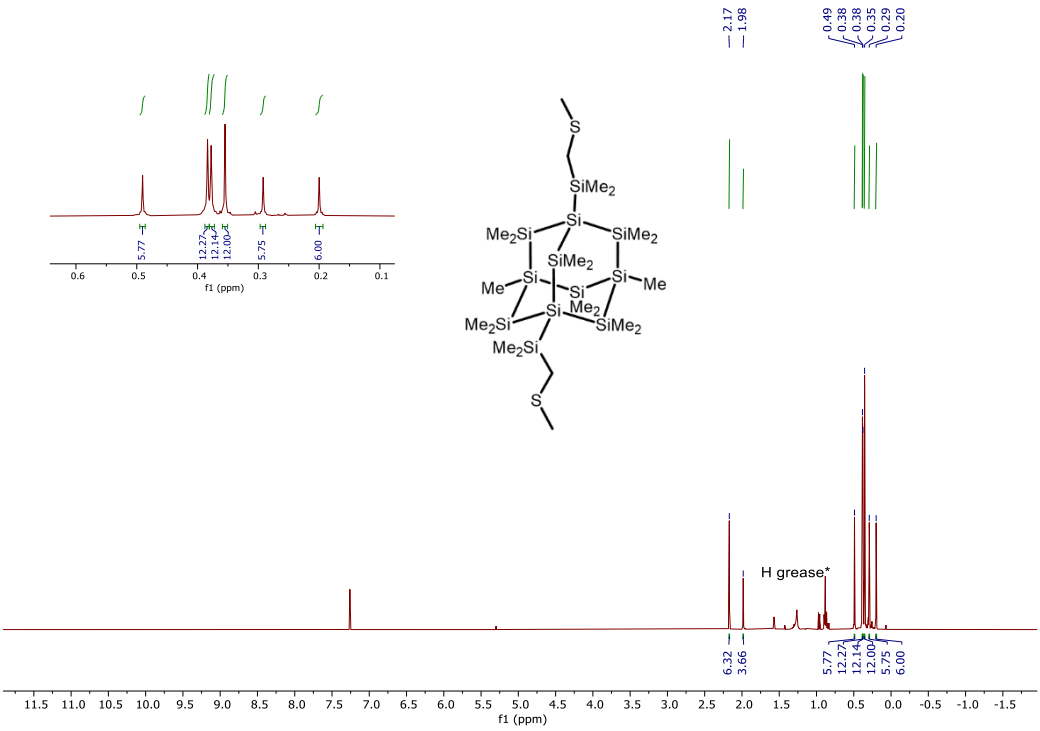


^{29}Si NMR (79 MHz, C_6D_6)

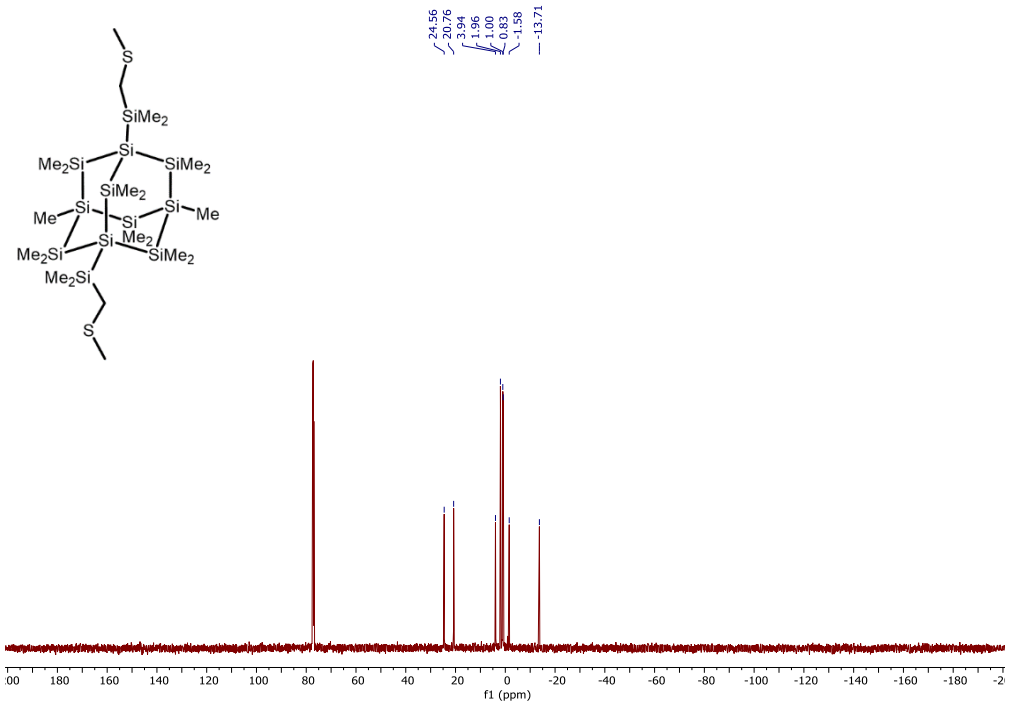


NMR Spectra of **10**

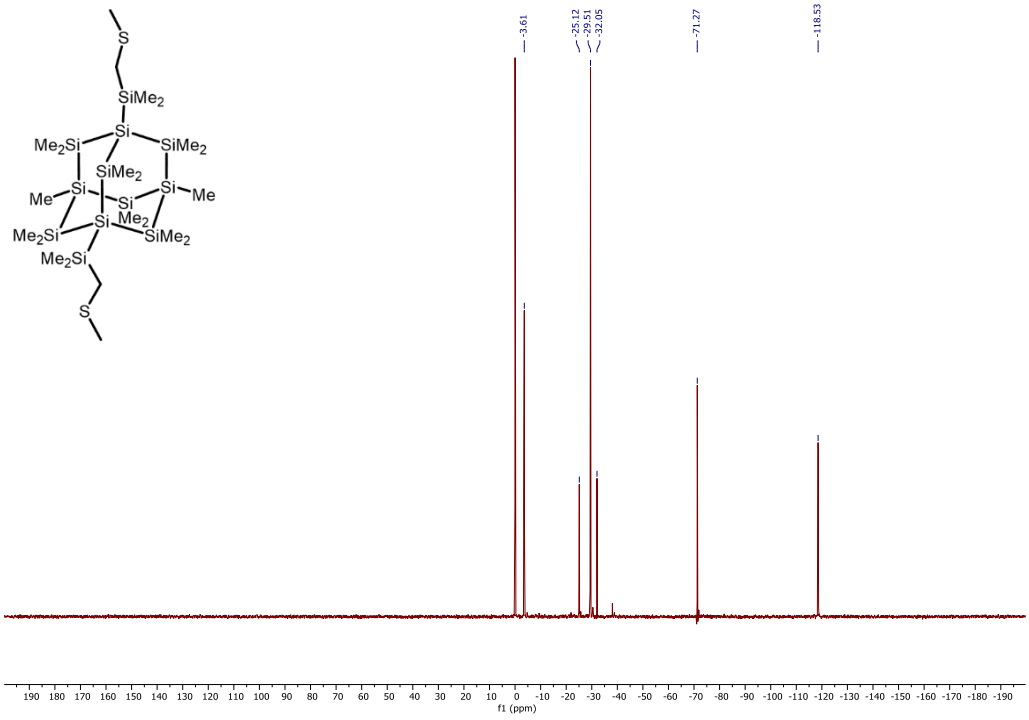
^{1}H NMR (400 MHz, $CDCl_3$)



^{13}C NMR (151 MHz, $CDCl_3$)

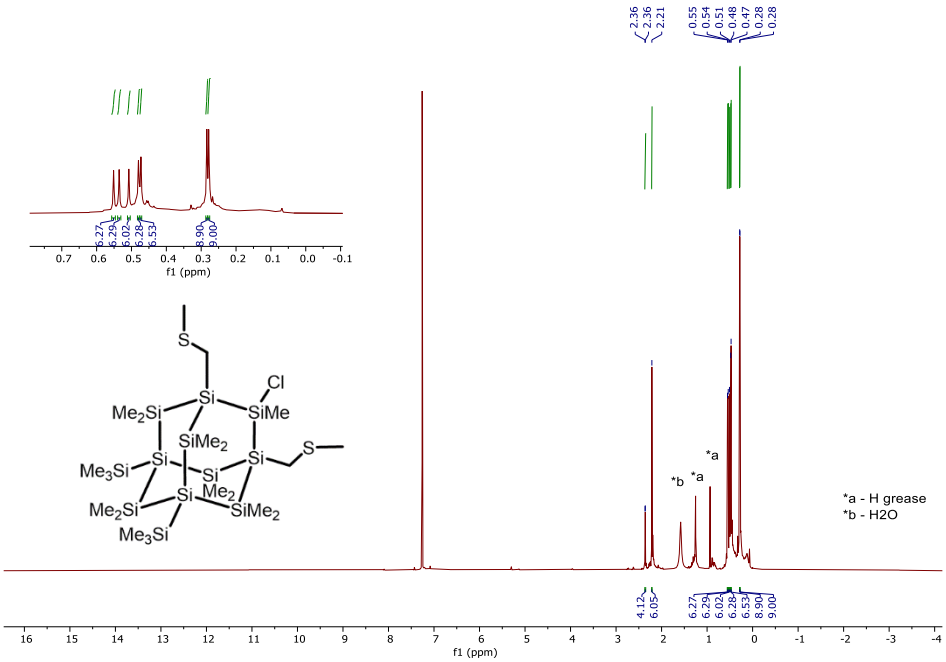


^{29}Si NMR (119 MHz, $CDCl_3$)

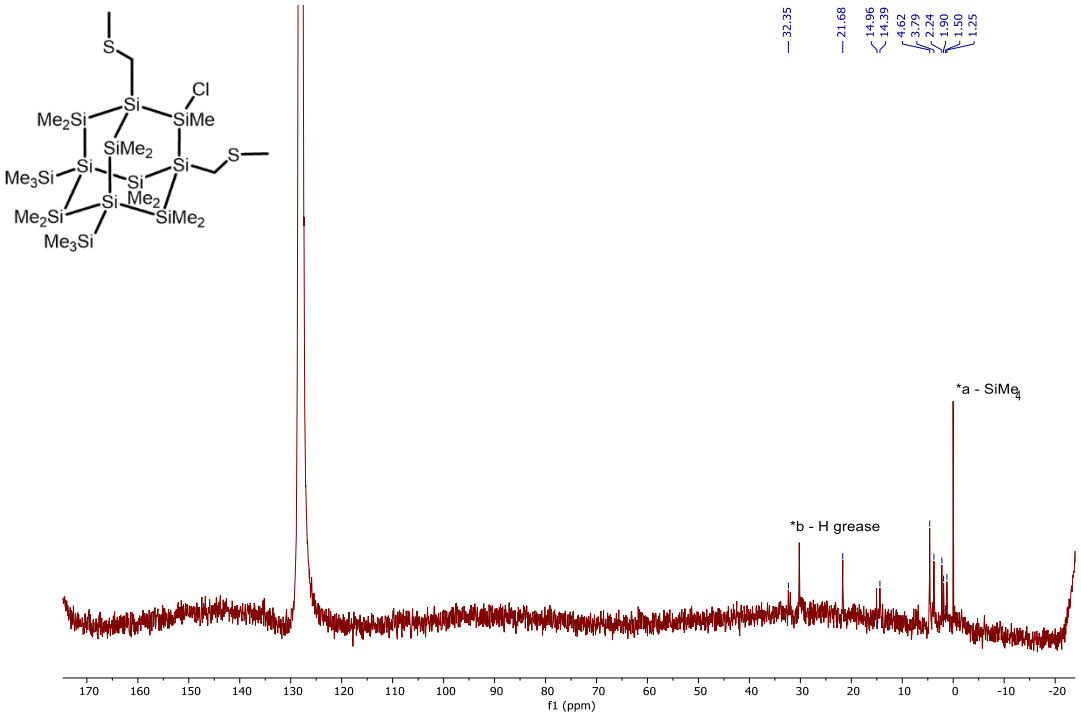


NMR Spectra of **12**

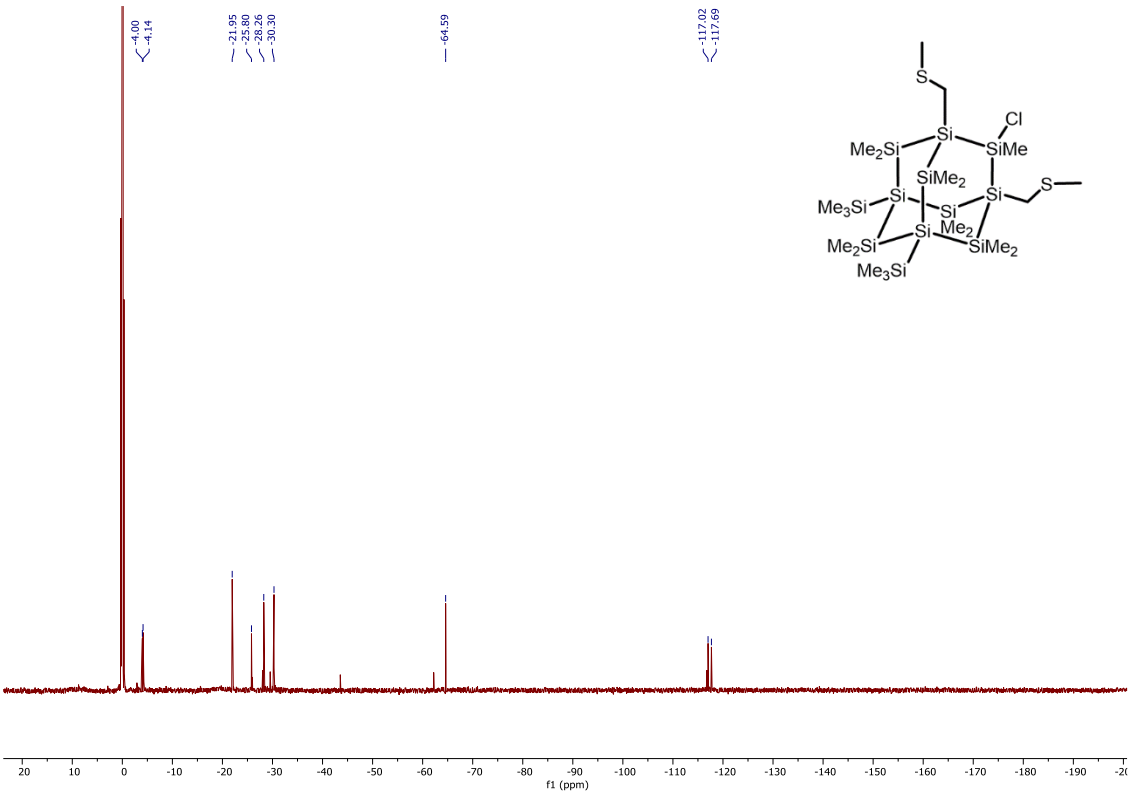
^{1}H NMR (400 MHz, $CDCl_3$)



^{13}C NMR (101 MHz, $CDCl_3$)



^{29}Si NMR (79 MHz, $CDCl_3$)



References

[1] Siu, T. C.; Imex Aguirre Cardenas, M.; Seo, J.; Boctor, K.; Shimono, M. G.; Tran, I. T.; Carta, V.; Su, T. A. *Angew. Chem. Int. Ed.* **2022**, *61* (31), e202206877.

[2] Zirngast, M.; Baumgartner, J.; Marschner, C. *Organometallics* **2008**, *27* (24), 6472–6478.

[3] Su, T. A.; Li, H.; Steigerwald, M. L.; Venkataraman, L.; Nuckolls, C. *Nat. Chem.* **2015**, *7* (3), 215–220.

Chapter 4. Oligosilane-Linked Sila-Adamantane Dumbbell Structures and Their Optical Properties

Preface

This chapter presents a manuscript in progress. I synthesized all compounds. Mr. McKinley Durham and Ms. Anika Manapul synthesized starting materials. Crystallographic data was obtained by Dr. Veronica Carta and Mr. Phillip Farias. Theoretical calculations were performed by Dr. Timothy A. Su.

Introduction

Dumbbell structures have been a subject of interest within a wide variety of fields ranging from drug delivery, organic electronics, photovoltaics and molecular machinery.[1-4] While this class molecules have been well studied within the carbon community, there remains few examples within the silicon community. One of the earliest examples of a dumbbell oligosilane structure was a linear silyl chain capped by two cyclopentasilanyl chains.[5] followed by dumbbells capped by other cyclic, or bicyclic structures.[6] While considering an expansion on the current scope of dumbbell structures, we proposed the possibility of using sila-adamantane (SiAd) as end caps for a dumbbell structure.

SiAd is a tricyclic cluster that is isostructural with the basic unit cell of bulk, crystalline silicon. It was first synthesized by Marschner and co-workers via Lewis acid mediated rearrangement of a tricyclic precursor.[7] Previously, we envisioned that SiAd

could be utilized as a model to explore the UV-vis absorbance differences in bridgehead versus bridge substitution and provided an atom-precise view on how nanocrystalline Si surface functionalization impacts fundamental optical properties.[8] Here, we sought to utilize SiAd as end caps for a dumbbell oligosilane structure to probe how the tricyclic cluster behaves when incorporated with a silyl chain. understand how changing the chain length or cluster end groups would alter molecular orbital environments of the dumbbell materials and impact physical effects.

Results and Discussion

Figure 4.1 Synthesis of symmetric dumbbell SiAds, **3** - **6**.

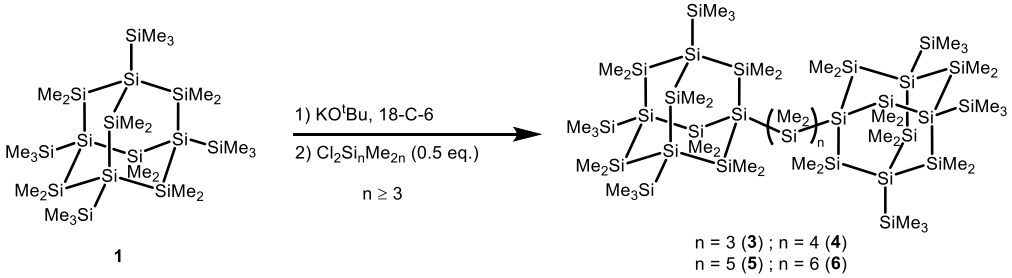


Table 4.1 Yields of dumbbell SiAds **3** - **6**. n ≤ 2 could not be formed.

n	Electrophile	% yield	Product
1	$ClSiMe_2Cl$	n/a	-
2	$ClSi_2Me_4Cl$	n/a	-
3	$ClSi_3Me_6Cl$	61%	**3**
4	$ClSi_4Me_8Cl$	38%	**4**
5	$ClSi_5Me_{10}Cl$	42%	**5**
6	$ClSi_6Me_{12}Cl$	45%	**6**

We were initially curious on dimerizing SiAd via installing dimethylsilylene subunits in between two SiAd end groups. We find that the dumbbell SiAds can be synthesized by forming the monoanion of **1** via potassium tert-butoxide mediated cleavage of a terminal trimethylsilyl group, followed by quenching with a α,ω-

dichloropermethyloligosilane (0.5 eq.) of varying length from n=1-6 (Figure 4.1, Table 4.1).[9] Following this synthetic method, we were able to synthesize dumbbell SiAds with three to six dimethylsilylene chain lengths. Chain lengths with less than three dimethylsilylene groups were attempted, but it seems that synthesis of shorter dumbbell SiAds are not feasible via potassium tert-butoxide chemistry, likely due to the steric demand imposed by the SiAd end groups.

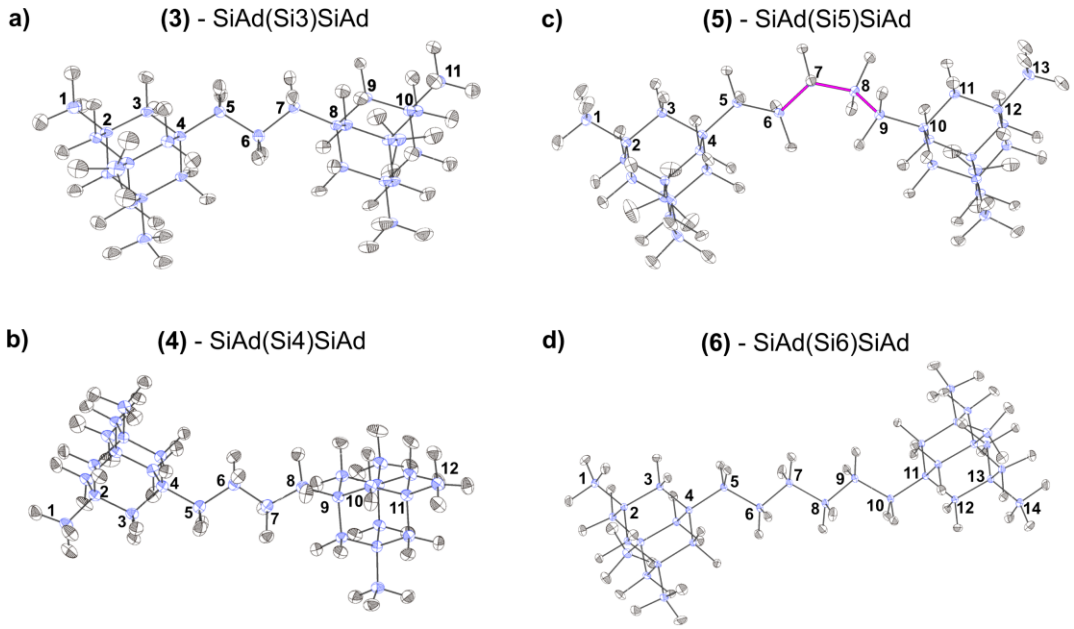


Figure 4.2 a) – d) Crystal structures of **3** through **6**. Bonds highlighted in purple display a gauche orientation. Solvent molecules and H atoms omitted for clarity. Si (blue), C (black).

Table 4.2 Relevant dihedral angles for dumbbell SiAds. Si atoms labeled correspond to longest Si chain. Red - anti, blue – transoid, yellow – gauche

	1-2-3-4	2-3-4-5	3-4-5-6	4-5-6-7	5-6-7-8	6-7-8-9	7-8-9-10	8-9-10-11	9-10-11-12	10-11-12-13	11-12-13-14
3	177.7(2)	-176.4(6)	-161.6(3)	-163.5(3)	-167.6(3)	-155.1(3)	-175.4(2)	179.0(2)	-	-	-
4	-179.9(9)	-179.7(9)	-159.5(10)	-160.4(7)	-160.4(7)	-160.4(7)	159.5(10)	-179.7(9)	179.9(10)	-	-
5	176.9(5)	-175.8(4)	-86.2(6)	-177.2(5)	98.1(4)	177.1(4)	162.4(5)	162.4(5)	179.0(4)	179.3(5)	-
6	-178.8(3)	-177.2(3)	-157.9(4)	-161.4(3)	177.9(4)	180.0(3)	177.9(4)	161.4(3)	157.8(4)	177.2(3)	-178.8(3)
7	-177.5(4)	176.0(4)	154.3(4)	170.5(3)	155.3(2)	171.5(15)	180.0(1)	174.9(9)	-	-	-

In addition to common spectroscopic methods of molecular characterization, we were also able to obtain crystallographic data via X-Ray diffraction analysis (Figure 4.2). The crystal structures of all dumbbell SiAds were determined by X-ray crystallographic

analysis and their relevant dihedral angles are described in Table 4.2. Here, each of the dumbbell SiAds have between 11 and 14 silicon atoms that form the backbone framework with the SiAd clusters imposing steric demands that influence the conformation of the dimethylsilylene linker units.

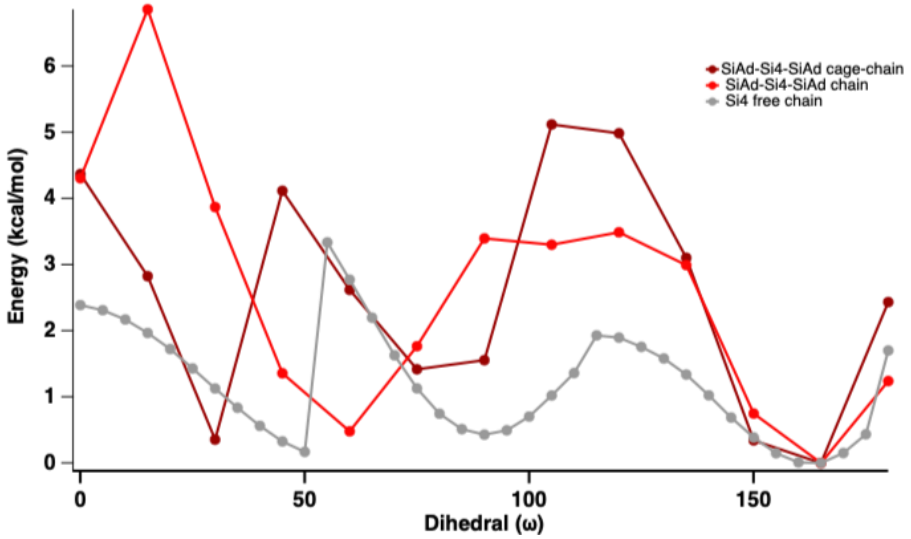


Figure 4.3. Dihedral scans of **4** along the chain linkage (red) and along the cage-chain (dark red). Dihedral scan of a linear Si_4Me_8 provided for context (grey).

A conformationally free linear silane chain typically contains a myriad of conformers in solution.[10] However, silyl chains can be locked in a conformation of choice by incorporating the chain within varying cyclic units.[11,12] We observe a similar conformation locking effect in these oligosilane linked dumbbell structures when investigating the torsion angles of **3** to **6**. Crystallographic data has revealed that there are two conformational locking mechanisms present here, where: 1) the Si atoms that are incorporated into the cluster ends are locked into *anti* dihedral angles analogous to carbon chain-tethered oligosilanes and 2) the Si atoms between the cluster ends are held at *transoid* or *gauche* dihedral angles due to the steric influence of the cluster ends. We also

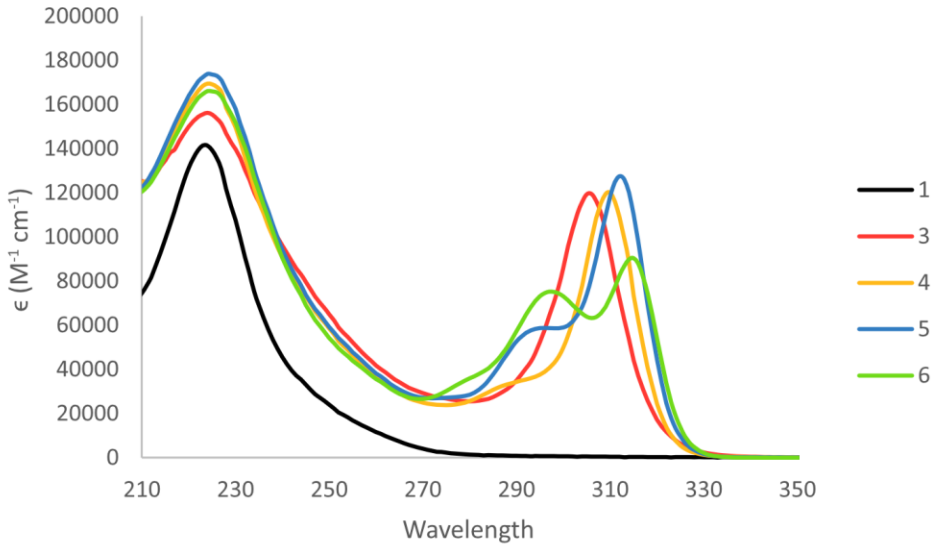


Figure 4.4 Experimental ultraviolet absorption spectra for 10 μM solutions of **1** and **3 – 6** in pentane.

Table 4.3 Scope of dumbbell SiAds and their ultraviolet absorption properties. *Data obtained from ref. [5]

	λ_1 [nm], ε_1 [M^{-1} cm^{-1}]	λ_2 [nm], ε_2 [M^{-1} cm^{-1}]	λ_3 [nm], ε_3 [M^{-1} cm^{-1}]
1*	225 nm, 141350	-	-
3	225 nm, 156170	-	306 nm, 119430
4	225 nm, 169420	286 nm, 31660	310 nm, 120030
5	225 nm, 173830	292 nm, 56500	312 nm, 127540
6	225 nm, 166120	297 nm, 75230	315 nm, 90459

note that the crystal structure of **5** contains a kinked, *gauche* conformation within the chain linkage. This infers that the barrier of rotation energy between transoid and ortho conformations in the chain linkages are likely smaller in energy for longer chains ($n \geq 5$). Indeed, even dihedral scans of **4** ($n = 4$) reveal energy wells near 80° and 160° for the chain linkage, with the *transoid* conformer being more favorable than the *guache* conformer by ~2 kcal/mol (Figure 4.3).

The structural nuances revealed by XRD and their dynamic nature is further revealed in their UV-vis absorbance characteristics. The dumbbell SiAds exhibit optical

properties of both a cluster and a linear silane chain characterized by high and low energy wavelengths of maximum absorption (Figure 4.4). The SiAd cluster components within the dumbbell SiAds have an absorbance signature (λ_1) at 225 nm and has a molar absorptivity ($\mathcal{E}_1$) higher than that of **SiAd** as a lone cluster (Table 4.3).[8] In addition to a cluster absorbance signature, we also observe a lower energy wavelength of maximum absorption (λ_3) that can be attributed to the silicon atoms that comprise the backbone of the dumbbell SiAds. As the backbone chain grows longer in length from **3** to **6**, the λ_3 absorbances red-shift from 306 nm to 315 nm respectively. The phenomenon of red-shifted absorbances as a function of silyl chain length is known to be attributed to increased σ – conjugation across the molecule.[13]

The linear absorbance signatures of these dumbbell structures are considerably different than that of previously reported linear permethylated silyl chains of comparable length. For example, **4** ($\lambda_3 = 310$ nm; $\varepsilon_3 = 1.2 \times 10^5$) is red-shifted by 25 nm and ε_3 is three times as intense as a permethylated, conformationally free $Si_{12}Me_{26}$ analogue ($\lambda_3 = 285$ nm; $\varepsilon_3 = 4.3 \times 10^4$).[14]

In accordance with the kinks that we observe in the oligosilane chains in our crystallographic data, we also find evidence of that these chains kink in solution, despite the steric bulk of the SiAd endgroups. Beginning with **4**, we observe the onset of a shoulder peak (λ_2) around 290 nm that grows in intensity as the Si bridges increase in length. To support that this blue-shifted absorbance peak arises from *gauche* defects, we performed TD-DFT calculations of *anti* and *gauche*-kinked **4, 5, 6** (Figure 4.5).

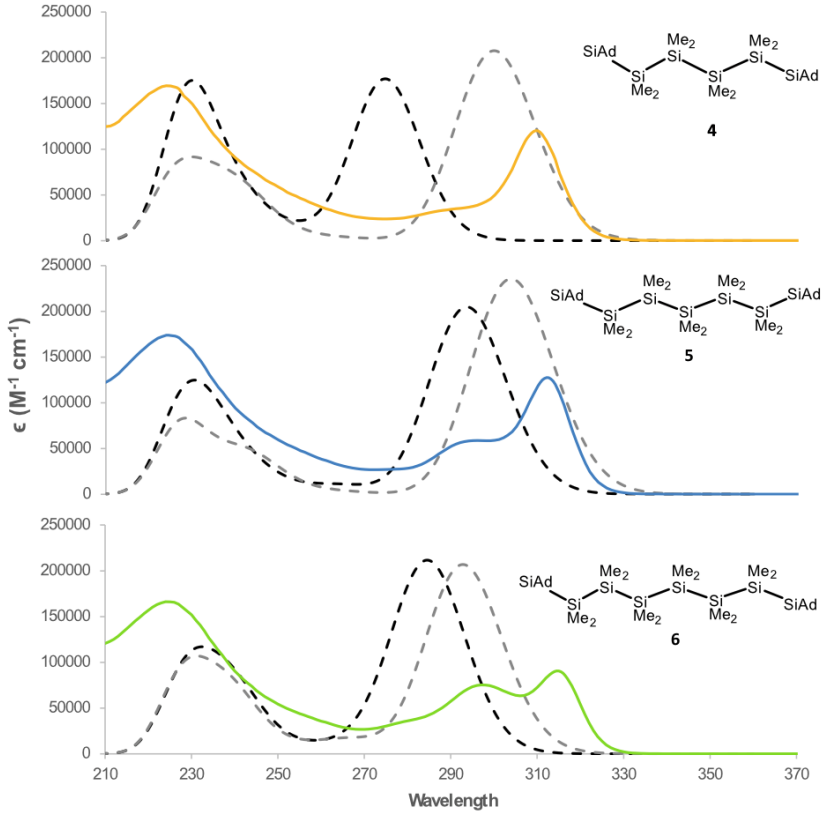


Figure 4.5 Experimental ultraviolet absorption spectra for 10 μM solutions of **4**, **5**, and **6** (solid yellow, blue and green respectively) in pentane. TD-DFT-calculated spectra (dotted black line – gauche ; dotted gray line – anti) at the PBE0/TZVP//BP86/TZVP level.

These findings suggest that as chain lengths increase, so too does the population of *gauche* conformers in solution. This increase is λ_2 (dotted black lines in Figure 4.5) accompanied by a decrease in λ_3 (dotted gray lines in Figure 4.5) intensity, the straight chain conformation. In **5**, the steric demand of the SiAd end groups are not sufficient to conformationally confine the linker groups to one conformation, resulting in significant growth of λ_2 for both **5** and **6**, seen in both the TD-DFT calculated spectra (Figure 4.5) and the experimental spectra (Figure 4.4). This onset of a higher energy peak (λ_2) has been observed for analogous oligosilane chains of similar length and also seem to red-

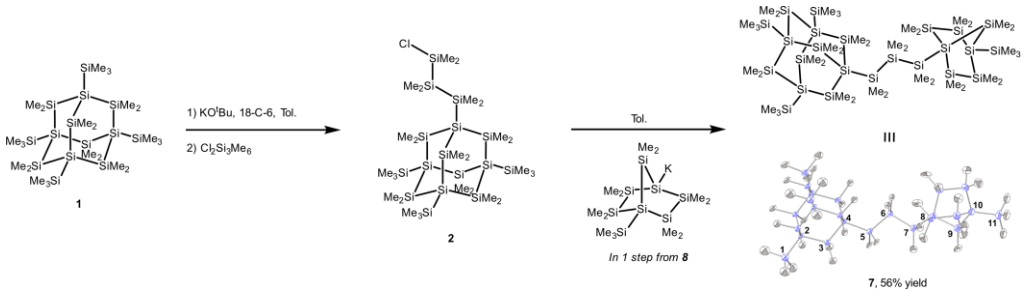


Figure 4.6 Synthesis of asymmetric dumbbell SiAd-Si_3Me_6-Si[2.2.1.] (**7**)

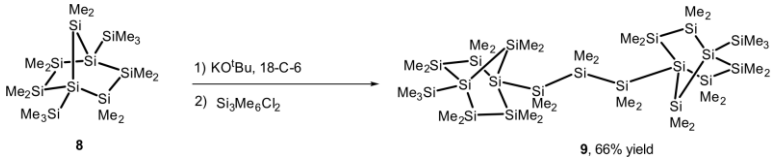


Figure 4.7 Synthesis of Si[2.2.1.]-$SiMe_2$-Si[2.2.1.] (**9**)

shift with increasing length.[15] It appears that as the dumbbells increase in length, the lower rotational barrier energy of the silyl chain linkage. This results in an increased population of gauche conformers in solution which is attributed to the rise of ε_2.

In addition to probing effect of chain length in dumbbell structures, we wanted to investigate how alternative cluster end groups could alter electronic properties while keeping the length of the molecule constant. To do this, we generated a silyl anion of **1** subsequently quenched the silyl anion with dichlorohexamethyltrisilane to yield **2**. We then generated the silyl anion of a Si[2.2.1.] cluster (**8**) and quenched it with **2** to yield an asymmetric dumbbell cluster, **9**, containing one SiAd and one Si[2.2.1.] end group. (Figure 4.6). To generate a dumbbell where both SiAd end groups are replaced with

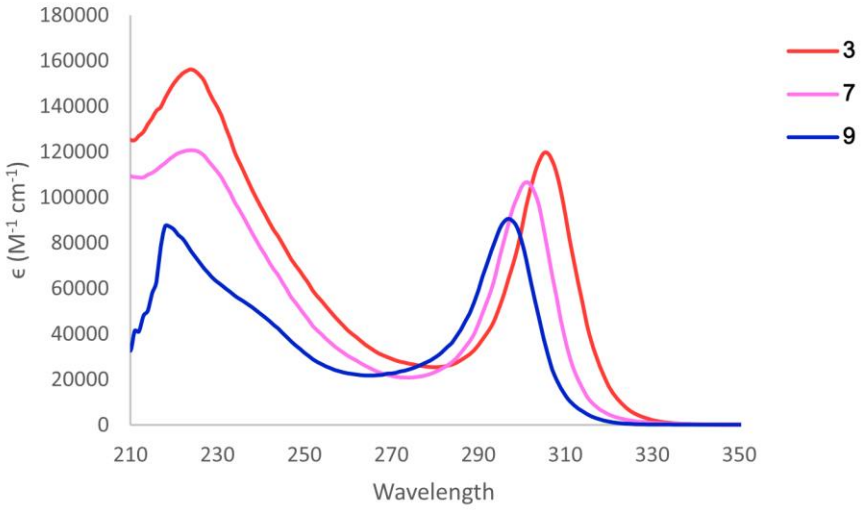


Figure 4.8 Experimental ultraviolet absorption spectra for 10 µM solutions of **3**, **7**, and **9** in pentane.

Table 4.4 Ultraviolet absorption properties of **3**, **7** and **9**

	λ_1 [nm], ε_1 [M^{-1} cm^{-1}]	λ_2 [nm], ε_2 [M^{-1} cm^{-1}]	λ_3 [nm], ε_3 [M^{-1} cm^{-1}]
3	225 nm, 156170	-	306 nm, 119430
7	225 nm, 120670	-	301 nm, 106640
9	218 nm, 87448	-	297 nm, 90666

Si[2.2.1.] clusters, we employed a similar method to the previous symmetrical dumbbells to yield **9** (Figure 4.7).

We also observed cluster dependent optical behavior by comparing the dumbbell absorbances of **3**, **7**, and **9** (Figure 4.8). These three dumbbells differ only in their end groups while the overall length of each dumbbell remains the same. Interestingly, the backbone chain absorbance (λ_3) has been blue shifted with increasing amounts of Si[2.2.1.] compared to **3**, which contains exclusively SiAd end groups (Table 4.4). Although **3**, **7** and **9** are comparable in length, the blue shifting of the lower energy absorption wavelength can be rationalized by the difference in the HOMO-LUMO gap between each dumbbell (Figure 4.9). Since SiAd is a larger cluster than Si[2.2.1.], it

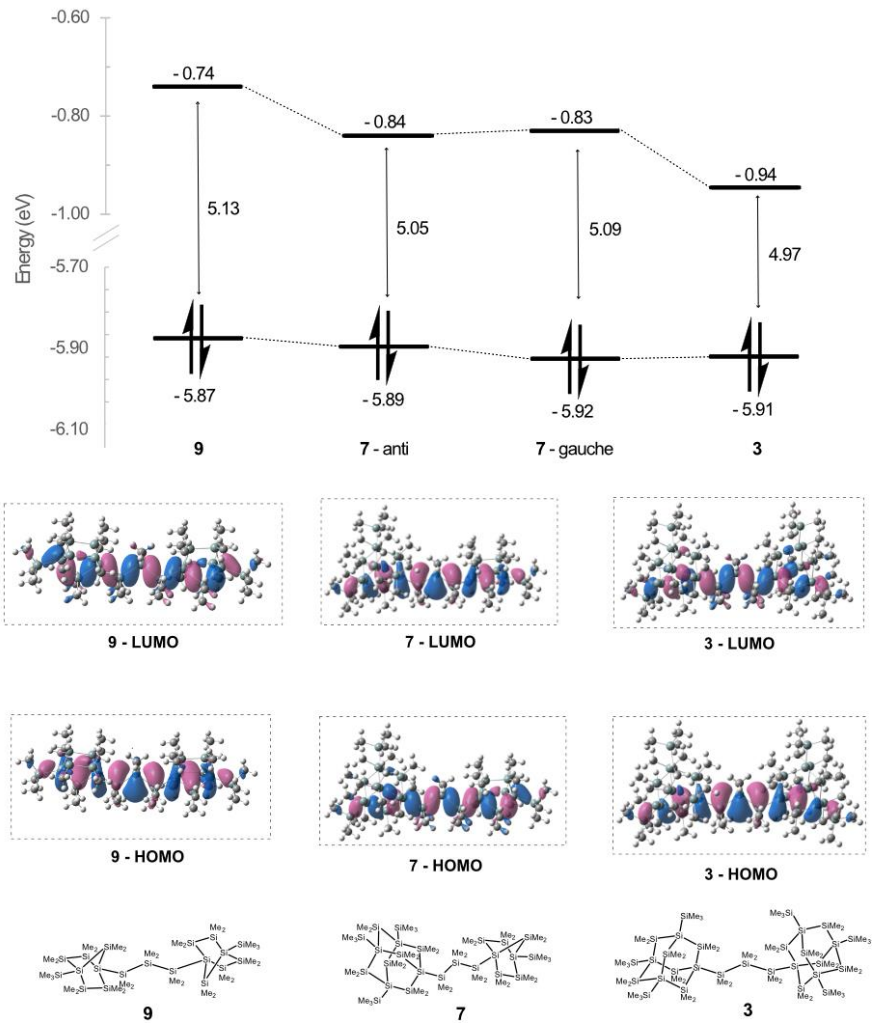


Figure 4.9 Molecular orbital diagrams of HOMO and LUMO of **9**, **7**, and **3**. Energy levels obtained from DFT-optimized structures at the M06-2X/6-31G**. MO surface plots of **9**, **7**, and **3** below.

confers more electronic delocalization and lowers the LUMO relative to that of Si[2.2.1.]. This results in larger HOMO-LUMO gaps for **9** relative to **7** and **3** and directly correlates to the overall 10 nm blue-shift of λ_3 between **9** and **3**.

We were also curious about the possibility of further functionalization of the dumbbell SiAds. To test this, we attempted to generate silyl dianions of **2** and **3** and subsequently quenched the dianions with chloromethyl methyl sulfide to obtain sulfur

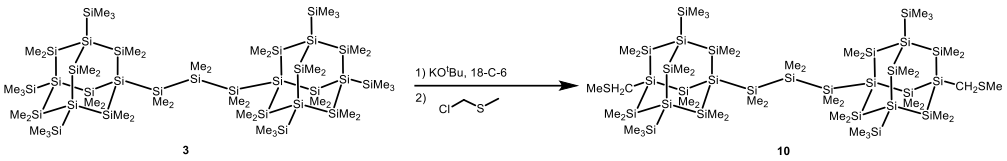


Figure 4.10 Synthesis of functionalized dumbbell **10**.

linker functionalized dumbbell SiAds, **10** and **11** (Figure 4.10). These derivatives of dumbbell SiAds may be suitable for further study in single molecule junction studies.

Conclusions

We report the synthesis of a tricyclic capped dumbbell structure with dimethylsilylene linker lengths between 3 and 6. We also display an example of an asymmetric dumbbell structure, **7**, and provide evidence of further functionalization of the dumbbells through synthesis of **10** and **11**. The optical properties of these dumbbell structures display a high energy, cluster absorption and a low energy, linear chain absorption. The high energy cluster absorption is higher than that of **1** as a lone cluster. The low energy linear chain absorption is 3 times as intense than that of a conformationally free, linear chain of comparable length, as seen when comparing wavelengths of maximum absorption between **4** and a permethylated Si12 analogue. The Si[2.2.1]. dumbbell structure, **9**, has a low energy wavelength absorption that is blue shifted compared to that of **3** which can be rationalized by the LUMO lowering effect that SiAd contains compared to the Si[2.2.1.] cluster. With the ability to functionalize these oligosilane dumbbells further, we intend to probe their charge transport properties.

References

[1] Xu C.; Wang B.; Sun S. *J. Am. Chem. Soc.* **2009**, *131*(12), 4216 – 4217

[2] Mahmoudi C.; Bulut I.; Jing J.; Heinrich B.; Mery S.; Heiser T.; Leveque P.; Steveler E.; Majdoub M.; Leclerc N. *Eur. J. Org. Chem.* **2021**, *2021*(22), 3170 – 3177

[3] Schroeder B. C.; et Al. *Angewandte Chemie* **2014**, *126*(47), 13084 – 13089

[4] Tseng H.; Vignon S. A.; Stoddart F. *Angewandte Chemie Int. Ed.* **2003**, *42*(13), 1491 – 1495

[5] Hengge E., Jenkner P. K. *Z. Anorg. Allg. Chem.* **1988**, *560*, 27 – 34

[6] Wallner A., Hlina J., Konopa T., Wagner H., Baumgartner J., Marschner C. *Organometallics* **2010**, *29*, 2600 – 2675

[7] J. Fischer, J. Baumgartner, C. Marschner, Science **2005**, *310*,825

[8] Siu, T. C.; Imex Aguirre Cardenas, M.; Seo, J.; Boctor, K.;Shimono, M. G.; Tran, I. T.; Carta, V.; Su, T. A. *Angew. Chem., Int. Ed.* **2022**, 61 (31), No. e202206877.

[9] Su, T. A.; Li, H.; Steigerwald, M. L; Venkataraman, L.; Nuckolls, C. *Nat. Chem.* **2015**, *7*, 215–220.

[10] Imhof R.; Antic D.; David D. E.; Michl J. *J. Phys. Chem. A.* **1997**, *101*(25), 4579 – 4586

[11] Fogarty H. A.; Tsuji H.; David D. E.; Ottosson C.; Ehara M.; Nakatsuji H.; Tamao K.; Michl J. *J. Phys. Chem. A.* **2002**, *106*(10), 2369 – 2373

[12] Fukazawa A.; Tsuji H.; Tamao K. *J. Am. Chem. Soc.* **2006**, *128*(21), 6800 – 6801

[13] (a) Miller R. D., Michl J. *Chem. Rev.* **1989**, *89*(6), 1359 – 1410 (b) Tsuji H., Michl J., Tamao K. *J. Org. Chem.* **2003**, *685*, 9 – 14 (c) Fukazawa A., Tsuji H., Tamao K. *J. Am. Chem. Soc.* **2006**, *128*, 6800 – 6801 (d) Bande A., Michl J. *Chem. Eur. J.* **2009**, *15*, 8504 – 8517 (e) Rooklin D. W., Schepers T., Raymond-Johansson M. K., Michl J. *Photochem. Photobiol. Sci.* **2003**, *2*, 511 – 517

[14] Boberski W.G., Allred A. L. *J. Org. Met. Chem.* **1975**, *88*, 65 – 72

[15] Kishida H., Tachibana H., Sakurai K., Matsumoto M., Abe S., Tokura Y. *J. Phys. Soc. Jpn.* **1996**, *65*(6), 1578 – 1581

Experimental

General Synthesis and Characterization Information

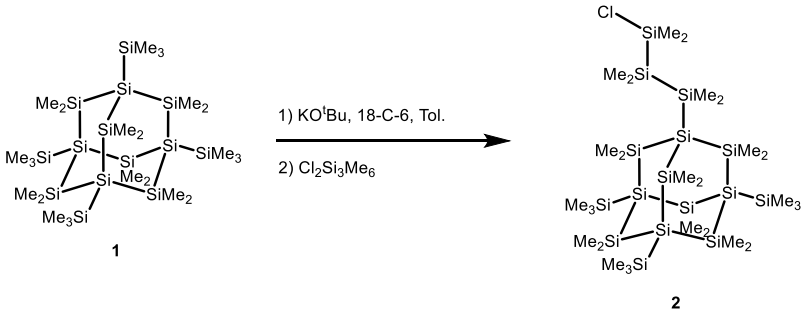
All reactions were performed in oven-dried or flame-dried glassware, unless otherwise stated. Reaction vessels were fitted with Teflon magnetic stir bars and rubber septa and reactions were conducted under nitrogen or argon on a Schlenk manifold or in a nitrogen-filled glovebox. Reaction solvents were purged with argon and dried over activated alumina columns through a JC Meyer solvent purification system, then stored over 4 Å molecular sieves. Automated flash chromatography was performed using a Yamazen Smart Flash AKROS system with Yamazen Premium silica columns.

Materials. All chemicals were purchased from commercial sources and used without further purification unless otherwise stated. **8** was prepared by previously reported described in Siu, T. C.; Imex Aguirre Cardenas, M.; Seo, J.; Boctor, K.;Shimono, M. G.; Tran, I. T.; Carta, V.; Su, T. A. *Angew. Chem., Int. Ed.* **2022**, 61 (31), No. e202206877

Instrumentation. ^{1}H NMR, ^{13}C NMR and ^{29}Si NMR were recorded on Bruker NEO 400 (400 MHz) or Bruker AV 600 (600 MHz) spectrometers. Chemical shifts for ^{1}H NMR are reported in parts per million downfield from tetramethylsilane and are referenced to residual protium in NMR solvents ($CHCl_3$, δ 7.26; C_6H_6, δ 7.16). Chemical shifts for ^{13}C NMR are reported in parts per million downfield from tetramethylsilane and are referenced to the center peaks of residual solvents ($CHCl_3$, δ 77.16; C_6H_6, δ128.06). Chemical shifts for silicon are reported in parts per million downfield from tetramethylsilane and are referenced to a tetramethylsilane internal standard. To compensate for the low isotopic abundance of ^{29}Si, the DEPT pulse sequence was employed for the amplification of the

signal. Data are represented as follows: chemical shift, multiplicity (s = singlet, d = doublet, t = triplet, m = multiplet, br = broad), coupling constants in Hertz, and integration. Low-resolution mass spectrometry (LRMS) was measured on a MALDI-TOF mass spectrometer instrument in the Analytical Chemistry Facility at UC Riverside. UV-vis absorbance spectra were obtained on a Cary 60 UV-vis Spectrophotometer in 1 cm cuvettes at concentrations of 10 μM in pentane.

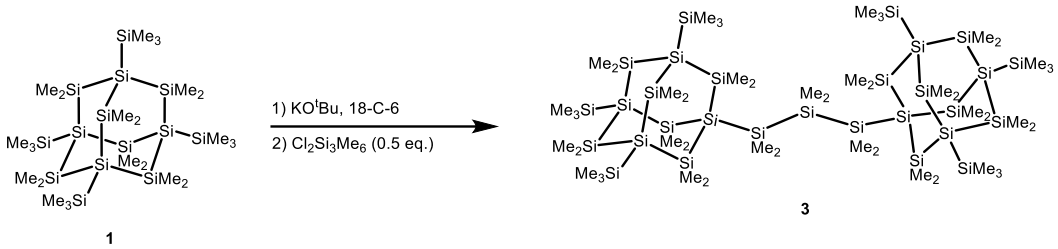
Preparation of **2**



An oven-dried 100 mL Schlenk flask was brought into a nitrogen-filled glovebox and subsequently equipped with a stir bar, **1** (0.150 g, 0.20 mmol, 1.0 eq.), potassium *tert*-butoxide (0.022 g, 0.20 mmol, 1.0 eq.) and 18-crown-6 (0.053 g, 0.20 mmol, 1.0 eq.), followed by toluene (20 mL). The resulting orange mixture was capped with a rubber septum, taken out of the glovebox and attached to a Schlenk manifold. The mixture was then left to stir overnight to allow sufficient time for formation of the silyl anion. The following day, 1,3-dichlorohexamethyltrisilane (0.048 g, 0.20 mmol, 1.0 eq.) was syringed into solution. The resulting mixture was left stirring for 30 min during which the mixture turned from orange to white. The reaction was then concentrated to dryness *in*

vacuo. The resulting solids were washed with dry pentane and the mixture was syringe filtered with a 0.22 µm syringe filter. Upon evaporation of the pentane filtrate, the crude product was obtained as a white waxy solid (0.274 g). ^{1}H NMR indicated that the crude product contained minor amounts of **3** as a byproduct. The crude reaction mixture was carried forward without further purification. ^{1}H NMR (400 MHz, C_6D_6) δ 0.61 (s, 18H), 0.61 (s, 9H), 0.60 (s, 9H), 0.52 (s, 6H), 0.52 (s, 6H), 0.43 (s, 6H), 0.36 (s, 27H). ^{13}C NMR (101 MHz, C_6D_6) δ 5.07, 4.72, 4.19, 4.11, 4.07, 3.92, 2.40. ^{29}Si NMR (79 MHz, C_6D_6) δ -4.61, -24.88, -26.18, -29.74, -38.93, -43.01, -111.72, -117.52. HRMS could not be obtained due to the sensitivity of silyl chloride groups.

Preparation of **3**

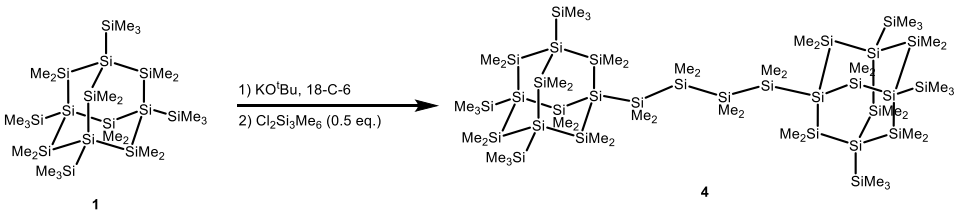


1 **3**

An oven-dried 100 mL Schlenk flask was cycled into a glove box and subsequently equipped with a stir bar, **1** (0.26 g, 0.35 mmol, 1.0 eq.), potassium tert-butoxide (0.039 g, 0.35 mmol, 1.0 eq.) and 18-crown-6 (0.091 g, 0.35 mmol, 1.0 eq.), followed by toluene (50 mL). The resulting orange mixture was capped with a rubber septum, taken out of the glovebox and attached to a Schlenk manifold. The mixture was then left to stir overnight to allow sufficient time for formation of the silyl anion. The following day, 1,3-dichlorohexamethyltrisilane (0.042 g, 0.17 mmol, 0.5 eq.) was syringed into solution. The

resulting mixture was left stirring for 30 min during which the mixture turned from orange to white. The reaction was then quenched with a 1 M hydrochloric acid solution (20 mL) and the organic and aqueous layers were separated. The aqueous layer was extracted with hexanes (3 x 50 mL) and the combined organic layers were brine-washed, dried over magnesium sulfate, then concentrated in vacuo. The crude product was purified by recrystallization with pentane to yield **3** as a white solid (0.32 g, 61% yield). XRD quality crystals were grown from a vapor diffusion method using toluene as the solvent and methanol as the anti-solvent. ^{1}H NMR (600 MHz, C_6D_6) δ 0.72 (s, 36H), 0.65 (s, 18H), 0.64 (s, 18H), 0.63 (s, 18H), 0.38 (s, 54H). ^{13}C NMR (151 MHz, C_6D_6) δ 5.09, 5.05, 4.14, 4.06, 3.31, -2.23. ^{29}Si NMR (79 MHz, $CDCl_3$) δ -4.91, -22.75, -24.76, -26.72, -37.38, -109.91, -117.21. LRMS (MALDI-TOF MS) for [$C_{48}H_{144}Si_{29}$+CH_3CN+H]: calculated = 1574.4920, found = 1574.63 [M+CH_3CN+H] $^{+}$

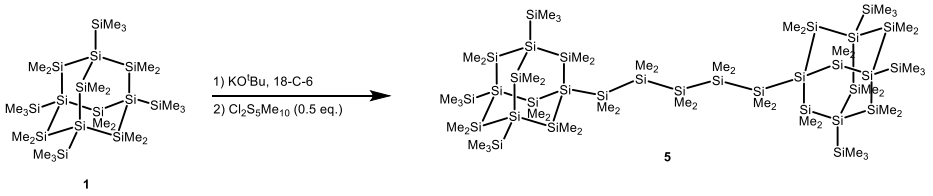
Preparation of **4**



An oven-dried 100 mL Schlenk flask was cycled into a glove box and was subsequently equipped with a stir bar, **1** (0.50 g, 0.66 mmol, 1.0 eq.), potassium tert-butoxide (0.075 g, 0.66 mmol, 1.0 eq.) and 18-crown-6 (0.175 g, 0.66 mmol, 1.0 eq.), followed by toluene (60 mL). The resulting orange mixture was capped with a rubber septum, taken out of the glovebox and attached to a Schlenk manifold. The mixture was

then left to stir overnight to allow sufficient time for formation of the silyl anion. The following day, 1,4-dichlorooctamethyltetrasilane (0.10 g, 0.33 mmol, 0.5 eq.) was syringed into solution. The resulting mixture was left stirring for 30 min during which the mixture turned from orange to white. The reaction was quenched with a 1 M hydrochloric acid solution (25 mL) and the organic and aqueous layers were separated. The aqueous layer was extracted with hexanes (3 x 70 mL) and the combined organic layers were brine-washed, dried over magnesium sulfate, then concentrated in vacuo. The crude product was purified by recrystallization with pentane to yield **4** as a white solid (0.20 g, 38% yield). XRD quality crystals were grown from a vapor diffusion method using toluene as the solvent and methanol as the anti-solvent. ^{1}H NMR (400 MHz, C_6D_6) δ 0.71 (s, 36H), 0.64 (s, 12H), 0.64 (s, 18H), 0.63 (s, 18H), 0.59 (s, 12H), 0.38 (s, 54H). ^{13}C NMR (101 MHz, C_6D_6) δ 4.72, 4.61, 3.79, 3.70, 2.78, -2.85. ^{29}Si NMR (79 MHz, C_6D_6) δ -4.65, -24.31, -24.52, -26.30, -34.51, -110.16, -117.22. LRMS (MALDI-TOF MS) for [$C_{50}H_{150}Si_{30}$ +CH_3CN+H]: calculated = 1632.5159, found = 1632.3 [M+CH_3CN+H] $^{+}$

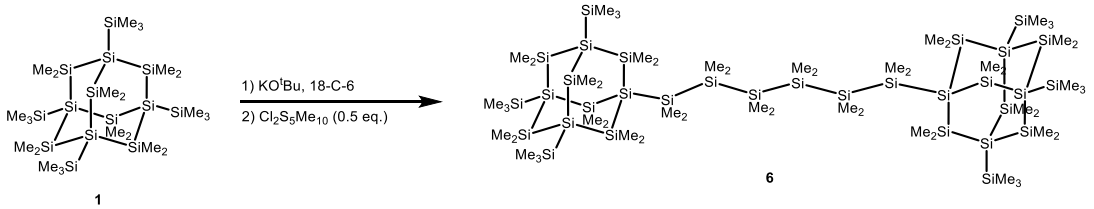
Preparation of **5**



An oven-dried 100 mL Schlenk flask was cycled into a glove box and was subsequently equipped with a stir bar, **1** (0.26 g, 0.34 mol, 1.0 eq.), potassium tert-butoxide (0.039 g, 0.34 mol, 1.0 eq.) and 18-crown-6 (0.091 g, mol, 1.0 eq.), followed by

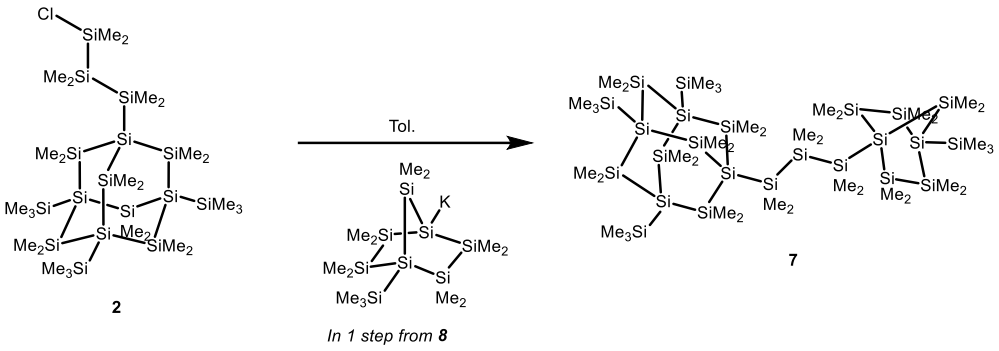
toluene (50 mL). The resulting orange mixture was capped with a rubber septum, taken out of the glovebox and attached to a Schlenk manifold. The mixture was then left to stir overnight to allow sufficient time for formation of the silyl anion. The following day, 1,5-dichlorodecamethylpentasilane (0.062 g, 0.1 mol, 0.5 eq.) was syringed into solution. The resulting mixture was left stirring for 30 min during which the mixture turned from orange to white. The reaction was quenched with a 1 M hydrochloric acid solution (20 mL) and the organic and aqueous layers were separated. The aqueous layer was extracted with hexanes (3 x 50 mL) and the combined organic layers were brine-washed, dried over magnesium sulfate, then concentrated in vacuo. The crude product was purified by recrystallization with pentane to yield **5** as a white solid (0.11 g, 42% yield). XRD quality crystals were grown from a vapor diffusion method using toluene as the solvent and methanol as the anti-solvent. ^{1}H NMR (400 MHz, C_6D_6) δ 0.70 (s, 36H), 0.64 (s, 18H), 0.63 (s, 12H), 0.63 (s, 18H), 0.57 (s, 12H), 0.51 (s, 6H), 0.37 (s, 54H). ^{13}C NMR (101 MHz, $CDCl_3$) δ 4.97, 4.60, 3.88, 3.81, 2.73, -2.91, -3.14. ^{29}Si NMR (79 MHz, $CDCl_3$) δ -4.93, -25.04, -25.55, -26.66, -34.12, -35.88, -110.88, -117.56. LRMS (MALDI-TOF MS) for $[C_{52}H_{156}Si_{31} + CH_3CN + H]$: calculated = 1690.5398, found = 1693.46 $[M+CH_3CN+H]^+$

Preparation of **6**



An oven-dried 100 mL Schlenk flask was cycled into a glove box and was subsequently equipped with a stir bar, **1** (0.51 g, 0.682 mmol, 1.0 eq.), potassium tert-butoxide (0.076 g, 0.682 mmol, 1.0 eq.) and 18-crown-6 (0.18 g, 0.682 mmol, 1.0 eq.), followed by toluene (50 mL). The resulting orange mixture was capped with a rubber septum, taken out of the glovebox and attached to a Schlenk manifold. The mixture was then left to stir overnight to allow sufficient time for formation of the silyl anion. The following day, 1,6-dichlorododecamethylhexasilane (0.14 g, 0.34 mmol, 0.5 eq.) was syringed into solution. The resulting mixture was left stirring for 30 min during which the mixture turned from orange to white. The reaction was quenched with a 1 M hydrochloric acid solution (20 mL) and the organic and aqueous layers were separated. The aqueous layer was extracted with hexanes (3 x 50 mL) and the combined organic layers were brine-washed, dried over magnesium sulfate, then concentrated in vacuo. The crude product was purified by recrystallization with pentane to yield **6** as a white solid (0.26 g, 45% yield). XRD quality crystals were grown from a vapor diffusion method using toluene as the solvent and methanol as the anti-solvent. ^{1}H NMR (400 MHz, C_6D_6) δ 0.69 (s, 36H), 0.63 (s, 18H), 0.62 (s, 18H), 0.61 (s, 12H), 0.55 (s, 12H), 0.48 (s, 12H), 0.37 (s, 54H). ^{13}C NMR (101 MHz, $CDCl_3$) δ 4.97, 4.58, 3.88, 3.81, 2.69, -3.19, -3.22. ^{29}Si NMR (79 MHz, $CDCl_3$) δ -4.90, -25.01, -26.10, -26.60, -35.19, -35.96, -110.95, -117.53. LRMS (MALDI-TOF MS) for [$C_{54}H_{162}Si_{32}$ + CH_3CN+H]: calculated = 1747.5559, found = 1749.56 [M+CH_3CN+H] $^{+}$

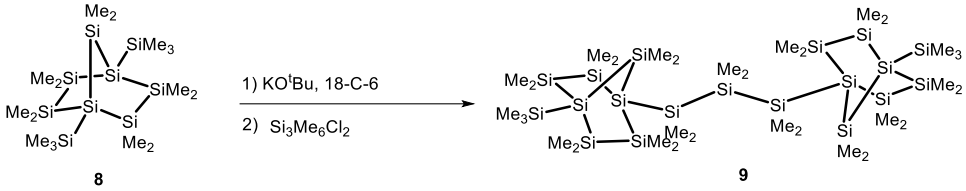
Preparation of **7**



An oven-dried 100 mL Schlenk flask was cycled into a glove box and was subsequently equipped with a stir bar, **8** (0.055 g, 0.11 mmol, 1.0 eq.), potassium tert-butoxide (0.013 g, 0.11 mmol, 1.0 eq.) and 18-crown-6 (0.030 g, 0.11 mmol, 1.0 eq.), followed by toluene (15 mL). The resulting orange mixture was capped with a rubber septum, taken out of the glovebox and attached to a Schlenk manifold. The mixture was then left to stir overnight to allow sufficient time for formation of the silyl anion. The following day, **2** (0.100 g, 0.11 mmol, 1.0 eq.) was dissolved in minimal dry toluene and syringed into solution. The resulting mixture was left stirring for 30 min during which the mixture turned from orange to white. The reaction was quenched with a 1 M hydrochloric acid solution (5 mL) and the organic and aqueous layers were separated. The aqueous layer was extracted with hexanes (3 x 25 mL) and the combined organic layers were brine-washed, dried over magnesium sulfate, then concentrated in vacuo. The crude product was purified by flash column chromatography in hexanes to yield **7** as a white solid (0.080 g, 56% yield). XRD quality crystals were grown from a vapor diffusion method using toluene as the solvent and methanol as the anti-solvent. ^{1}H NMR (400 MHz, C_6D_6) δ 0.51 (s, 18H), 0.48 (s, 9H), 0.47 (s, 9H), 0.45 (s, 6H), 0.41 (s, 6H), 0.37 (s. 6H),

0.32 (s, 6H), 0.31 (s, 6H), 0.29 (s, 6H), 0.29 (s, 9H), 0.27 (s, 27H), 0.23 (s, 9H). ^{13}C NMR (151 MHz, $CDCl_3$) δ 4.84, 4.46, 3.75, 3.26, 2.55, 1.44, 0.98, -0.35, -0.85, -1.32, -1.70, -3.32. ^{29}Si NMR (119 MHz, $CDCl_3$) δ -4.88, -5.50, -13.86, -21.93, -25.02, -25.98, -26.58, -31.77, -31.93, -38.47, -49.97, -110.89, -117.57, -118.47, -124.11. LRMS (MALDI-TOF MS) for [$C_{39}H_{117}Si_{24}$ + CH_3CN + H]: calculated = 1314.4196, found = 1314.21 [M+H+CH_3CN] $^+$

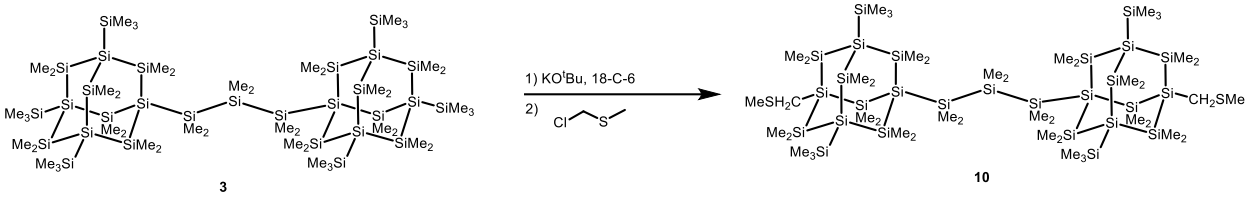
Preparation of **9**



An oven-dried 100 mL Schlenk flask was cycled into a glove box and was subsequently equipped with a stir bar, **8** (0.50 g, 1.1 mmol, 1.0 eq.), potassium tert-butoxide (0.12 g, 1.1 mmol, 1.0 eq.) and 18-crown-6 (0.29 g, 1.1 mmol, 1.0 eq.), followed by toluene (50 mL). The resulting orange mixture was capped with a rubber septum, taken out of the glovebox and attached to a Schlenk manifold. The mixture was then left to stir overnight to allow sufficient time for formation of the silyl anion. The following day, 1,3-dichlorohexamethyltrisilane (0.14 g, 0.55 mmol, 0.5 eq.) was syringed into solution. The resulting mixture was left stirring for 30 min during which the mixture turned from orange to white. The reaction was quenched with a 1 M hydrochloric acid solution (20 mL) and the organic and aqueous layers were separated. The aqueous layer was extracted with hexanes (3 x 50 mL) and the combined organic layers were brine-

washed, dried over magnesium sulfate, then concentrated in vacuo. The crude product was purified by flash column chromatography in hexanes to yield **9** as a white solid (0.080 g, 56% yield). ^{1}H NMR (600 MHz, C_6D_6) δ 0.70 (s, 12H), 0.66 (s, 12H), 0.63 (s, 6H), 0.60 (s, 12H), 0.56 (s, 12H), 0.50 (s 12H), 0.50 (s, 12H) 0.44 (s, 18H). ^{13}C NMR (151 MHz, C_6D_6) δ 3.46, 1.67, 1.06, -0.00, -0.56, -1.01, -1.47, -3.42. ^{29}Si NMR (119 MHz, C_6D_6) δ -5.31, -14.03, -24.76, -31.43, -40.04, -118.49, -123.32.

Synthesis of 10

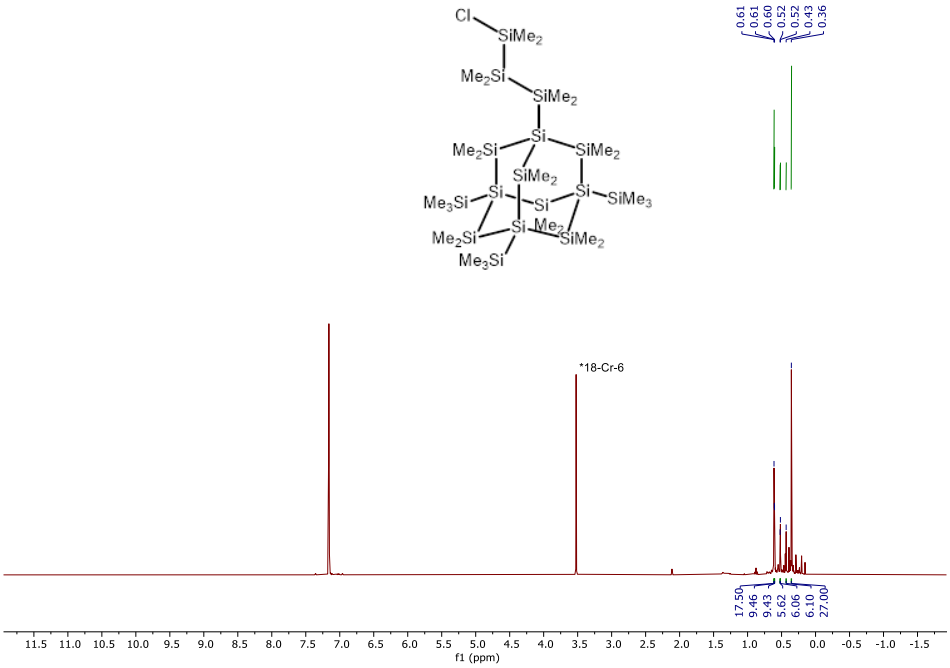


An oven-dried 20 mL glass vial was cycled into a glove box and was subsequently equipped with a stir bar, **3** (0.10 g, 0.065 mmol, 1.0 eq.), potassium tert-butoxide (0.015 g, 0.13 mmol, 2.0 eq.) and 18-crown-6 (0.034 g, 0.13 mmol, 2.0 eq.), followed by toluene (5 mL). The resulting yellow mixture was left to stir overnight to allow sufficient time for formation of the silyl anion. The following day, the vial cap was swapped with a rubber septum before being taken out of the glovebox. Then, chloro methyl methylsulfide (0.013 g, 0.13 mmol, 2.0 eq.) was syringed into solution upon which the mixture turned from yellow to clear. The reaction was quenched with a 1 M hydrochloric acid solution (5 mL) and the organic and aqueous layers were separated. The aqueous layer was extracted with hexanes (3 x 10 mL) and the combined organic layers were brine-washed, dried over magnesium sulfate, then concentrated in vacuo. The

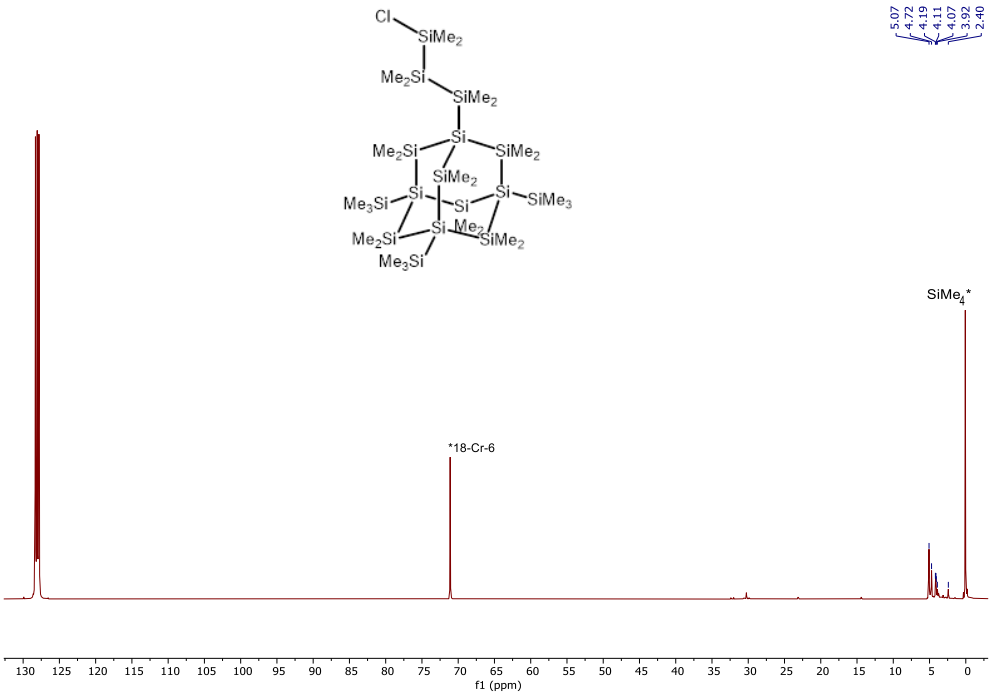
crude product was purified by flash column chromatography from pure hexanes to 60% hexanes and 40% dichloromethane to yield **10** as a white solid (0.029 g, 30% yield). ^{1}H NMR (400 MHz, C_6D_6) δ 2.39 (s, 4H), 1.95 (s, 6H), 0.79 (s, 12H), 0.74 (s, 12H), 0.73 (s, 12H), 0.71 (s, 12H), 0.70 (s, 12H), 0.64 (s, 6H), 0.63 (s, 6H), 0.62 (s, 6H), 0.62 (s, 6H), 0.37 (s, 36H). ^{13}C NMR (101 MHz, C_6D_6) δ 21.95, 15.97, 5.01, 4.93, 4.83, 4.06, 3.92, 3.11, 2.99, 2.44, 2.20, 1.42, -2.37. ^{29}Si NMR (79 MHz, C_6D_6) δ -4.40, -21.37, -22.13, -24.03, -26.01, -27.32, -28.97, -69.04, -108.10, -115.26.

NMR Spectra of **2**

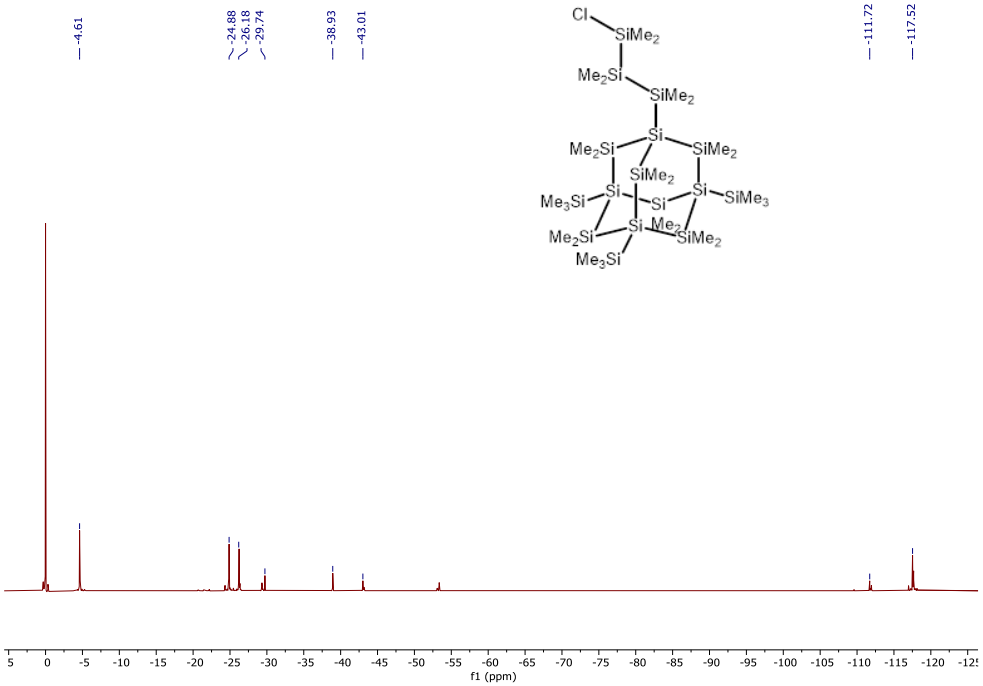
^{1}H NMR Spectrum (400 MHz, C_6D_6):



^{13}C NMR Spectrum (151 MHz, C_6D_6):

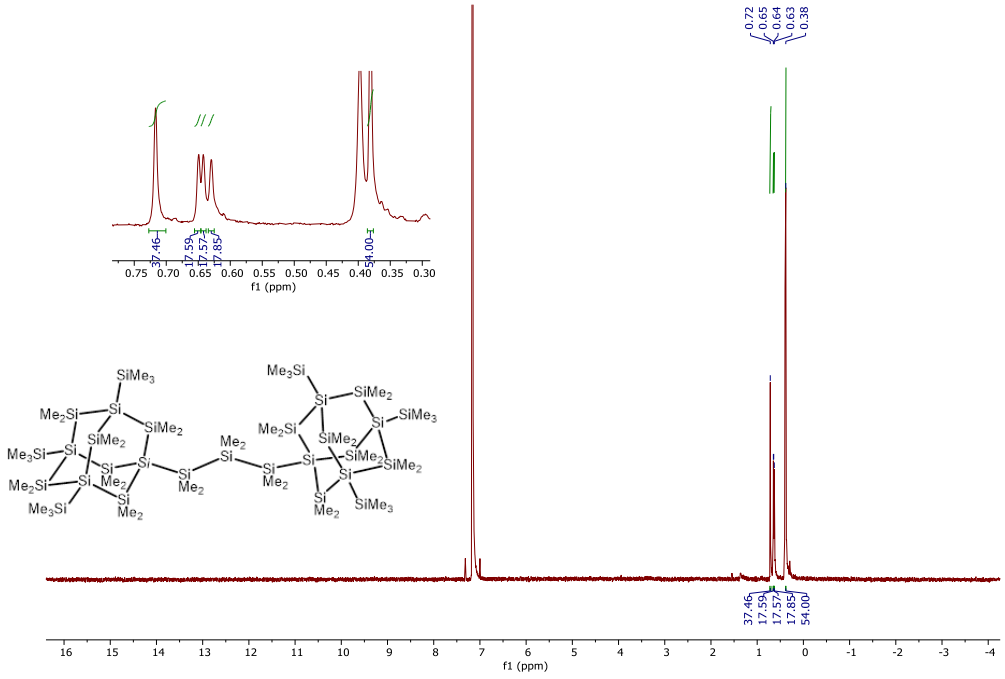


^{29}Si NMR (79 MHz, $CDCl_3$)

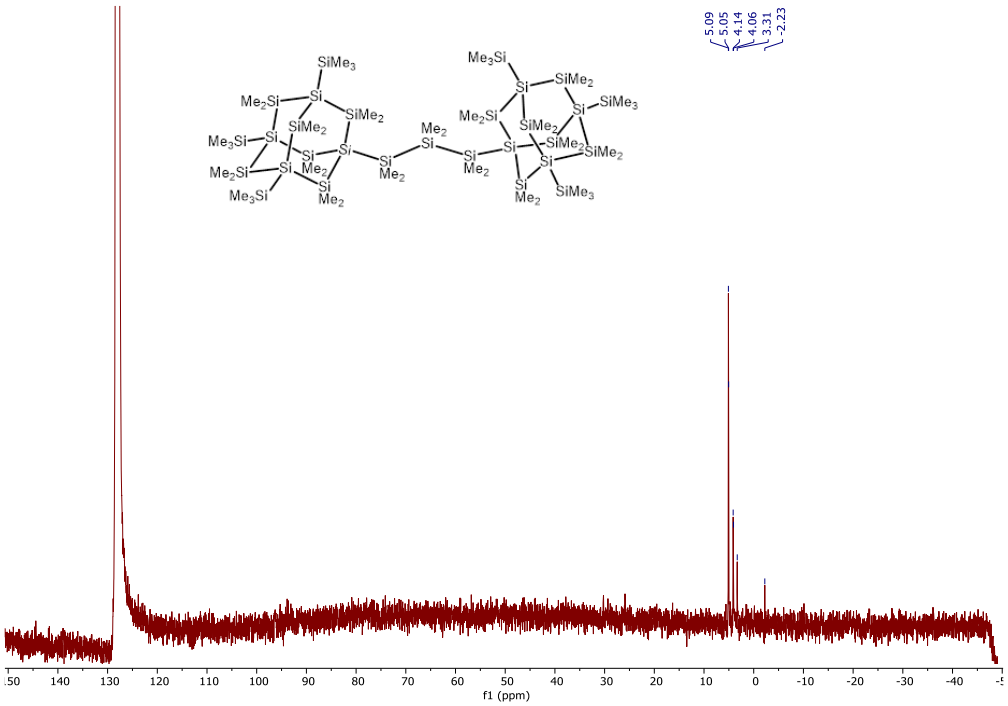


NMR Spectra of **3**

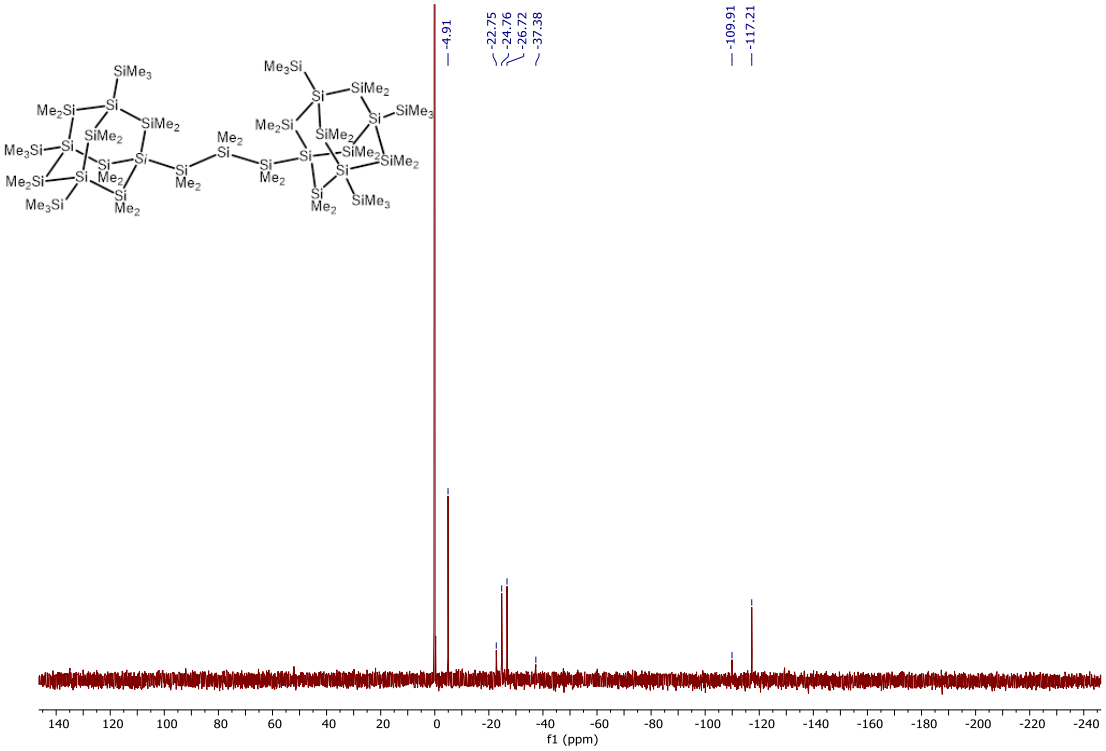
^{1}H NMR Spectrum (600 MHz, C_6D_6):



^{13}C NMR Spectrum (151 MHz, C_6D_6):

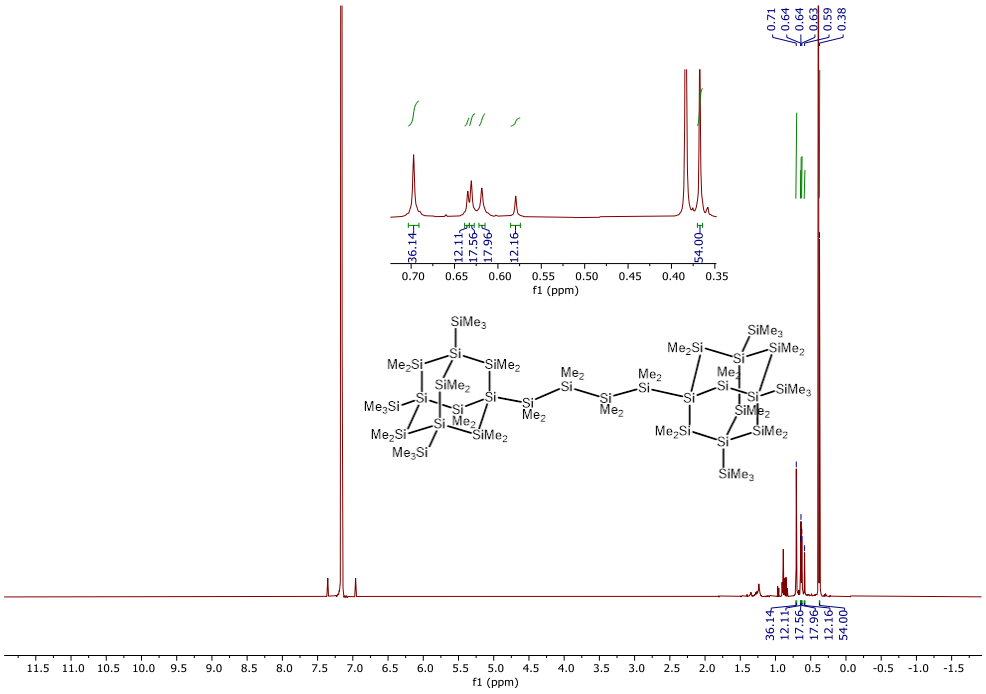


^{29}Si NMR (79 MHz, $CDCl_3$)

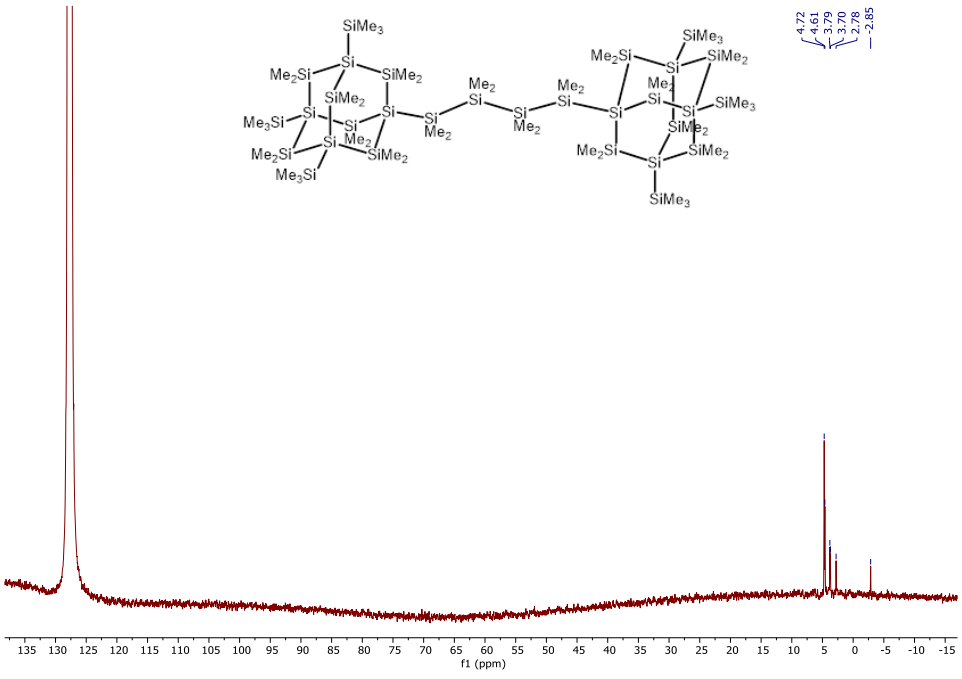


NMR Spectra of **4**

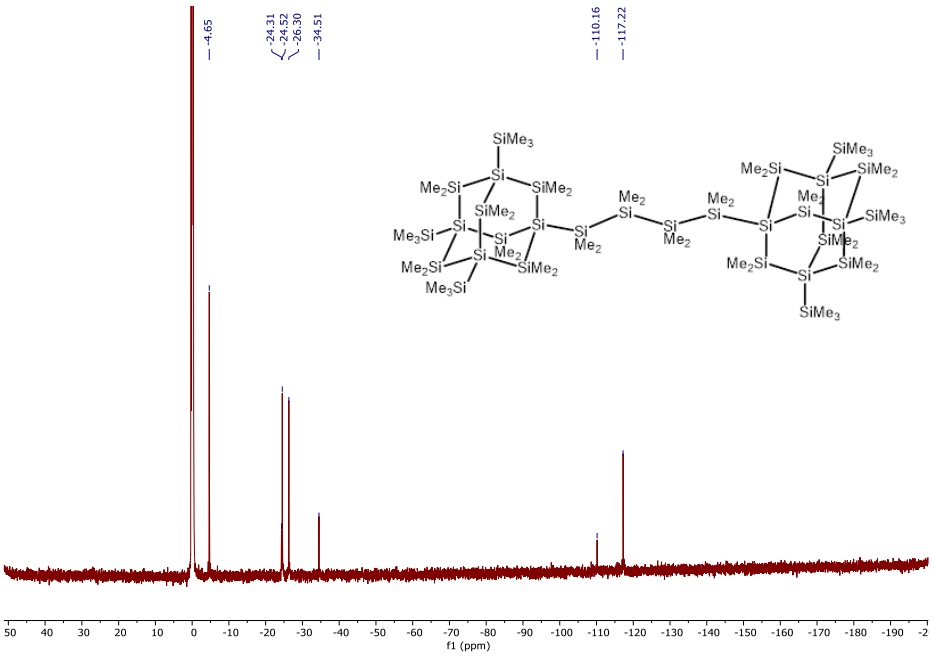
^{1}H NMR Spectrum (400 MHz, C_6D_6):



^{13}C NMR Spectrum (101 MHz, C_6D_6):

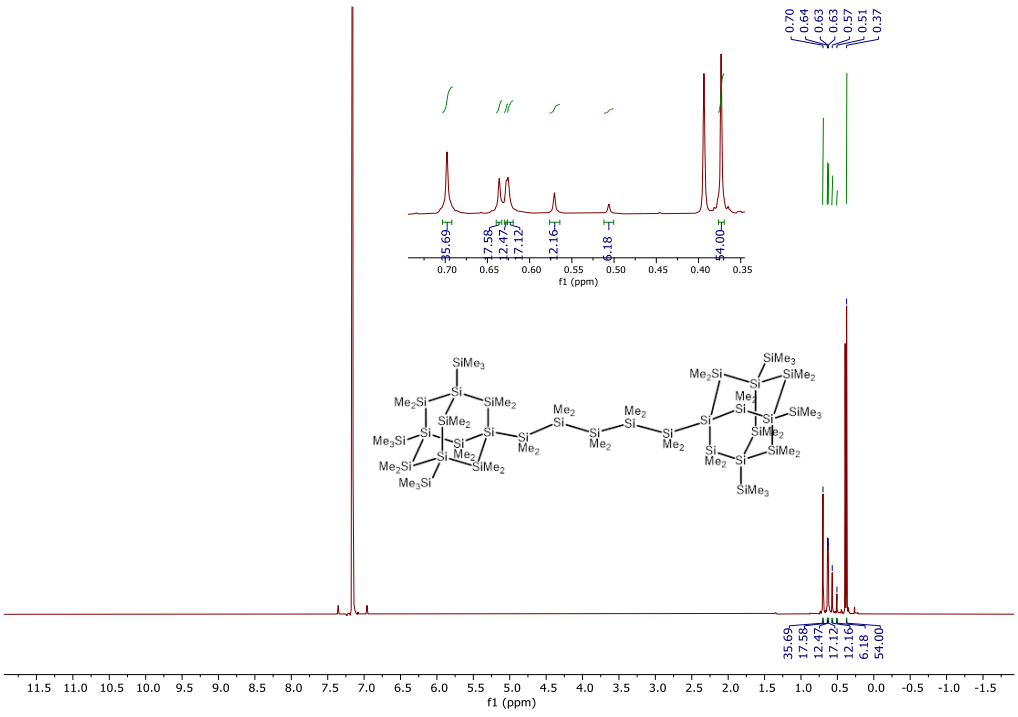


^{29}Si NMR Spectrum (79 MHz, C_6D_6):

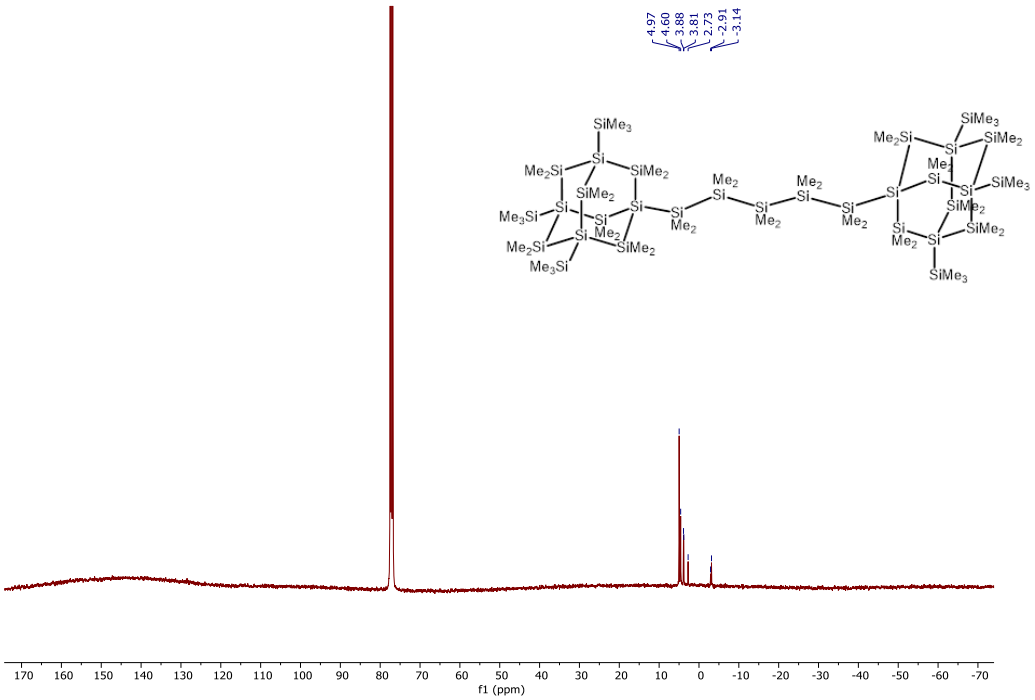


NMR Spectra of **5**

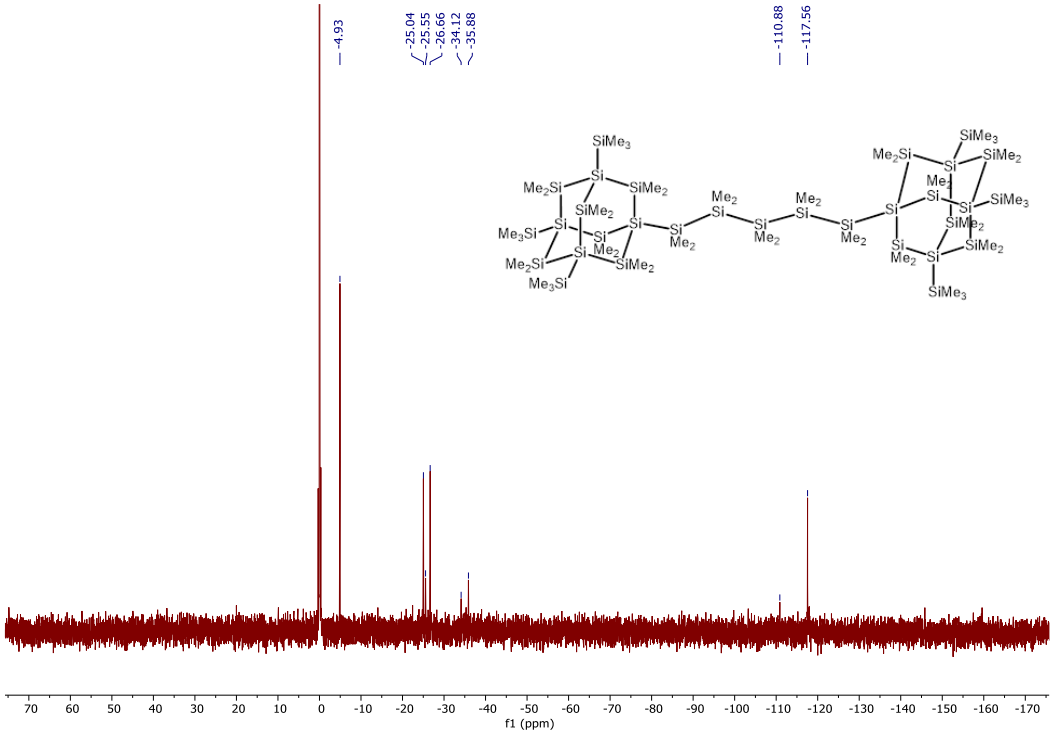
^{1}H NMR Spectrum (400 MHz, C_6D_6):



^{13}C NMR (101 MHz, $CDCl_3$):

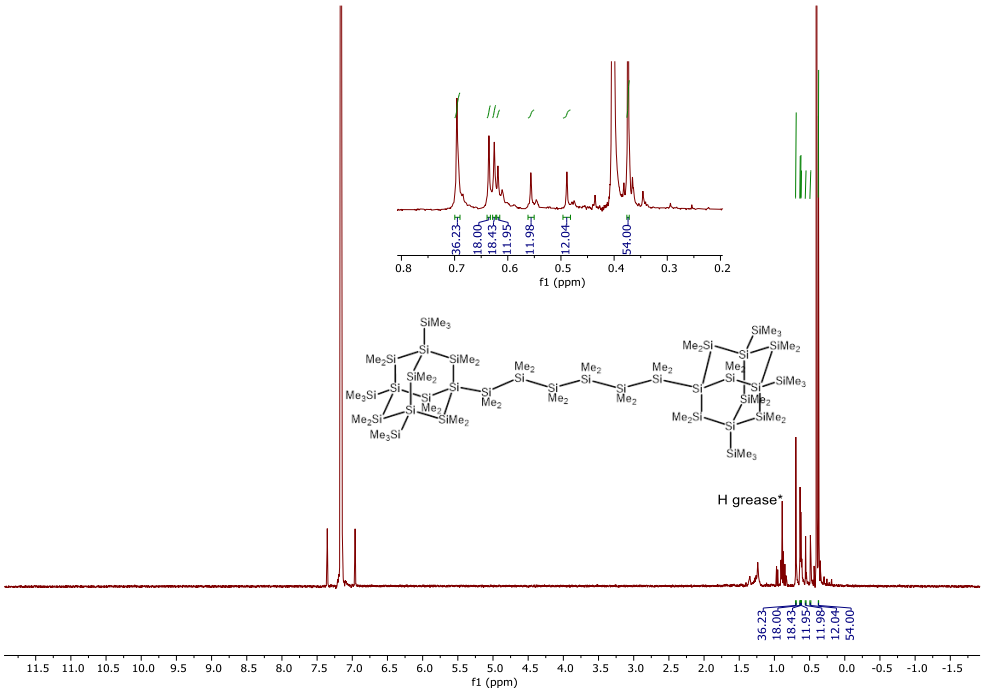


^{29}Si NMR (79 MHz, $CDCl_3$):

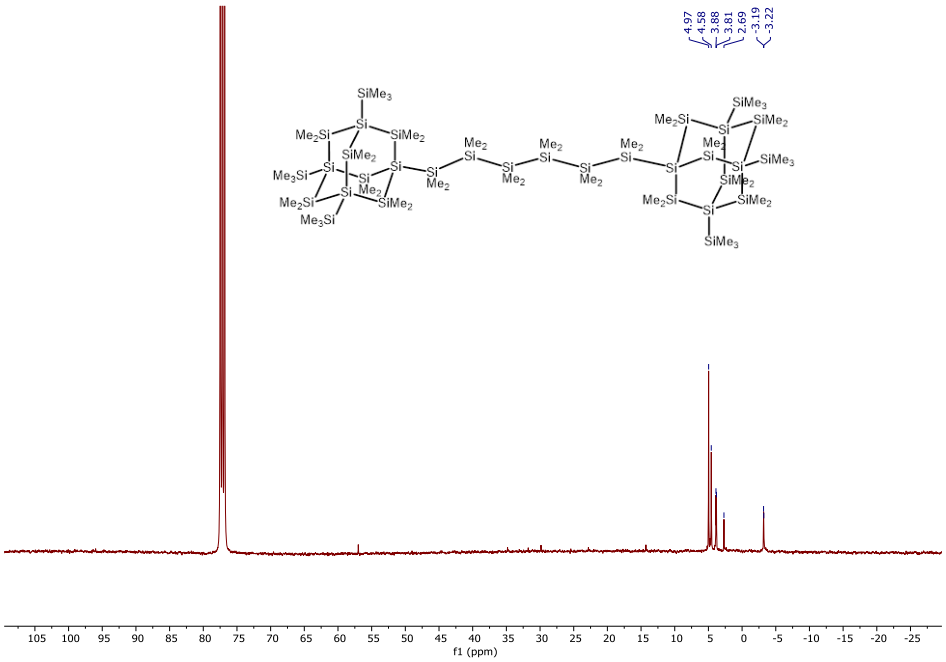


NMR Spectra of **6**

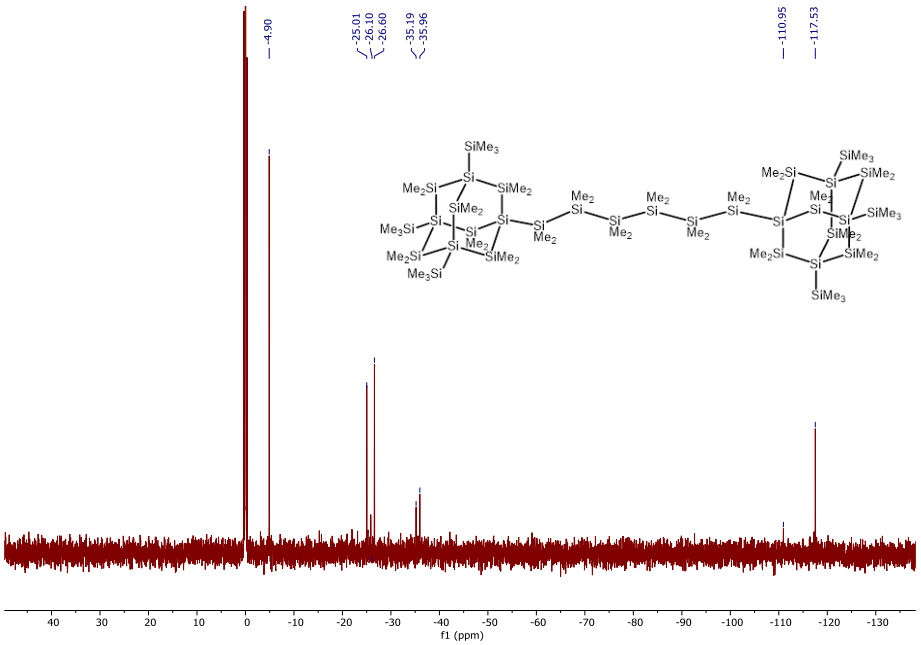
^{1}H NMR (400 MHz, C_6D_6):



^{13}C NMR (101 MHz, $CDCl_3$):

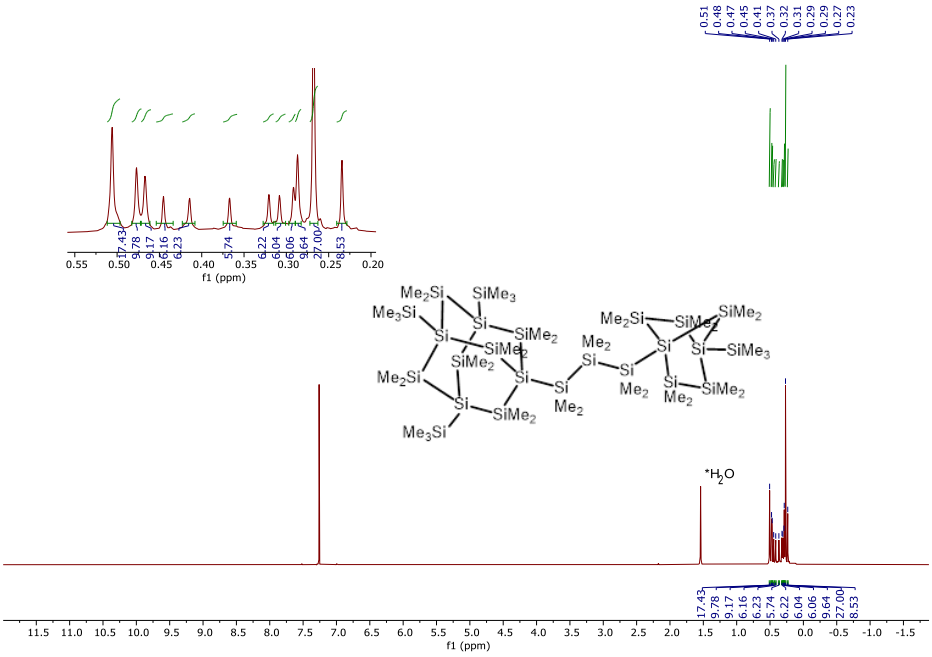


^{29}Si NMR (79 MHz, $CDCl_3$):

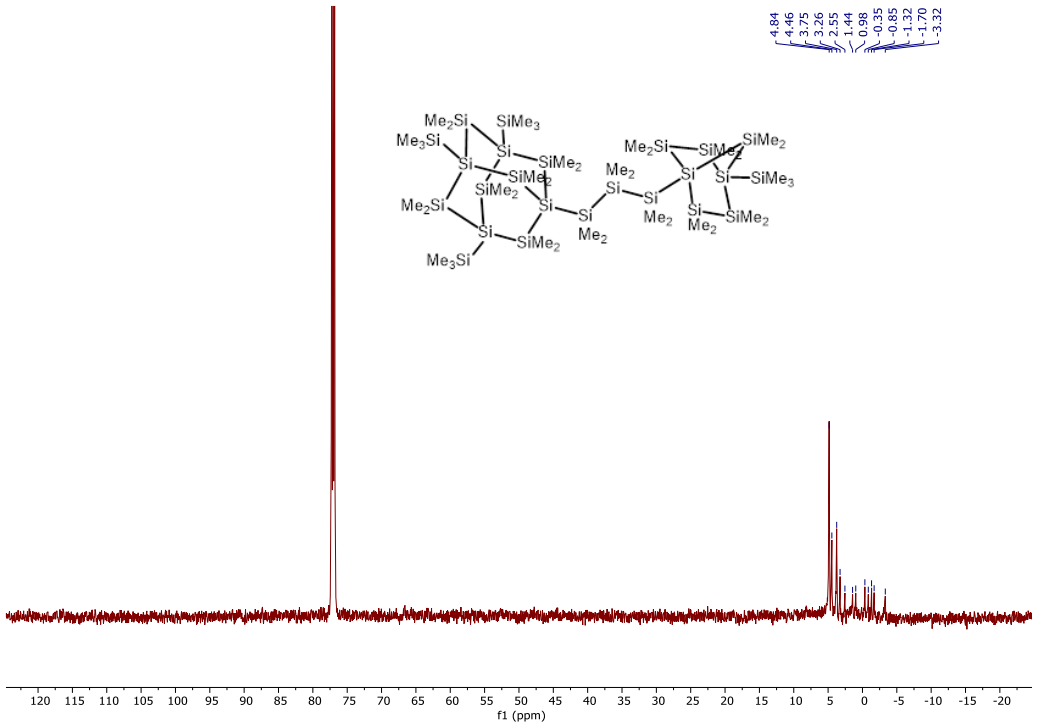


NMR Spectra of **7**

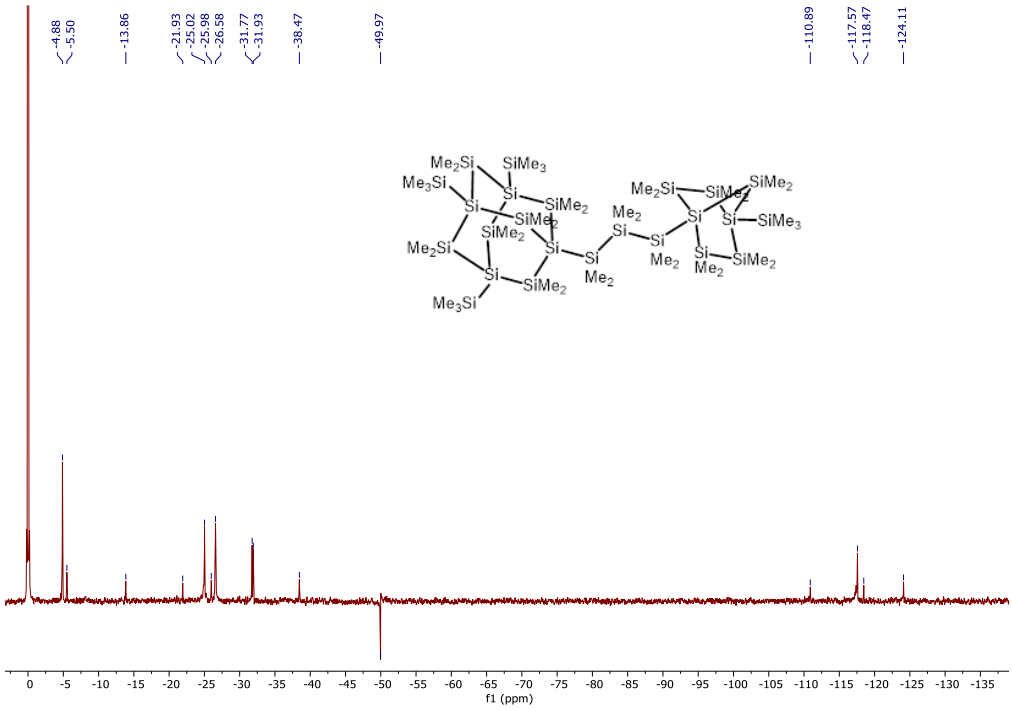
^{1}H NMR (400 MHz, $CDCl_3$):



^{13}C NMR (151 MHz, $CDCl_3$):

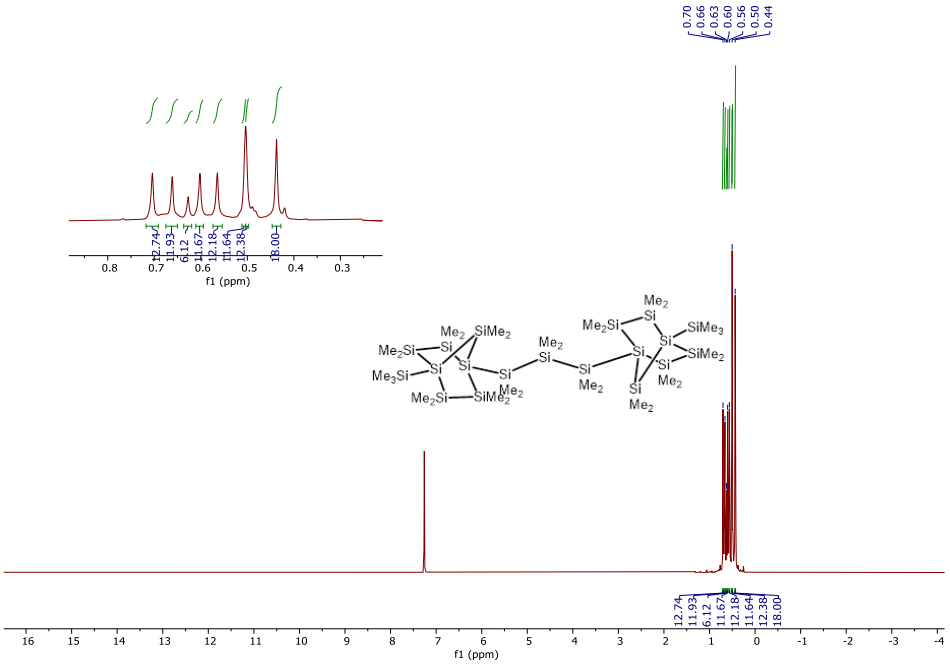


^{29}Si NMR (119 MHz, $CDCl_3$):

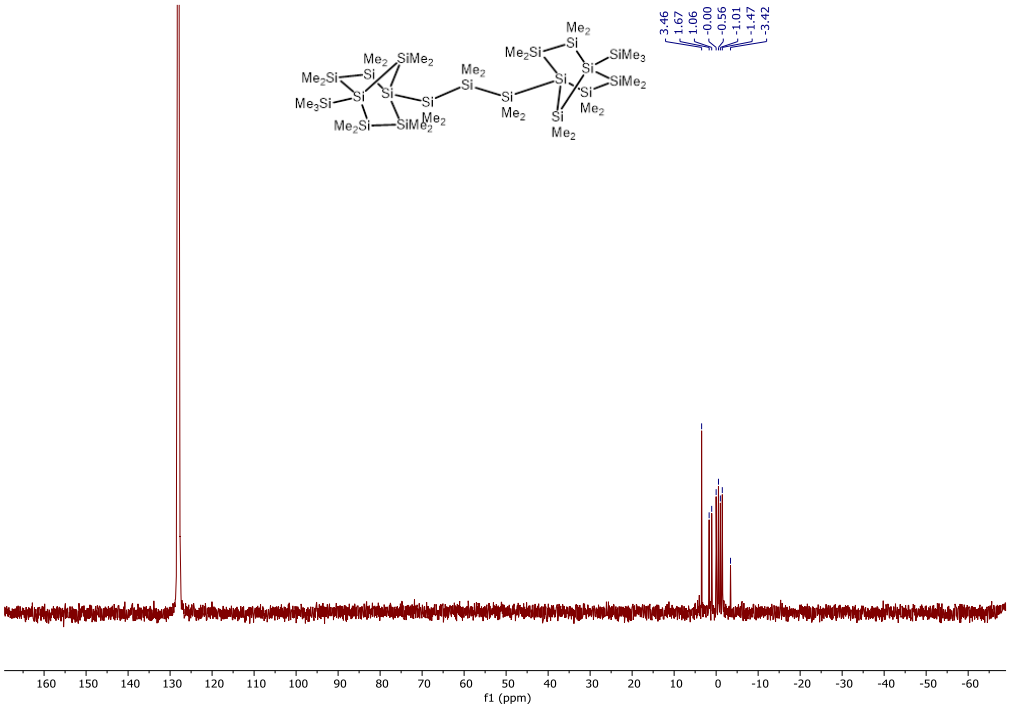


NMR Spectra of **9**

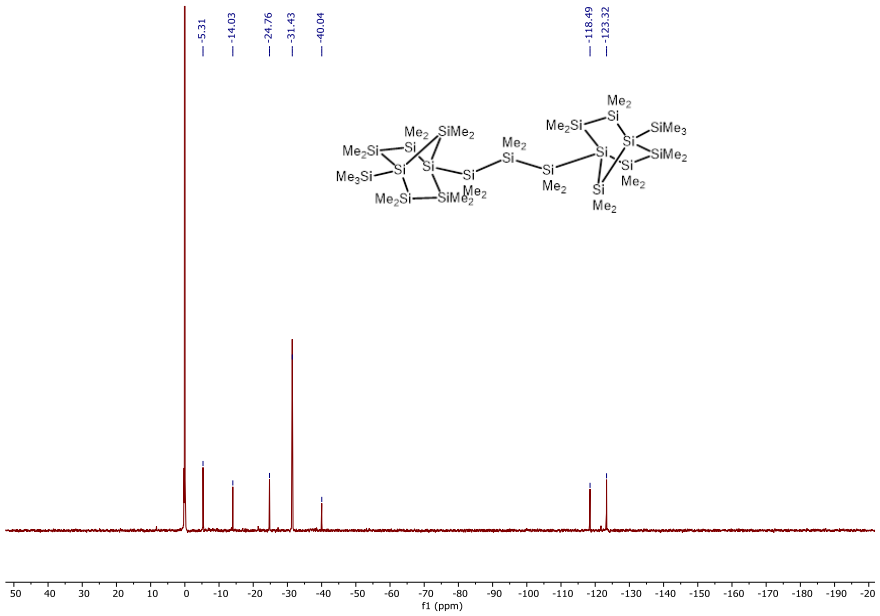
^{1}H NMR (600 MHz, C_6D_6):



^{13}C NMR (151 MHz, C_6D_6):

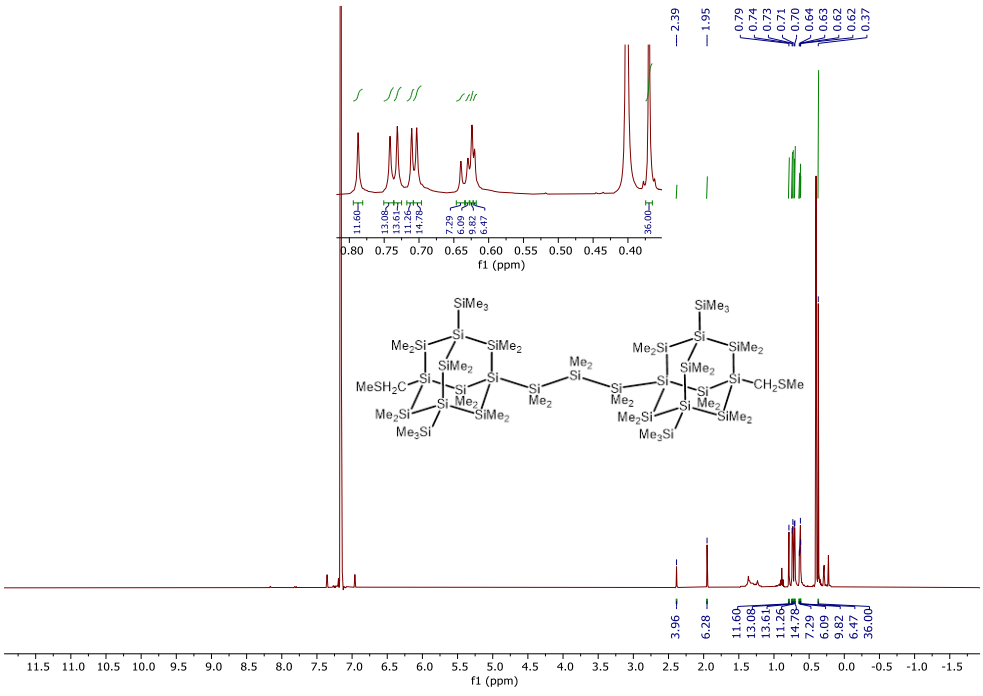


^{29}Si NMR (119 MHz, C_6D_6):

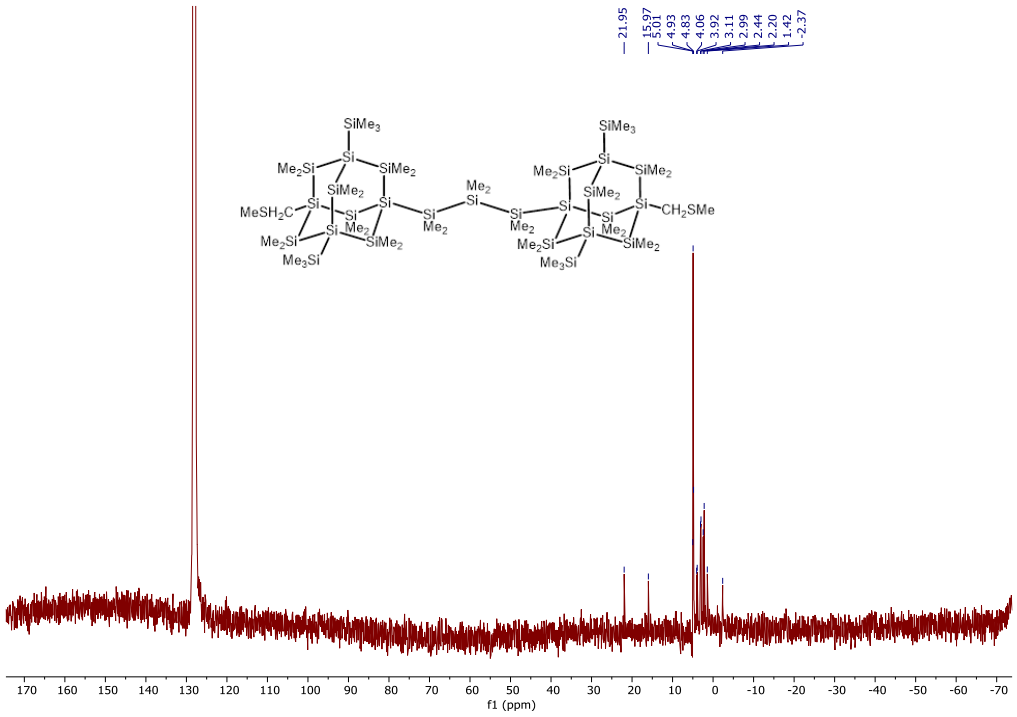


NMR Spectra of **10**

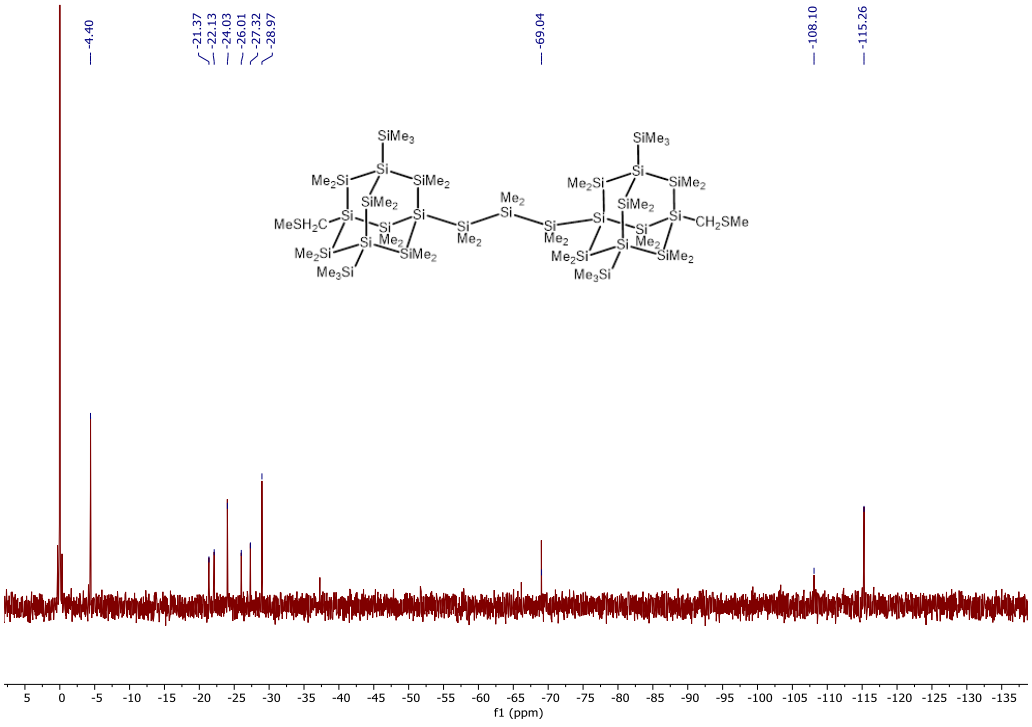
^{1}H NMR (400 MHz, C_6D_6):



^{13}C NMR (101 MHz, C_6D_6):



^{29}Si NMR (79 MHz, C_6D_6):



Crystallographic Data collection

Single crystals suitable for X-ray diffraction were grown by vapor diffusion of methanol into toluene. A colourless crystal (plate, approximate dimensions 0.29 × 0.19 × 0.05 mm^3) was placed onto the tip of a MiTeGen pin and mounted on a Bruker Venture D8 diffractometer equipped with a PhotonIII detector at 147.00 K. The data collection was carried out using Cu Kα radiation (λ = 1.54178 Å, IμS micro-source) with a frame time of 5 seconds and a detector distance of 40 mm. A collection strategy was calculated and complete data to a resolution of 0.82 Å with a redundancy of 8.3 were collected. The frames were integrated with the Bruker SAINT[1] software package using a narrow-frame algorithm to 0.84 Å resolution. Data were corrected for absorption effects using the multi-scan method (SADABS).[2]

Structure solution and refinement of 3

The space group P-1 was determined based on intensity statistics and systematic absences. The structure was solved using the SHELX suite of programs[3] and refined using full-matrix least-squares on F^2 within the OLEX2 suite.[4] An intrinsic phasing solution was calculated, which provided most non-hydrogen atoms from the E-map. Full-matrix least squares / difference Fourier cycles were performed, which located the remaining non-hydrogen atoms. All non-hydrogen atoms were refined with anisotropic displacement parameters. The hydrogen atoms were placed in ideal positions and refined as riding atoms with relative isotropic displacement parameters. Disorder was modelled for the solvent toluene molecules and for some $SiMe_3$ groups. The final full matrix least squares refinement converged to R1 = 0.1705 and wR2 = 0.4485 (F^2, all data). The goodness-of-fit was 1.022. On the basis of the final model, the calculated density was 1.071 g/cm^3 and F(000), 1926 e^-.

[1]SAINT, V8.30A, Bruker Analytical X-Ray Systems, Madison, WI, 2012.

[2]SADABS, 2.03, Bruker Analytical X-Ray Systems, Madison, WI, 2016.

[3]G. M. Sheldrick, Acta Cryst. A64, 112 - 122 (2008). Sheldrick, G.M. (2015). Acta Cryst. A71, 3-8.

[4]O. V. Dolomanov, L. J. Bourhis, R. J. Gildea, J. A. K. Howard and H. Puschmann, J. Appl. Crystallogr., 2009, 42, 339–341.

Crystal data and structure refinement for 3

Empirical formula	C65.50 H164 Si29	
Formula weight	1766.57	
Crystal color, shape, size	colourless plate, 0.29 × 0.19 × 0.05 mm^3	
Temperature	147.0 K	
Wavelength	1.54178 Å	
Crystal system, space group	Triclinic, P-1	
Unit cell dimensions	a = 12.6633(9) Å	α = 65.368(4)°.
	b = 20.4383(14) Å	β = 82.880(5)°.
	c = 23.4891(18) Å	γ = 89.271(4)°.
Volume	5478.4(7) $Å^3$	
Z	2	
Density (calculated)	1.071 g/cm^3	
Absorption coefficient	3.363 mm^{-1}	
F(000)	1926	

Data collection

Diffractometer	Bruker D8 Venture
Theta range for data collection	2.087 to 66.594°.
Index ranges	-15<=h<=15, -24<=k<=24, -27<=l<=27
Reflections collected	92689
Independent reflections	18479 [R_{int} = 0.0996]
Observed Reflections	14438
Completeness to theta = 66.594°	95.5 %

Solution and Refinement

Absorption correction	Semi-empirical from equivalents
Max. and min. transmission	0.7533 and 0.4713
Solution	Intrinsic methods
Refinement method	Full-matrix least-squares on F^2
Weighting scheme	$w = [\sigma^2 Fo^2 + AP^2 + BP]^{-1}$, with
	$P = (Fo^2 + 2\,Fc^2)/3$, A = 0.125, B = 228
Data / restraints / parameters	18479 / 1598 / 835
Goodness-of-fit on F^2	1.022
Final R indices [I>2σ(I)]	R1 = 0.1705, wR2 = 0.4260
R indices (all data)	R1 = 0.2045, wR2 = 0.4485
Largest diff. peak and hole	1.512 and -0.886 $e.Å^{-3}$

Twin Details

Type, twin law	pseudomerohedral, -1 0 0, 0 -1 0, -0.44 -1 1

Twin element, domain ratio	180° rotation around *c*, 0.08:99.92

Structure solution and refinement for 4

The space group P 2/c was determined based on intensity statistics and systematic absences. The structure was solved using the SHELX suite of programs[3] and refined using full-matrix least-squares on F^2 within the OLEX2 suite.[4] An intrinsic phasing solution was calculated, which provided most non-hydrogen atoms from the E-map. Full-matrix least squares / difference Fourier cycles were performed, which located the remaining non-hydrogen atoms. Disorder over a special position was modelled for a toluene molecule. All non-hydrogen atoms were refined with anisotropic displacement parameters, beside the disorder toluene molecules. The hydrogen atoms were placed in ideal positions and refined as riding atoms with relative isotropic displacement parameters. The final full matrix least squares refinement converged to R1 = 0.0777 and wR2 = 0.2339 (F^2, all data). The goodness-of-fit was 1.053. On the basis of the final model, the calculated density was 1.075 g/cm^3 and F(000), 1856 e^-.

Crystal data and structure refinement for 4

Empirical formula	C57 H166 Si30	
Formula weight	1694.59	
Crystal color, shape, size	colourless plate, 0.131 × 0.12 × 0.02 mm^3	
Temperature	147.0 K	
Wavelength	1.54178 Å	
Crystal system, space group	Monoclinic, P 1 2/c 1	
Unit cell dimensions	a = 21.1011(13) Å	α = 90°.
	b = 12.7707(6) Å	β = 101.503(4)°.
	c = 19.8281(11) Å	γ = 90°.
Volume	5235.9(5) $Å^3$	
Z	2	
Density (calculated)	1.075 g/cm^3	
Absorption coefficient	3.603 mm^{-1}	
F(000)	1856	

Data collection

Diffractometer	Bruker D8 Venture
Theta range for data collection	2.137 to 66.595°.
Index ranges	-25<=h<=25, -15<=k<=15, -23<=l<=20
Reflections collected	124783
Independent reflections	9261 [R_{int} = 0.1785]
Observed Reflections	5698
Completeness to theta = 66.595°	100.0 %

Solution and Refinement

Absorption correction	Semi-empirical from equivalents
Max. and min. transmission	0.7533 and 0.6191
Solution	Intrinsic methods
Refinement method	Full-matrix least-squares on F^2
Weighting scheme	$w = [\sigma^2 Fo^2 + AP^2 + BP]^{-1}$, with
	$P = (Fo^2 + 2\,Fc^2)/3$, A = 0.087, B = 20.7
Data / restraints / parameters	9261 / 164 / 432
Goodness-of-fit on F^2	1.053
Final R indices [$I>2\sigma(I)$]	R1 = 0.0777, wR2 = 0.1975
R indices (all data)	R1 = 0.1307, wR2 = 0.2339
Largest diff. peak and hole	1.199 and -0.787 $e.Å^{-3}$

Structure solution and refinement of 5

The space group P-1 was determined based on intensity statistics and systematic absences. The structure was solved using the SHELX suite of programs[3] and refined using full-matrix least-squares on F^2 within the OLEX2 suite.[4] An intrinsic phasing solution was calculated, which provided most non-hydrogen atoms from the E-map. Full-matrix least squares / difference Fourier cycles were performed, which located the remaining non-hydrogen atoms. All non-hydrogen atoms were refined with anisotropic displacement parameters. The hydrogen atoms were placed in ideal positions and refined as riding atoms with relative isotropic displacement parameters. The final full matrix least squares refinement converged to R1 = 0.0519 and wR2 = 0.1526 (F^2, all data). The goodness-of-fit was 1.058. On the basis of the final model, the calculated density was 1.051 g/cm^3 and F(000), 1854 e^-.

Crystal data and structure refinement for 5

Empirical formula	C111 H320 Si62	
Formula weight	3397.23	
Crystal color, shape, size	colourless plate, 0.27 × 0.16 × 0.04 mm^3	
Temperature	100.0 K	
Wavelength	1.54184 Å	
Crystal system, space group	Triclinic, P-1	
Unit cell dimensions	a = 12.500(3) Å	α = 94.622(8)°.
	b = 17.031(3) Å	β = 90.477(9)°.
	c = 25.308(4) Å	γ = 91.226(10)°.
Volume	5368.9(19) $Å^3$	
Z	1	
Density (calculated)	1.051 g/cm^3	
Absorption coefficient	3.620 mm^{-1}	
F(000)	1854	

Data collection

Diffractometer	Bruker D8 Venture
Theta range for data collection	2.603 to 68.438°.
Index ranges	-15<=h<=14, -20<=k<=20, -30<=l<=30
Reflections collected	116725
Independent reflections	19550 [R_{int} = 0.0574]
Observed Reflections	16273
Completeness to theta = 67.684°	99.7 %

Solution and Refinement

Absorption correction	Semi-empirical from equivalents
Max. and min. transmission	0.7531 and 0.5674
Solution	Intrinsic methods
Refinement method	Full-matrix least-squares on F^2
Weighting scheme	$w = [\sigma^2 Fo^2 + AP^2 + BP]^{-1}$, with
	$P = (Fo^2 + 2\,Fc^2)/3$, A = 0.069, B = 10.8
Data / restraints / parameters	19550 / 254 / 829
Goodness-of-fit on F^2	1.058
Final R indices [$I>2\sigma(I)$]	R1 = 0.0519, wR2 = 0.1411
R indices (all data)	R1 = 0.0642, wR2 = 0.1526
Largest diff. peak and hole	0.974 and -0.483 $e.Å^{-3}$

Structure solution and refinement of 6

The space group P-1 was determined based on intensity statistics and systematic absences. The structure was solved using the SHELX suite of programs[3] and refined using full-matrix least-squares on F2 within the OLEX2 suite.[4] An intrinsic phasing solution was calculated, which provided most non-hydrogen atoms from the E-map. Full-matrix least squares / difference Fourier cycles were performed, which located the remaining non-hydrogen atoms. All non-hydrogen atoms were refined with anisotropic displacement parameters. The final full matrix least squares refinement converged to R1 = 0.0417 and wR2 = 0.0962 (F^2, all data). The goodness-of-fit was 1.079. On the basis of the final model, the calculated density was 1.066 g/cm^3 and F(000), 934 e^-.

Crystal data and structure refinement for 6

Empirical formula	C54 H162 Si32	
Formula weight	1710.71	
Crystal color, shape, size	colourless plate, 0.27 × 0.18 × 0.04 mm^3	
Temperature	105.00 K	
Wavelength	0.71073 Å	
Crystal system, space group	Triclinic, P-1	
Unit cell dimensions	a = 11.7209(5) Å	α = 95.934(2)°.
	b = 12.0739(5) Å	β = 98.208(2)°.
	c = 20.5810(9) Å	γ = 110.447(2)°.
Volume	2664.0(2) $Å^3$	
Z	1	
Density (calculated)	1.066 g/cm^3	
Absorption coefficient	0.399 mm^{-1}	
F(000)	934	

Data collection

Diffractometer	Bruker D8 Venture
Theta range for data collection	1.825 to 27.539°.
Index ranges	-15<=h<=15, -15<=k<=15, -26<=l<=26
Reflections collected	67943
Independent reflections	12269 [R_{int} = 0.0687]
Observed Reflections	9428
Completeness to theta = 25.242°	99.8 %

Solution and Refinement

Absorption correction	Semi-empirical from equivalents
Max. and min. transmission	0.7456 and 0.7003
Solution	Intrinsic methods
Refinement method	Full-matrix least-squares on F^2
Weighting scheme	$w = [\sigma^2 Fo^2 + AP^2 + BP]^{-1}$, with
	$P = (Fo^2 + 2\,Fc^2)/3$, A = 0.010, B = 3.52
Data / restraints / parameters	12269 / 0 / 415
Goodness-of-fit on F^2	1.079
Final R indices [I>2σ(I)]	R1 = 0.0417, wR2 = 0.0878
R indices (all data)	R1 = 0.0607, wR2 = 0.0962
Largest diff. peak and hole	0.560 and -0.298 $e.Å^{-3}$

Structure solution and refinement of 7

The space group P $2_1/m$ was determined based on intensity statistics and systematic absences. The structure was solved using the SHELX suite of programs[3] and refined using full-matrix least-squares on F^2 within the OLEX2 suite.[4] An intrinsic phasing solution was calculated, which provided most non-hydrogen atoms from the E-map. Full-matrix least squares / difference Fourier cycles were performed, which located the remaining non-hydrogen atoms. All non-hydrogen atoms were refined with anisotropic displacement parameters. The hydrogen atoms were placed in ideal positions and refined as riding atoms with relative isotropic displacement parameters. The molecule is on a special position and is partially disordered. Disorder over a symmetry element was also modelled for a toluene solvent molecule with total occupancy 0.5. The crystal suffers from solvent loss, twinning, and low peak intensity at high angles. The twin law is: -1 0 0, 0 -1 0, 0.154 0 1. The final full matrix least squares refinement converged to R1 = 0.1626 and wR2 = 0.4642 (F^2, all data). The goodness-of-fit was 1.765. On the basis of the final model, the calculated density was 0.996 g/cm^3 and F(000), 1442 e^-.

Crystal data and structure refinement for 7

Empirical formula	C43.50 H124 Si24	
Formula weight	1321.58	
Crystal color, shape, size	colourless plate, 0.22 × 0.16 × 0.01 mm^3	
Temperature	100.0 K	
Wavelength	1.54178 Å	
Crystal system, space group	Monoclinic, P 1 21/m 1	
Unit cell dimensions	a = 15.5015(12) Å	α = 90°.
	b = 17.0889(16) Å	β = 94.099(7)°.
	c = 16.6810(17) Å	γ = 90°.
Volume	4407.6(7) $Å^3$	
Z	2	
Density (calculated)	0.996 g/cm^3	
Absorption coefficient	3.416 mm^{-1}	
F(000)	1442	

Data collection

Diffractometer	Bruker D8 Venture
Theta range for data collection	2.586 to 67.524°.
Index ranges	-18<=h<=18, -19<=k<=20, -19<=l<=19
Reflections collected	72145
Independent reflections	8126 [R_{int} = 0.1915]
Observed Reflections	5492
Completeness to theta = 67.524°	98.6 %

Solution and Refinement

Absorption correction	Semi-empirical from equivalents
Max. and min. transmission	0.7528 and 0.5923
Solution	Intrinsic methods
Refinement method	Full-matrix least-squares on F^2
Weighting scheme	$w = [\sigma^2 Fo^2 + AP^2 + BP]^{-1}$, with
	$P = (Fo^2 + 2\,Fc^2)/3$, A = 0.20, B = 0.00
Data / restraints / parameters	8126 / 645 / 419
Goodness-of-fit on F^2	1.765
Final R indices [$I>2\sigma(I)$]	R1 = 0.1626, wR2 = 0.4253
R indices (all data)	R1 = 0.2065, wR2 = 0.4642
Largest diff. peak and hole	1.775 and -0.889 $e.Å^{-3}$

Twin Details

Type, twin law	Non merohedral, -1 0 0, 0 -1 0, 0.154 0 1

Twin element, domain ratio	180˚ rotation around *c*

References

[1] SAINT, V8.30A, Bruker Analytical X-Ray Systems, Madison, WI, 2012.

[2] SADABS, 2.03, Bruker Analytical X-Ray Systems, Madison, WI, 2016.

[3] G. M. Sheldrick, Acta Cryst. A64, 112 - 122 (2008). Sheldrick, G.M. (2015). Acta Cryst. A71, 3-8.

[4] O. V. Dolomanov, L. J. Bourhis, R. J. Gildea, J. A. K. Howard and H. Puschmann, J. Appl. Crystallogr., 2009, 42, 339–341.

Chapter 5: Synthesis and Structure of a $Si_{10}C_1$ Trishomocubane

Preface

This chapter presents a manuscript in progress. I synthesized all compounds. Mr. McKinley Durham and Mr. Fernando Alfaro synthesized starting materials. Crystallographic data was obtained by Dr. Veronica Carta.

Introduction

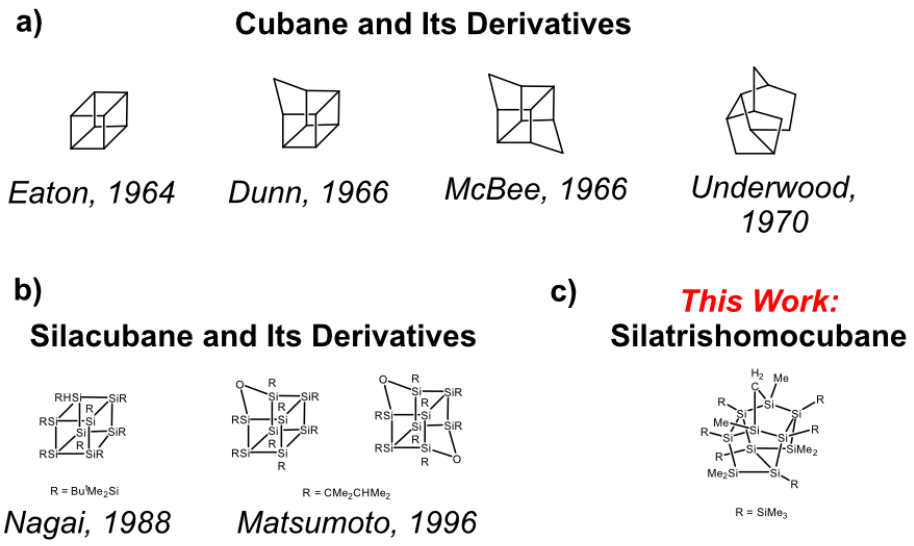


Figure 5.1 a) Earliest examples of cubane, homocubane, bishomocubane and trishomocubane. b) Earliest examples of silacubane, oxahomocubane, oxabishomocubane. c) This work discloses the first synthesis of sila-trishomocubane that contains Group 14 elements exclusively.

Since the synthesis of cubane by Eaton and Cole in 1964,[1] there have been plenty of follow up studies resulting in numerous derivatives containing the carbon cubic framework. (Figure 5.1a). The innately high bond strains in cubane had made them suitable for high density fuel applications post functionalization.[2] Shortly afterwards, homologues of cubane arose from the introduction of one, two or three methylene groups

in the cubane framework, resulting in homo, bishomo and trishomocubanes respectively.[3–5] The unique geometries of cubane homologues had allowed them to find uses in some biological applications as effective σ receptor ligands.

As group 14 chemistry developed, Nagai and coworkers had synthesized an all-silicon analogue of cubane**,** sila-cubane. Matsumoto and coworkers were subsequently able to insert oxygen atoms into the sila-cubane framework, enabling the synthesis of sila-oxahomocubanes (Figure 5.1b). Additionally, trishomocubane scaffolds have been discovered in polyanionic clusters composed bismuth, arsenic, phosphorus or antimony.[7–9] This report extends upon oligosilane derivatives containing the octasilacubane framework by disclosing the synthesis of sila-trishomocubane (Figure 5.1c). To the best of our knowledge, this is the first reported synthesis towards sila-trishomocubane and the only derivative of octasilacubane containing exclusively Group 14 elements in the core framework.

The discovery of sila-trishomocubane was quite unexpected as we were designing precursors towards sila-diamantane (SiDi) inspired from carbon diamantane and oligosilane literature. Based on relevant literature,[10] we aimed to synthesize precursors that contain the same or similar Si_xMe_y composition as SiDi and contain the same or similar number of cycles as the target molecule, pentacyclic SiDi. During our search for easily accessible precursors, we found that bicycloheptasilane could be dimerized and separated by one dimethylsilylene spacer unit, thus affording a tetracyclic molecule that was a similar match with SiDi.

Results and Discussion

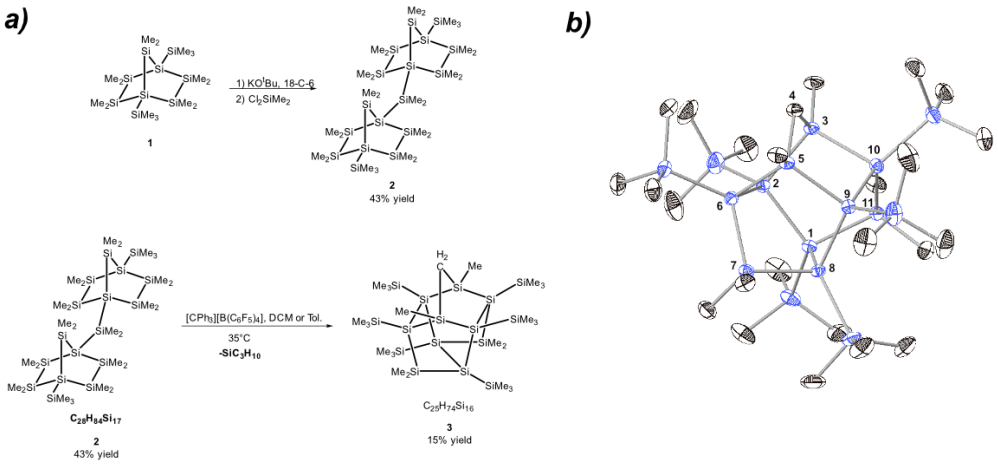


Figure 5.2 a) Synthesis of sila-trishomocubane, **3**, via isomerization of **2**. b) Crystal structure of **3**. H atoms and solvent molecules omitted for clarity. Si – blue, C – black. Core Si framework labelled 1 – 11 (4 is Carbon).

Table 5.1 Relevant Si-Si-Si bond angles for **3**.

	1-2-3	2-3-4	3-4-5	4-5-6	5-6-7	6-7-8	7-8-9	8-9-10	9-10-11	10-11-1	11-1-2
3	104.2° (2)	105.9° (4)	104.1° (10)	104.1° (3)	101.1° (2)	96.2° (2)	102.9° (2)	105.7° (2)	105.7° (2)	96.2° (2)	102.9° (2)

Starting from bicycloheptasilane, **1**, a silyl anion was generated via potassium tert-butoxide followed by quenching with 0.5 eq. of dichlorodimethylsilane to afford the dumbbell oligosilane **2**. Then, **2** was subjected to Lewis acid mediated isomerization with heating to 35°C in dichloromethane or toluene. We have found that the starting material does not undergo isomerization at room temperature, even after several days. During the rearrangement, we observe the loss of tetramethylsilane and hexamethyldisiloxane concomitant with the observation of new peaks that are distinct from that of the starting material. Upon purification and characterization via NMR and X-ray crystallography, the product was determined to be a D_3 symmetric sila-trishomocubane, **3** (Figure 5.2b).

Observation of this molecule yields some interesting mechanistic behaviors not seen in previously known oligosilane isomerization literature. For example, we observe a cyclization behavior of tetracyclic **2** into pentacyclic **3**. Prior literature has provided many examples of oligosilanes that conserve the number of cycles from a starting material to its isomerized product.[10a,11,12,13] To the best of our knowledge, there is only one other example of cyclization behavior disclosed by Marschner when his group had found that $Al(Fe)Cl_3$-catalyzed rearrangement of acyclic oligosilanes that contained one preinstalled, internal methylene group could promote cyclization into cyclic or bicyclic compounds.[14] Our system, however, exhibits cyclization behavior without the preinstallation of a methylene.

We also note that the stoichiometry of the precursor and product do not match each other as evidenced by the loss of $-SiC_3H_{10}$ in stoichiometry from **2** to **3**. This is highly unusual given that rearrangement products typically retain Si_xMe_y composition or match a tetramethylsilane elimination stoichiometry. It appears that the precursor **2** fragments beyond the elimination of tetramethylsilane before subsequently isomerizing into a thermodynamically favorable structure. The observation of hexamethyldisiloxane is another elimination product that has not been previously reported.

While corroborating with the carbon literature, D_3-symmetric trishomocubane is identified as the most thermodynamically stable isomer among the cage structures with the formula $C_{11}H_{14}$.[15, 16] Despite this, it is constructed of strained C-C-C bond angles that are significantly deviated from tetrahedral at 92.5° - 106.8°.[17] Inspection of the crystallographic data of **3** also reveals ring strain in which the Si-Si-Si bond angles

comprising the cluster framework are held between 96.2°(2) and 105.9°(4), which implies that ring strain is present here as well albeit lesser than that of its carbon analogue (Table 5.1). Despite the relatively strained bond angles, there appears to be significant stabilization from the six quaternary Si centers that allow for the formation of **3**. This thermodynamic balance between σ-conjugation from branching and destabilizing steric interactions from ring strain is a common modality across oligosilane rearrangements that is exhibited here as well.[13] We are currently investigating both the driving force behind the aforementioned cyclization behavior and the nuances of the thermodynamic balance that allows for the formation of **3**.

Our group had previously been successful in establishing a scope of derivatized sila-adamantanes via potassium tert-butoxide mediated silanide chemistry and we attempted to apply similar functionalization methods to **3**.[18] However, these attempts were unsuccessful and yielded a decomposition of products upon addition of potassium *tert*-butoxide. Similarly, this has been noted in the trishomocubane literature, where methods for functionalizing adamantane were ineffective for trishomocubane functionalization.[19] This is attributed to the higher reactivity of the strained bridge atoms over bridgehead atoms.

Conclusions

We disclose the first synthesis of sila-trishomocubane, **3**, via Lewis acid mediated isomerization of a dumbbell-like oligosilane **2**. We observe a rare cyclization behavior that rearranges our tetracyclic starting material to a pentacyclic product. We also observe

a loss of stoichiometry in the product that is inequivalent to loss of $SiMe_4$. It also appears that maximizing the number of quaternary Si centers between the starting material and product provides higher thermodynamic stability that overcomes minor strain energy in the product.

References

[1] Eaton P. E., Cole T. W. Jr. *J. Am. Chem. Soc.* **1964**, *86*, 962

[2] (a) Schmidt M. W., Gordon M. S., Boatz J. A. *Internation Journal of Quantum Chemistry* **2000**, *76*, 434 – 446 (b) Roy G. D. *Journal of Propulsion and Power* **2000**, *16*(4), 546

[3] Dunn G. L., DiPasquo V. J., Hoover J. R. E. *Tetrahedron Lett.* **1966**, *7*(31), 3737 – 3742

[4] McBee E. T., Dilling W. L., Braendiin H. P. *J. Org. Chem.* **1962**, *27*(7), 2704 – 2710

[5] Underwood G. R., Ramamoorthy B. *Tetrahedron Lett.* **1970**, *47*, 4125 – 4127

[6] (a) Oliver D. W., Dekker T. G., Snyckers F. O., Fourie T. G. *J. Med. Chem.* **1991**, *34*, 851 – 854 (b) Kassiou M., Nguyen V. H., Knott R., Christie M. J., Hambley T. W. *Bioorganic & Medicinal Chemistry Letters* **1996**, *6*(6), 595 – 600

[7] Belin C. H. E. *J. Am. Chem. Soc.* **1980**, *102*, 6036 – 6040

[8] Weinert B., Eulenstein A. R., Ababei R., Dehnen S. *Angew. Chem. Int. Ed.* **2014**, *53*, 4704 – 4708

[9] Hanauer T., Korber N. *Z. Anorg. Allg. Chem.* **2006**, *632*, 1135 – 1140

[10] (a) Fischer J., Baumgartner J., Marschner C. *Science* **2005**, *310*(5749), 825 (b) Gund T. M., Schleyer P. v. R., Gund P. H., Wipke T. W. *J. Am. Chem. Soc.* **1975**, *97*(4), 743 – 751

[11] Ishikawa, M.; Iyoda, J.; Ikeda, H.; Kotake, K.; Hashimoto, T.; Kumada, M. *J. Am. Chem. Soc.* **1981**, *103* (16), 4845–4850.

[12] Ishikawa, M.; Watanabe, M.; Iyoda, J.; Ikeda, H.; Kumada, M. *Organometallics* **1982**, *1* (2), 317–322.

[13] Blinka, T. A.; West, R. *Organometallics* **1986**, *5* (1), 128–133.

[14] Wagner H., Baumgartner J., Marschner C. *Organometallics* **2011**, *30*, 3939 – 3954

[15] Levandovsky, I. A.; Sharapa, D. I.; Cherenkova, O. A.; Gaidai, A. V.; Shubina, T. E. *Russ. Chem. Rev.* **2010**, *79* (11), 1005.

[16] Marchand, A. P. *Chem. Rev.* **1989**, *89* (5), 1011–1033.

[17] Kent, G. J.; Godleski, S. A.; Osawa, E.; Schleyer, P. von R. *J. Org. Chem.* **1977**, *42* (24), 3852–3859.

[18] Siu, T. C.; Imex Aguirre Cardenas, M.; Seo, J.; Boctor, K.; Shimono, M. G.; Tran, I. T.; Carta, V.; Su, T. A. *Angewandte Chemie International Edition* **2022**, *61* (31), e202206877.

[19] A. Godleski, S.; R. Schleyer, P. v; Ōsawa, E.; J. Kent, G. *Journal of the Chemical Society, Chemical Communications* **1974**, *0* (23), 976b–9977.

Experimental

General Synthesis and Characterization Information

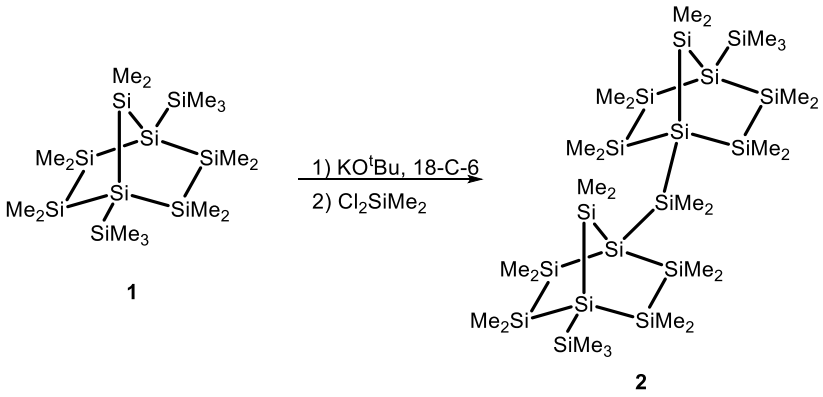
All reactions were performed in oven-dried or flame-dried glassware, unless otherwise stated. Reaction vessels were fitted with Teflon magnetic stir bars and rubber septa and reactions were conducted under nitrogen or argon on a Schlenk manifold or in a nitrogen-filled glovebox. Reaction solvents were purged with argon and dried over activated alumina columns through a JC Meyer solvent purification system, then stored over 4 Å molecular sieves. Automated flash chromatography was performed using a Yamazen Smart Flash AKROS system with Yamazen Premium silica columns.

Materials. All chemicals were purchased from commercial sources and used without further purification unless otherwise stated. **1** was prepared by previously reported methods described in Siu, T. C.; Imex Aguirre Cardenas, M.; Seo, J.; Boctor, K.;Shimono, M. G.; Tran, I. T.; Carta, V.; Su, T. A. *Angew. Chem., Int. Ed.* **2022**, 61 (31), No. e202206877.

Instrumentation. ^{1}H NMR, ^{13}C NMR and ^{29}Si NMR were recorded on Bruker NEO 400 (400 MHz) or Bruker AV 600 (600 MHz) spectrometers. Chemical shifts for ^{1}H NMR are reported in parts per million downfield from tetramethylsilane and are referenced to residual protium in NMR solvents ($CHCl_3$, δ 7.26; C_6H_6, δ 7.16). Chemical shifts for ^{13}C NMR are reported in parts per million downfield from tetramethylsilane and are referenced to the center peaks of residual solvents ($CHCl_3$, δ 77.16; C_6H_6, δ128.06). Chemical shifts for silicon are reported in parts per million downfield from tetramethylsilane and are referenced to a tetramethylsilane internal standard. To compensate for the low isotopic

abundance of ^{29}Si, the DEPT pulse sequence was employed for the amplification of the signal. Data are represented as follows: chemical shift, multiplicity (s = singlet, d = doublet, t = triplet, m = multiplet, br = broad), coupling constants in Hertz, and integration. High-resolution mass spectrometry (HRMS) was recorded on either an Agilent 7200 GCMS-QTOF in methane chemical ionization mode, or a Waters XEVO G2XS QToF mass spectrometer equipped with a UPC2 SFC inlet, electrospray ionization (ESI) probe, atmospheric pressure chemical ionization (APCI) probe, and atmospheric solids analysis probe (ASAP+). Low-resolution mass spectrometry (LRMS) was measured on a MALDI-TOF mass spectrometer instrument in the Analytical Chemistry Facility at UC Riverside.

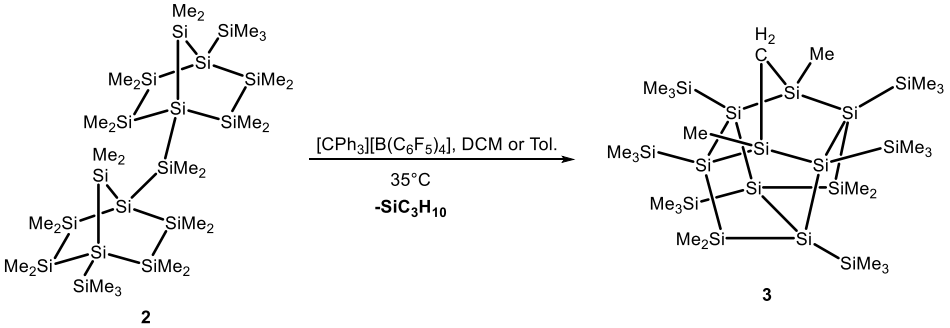
*Synthesis of **2**:*



An oven-dried 100 mL Schlenk flask was cycled into a glove box and equipped with a stir bar. **1** (0.68 g, 1.38 mmol, 1.0 equiv.), potassium tert-butoxide (0.16 g, 1.38 mmol, 1.0 equiv.) and 18-crown-6 (0.36 g, 1.38 mmol, 1.0 equiv.) were added, followed by toluene (50 mL). The resulting orange mixture was capped with a rubber septum and left to stir overnight. The reaction flask was then removed from the glovebox and attached to

a Schlenk manifold under nitrogen upon which dichlorodimethylsilane (0.089 g, 0.69 mmol, 0.5 equiv.) was syringed into solution. The resulting mixture was left stirring for 30 min during which the mixture turned from orange to cloudy white. The reaction was quenched with a 1 M hydrochloric acid solution (10 mL) and the organic and aqueous layers were separated. The aqueous layer was extracted with hexanes (3 x 100 mL) and the combined organic layers were brine-washed, dried over magnesium sulfate, then concentrated *in vacuo*. The crude product was purified by flash column chromatography in hexanes to yield **2** as a white solid (0.26 g, 43% yield). ^{1}H NMR (400 MHz, C_6D_6) δ 0.65 (s, 6H), 0.61 (s, 12H), 0.53 (s, 12H), 0.52 (s, 12H), 0.40 (s, 12H), 0.39 (s, 12H), 0.33 (s, 18H). ^{13}C NMR (151 MHz, C_6D_6) δ 7.52, 4.50, 2.94, 1.00, 0.41, 0.00, -0.45. ^{29}Si NMR (79 MHz, C_6D_6) δ -5.24, -13.12, -20.62, -31.16, -31.72, -112.55, -124.39. LRMS (MALDI-TOF MS) for [$C_{28}H_{84}Si_{17}$]: calculated = 896.2651, found = 938.1152 $[M+CH_3CN+H]^+$

*Synthesis of **3**:*

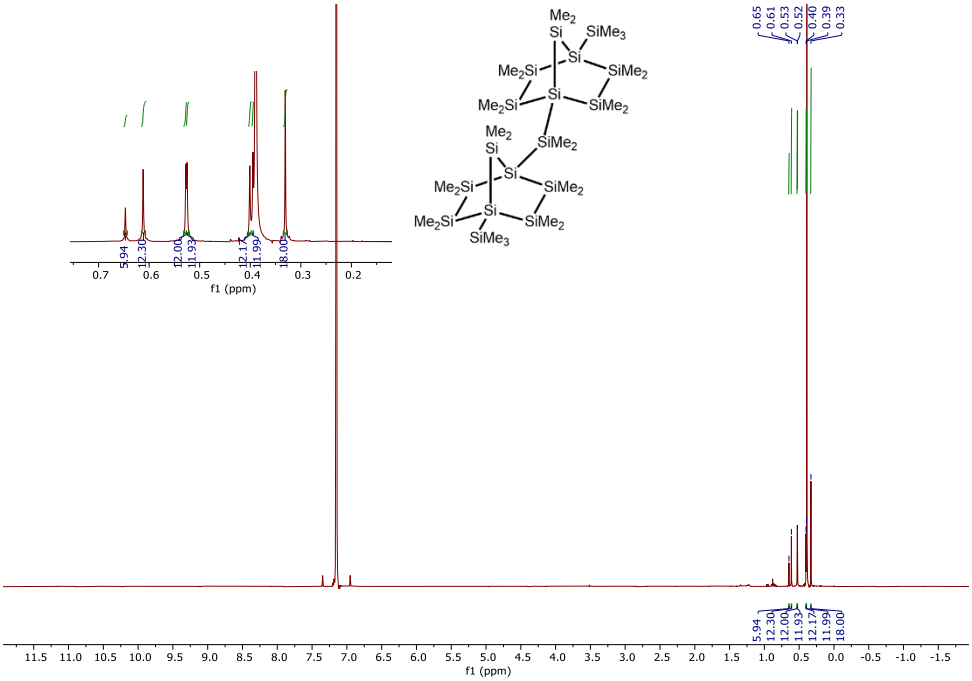


An oven-dried 250 mL high pressure tube was cycled into a glove box and was subsequently equipped with a stir bar, **2** (0.50 g, 0.56 mmol, 1.0 eq.) followed by trityl

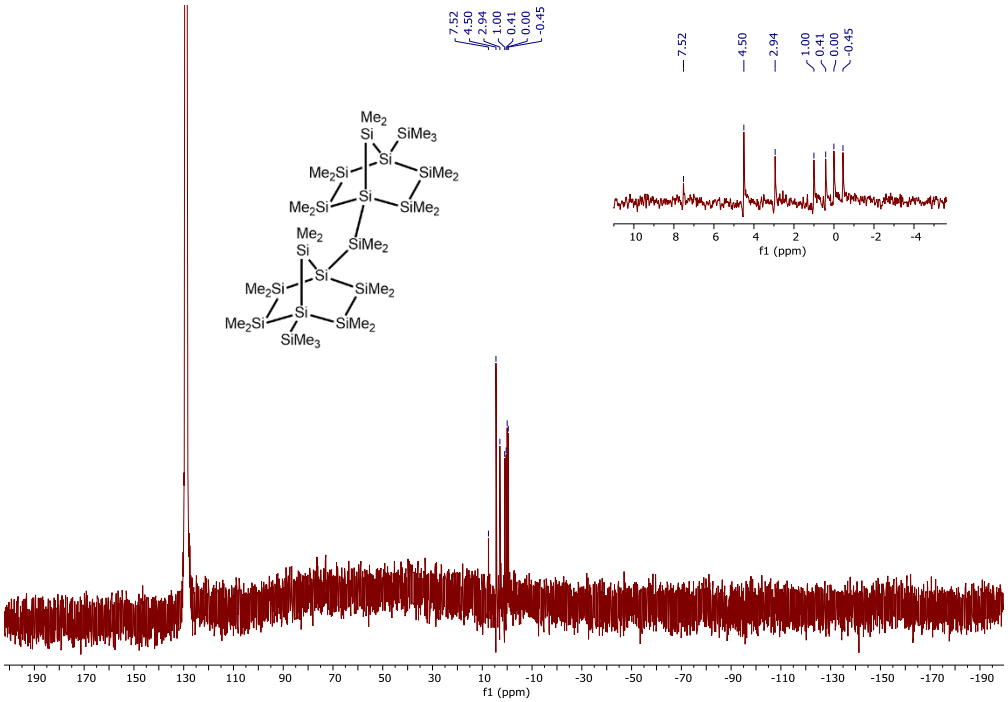
tetrakis(pentafluorophenyl)borate (0.18 g, 0.195 mmol, 0.40 eq.) and dichloromethane (50 mL). The reaction vial was then placed into a heating block upon which the reaction was heated to 35°C. The following day, the reaction had went from a cloudy orange to a more translucent golden brown and ^{1}H NMR monitoring of the reaction had shown the starting material peaks had disappeared and new product peaks had emerged. The reaction was then taken out of the glovebox and quenched with a 1 M hydrochloric acid solution (10 mL) and the organic and aqueous layers were separated. The aqueous layer was extracted with hexanes (3 x 50 mL) and the combined organic layers were brine-washed, dried over magnesium sulfate, then concentrated in vacuo. The crude product was purified by flash column chromatography in hexanes to yield **3** as a waxy solid (0.083 g, 15% yield). XRD quality crystals were grown from a vapor diffusion method using chloroform as the solvent and methanol as the anti-solvent. ^{1}H NMR (400 MHz, C_6D_6) δ 0.73 (s, 2H), 0.72 (s, 6H), 0.67 (s, 6H), 0.64 (s, 6H), 0.44 (s, 18H), 0.39 (s, 9H), 0.38 (s, 27H). ^{13}C NMR (101 MHz, C_6D_6) δ 6.38, 4.17, 3.35, 3.27, 0.85, 0.44, -0.32. ^{29}Si NMR (79 MHz, C_6D_6) δ 1.01, -6.15, -6.31, -7.59, -14.09, -103.20, -111.15, -121.02. HRMS (TOF MS ASAP+) for [$C_{25}H_{74}Si_{16}$+CH_3CN+H]: calculated = 863.2364, found = 864.10 [M+CH_3CN+H]$^{+}$

NMR Spectra of **2**:

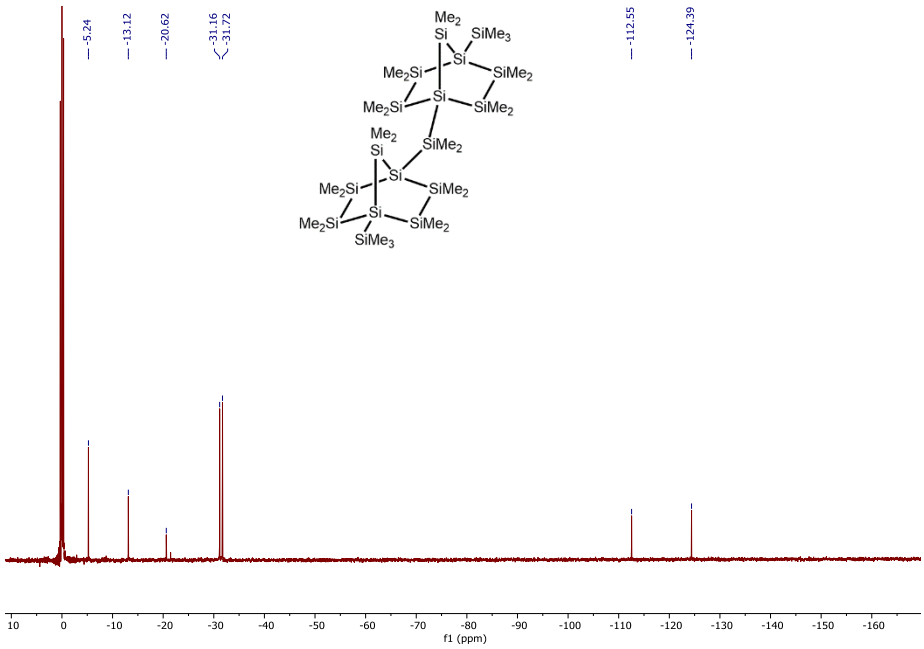
^{1}H NMR (400 MHz, C_6D_6)



^{13}C NMR (151 MHz, C_6D_6)

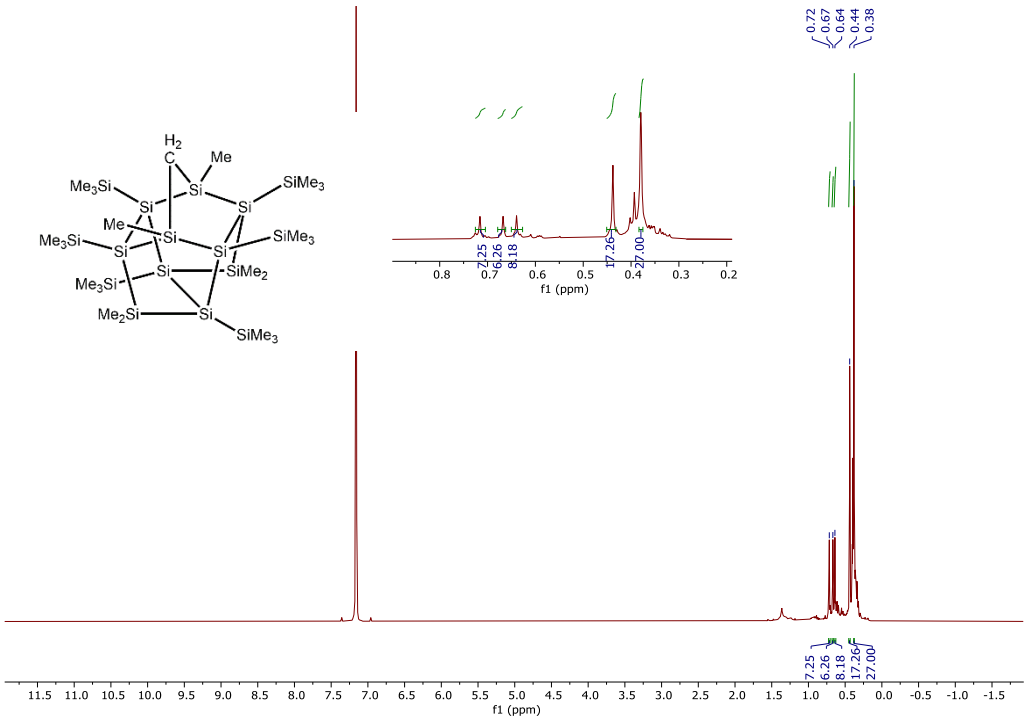


^{29}Si NMR (79 MHz, C_6D_6)

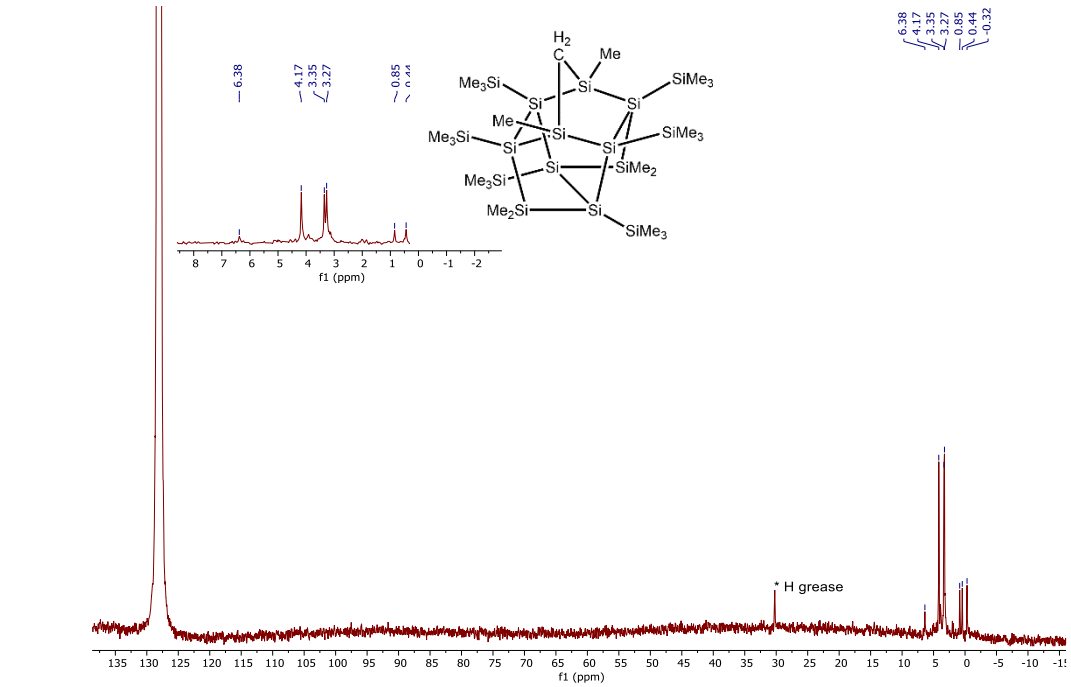


NMR Spectra of **3**:

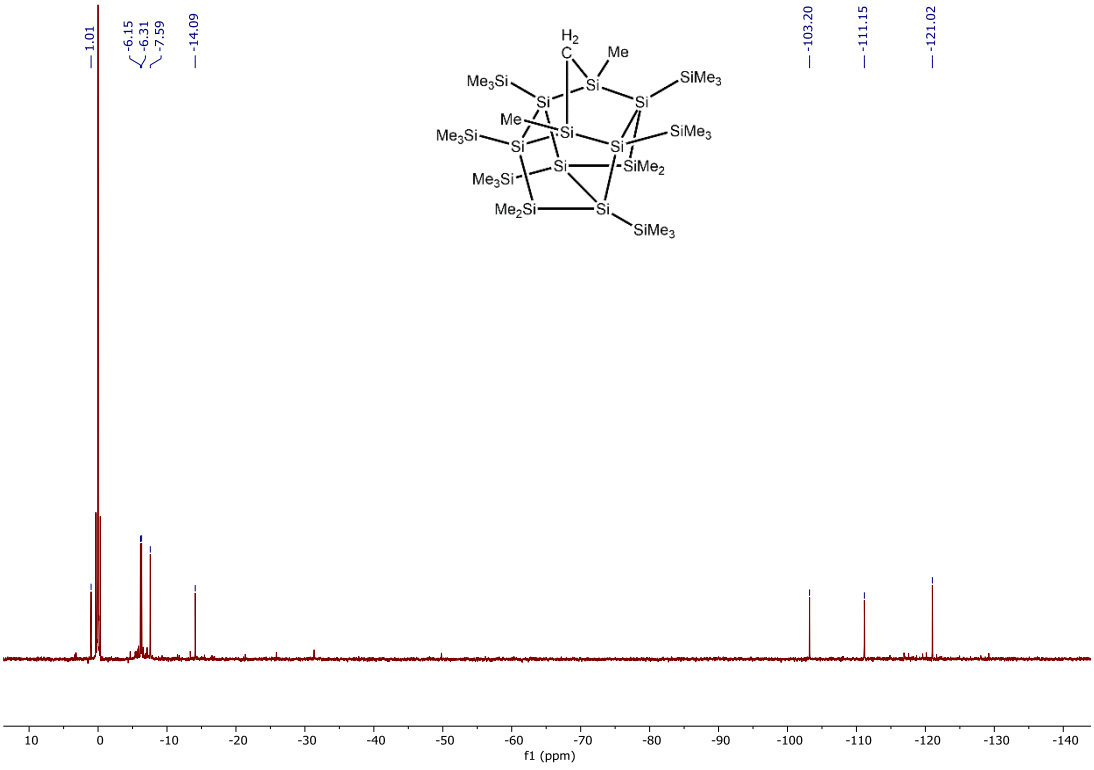
^{1}H NMR (400 MHz, C_6D_6)



^{13}C NMR (151 MHz, C_6D_6)



^{29}Si NMR (79 MHz, C_6D_6)



Crystallographic Data collection

Single crystals suitable for X-ray diffraction were grown by vapor diffusion of EtOH into $CHCl_3$. A colourless crystal (block, approximate dimensions 0.32 × 0.31 × 0.06 mm^3) was placed onto the tip of a MiTeGen pin and mounted on a Bruker Venture D8 diffractometer equipped with a PhotonIII detector at 100.00 K. The data collection was carried out using Mo Kα radiation (λ = 0.71073 Å, IμS micro-source) with a frame time of 3 seconds and a detector distance of 40 mm. A collection strategy was calculated and complete data to a resolution of 0.77 Å were collected. The frames were integrated with the Bruker SAINT[1] software package using a narrow-frame algorithm to 0.77 Å resolution. Data were corrected for absorption effects using the multi-scan method (SADABS).[2] Please refer to Table 1 for additional crystal and refinement information.

Structure solution and refinement

The space group C 2/c was determined based on intensity statistics and systematic absences. The structure was solved using the SHELX suite of programs[3] and refined using full-matrix least-squares on F^2 within the OLEX2 suite.[4] An intrinsic phasing solution was calculated, which provided most non-hydrogen atoms from the E-map. Full-matrix least squares / difference Fourier cycles were performed, which located the remaining non-hydrogen atoms. All non-hydrogen atoms were refined with anisotropic displacement parameters. The hydrogen atoms were placed in ideal positions and refined as riding atoms with relative isotropic displacement parameters. The structure crystalizes with Z' = 0.5. The final full matrix least squares refinement converged to R1 = 0.0295 and wR2 = 0.0741 (F^2, all data). The goodness-of-fit was 1.053. On the basis of the final model, the calculated density was 1.052 g/cm^3 and F(000), 1792 e^-.

Crystal data and structure refinement for 3

Empirical formula	C25 H74 Si16	
Formula weight	824.28	
Crystal color, shape, size	colourless block, 0.32 × 0.31 × 0.06 mm^3	
Temperature	100.00 K	
Wavelength	0.71073 Å	
Crystal system, space group	Monoclinic, C 1 2/c 1	
Unit cell dimensions	a = 20.7259(18) Å	α = 90°.
	b = 11.3770(17) Å	β = 105.265(4)°.
	c = 22.885(3) Å	γ = 90°.
Volume	5205.8(11) $Å^3$	
Z	4	
Density (calculated)	1.052 g/cm^3	
Absorption coefficient	0.407 mm^{-1}	
F(000)	1792	

Data collection

Diffractometer	Bruker D8 Venture
Theta range for data collection	2.060 to 27.507°.
Index ranges	-26<=h<=22, -14<=k<=14, -29<=l<=29
Reflections collected	66680
Independent reflections	5975 [R_{int} = 0.0633]
Observed Reflections	5056
Completeness to theta = 25.242°	99.7 %

Solution and Refinement

Absorption correction	Semi-empirical from equivalents
Max. and min. transmission	0.7456 and 0.6810
Solution	Intrinsic methods
Refinement method	Full-matrix least-squares on F^2
Weighting scheme	$w = [\sigma^2 Fo^2 + AP^2 + BP]^{-1}$, with
	$P = (Fo^2 + 2\,Fc^2)/3$, A = 0.031, B = 4.50
Data / restraints / parameters	5975 / 0 / 198
Goodness-of-fit on F^2	1.053
Final R indices [I>2σ(I)]	R1 = 0.0295, wR2 = 0.0683
R indices (all data)	R1 = 0.0386, wR2 = 0.0741
Largest diff. peak and hole	0.336 and -0.260 $e.Å^{-3}$

References

[1] SAINT, V8.30A, Bruker Analytical X-Ray Systems, Madison, WI, 2012.

[2] SADABS, 2.03, Bruker Analytical X-Ray Systems, Madison, WI, 2016.

[3] G. M. Sheldrick, Acta Cryst. A64, 112 - 122 (2008). Sheldrick, G.M. (2015). Acta Cryst. A71, 3-8.

[4] O. V. Dolomanov, L. J. Bourhis, R. J. Gildea, J. A. K. Howard and H. Puschmann, J. Appl. Crystallogr., 2009, 42, 339–341.